Random walk models for intracellular transport: the role of inhomogeneity and anisotropy

Dissertation

zur Erlangung des Grades
des Doktors der Naturwissenschaften
der Naturwissenschaftlich-Technischen Fakultät
der Universität des Saarlandes

von

Anne Elisabeth Hafner

Saarbrücken

2018

Tag des Kolloquiums:
18.12.2018

Dekan:
Prof. Dr. Guido Kickelbick

Vorsitzender:
Prof. Dr. Romanus Dyczij-Edlinger

Berichterstatter/innen:
Prof. Dr. Dr. h.c. Heiko Rieger
Prof. Dr. Ludger Santen
Prof. Dr. Cécile Appert-Rolland

Akad. Beisitzer:
Dr. Hendrik Hähl

Zusammenfassung

Intrazellulärer Transport ist ein komplexes Zusammenspiel zwischen Zytoskelett, Motorproteinen und Cargo. Das Zytoskelett ist räumlich stark inhomogen und anisotrop. Während Mikrotubuli ein radiales Netzwerk mit Zentrum im Zellinneren bilden, sind Aktinfilament mit willkürlicher Anordnung auf den Kortex beschränkt. Verschiedene Motorproteine binden an ein Cargoteilchen und transportieren es entlang des Zytoskeletts. Dabei erfährt das Teilchen stochastische Übergänge zwischen Phasen gerichteten Transports und Phasen des Stillstands. Wie dieses Zusammenspiel die Diffusion und die Effizienz des Transports beeinflusst ist unklar. Random Walk Modelle bilden einen theoretischen Zugang zu Transportprozessen in Zellen. Allerdings wurde der Einfluss des Zytoskeletts, der Motorproteine und der Arrestzustände in der Literatur bisher nur separat behandelt. Im Rahmen dieser Arbeit werden Random Walk Modelle behandelt, die das Zusammenspiel der drei Schlüsselkomponenten intrazellulären Transports berücksichtigen. Mittels dieser kann der Einfluss dieses Zusammenspiels auf anomale Diffusion und First Passage Events systematisch untersucht werden. Analytische Berechnungen und Monte Carlo Simulationen prognostizieren das Aufkommen transienter anomaler Diffusion und zeigen, dass die Effizienz verschiedener Transportprozesse durch die Inhomogenität und die Anisotropie des Zytoskeletts erhöht wird.

Abstract

Intracellular transport is an intricate interplay between the cytoskeleton, the motor proteins, and the cargo. The cytoskeleton exhibits a complex spatial organization which is generally inhomogeneous and anisotropic. Microtubules radiate from the cell center, whereas actin filaments randomly populate the cortex. Several motors of diverse species attach to a single cargo and carry it along the cytoskeleton. Thereby, cargoes exhibit stochastic transitions between phases of directed motion and reorienting arrest states at filament crossings. How this interplay effects anomalous diffusion and the efficiency of targeted transport is elusive. Coarse grained random walk models provide a powerful tool to approach transport processes inside cells. But so far, the impact of the cytoskeleton architecture, the motor activity, and the transient arrest states of the cargo are considered separately in the literature. Here, we present unified random walk models which incorporate the three key components of intracellular transport and enable us to elucidate how their interplay effects anomalous diffusion and first passage events. With the aid of analytic considerations and extensive Monte Carlo simulations, we show that transient crossovers in anomalous diffusion arise and that the efficiency of various intracellular transport tasks is substantially increased by the inhomogeneity and anisotropy of the cytoskeleton.

Publications

Results of this thesis are published in the following peer-reviewed journals:

[Hafner2018]
A. E. Hafner and H. Rieger.
Spatial cytoskeleton organization supports targeted intracellular transport.
Biophys. J., 114:1420-1432, 2018.

[Hafner2016]
A. E. Hafner and H. Rieger.
Spatial organization of the cytoskeleton enhances cargo delivery to specific target areas on the plasma membrane of spherical cells.
Phys. Biol., 13:066003, 2016.

[Hafner2016B]
A. E. Hafner, L. Santen, H. Rieger and M. R. Shaebani.
Run-and-pause dynamics of cytoskeletal motor proteins.
Sci. Rep., 6:37162, 2016.

Conference contributions

Moreover, results of this thesis were presented at the following conferences:

10/17 Conference "Cell Physics"
Saarland University, Saarbrücken, Germany
Talk: Spatial cytoskeleton organization supports targeted intracellular transport

07/17 Summer school "Fundamental Problems in Statistical Physics XIV"
Bruneck, Italy
Poster: Spatial cytoskeleton organization supports targeted intracellular transport

03/17 Meeting "Circle Meeting Biological Physics 2017"
EMBL Advanced Training Centre, Heidelberg, Germany
Talk: Spatially inhomogeneous cytoskeleton promotes targeted intracellular transport

01/17 Workshop "Biology for Physics: Is there new Physics in living matter?"
PRBB, Barcelona, Spain
Poster: Impact of the cytoskeleton architecture on intracellular transport efficiency to specific membranous targets

10/16 Science Slam "2. Science Slam der DFG-Verbundprojekte@UdS"
Saarland University, Homburg, Germany
Talk: Random search processes in and of cells

07/16 Conference "StatPhys 26"
Centre de Congres de Lyon, Lyon, France
Poster: Spatially inhomogeneous search strategies for intracellular transport to targets on the membrane: a random velocity model

06/16 Conference "Cell Physics"
Saarland University, Saarbrücken, Germany
Poster: Spatially inhomogeneous search strategies for intracellular transport to targets on the membrane: a random velocity model
Poster: Run-and-tumble dynamics of cytoskeletal motor proteins

05/16 Summer Camp "Summer Camp des SFB 1027"
Konferenzzentrum Schloss Waldthausen, Mainz, Germany
Poster: Intracellular transport during cell polarization

05/16 Meeting "Circle Meeting Biological Physics 2016"
IPGG, Paris, France
Talk: Spatially inhomogeneous search strategies for intracellular transport – a random velocity model

03/16 Conference "80. Jahrestagung der Deutschen Physikalischen Gesellschaf"
Universität Regensburg, Regensburg, Germany

Talk: Impact of detachment frequency on transport dynamics of cytoskeletal motor proteins
Poster: Spatially inhomogeneous search strategies for intracellular transport to targets on the membrane: a random velocity model

09/15 Symposium “Physics of Cancer”
BBZ, Leipzig, Germany
Poster: Spatially inhomogeneous search strategies during intracellular transport

06/15 Summer Camp “Summer Camp des SFB 1027”
Physikzentrum, Bad Honnef, Germany
Poster: Efficient search strategies in spatially inhomogeneous cells

05/15 Workshop “Random Walks and Non-Linear Dynamics in the Life of Cells”
MPI PKS, Dresden, Germany
Poster: Anomalous transport in complex dendrites – geometrical considerations

04/15 Meeting “Circle Meeting Biological Physics 2015”
AMOLF, Amsterdam, Netherlands
Talk: Analytical approach to the intermittent motion of self-propelled particles

03/15 Conference “79. Jahrestagung der Deutschen Physikalischen Gesellschaft”
Technische Universität Berlin, Berlin, Germany
Talk: Anomalous transport in complex dendrites – geometrical considerations

Contents

List of Figures

List of Tables

Nomenclature

Model parameters used in Chapter 4

κ_w	probability to switch from motion to waiting state
κ_m	probability to switch from waiting to motion state
ℓ	step length
$\mathcal{F}(\ell)$	step length distribution
$\lambda = \langle \ell^2 \rangle / \langle \ell \rangle^2$	width of the step length distribution
P_0^M	probability to start the walk in the motion state
p	processivity
$\mathcal{R}(\phi)$	rotation angle distribution
$\mathcal{R}$	Fourier transform of $\mathcal{R}(\phi)$
$\mathcal{A}{=}p + \mathcal{R} - p\mathcal{R}$	generalized anisotropy

Model parameters used in Chapter 5

R_m	cell radius
δ	width of the actin cortex
α_exit	opening angle of the narrow escape
R_d	detection radius of the reaction problem
v	effective speed of the cargo
$k_{m\to w}$	rate to switch from motion to waiting state
$k_{w\to m}$	rate to switch from waiting to motion state
ω	processivity of the cargo
$f(\alpha_\mathrm{rot})$	rotation angle distribution
p_antero	probability for radially outward motion in the cell interior
q_K, q_D, q_M	probability for radially outward, inward, and random motion in the cortex

Abbreviations

ADP	adenosin diphosphate
ATP	adenosine triphosphate
cAMP	cyclic adenosine monophosphate
CTL	cytotoxic T lymphocyte
CTRW	continuous time random walk
DNA	deoxyribonucleic acid
ERM	ezrin, radixin, moesin
FPT	first passage time
mRNA	messenger ribonucleic acid
MAP	microtubule associated protein
MFPT	mean first passage time
MMT	total mean motion time
MSD	mean square displacement
MTOC	microtubule organizing center
MWT	total mean waiting time
Pi	phosphate ion
(# waiting periods)	total mean number of waiting states

Chapter 1.

Introduction and Motivation

> "What is Life?", Erwin Schrödinger, 1944 [1]

Since the beginning of time, people wonder about the complexity of life. It appears to be obvious how to distinguish between living and non-living matter. Animals, plants, and fungi are living; a cloud, a stone, a car is not. However, to define the properties which are distinctive of life is challenging. Presumably the most striking difference is that living systems are made up of cells [2]. Cells are often referred to as the "building blocks of life" [3]. Even though a unequivocal definition of a cell is lacking, cells share the same fundamental properties [2, 4, 5]: Cells are able to reproduce and transmit genetic information. Cells consume energy to regulate their function and maintain a specific internal organization. Cells are able to communicate with their environment and adapt to external stimuli. And cells are able to arrange into complex multi-cellular organisms. The astonishing complexity of life which emerges out of these basic properties of cells is believed to arise due to the interplay between "chance and necessity" [6] and is captured in biological concepts such as evolution, heredity, or fitness. Nonetheless, a quantitative understanding of living systems necessitates an interactive collaboration between diverse disciplines, such as physics, biology, chemistry, or computer science, with their respective scientific background, experimental techniques, and theoretical models, see for instance [7]. Even more than 70 years after Schrödinger's famous article [1], the physical principles behind "What is Life?" are far from being fully understood.

In this thesis, the focus is on one crucial aspect of life, namely active intracellular transport. The biological background is provided in Chapter 2.

The correct delivery of intracellular cargo is vital for the function of cells and organisms. A myriad of cargo particles, such as cell organelles or macromolecules, have to be transported from their source to specific target locations. Processes as diverse as secretion, signal transduction, cell division and migration, or muscle contraction rely on active intracellular transport [2]. A prominent example occurs during immune response. Specialized T cells scan organisms for pathogen-infected or tumorigenic cells [2]. When

getting into contact with a pathological cell, T cells form a close connection to it, which is called immunological synapse. Toxic material is then actively transported and exclusively released at the synapse to ensure the killing of the pathological cell [2, 8–14]. A malfunction of active intracellular transport is related to diverse severe diseases, such as Alzheimer's or dementia, e.g. [15]. Active intracellular transport is a complex non-equilibrium process which involves the cytoskeleton, molecular motors, and the cargo. The cytoskeleton of metazoan cells is a highly complex filament network composed of microtubules, actin filaments, and intermediate filaments [2]. In general, the cytoskeleton exhibits a complex, space-dependent structure which is highly inhomogeneous and anisotropic. Actin filaments are randomly accumulated in the cell cortex, whereas microtubules radiate from the center of the cell [2]. Specialized motor proteins walk actively along the cytoskeleton filaments by continuously consuming energy [2]. Simultaneously, they attach to a cargo and drag it along the filaments. Kinesin and dynein motors facilitate long-range transport along microtubules, while myosins manage short-range transport on actin filaments [2, 16]. Typically, a single cargo is dragged along the cytoskeleton with the aid of several motors of diverse species [17–31]. In order to guarantee efficient cargo delivery, the activity of a motor species is regulated by the cell [19–28, 31, 32]. When navigating through the cell, large cargo-motor complexes frequently pause at filament crossings of the cytoskeleton until they either overcome the barrier or switch to another filament [29, 33–38]. Hence, intracellular cargo undergoes a stochastic motion pattern with random alternations between directed transport along the cytoskeleton and reorienting arrest states.

In essence, intracellular transport is a stochastic process which is shaped by the interplay between three key players: the cytoskeleton with its spatial architecture, the molecular motors with their respective activity, and the cargo with its random alternations between active motion and reorienting arrest states. How a cell regulates intracellular transport by taking advantage of this interplay is elusive.

Due to its complexity, modeling intracellular transport is a challenging theoretical task. But, the stochastic motion pattern suggests a random walk approach. Coarse grained models which consider the effective cargo motion but ignore the microscopic stepping of individual motor proteins provide a powerful approach to active transport on a cellular scale. The state of the art in modeling intracellular transport with the aid of random walks is provided in Chapter 3. A particular focus is on two aspects of intracellular transport: anomalous diffusion, which is frequently observed inside cells, e.g. [39–55], and first passage events, which quantify the crucial temporal efficiency of targeted transport. Standard random walk models for asymptotic anomalous diffusion rely on a breakdown of the central limit theorem and take advantage of broad distributions and long-range correlations in the walker's trajectory [56–61]. But, anomalous diffusion can also occur on short and intermediate timescales without the need for broad distributions or long-range correlations. Random walks in anisotropic, directed environments, such as the cytoskeleton [62, 63], and random walks with stochastic trapping events [64], similar to the pausing states experienced by intracellular cargo, show non-trivial transient anomalous diffusion. Whether the observed anomalous diffusion in biological experiments maintains in the long time limit or whether it is only a transient effect is

obscure [65–67]. First passage times specify the time it takes a cargo to reach a target for the first time. In the context of various search problem, intermittent strategies with stochastic transitions between a slow detective phase and a fast non-reactive phase are shown to be advantageous, e.g. [68–75]. Such random walks are typically studied in homogeneous, isotropic environments. But, this assumption is not valid for intracellular transport processes which cover the whole cell range. Very recently, the effect of the exact topology of the cytoskeleton on intracellular transport has gained scientific interest [76–80].

However, up to now the impact of the cytoskeletal architecture, the motor activity, and pauses of the cargo have been studied separately in the literature, as discussed in Chapter 3. In this thesis, we present unified random walk models which incorporate the three key properties of intracellular transport and enable us to elucidate how the interplay effects anomalous diffusion and first passage events. A specific focus is on the role of the inhomogeneity and anisotropy of the cytoskeleton.

In Chapter 4, we identify the influence of the local anisotropy of the cytoskeleton, the motor behavior, and the waiting frequency of the cargo on intracellular diffusion [Hafner2016B]. At first, a random walk model is introduced to investigate the unidirectional motion of cargo along a single, polarized filament which is frequently interrupted by waiting states. Within an analytic framework, we derive an exact expression of the probability density function of the tracer's displacement. The resulting mean square displacement reveals complex anomalous diffusion. Crossovers between different anomalous regimes occur on short and intermediate timescales. By monitoring the temporal evolution of the anomalous exponent over all timescales we show that the observed anomaly is a highly transient effect based on aging processes out of a predefined initial state. The impact of the initial state and the measurement procedure is of crucial importance for the interpretation of experimental results. Anomalous diffusion of intracellular cargo on two-dimensional anisotropic networks was studied in [Hafner2014]. The model and main results are briefly recapitulated in Chapter 4. Our understanding of the observed anomaly is significantly deepened here by studying the anomalous exponent over all timescales and by investigation of the long time limit. We show that the crossover time to asymptotic diffusion and the long time diffusion constant varies by several orders of magnitude in response to the arrest frequency of the cargo.

Chapter 5 is dedicated to the temporal efficiency of intracellular search strategies [Hafner2016, Hafner2018]. We introduce a random walk model to study the transport of intracellular cargo on a cytoskeleton which is very inhomogeneous on a cellular scale. The tracer particle experiences radial transport in the cell interior, whereas multi-directional transport is restricted to a cortex underneath the plasma membrane. With the aid of extensive Monte Carlo simulations, we systematically analyze how the interplay between the structural characteristics of the cytoskeleton, the motor activity, and the pausing frequency of the cargo effects the efficiency of targeted intracellular transport. We consider three paradigmatic tasks: the narrow escape problem, which models transport to a specific area on the plasma membrane,

the reaction problem, which evaluates the time until fusion of two reactants within the cell, and the reaction-escape problem, which emerges when two particles first have to react inside the cell before the product particle is transported to a narrow exit on the plasma membrane. By taking into account different physiological conditions, we show that a cell is able to regulate the efficiency of diverse transport tasks by control of the cytoskeleton architecture, the motor activity, and the cargo's waiting frequency. A spatially inhomogeneous cytoskeleton with a thin actin cortex is generally advantageous to its homogeneous counterpart.

The results of this thesis are discussed in Chapter 6.

Chapter 2.

Biology of intracellular transport

Contents

2.1. Basic components of cells

Life is inevitably connected to biological cells. All organisms ranging from unicellular organisms, as for instance bacteria, to complex multi-cellular organisms, such as animals, plants, and fungi, are composed of cells [2, 5]. Besides the astonishing diversity of life, cells share the same fundamental protperties [4]. All cells emerge by division of existing cells. All cells contain a hereditary genetic information which is mandatory for the regulation of cell function. All cells are open systems which communicate with their surrounding and obtain and consume energy. And all cells have a complex, but highly organized internal structure.

Apart from their similarities, cells are very diverse in their appearance and function. A main difference is the organization of the genetic material due to which cells are classified into two types: *prokaryotes* (Greek: “before nucleus”) and *eukaryotes* (Greek:

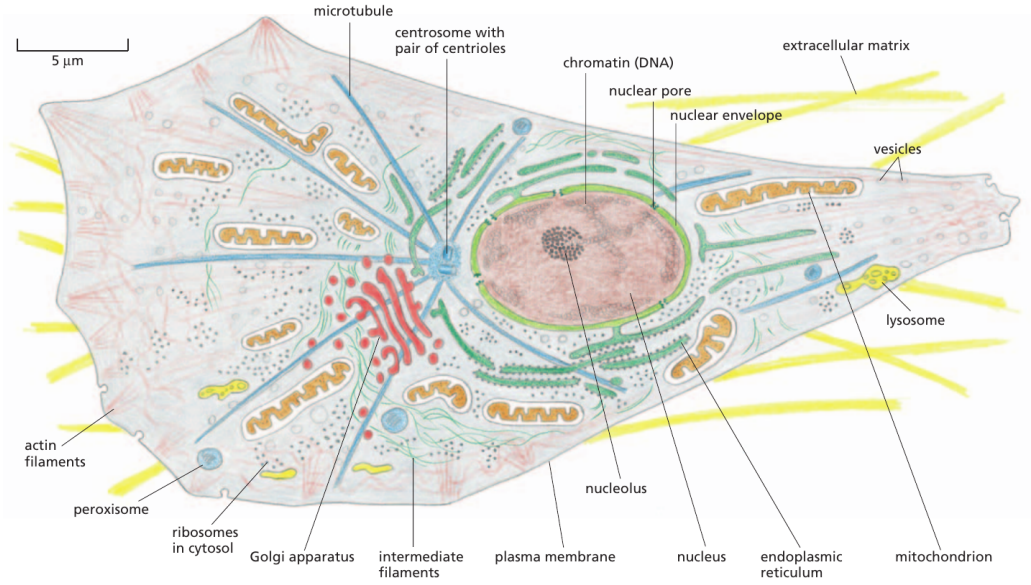

Figure 2.1.: Eukaryotic cell. The cell interior is framed by the plasma membrane. The most prominent cell organelle is the nucleus which contains the genetic material. Apart from the nucleus, the cytoplasm is filled with organelles, such as mitochondria, endoplasmic reticulum, Golgi complex, and diverse functional vesicles. Reprint of [2], Molecular Biology of the Cell by Alberts, reproduced with permission of Taylor & Francis Group in the format Thesis/Dissertation via Copyright Clearance Center.

"well nucleus") [2, 5]. Prokaryotes are single-celled microorganisms, such as bacteria or archaea. Typically, they posses a diameter of 1 μm - 2 μm. Eukaryotes can be either unicellular or multicellular organisms, as for instance protists, animals, plants, and fungi. Eukaryotic cells have a diameter of 5 μm - 100 μm [2, 5].

Prokaryotic and eukaryotic cells are bound by a *plasma membrane* which is interspersed with several proteins and channels so that each cell is able to interact with its surrounding [2]. The interior of a cell is called *cytoplasm*, although the nucleus is excluded in some definitions [2]. The cytoplasm consists of an aquaeous substance called *cytosol* and, in the case of eukaryotic cells, a large variety of biomolecules and functional structures collectively known as *cell organelles* [2, 4, 5]. Figure 2.1 displays the main components of an eukaryotic cell. Typical organelles are listed below [2, 4, 5, 65].

- The *nucleus* is a prominent membrane-bound organelle which contains the genetic material in form of DNA (deoxyribonucleic acid) [2].
- *Mitochondria* are membrane-enclosed organelles responsible for the synthesis of ATP (adenosine triphosphate) which is the main source of energy inside cells [2]. Mitochondria contain their own ribosomes and DNA. According to the endosymbiotic theory, mitochondria once lived freely as prokaryotes which were internalized by ancestral eukaryotic cells for symbiotic reasons [4, 5].

- *Ribosomes* catalyze the synthesis of proteins by translation of mRNA (messenger ribonucleic acid), which is a single-stranded, transcripted piece of DNA produced in the nucleus [2].

- The *endoplasmic reticulum* is a membrane-bound organelle with a tubular structure. It is the site of protein and lipid synthesis. According to the number of associated ribosomes the endoplasmic reticulum is categorized as rough (many ribosomes) or smooth (less ribosomes) [2, 65].

- The *Golgi complex* is a membrane-bound organelle located close to the nucleus. It modifies and sorts proteins and lipids which were transported from the endoplasmic reticulum in vesicles for final target delivery [2, 65].

- *Vesicles* are small, spherical organelles enclosed by a membrane which store diverse material. They fulfill a variety of functions and are involved in transport processes inside cells [2].

- *Lysosomes* are vesicles which are mainly responsible for degradation of biomolecules. For that purpose they are filled with digestive enzymes [2, 65].

- *Peroxisomes* are vesicles which are in charge of the catabolism of fatty acids [2].

- *Endosomes* are vesicle which are formed via endocytosis [2]. During *endocytosis* extracelluar material is transferred into the cell by invagination of the plasma membrane. The opposite process where a vesicle fuses with the membrane in order to release its material to the extracellular space is called *exocytosis* [2].

In contrast to the complex organization of eukaryotic cells, prokaryotes have a relatively simple internal organization. They lack a nucleus, compartmentalized organelles, and a complex cytoskeleton [4, 5]. In the following, the focus will be on the metazoan lineage of eukaryotic cells.

2.2. Cytoskeleton

In order to maintain a cell's mechanical stability , to adjust cell shape, to drive cell motility and division, and to actively transport intracellular cargo , cells are equipped with a highly complex, dynamic filament network, the so-called *cytoskeleton* [2, 81, 82]. The cytoskeleton of eukaryotic cells is composed of three different filament species: *microtubules*, *actin filaments* and *intermediate filaments*, as sketched in Fig. 2.1 [2]. The filaments are assembled in a regular, periodic structure by distinct protein species and undergo a frequent turnover of polymerization and depolymerization [2]. Specialized *accessory proteins* control the assembly of the filaments and cross-link them into networks. These networks exhibit a characteristic structure and spatial distribution inside a cell, as shown in Fig. 2.2 [2]. Consequently the cytoskeleton is a dynamic network which is able to adjust to specific tasks and environmental conditions.

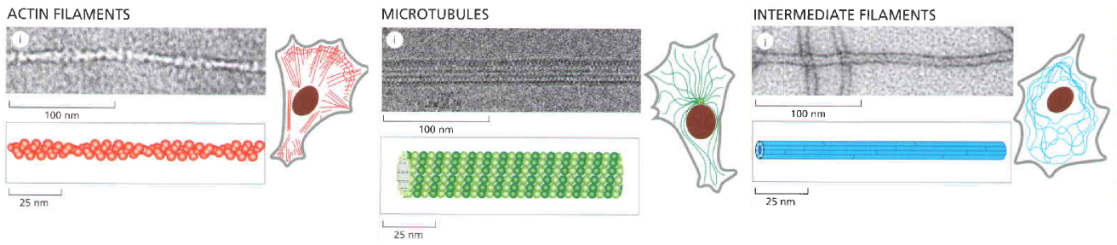

Figure 2.2.: Cytoskeletal filament species. The cytoskeleton is composed of three different filament types. Actin filaments, microtubules and intermediate filaments have a specific composition and spatial distribution within a cell. Reprint of [2], Molecular Biology of the Cell by Alberts, reproduced with permission of Taylor & Francis Group in the format Thesis/Dissertation via Copyright Clearance Center.

2.2.1. Microtubules

Microtubules are composed of heterodimeric *tubulin* subunits. A tubulin heterodimer consist of α- and β-tubulin and has a length of 8 nm [2, 83]. Tubulin assembles axially into linear *protofilaments*. The assembly occurs in a regular way such that an α-tubulin is always linked to a β-tubulin [2]. On average 13 protofilaments are then laterally connected to a hollow cylindrical microtubule with a diameter of 25 nm [2]. The asymmetry of the tubulin subunits leads to an intrinsic *polarity* of the assembled filament, as shown in Fig. 2.3 [2]. The end with an exposed β site is called plus end, whereas the one with an exposed α site is referred to as the minus end of the microtubule [2]. Due to their structure microtubules are very stiff filaments with a *persistence length* (average length scale at which no bending of the filament occurs) of a few millimeters [2]. Moreover, microtubules are dynamic filaments which undergo a dynamic instability, one end performs stochastic transitions between polymerization and depolymerization [2]. In general the minus end is known to be less dynamic than the plus end [84, 85]. Microtubules manage long-range intracellular transport and are key players during cell division [2].

2.2.2. Actin filaments

Actin filaments are built of globular *actin* which assemble head-to-tail and thus result in a polarized protofilament. An actin filament is formed out of two of these protofilaments which intertwine in a helical fashion as shown in Fig. 2.3 [2]. They are the thinnest of the cytoskeletal filaments and have a diameter of 5 nm - 9 nm [2]. Due to their structure, actin filaments are much more flexible than microtubules which is manifested by a persistence length of the order of 10 μm [2]. Just as microtubules, actin filaments are very dynamic and mainly perform treadmilling, i.e. one end depolymerizes while the other end polymerizes at the same time [2]. Actin filaments are involved in muscle contraction, manage active intracellular transport, maintain the mechanical stability of cells, and drive cell motility [2].

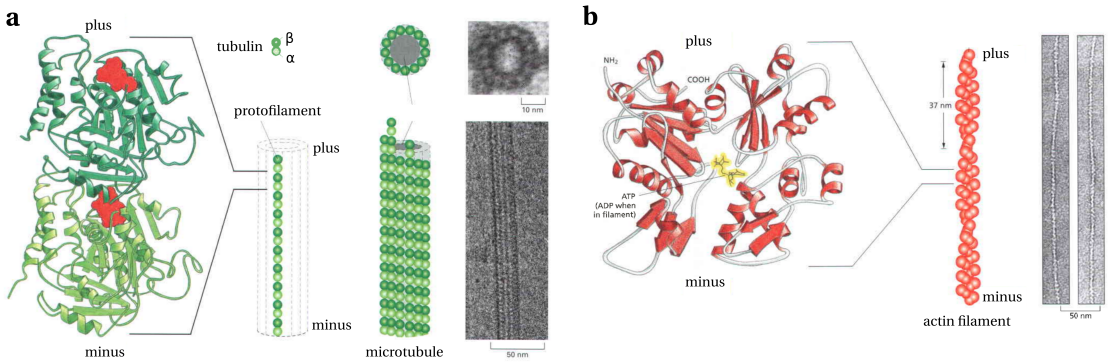

Figure 2.3.: Structure of microtubules and actin filaments. (**a**) Microtubules are built up of tubulin subunits, whereas (**b**) actin filaments are composed of actin proteins. The asymmetry of the subunits leads to the polar structure of the assembled filaments. Reprint of [2], Molecular Biology of the Cell by Alberts, reproduced with permission of Taylor & Francis Group in the format Thesis/Dissertation via Copyright Clearance Center.

2.2.3. Intermediate filaments

Intermediate filaments are assembled by a broad class of *intermediate filament proteins* [2,82]. The fibers have an average diameter of 10 nm, which is the name-giving quantity. Intermediate filaments are easily deformable and have a persistence length of less than 1 μm [2]. The main task of intermediate filaments is the support of the structural stability of cells [2, 82]. For instance, one species of intermediate filaments, called lamins, backs the nucleus, while others spread throughout the cytoplasm [2]. In contrast to actin and microtubules, intermediate filaments are neither polar nor involved in active intracellular transport [2]. Therefore, intermediate filaments will be neglected in the following.

2.2.4. Accessory proteins and the cytoskeleton architecture

With the aid of a variety of accessory proteins, cytoskeletal filaments are structured into specific networks. Accessory proteins regulate the dynamics and the location of filaments, they interlink them to complex meshworks, and connect them to the plasma membrane either by directly attaching to the filaments or to the free filament subunits in the cytosol [2]. A cell is thus able to control the structure of the cytoskeleton via different accessory proteins [2].

In most animal cells microtubules are nucleated at the central centrosome which acts as a *microtubule organizing center* (MTOC) [2]. Nucleation takes place at the minus end of the microtubule which is solidly fixed to the MTOC [83–85]. Since polymerisation occurs at the plus end, microtubules are growing towards the cell periphery [2]. Approximately 10^2-10^3 microtubules compose an astral structure within the cell [86–88], as indicated in Fig. 2.4, a. Accessory proteins of microtubules are collectively called *microtubule-associated proteins* (MAPs). MAPs influence the dynamics of individual filaments and connect microtubules to networks [2,83]. For instance the distinct spacing

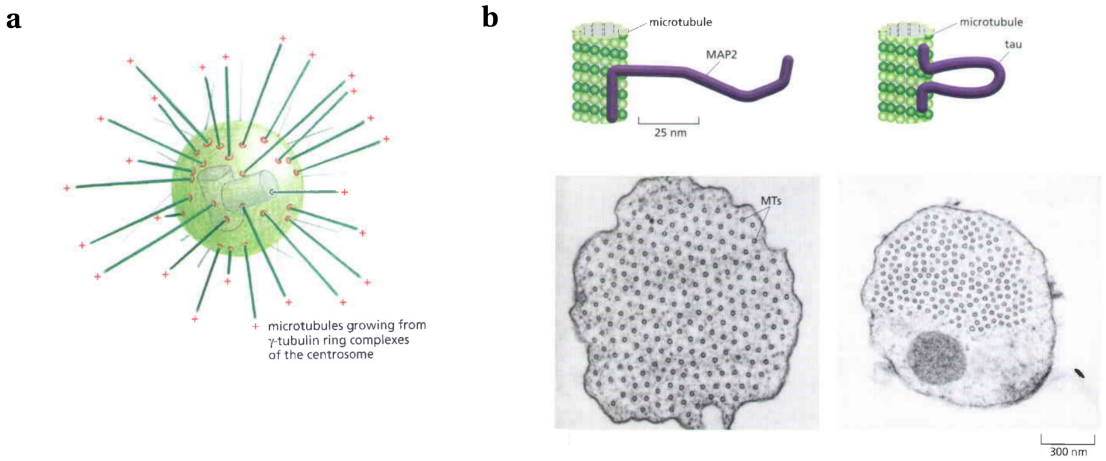

Figure 2.4.: Structure of microtubule networks. (**a**) In cells with a centrosome microtubules mainly nucleate at the central MTOC and project in a radial manner, thus forming an astral network. (**b**) Microtubule bundles in neurons formed by MAP2 (left) and tau (right) show different spacings between individual microtubules. Reprint of [2], Molecular Biology of the Cell by Alberts, reproduced with permission of Taylor & Francis Group in the format Thesis/Dissertation via Copyright Clearance Center.

between individual microtubules in neurons is achieved by the action of MAPs such as MAP2 or tau, see Fig. 2.4, b [2].

Actin filaments are mainly nucleated underneath the plasma membrane [2]. In analogy to microtubules, there are several accessory proteins specific to actin filaments which influence their dynamics and link them to networks [2]. Actin filaments are interconnected by bundling and web-forming proteins [2]. They lead to distinct networks with different architecture and mechanical properties, see for instance [82, 89], as indicated in Fig. 2.5. Bundling proteins, such as fimbrin and α-actinin, form aligned, parallel or anti-parallel bundles of actin filaments [2]. Such bundles can be found in cell protrusions like filopodia, which sensor the surrounding, or in stress fibers, which indicate cell adhesion to a substrate and exert forces [2]. Contrarily, web-forming proteins, such as spectrin or filamin, cross-link actin filaments to complex networks [2]. Spectrin is mainly found underneath the plasma membrane, whereas filamin is responsible for membrane projections called lamellipodia which are necessary for cell migration [2]. The protein complex Arp2/3 induces actin branches which emanate at distinct angles of 70° from the parent filament [90, 91]. Spectrin and proteins of the ERM (ezrin, radixin, moesin) family are able to tether actin filaments to the plasma membrane where they form a dense meshwork, the so-called *actin cortex* [2, 92, 93]. The actin cortex forms a well defined, thin shell underneath the plasma membrane with a width of 0.1 μm - 1 μm [2, 93–95]. The cortex consists of relatively short filament segments of length < 1 μm [96] which point in roughly isotropic directions [2, 93]. The exact distribution of orientations is objective of ongoing research, but there is recent evidence that actin filaments in cellular blebs are tangentially oriented to the membrane [97]. The *mesh size*

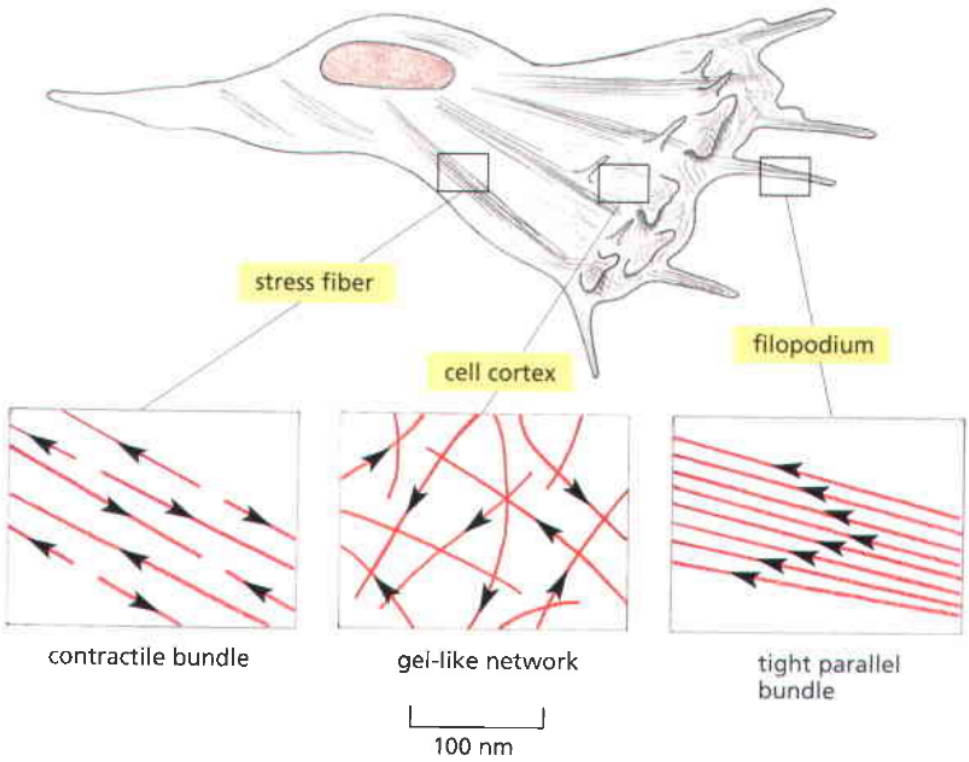

Figure 2.5.: Structure of actin networks. Actin filaments are linked via two types of accessory proteins: bundling and web-forming proteins. Bundling proteins form aligned, parallel or anti-parallel bundles of actin filament which can be found in cell protrusions, such as filopodia, or stress fibers. In contrast web-forming proteins lead to a complex, random network of actin filaments in the cell cortex. The polarity of individual actin filaments is indicated by the arrowhead which points to the actin minus end. Reprint of [2], Molecular Biology of the Cell by Alberts, reproduced with permission of Taylor & Francis Group in the format Thesis/Dissertation via Copyright Clearance Center.

of the cortex, which reflects the average distance between neighboring filaments, varies between 20 nm - 250 nm, but is typically given by 100 nm [93, 96, 98, 99].

Microtubule and actin networks are interconnected by specific accessory proteins, as reviewed in [100]. Approximately 10% of all microtubules are stably linked to the actin cortex [83,101–104] and some +TIPs thereby align microtubules and actin filaments [105]. In general, the cytoskeleton of metazoan cells which are rounded in suspension, mitosis, and amoeboid-like motion [93,106–108] is very inhomogeneous and anisotropic. An astral network of microtubules invades the whole cell, whereas actin filaments form a random cortex [2].

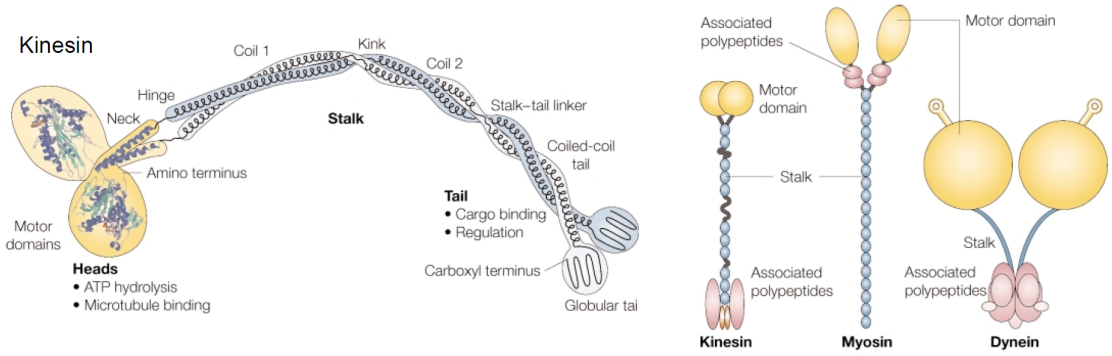

Figure 2.6.: Structure of molecular motors. All three types of motor proteins consist of a head domain which walks along cytoskeletal filaments and a tail domain which mediates specific cargo binding. Reprint of [109]. Reprinted by permission from Springer Customer Service Centre GmbH: Springer Nature, Nature Reviews Molecular Cell Biology, Walking on two heads: the many talents of kinesin, Woehlke, G. and Schliwa, M., Copyright (2000), (`http://dx.doi.org/10.1038/35036069`); permission conveyed through Copyright Clearance Center, Inc.

2.3. Molecular motors

The cytoskeleton serves as track for *molecular motors*. Molecular motors are specialized accessory proteins which actively walk along the cytoskeletal filaments powered by the hydrolysis of ATP [2]. They thus facilitate active intracellular transport, but are also involved in muscle contraction and ciliary beating, cell locomotion and cell division [2]. Topical reviews on molecular motors include [32, 109–112].

Three different classes of motor proteins exist in eukaryotic cells: *kinesins*, *dyneins*, and *myosins* [2]. They vary according to the associated filament type, the walking direction, and the bound cargo [2]. Myosins move along actin filaments, whereas kinesins and dyneins walk along microtubules. Individual motor proteins exhibit predefined direction which is determined by the polarity of the cytoskeletal filaments [2].

Each motor protein is composed of a *motor domain*, or head, and a *tail domain* which are connected by a stalk, as shown in Fig. 2.6 [109]. The tail domain has a specific binding site to attach to intracellular cargo, such as cell organelles (e.g. vesicles, mitochondria, Golgi stacks) and intracellular macromolecules (e.g. mRNA, centrosomes, cytoskeletal filaments, viruses) [2, 32, 109–112]. In contrast to the head, the tail domain is highly specific which accounts for the diversity of cargo and function performed by motor proteins [109]. The head domain binds to the filament, hydrolyzes ATP, and drives the motion of the motor proteins. Its structure is largely conserved among the three motor species [109] and may be monomeric, dimeric, trimeric or tetrameric [112]. Each head of the motor domain contains a specific filament- and at least one ATP-binding site [2, 109]. The occupancy of the ATP-site determines the binding of the head to the filament. Hydrolysis of ATP ($\mathrm{ATP} \rightleftharpoons \mathrm{ADP} + \mathrm{P_i}$) drives a *mechanochemical cycle* which

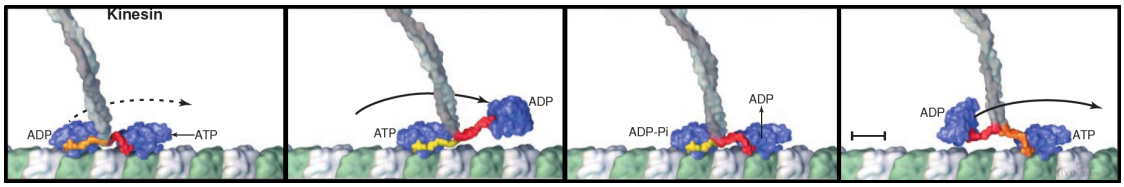

Figure 2.7.: Hand-over-hand movement of a single motor. Conventional kinesin coordinates the mechanochemical cylcles of the head dimer to move processively along microtubules. Reprint of [110]. From Vale, R. D. and Milligan, R. A., The way things move: looking under the hood of molecular motor proteins, Science, 288:88-95, 2000, (`http://dx.doi.org/10.1126/science.288.5463.88`). Reprinted with permission from AAAS.

basically consists of filament attachment of the head, amplified conformational change of the motor, filament detachment of the head, conformational relaxation, and filament reattachment [2, 32, 109–112]. Consequently, molecular motors convert the chemical energy provided by the hydrolysis of ATP into mechanical energy to propel themselves in distinct steps of a few nanometers along the cytoskeletal filaments [2, 32, 109–112].

2.3.1. Movement pattern of motor proteins

Some motor proteins are able to perform multiple steps before dissociation of the filament, a characteristic referred to as *processivity*, whereas non-processive motors take only one step before dissociation [2, 109, 112]. Processivity is believed to originate from a high *duty ratio*, i.e. the motor stays attached to the filament for a long time period during one mechanochemical cycle [2, 109, 113], and the ability to coordinate the heads of the motor [2, 110, 114]. Processive and non-processive motors are specialized for different tasks [2, 112].

A typical example of a non-processive motor is myosin-II. Myosin-II is specialized for fast interactions with actin filaments [112]. It is the main player in muscle contraction for which a large array of non-intervening motors is crucial [2]. Many myosin-II motors perform one step along the filament and directly detach again to not impede the motion of other motors [110, 112].

In contrast, most motor proteins which are involved in intracellular transport, such as kinesin-1, cytoplasmic dynein-1, and myosin-V, are processive homodimers with finite *run length* [2, 32, 115–119]. By coordination of the two heads kinesin-1 and myosin-V move in a so-called *hand-over-hand motion pattern* along the filament [32, 110, 114, 120–122]. Thereby, one head is propelled forward at a time in a concerted manner. The rear head detaches, passes the leading head and reattaches to the filament in front of the former leading head, as shown in Fig. 2.7 [2, 32, 110]. The heads of cytoplasmic dynein-1 are less well coordinated and allow for multiple, consecutive steps of the same head [123–128].

Due to the finite run length, single motor proteins frequently perform cycles of directed motion along the filaments and undirected motion in the crowded cytoplasm [2, 65, 129].

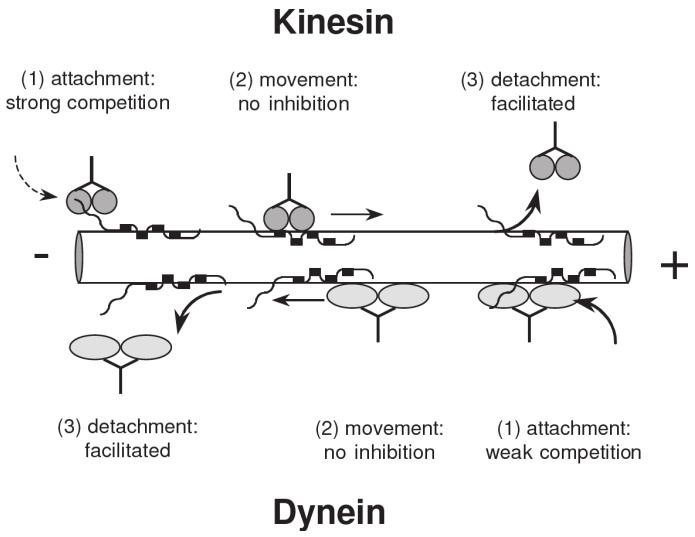

Figure 2.8.: Impact of MAP tau on the motion of motor proteins. The MAP tau competes with binding and facilitates unbinding events of kinesin and dynein motors on microtubules. Reprint of [130], Trinczek, B. *et al.*, Journal of Cell Science, 1999, 112, 14, 2355-2367 (`http://jcs.biologists.org/content/112/14/2355.long`), Journal of Cell Science by Company of Biologists, reproduced with permission of COMPANY OF BIOLOGISTS LTD. in the format Republish in a thesis/dissertation via Copyright Clearance Center.

Accessory proteins are able to regulate the detachment and reattachment frequency of motor proteins. For instance the MAP tau competes with the binding and facilitates the unbinding of kinesin and dynein motors, as sketechd in Fig. 2.8 [130]. And the protein complex dynactin, which is important for dynein cargo linkage, improves the processivity of dynein motors [32, 111, 119].

2.3.2. Kinesin

The kinesin family is very large and can be classified into 14 subfamilies [131]. Kinesins are involved in cell division and facilitate intracellular transport [2]. Most kinesins move towards the plus end of microtubules, but there is also one group moving in minus direction [2]. A paradigmatic member of the kinesin family which is responsible for intracellular transport is conventional kinesin, or kinesin-1, which moves in the microtubule plus direction [2, 32, 109]. Its motor domain is a homodimer and each head features a single ATP-binding [32, 109, 110]. Per ATP hydrolysis, it takes 8 nm-steps along a microtubule protofilament and thus propagates from one tubulin subunit to the next on a timescale of about 10 ms [2, 32, 109, 110, 132, 133]. Kinesin-1 is a processive motor which *in vitro* can take several hundred steps before detaching from the filament, which leads to total walking distances of about 1.1 μm [32, 110, 115, 116]. The speed of kinesins varies largely within the family from 0.02 μm/s to 3 μm/s [2, 109, 134].

2.3.3. Dynein

Dynein motors are classified into axenomal and cytoplasmic dynein [32]. Axenomal dyneins are mainly involved in flagella or cilia beating, see for instance [135]. Whereas cytoplasmic dynein-1 manages active transport along the microtubule minus direction [2]. Its function is closely connected to the protein complex dynactin which enhances its processivity and links it to cargo [32, 111, 119]. Dyneins move processively for distances of up to 1.9 μm [124,125] at speeds of up to 14 μm/s [2,136]. The step size of cytoplasmic dynein-1 depends on its load; it takes 8 nm steps at high load and up to 32 nm at zero load [32, 136, 137].

2.3.4. Myosin

Myosins facilitate active transport and muscle contraction along actin filaments [2]. The myosin family is very diverse and can be divided into 18 subfamilies [112]. All of them but myosin-VI walk towards the plus end of actin filaments [2]. Amongst them, myosin-II drives muscle contraction, whereas unconventional myosin-V is mainly responsible for active intracellular transport [2, 32]. Myosin-II is a non-processive motor, but myosin-V is highly processive [110, 117, 138]. With its homodimeric motor domain myosin-V takes distinct steps of 36 nm from one actin helix to the next [112, 117, 138]. The speed of myosin motors ranges from 0.2 μm/s - 60 μm/s [2].

In the following, kinesin, dynein, and myosin will generally refer to kinesin-1, cytoplasmic dynein-1, and myosin-V.

2.4. Intracellular transport

Intracellular transport is of utmost importance for cells and transport failures are connected to a variety of severe diseases, see for instance [15]. *Cargo particles*, such as organelles (e.g. vesicles, mitochondria, Golgi stacks) and biomolecules (e.g. mRNA, ribosomes, centrosomes, cytoskeletal filaments, viruses), usually arise in one area of the cell, but are needed in some other region [2, 32, 109, 111, 112, 139]. Consequently, cargo has to be transferred within the cell.

Cargo particles can be passively transported within the cytosol by diffusion [2, 65]. *Passive diffusion* is driven by thermal fluctuations [65], but has some drawbacks [65]. Passive motion in the cytosol is often too slow to travel over long distances within the cell [65]. This is especially critical in the case of axons of mammalian neurons which might be several meters long [2]. Moreover, the cytoplasm constitutes a highly crowded environment which merely allows for subdiffusive motion of intracellular cargo. The degree of subdiffusion depends on the particle radius [39–41, 50, 51, 55]. Hence larger cargoes, such as vesicles or mitochondria, are effectively stationary in the cytoplasm. Furthermore, passive diffusion is an unbiased process [65]. Consequently there is no net transport in a specific direction which is important for many intracellular transport tasks.

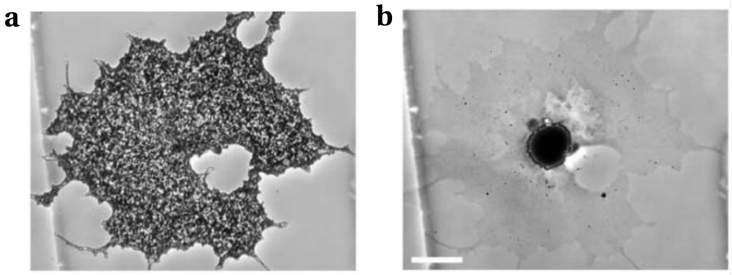

Figure 2.9.: Regulation of motor proteins in melanophores. The dispersion (**a**) and aggregation (**b**) of pigment granules in melanophores is tightly controlled by signaling processes. Reprint of [147]. Reprinted from Current Biology, 13, Rodionov, V. *et al.*, Switching between microtubule- and actin-based transport systems in melanophores is controlled by cAMP levels, 1837-1847, Copyright (2003), (`https://doi.org/10.1016/j.cub.2003.10.027`), with permission from Elsevier; permission conveyed through Copyright Clearance Center, Inc.

These disadvantages can be solved with the aid of *active transport* along cytoskletal filaments empowered by molecular motors [65]. By ATP consumption, molecular motors manage fast, directed transport of diverse cargo particles over long distances within a cell [2]. However, active intracellular transport faces its own difficulties. The following questions will be addressed below: How is a cargo-motor complex formed? How does a cargo-motor complex move along the complex cytoskeleton? And how is active intracellular transport regulated in order to allow for efficient cargo delivery?

2.4.1. Movement pattern of cargo-motor complexes

Active intracellular transport involves a complex interplay between the cytoskeleton, the motors, and the cargo. Cargo delivery necessitates transport over the whole cell range. Long-range transport by kinesins and dyneins along radial microtubules is supplanted by short-range transport along multi-directional actin filaments in the cortex with the aid of myosins [2, 16, 112, 138, 140–142].

Nowadays there is overwhelming evidence that many motors of diverse species are connected to a single cargo simultaneously, forming a *cargo-motor complex* [17–31]. The motion pattern of such a complex differs significantly from the one of a single motor. It is not necessarily unidirectionally but rather "saltatory" [21, 22, 30, 143, 144]. This erratic motion may be advantageous to manoeuvre around roadblocks on filaments or to facilitate cargo reactions [144]. Furthermore, run lengths are increased [25] and cargo can more easily switch between the microtubule and the actin network [24, 36, 140–142, 145, 146] even without an intermediate unbound, diffusive state [24].

But the linkage of opposing motors to a single cargo provides the need for a regulation mechanism to ensure efficient cargo delivery despite the competition between diverse motors [19–28, 31, 32]. The regulation of intracellular transport is not fully understood. But the *activity* of specific motor species can be tuned with the aid of signaling processes. A

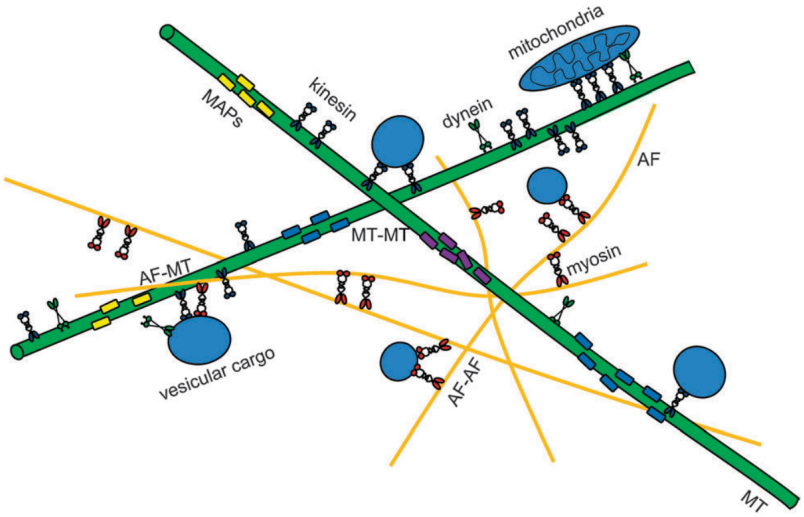

Figure 2.10.: Cargo motion on complex cytoskeleton. Cargo-Motor complexes are frequently faced with roadblocks (accessory proteins, other motors, cargo) and filament crossings which hinder their motion. Reprint of [37]. Reproduced from Lakadamyali, M., Navigating the cell: how motors overcome roadblocks and traffic jams to efficiently transport cargo, Physical Chemistry Chemical Physics, 16:5907, 2014 (`http://dx.doi.org/10.1039/C3CP55271C`) with permission of the PCCP Owner Societies; permission conveyed through Copyright Clearance Center, Inc.

prominent example is the transport of pigment granules in melanophores, which involves both the actin and the microtubule network [19, 146, 147]. The activity level of diverse motor proteins is controlled by the intracellular concentration of cAMP (cyclic adenosine monophosphate). High concentrations stimulate kinesin motors, intermediate values myosin motors, and low levels of cAMP promote dynein motors [147]. Accordingly, a dispersion of pigment granules throughout the cell or their accumulation at the center is achieved which induces a change in melanophore coloration, as shown in Figure 2.9 [2]. Furthermore, transport to the nucleus is enhanced in cells which are infected with adenoviruses [148]. In Drosophila, the absence or presence of the transacting factor Halo triggers transport of lipid droplets to the cell center or periphery [21,149]. And, accessory proteins impact the activity of molecular motors. For instance, the MAP tau regulates the number of active motor proteins attached to a cargo [25] by hindering the attachment of kinesin and dynein motors and facilitating their detachment [130]. Moreover, the protein complex dynactin is crucial for the linkage between cargo and dynein, it regulates the directionality of cargo transport, and improves dynein's processivity [20,32,111,119,150].

During intracellular transport, cargo-motor complexes face diverse road blocks along the cytoskeleton, as sketched in Fig. 2.10 [37]. This results in a stochastic movement pattern of a cargo-motor complex: periods of directed, active transport along the cytoskeleton are frequently interrupted by effectively stationary states [65, 129]. Such *pauses* arise out of several reasons.

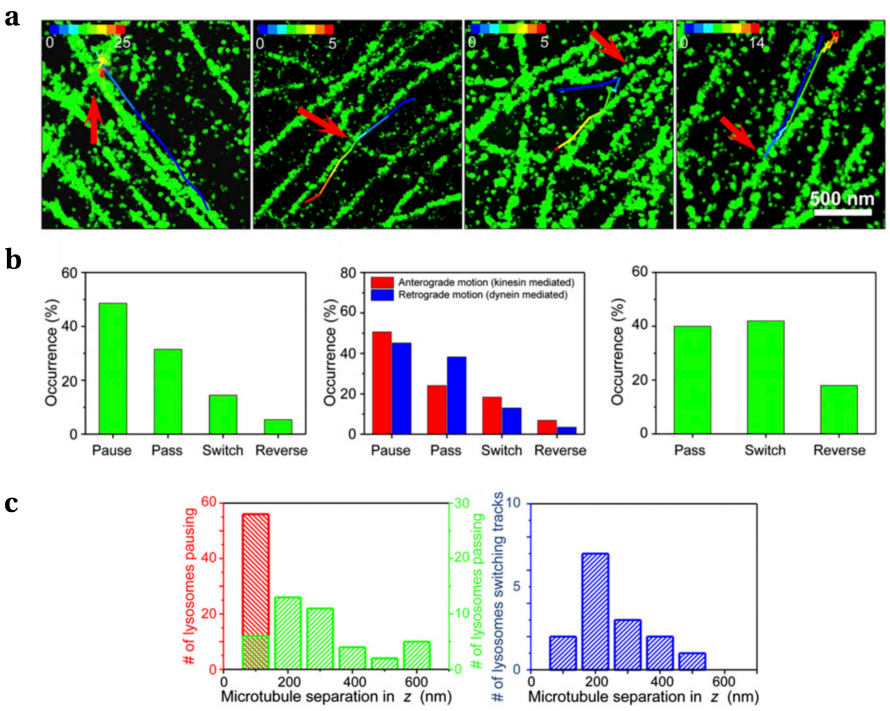

Figure 2.11.: Cargo motion on complex cytoskeleton - pausing events. (**a**) Lysosomes moving on a microtubule network either pause, pass, switch track, or reverse direction at crossings. (**b**) Percentage of lysosome behavior at network crossings (left), divided into anterograde and retrograde motion (middle), and under the condition of prior pausing (right). (**c**) Percentage of pausing, passing and switching events at microtubule crossings as a function of the axial separation of microtubules. Reprint of [29]. Reprinted from Bálint, Š. *et al.*, Correlative live-cell and superresolution microscopy reveals cargo transport dynamics at microtubule intersections, P. Natl. Acad. Sci. USA, 110:3375-3380, 2013, (`https://doi.org/10.1073/pnas.1219206110`), with permission from PNAS.

Stochastic detachment events from the cytoskeleton may cause stationary states. Motor proteins undergo detachment and reattachment processes either out of chemical reasons or facilitated by accessory proteins [2]. When detached of the filament, the motion of a cargo-motor complex in the surrounding cytoplasm is strongly subdiffusive and closely confined to the detachment point due to the crowdedness of the cytoplasm [39–41, 50, 51, 55]. Consequently, such excursions in the cytoplasm are effectively stationary. But since several motors are attached to a single cargo [17–31], a full dissociation of the cargo-motor complex is rather unlikely [31].
Mechanically constricting filament crossings of the cytoskeleton also cause pausing events [29, 33–38]. The movement of cargo-motor complexes through the cytoskeleton has recently been investigated both *in vitro* [33–36] and *in vivo* [29, 38]. According to these studies, the origin of stationary states are filament crossings of the cytoskeleton - probably since the cytoskeletal mesh size, which is reminiscent of the mean distance between network intersections, is typically smaller than the processive run lengths of

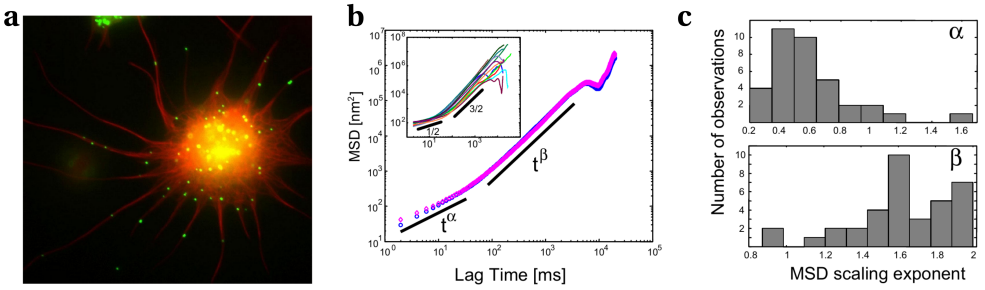

Figure 2.12.: Anomalous diffusion during active transport. (**a**) The motion of peroxisomes (green) is tracked during transport along microtubules (red) in Drosophila cells. (**b**) The MSD of peroxisomes exhibits a crossover from sub- to superdiffusion at intermediate timescales. (**c**) Short time and long time anomalous exponents are distributed in sub- and superdiffusive regimes, respectively. Reprint of [46]. Reprinted from Kulić, I. M. *et al.*, The role of microtubule movement in bidirectional cargo transport, P. Natl. Acad. Sci. USA, 105:10011-10016, 2008, (`https://doi.org/10.1073/pnas.0800031105`), Copyright (2008) National Academy of Sciences, with permission from PNAS.

individual motors and consequently cargo-motor complexes [25, 34, 65, 151]. Cargo-motor compounds actively propagate from intersection to intersection. Whenever the complex reaches an intersection node it pauses there until it either overcomes the constriction and passes it on the same track or until it changes direction by reversion or track switching [29, 33–35, 38], as shown in Fig. 2.11, a and b. The waiting time at a network intersection is of the order of seconds [29, 146, 152] and depends on the size of the cargo and the axial separation of the crossing filaments [29,38], see Fig. 2.11, c.

In essence, the motion pattern of cargo-motor compounds reflects the complex, crowded environment they are living in [65]. The interplay between motor activities and cytoskeleton architecture results in a stochastic motion pattern of the cargo with random transitions between active directed transport and reorienting pauses. How this interplay effects intracellular transport properties, such as anomalous diffusion and temporal efficiency, is elusive.

2.4.2. Anomalous diffusion during intracellular transport

In normal diffusion, the mean square displacement (MSD), which is a measure for the amount of space a particle explores in a given time, is a linear function in time $\langle r^2 \rangle = 2dDt$ (MSD: $\langle r^2 \rangle$, dimension: d, diffusion coefficient: D, time: t). Contrarily, the dependence is given by a power-law $\langle r^2 \rangle = 2dDt^\alpha$ in case of anomalous diffusion [61,153]. Subdiffusion is characterized by $\alpha < 1$ and thus a slower particle spreading than found during normal diffusion. Whereas superdiffusion is determined by $\alpha > 1$. Note that a more elaborate introduction to diffusion will be given in Chapter 3. Remarkably, anomalous diffusion is observed in various contexts of intracellular transport [55].

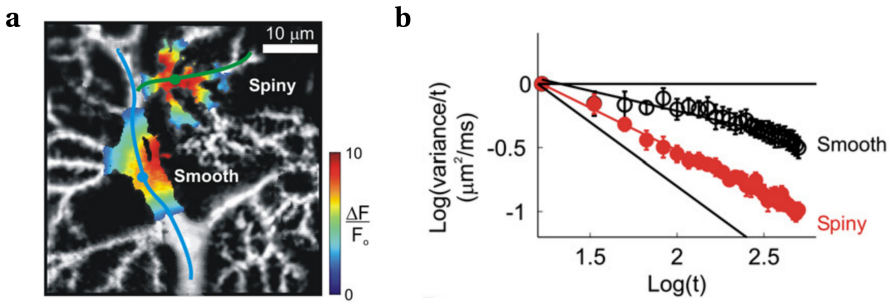

Figure 2.13.: Subdiffusion in spiny dendrites. (**a**) Neuron with smooth (blue line) and spiny (green line) dendrites. (**b**) Spines lead to a more pronounced subdiffusion than observed in smooth dendrites. Reprint of [48]. Reprinted from Neuron, 52, Santamaria, F. *et al.*, Anomalous diffusion in Purkinje cell dendrites caused by spines, 635-648, Copyright (2006), (`https://doi.org/10.1016/j.neuron.2006.10.025`), with permission from Elsevier; permission conveyed through Copyright Clearance Center, Inc.

Anomalous subdiffusion is a hallmark of motion in the crowded cytoplasm. Approximately $10 - 50\%$ of the cytoplasmic volume is occupied with small solutes, macromolecules, cell organelles and cytoskeletal filaments [50, 65, 154]. As a consequence, subdiffusion is observed for various tracer particles [55], such as mRNA or chromosomal loci moving in the cytoplasm of E. coli cells [53, 54] and lipid granules in living yeast cells [52]. The degree of the anomaly depends on both the size of the tracer particle and the occupation of the cytoplasm [39–41, 50, 51].

Anomalous diffusion is also reported during active transport of tracer particles along the cytoskeleton [42–47]. Remarkably, non-trivial crossovers from sub- to superdiffusion and vice versa are found. For instance a population of rapide peroxisomes which are moving in unison along the microtubule network of Drosophila cells shows subdiffusive dynamics at short timescales and exhibit a crossover to superdiffusion at intermediate timescales, as shown in Fig. 2.12 [46]. In contrast, crossovers from super- to subdiffusive regimes are reported for the motion of engulfed microspheres [42, 43] and endosomes [45] along microtubule networks of eukaryotic cells.

Subdiffusion can also arise due to trapping events. For instance, anomalous subdiffusion is observed during the motion of tracer particles in dendrites of neurons [48, 49], as shown in Fig. 2.13. The dendrites of neurons possess small membrane protrusions, called spines, which effectively trap tracer particles and thus lead to subdiffusion [48, 49, 155] [Hafner2014].

Consequently, cells can benefit from subdiffusion [156, 157]. Despite the lower space exploration, a cell is able to regulate the spatio-temporal distribution and reactivity of intracellular particles with the aid of subdiffusion [48–50, 53, 55, 156, 157].

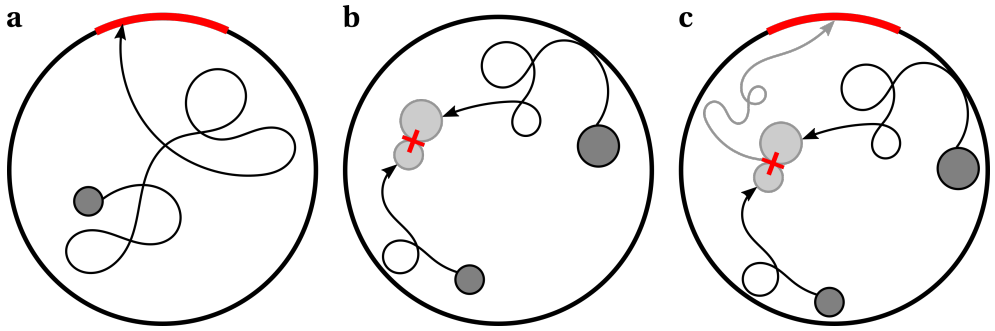

Figure 2.14.: Intracellular search processes. Paradigmatic search processes which occur during active intracellular transport are (**a**) the narrow escape problem which emerges during transport to a specific region on the plasma membrane, (**b**) the reaction problem which considers the arrival of a searcher at a motile or immotile target, and (**c**) the combined reaction-escape problem which occurs when cargo must be delivered to a narrow area on the plasma membrane only after tethering to another particle beforehand.

2.4.3. Search processes during intracellular transport

Intracellular transport aims to deliver cargo at specific target locations which defines distinct search processes. Such intracellular search processes occur on a "trial and error" basis [158]. In general, there is no direct connection between searcher and target and the searcher does neither know the shortest path to the target nor its exact position. Hence, intracellular search is a stochastic process and targets are only identified with the aid of cognate pairs of proteins, such as coat proteins, tethers, Rabs and SNAREs [159, 160]. These proteins are found on both searcher and target and work in a key-lock principle to ensure correct cargo delivery [159, 160]. Consequently, the stochastic nature of intracellular transport with random alternations between active, directed motion and reorienting waiting states enhances the exploration of intracellular space and thus the probability of target detection [161].

A cell has to fulfill many different transport task and searcher and target may be very diverse in terms of size, dynamics and location [2]. In general, the searcher is a cargo which is actively transported along the cytoskeleton with the aid of motor proteins, whereas the target can either be motile or immotile. Frequently encountered tasks of active intracellular transport can be summarized by the narrow escape problem, the reaction problem and the combined reaction-escape problem, as sketched in Fig. 2.14.

The narrow escape problem

Some cargo particles have to be transported from a position within the cell, often from a position close to the nucleus, to a narrow target region alongside the plasma membrane. A prominent example occurs during directed secretion by cytotoxic T lymphocytes (CTL or T cell). Specialized T cells scan organisms for virus-infected or tumorigenic cells [2]. When getting into contact with a pathogenic cell, T cells form a close connection to it,

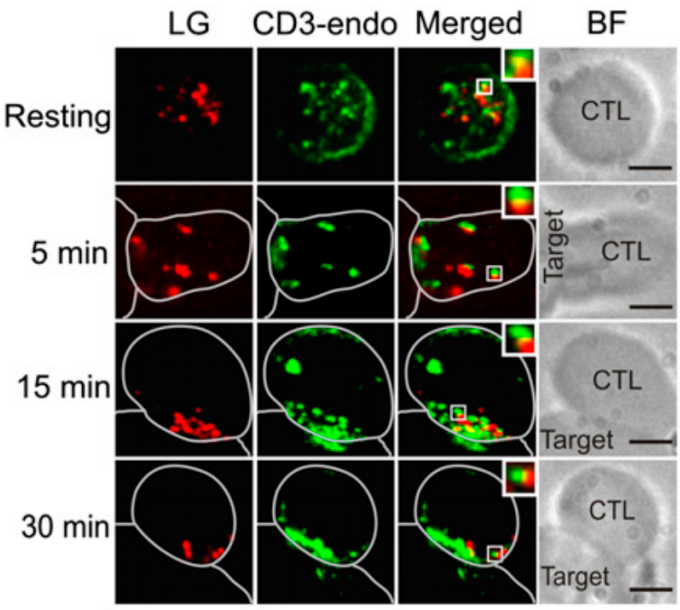

Figure 2.15.: Release of lytic granules at the immunological synapse of T cells. The temporal evolution of the accumulation of lytic granules (red) and CD3-endosomes (green) at the synapse is shown for T cells connected to a pathogenic target cell. The docking and release of lytic granules requires the tethering with CD3-endosomes beforehand. Note that the immunological synapse is the contact zone between T cell and target cell. Reprint of [12], Qu *et al.*, The Journal of Immunology, 186:6894-6904, 2011, (`http://dx.doi.org/10.4049/jimmunol.1003471`); with permission of Copyright 2011, The American Association of Immunologists, Inc.

which is called immunological synapse [2, 8–14]. Toxic material bound in lytic granules is then actively transported and exclusively released at the synapse to ensure the killing of the pathogenic cell [2, 8–14]. The immunological synapse typically has a diameter of the order of 1 μm and thus constitutes a narrow opening in the plasma membrane of T cells [2, 8–14]. Other examples involve the closing of plasma membrane disruptions by patch vesicles [162–164], the transport of lysosomes to parasitic invasion sites in the plasma membrane [165], the transport of vesicles to neurite outgrowth site [166], or the accumulation of polarity regulating proteins, such as Cdc42 in budding yeast or Rac in canine kidney cells, at a specific site on the plasma membrane [167, 168].

The stochastic search for a narrow region on the plasma membrane of a cell is reminiscent of the so-called narrow escape problem coined by Holcman, Schuss, and Singer [169–175]. The narrow escape problem is traditionally studied in the context of passively diffusing particles. Examples involve ions searching for open channels in the plasma membrane [2, 129], mRNA looking for nuclear pores to exit the nucleus [2, 176, 177], or calcium and other signaling molecules confined in subcellular compartments [2, 178].

The reaction problem

Besides the narrow escape problem, intracellular cargo also has to react with other motile particles or has to reach immotile cell organelles, such as the nucleus, within the cell. For instance late endosomes fuse with lysosomes for disposal [2, 179], and mitochondria are shipped to regions which demand for ATP [2,139]. In the secretory pathway, vesicles derived from the endoplasmic reticulum are transported to the Golgi complex for dispatch to their terminal [2]. When entering the cell by endocytosis, diverse viruses, such as influenza virus or HIV, hijack molecular motors to get rapidly transported to the nucleus in order to release their genome [2, 180, 181].

The reaction-escape problem

In specific cases, cargo must dock at a narrow area on the plasma membrane only after tethering with another particle beforehand. Such search processes are two-fold and combine the reaction and the escape problem. For instance, lytic granules have to pair with endosomes before they are released at the immunological synapse of T cells, as shown in Fig. 2.15 [12]. The docking and release of lytic granules at the synapse is thereby promoted by the prior tethering with endosomes which are loaded with CD3 receptors [12].

2.5. Summary

Active intracellular transport is vital to maintain the correct function of cells and organisms. Cargo, such as cell organelles or macromolecules, has to be transferred from its source to specific target locations. In order to facilitate cargo delivery, cells are equipped with a highly complex cytoskeleton network, which is highly inhomogeneous and anisotropic. Whereas microtubules emerge radially from the central MTOC, actin filaments populate the cell cortex and exhibit diverse orientations. Molecular motors empower intracellular transport. They actively walk along the cyotskeletal filaments by ATP consumption while being attached to cargo particles. The movement pattern of cargo-motor complexes reflects the complex, crowded environment they are living in. They exhibit a stochastic motion with random alternations between directed transport along the cytoskeleton and reorienting pauses, most likely due to mechanically constricting filament crossings. The motor activity levels and the cytoskeleton architecture dramatically influence the erratic motion pattern of intracellular cargo. To investigate how a cell regulates the diffusive properties and the search efficiency of intracellular cargo is a challenging theoretical task. But, the stochastic motion pattern of intracellular cargo suggests a random walk approach.

Chapter 3.

Modeling of intracellular transport: a random walk review

Contents

3.1. Basic concepts of random walks

3.1.1. History of random walks

In 1828, the botanist Robert Brown studied the motion of pollen suspended in water, which is nowadays referred to as Brownian motion [182, 183]. Basic concepts of random walks were already investigated in 1900 within the theory of finanical speculations by Louis Bachelier [153, 184]. However, the term "random walk" was introduced by Karl Pearson in 1905. When he was studying the motion of mosquitoes which spread malaria [60, 153, 185], he was faced with "the problem of the random walk" [186–188]:

> "A man starts from a point $\mathcal{O}$ and walks l yards in a straight line; he then turns through any angle whatever and walks another l yards in a second straight line. He repeats this process n times. I require the probability that after these n stretches he is at a distance between r and $r + \delta r$ from his starting point, $\mathcal{O}$." [186]

Related problems were addressed by Albert Einstein and Marian Smoluchowski near-term in 1905 and 1906 [189–191].

Since then, many specialized random walk models have been introduced and the theory of random walks has become a powerful approach to study stochastic processes in fields as diverse as economics, psychology, computer science, physics, chemistry, and biology [153]. In the following, a brief introduction to the theory of random walks is given according to [60, 192].

3.1.2. Stochastic processes

A *stochastic variable* Z is a variable which takes random values. It is determined by a (continuous or discrete) set of possible values z and a probability density function over this set $p(z)$ [192]. *Probability density functions* are non-negative and normalized [192]

$$p(z) \geqslant 0, \qquad \int p(z)\,\mathrm{d}z = 1. \tag{3.1}$$

Note that the probability density function of a random variable Z with discrete values labeled by j can be written with the aid of the Dirac delta function as [60]

$$p(z) = \sum_j p_j \delta(z - j). \tag{3.2}$$

The *cumulative distribution function* determines the probability that the stochastic variable Z takes a value smaller than or equal to z [192]

$$F(z) = \mathrm{Prob}(Z \leqslant z) = \int_{-\infty}^{z} p(z')\mathrm{d}z'. \tag{3.3}$$

The average or expectation value of any function $f(Z)$ is given by [192]

$$\langle f(Z)\rangle = \int f(z)p(z)\,\mathrm{d}z \tag{3.4}$$

and the *m-th moment* of a stochastic variable Z is

$$\mu_m = \langle Z^m\rangle = \int z^m p(z)\mathrm{d}z. \tag{3.5}$$

In particular, $\mu_1{=}\langle Z\rangle$ is the *mean* value, $\mu_2{=}\langle Z^2\rangle$ the *mean square* value, and $\sigma^2{=}\langle(Z - \langle Z\rangle)^2\rangle{=}\mu_2 - \mu_1^2$ is the *variance* of the stochastic variable Z [192].

The *characteristic function* of a stochastic variable Z is defined by [192]

$$G(k) = \langle \mathrm{e}^{ikZ} \rangle \tag{3.6}$$

and generates its moments according to

$$G(k) = \sum_{m=0}^{\infty} \frac{(ik)^m}{m!} \mu_m. \tag{3.7}$$

Probability density functions which frequently occur in physics are the exponential distribution

$$p(z) = \begin{cases} \lambda \exp(-\lambda z), & z \geqslant 0 \\ 0, & z < 0 \end{cases} \tag{3.8}$$

with mean $1/\lambda > 0$ and the gaussian distribution

$$p(z) = \frac{1}{\sqrt{2\pi\sigma^2}} \mathrm{e}^{-\frac{(z-\mu)^2}{2\sigma^2}}, \qquad -\infty < z < \infty \tag{3.9}$$

with mean μ and variance σ^2.

A *stochastic process* is a function $X_Z(t) = f(Z,t)$ of a random variable Z and time t [192]. Stochastic processes thus describe a quantity which evolves in time in a non-deterministic manner. However, averaged quantities may give insight into the laws underlying the stochastic process [192].

Many stochastic phenomena which are common in nature further exhibit the so-called *Markov property*. In Markov processes the next state only depends on the current state, but not on any other previous state of the stochastic process [192]. A paradigmatic stochastic process with the Markovian property is Brownian motion.

The temporal evolution of the probability density function $p(x,t)$ for the Markovian process $X_Z(t)$ to take a value x at time t is determined by the *master equation* [192]. In case of a continuous range of X it reads

$$\frac{\partial p(x,t)}{\partial t} = \int \left[W(x|x')p(x',t) - W(x'|x)p(x,t) \right] \mathrm{d}x', \tag{3.10}$$

whereas for a discrete set of values labeled with j it is given by

$$\frac{\mathrm{d}p_j(t)}{\mathrm{d}t} = \sum_j \left[W_{jj'}p_{j'}(t) - W_{j'j}p_j(t) \right]. \tag{3.11}$$

Thereby, $W(x|x') \geqslant 0$ ($W_{jj'} \geqslant 0$) is the transition rate from a state x' to a state x (from j' to j). Consequently, the master equation is a gain-loss equation [192]. The first term describes the gain of state x (j) by transitions from state x' to x (from j' to j), whereas the second term is associated to a loss of state x (j) by transitions from x to x' (from j to j').

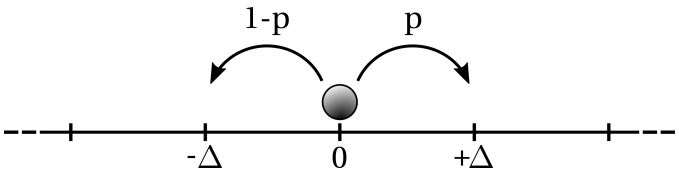

Figure 3.1.: 1D random walk. On a one-dimensional lattice a walker moves one increment Δ to the right with probability p and to the left with probability $(1-p)$ per discrete time step.

3.1.3. Simple random walk

A *random walk* is a stochastic process which describes the position of a walker who changes its direction as a function of time t. The random walk in discrete time is based on steps, while the one in continuous time is based on velocities [193]. From a mathematical perspective, a random walk is a sum of (often independent and identically distributed) random variables [60]. For illustration, consider a simple random walk in discrete space and time. The walker starts at the origin of a one-dimensional lattice. Note that it is generally beneficial to choose the initial condition $X(t=0)=0$. Per discrete time step Δt, the walker moves one increment Δ to the right with probability p or to the left with probability $(1-p)$, as sketched in Fig. 3.1. The displacement per time step is an independent and identically distributed random variable $Z_n \in \{+\Delta, -\Delta\}$. The total displacement, or the position, of the random walker at time step n is a stochastic process X_n given by the sum of the individual displacements [60]

$$X_n = \sum_{j=1}^{n} Z_j. \tag{3.12}$$

The temporal evolution of the probability $p_{n,j}$ to find the walker at position j at time step n is determined by [60]

$$p_{n,j} = p p_{n-1,j-\Delta} + (1-p) p_{n-1,j+\Delta}. \tag{3.13}$$

By assuming that the mean as well as the mean square displacements per step are finite, it can be shown that the probability density function $p(x,t)$ to find the walker at time t at position x in the continuous time and space limit ($\Delta \to 0$, $\Delta t \to 0$) is given by [60]

$$\frac{\partial}{\partial t} p(x,t) = -v \frac{\partial}{\partial x} p(x,t) + D \frac{\partial^2}{\partial x^2} p(x,t), \tag{3.14}$$

which is the *diffusion equation* with diffusion coefficient D in the presence of a constant drift v [60]. The diffusion equation can be solved with the aid of Fourier transformation, such that the probability density function of the random walker is [60]

$$p(x,t) = \frac{1}{\sqrt{4\pi D t}} \exp\left\{ -\frac{(x-vt)^2}{4Dt} \right\}. \tag{3.15}$$

This reflects the *central limit theorem*, which states that the probability density function of a sum of random variables which are independent and have identical probability density functions with finite mean and mean square converges to a Gaussian density [153].

3.1.4. Anomalous diffusion

In principle, the probability density function of a random walker's displacement can be derived by solving the corresponding master equation. The displacement probability density function enables the quantification of macroscopic physical observables, such as the diffusive properties of the walk.

At the beginning of the 20th century, Einstein and Smoluchowski found a fundamental relation between the mean square displacement of Brownian particles and the diffusion coefficient [61, 189]

$$D \propto \langle \Delta x^2 \rangle / t. \tag{3.16}$$

Hence, studying the mean square displacement (MSD) $\langle \Delta x^2 \rangle$, which is a measure for the amount of space a walker explores in a given time interval, gives information about the diffusive properties of a random walk [61, 153].

In general, the average value is considered to be an *ensemble average* [153]

$$\langle \Delta x^2(t) \rangle_{\text{ens}} = \int_{-\infty}^{\infty} (x(t) - x(0))^2 \, p(x,t) \, \mathrm{d}x. \tag{3.17}$$

i.e. an average over many independent realizations of the random walk which corresponds to the probabilistic definition given in Eq. 3.5. Usually, it is beneficial to fix $x(0) = 0$. However, due to the lack of a sufficient amount of such realizations in experiments a *moving time average* is often used [153]

$$\langle \Delta x^2(t) \rangle_{\text{time}} = \frac{1}{T-t} \int_{0}^{T-t} (x(t+\tau) - x(\tau))^2 \, \mathrm{d}\tau, \tag{3.18}$$

for which only a single trajectory of duration $T \gg 1$ is needed. Ensemble and moving time average are equal for ergodic processes [153].

Without any drift, according to Eq. 3.15 the MSD of a Brownian particle in 1D yields

$$\langle \Delta x^2(t) \rangle = \int_{-\infty}^{\infty} x^2 P(x,t) \, \mathrm{d}x = \frac{1}{\sqrt{4\pi D t}} \int_{-\infty}^{\infty} x^2 \exp\left(-\frac{x^2}{4Dt}\right) \mathrm{d}x = 2Dt \ . \tag{3.19}$$

Accordingly, normal diffusion is determined by the MSD being linear in time which is a consequence of the central limit theorem [61].

However, according to the specific properties of a random walk in d dimensions the functional dependence between MSD and time generally is a power-law

$$\langle \Delta x^2(t) \rangle = 2dK_\alpha t^\alpha \ , \tag{3.20}$$

with the *anomalous exponent* α [61, 194] and the *generalized diffusion constant* $[K_\alpha] = \mathrm{m}^2\mathrm{s}^{-\alpha}$ [61, 194]. *Anomalous diffusion* is observed in various contexts and is classified according to the anomalous exponent [61]. *Normal Brownian diffusion* is determined by α=1, whereas *subdiffusion* is defined by $0<\alpha<1$. An anomalous exponent of $\alpha>1$ is characteristic for *superdiffusion* and *ballistic motion* corresponds to α=2 [61].

3.1.5. First passage events

Search processes are very common in nature and occur on all lengthscales [72]. Animals are searching for beneficial habitats, a bacterium is looking for nutrients, or intracellular cargo is transported to a target site within the cell. When the searcher has low cognitive abilities and no hint on the target position, the search process is random and can be well described with the aid of random walks [72].

The efficiency of a random search process can be measured in terms of various first passage quantities, as for instance the consumed energy upon target detection. However, in most applications it is essential to minimize the time needed until the target is found, which is the so-called *first passage time* [72]. The first passage time is a random variable [192]. The investigation of the probability density function of first passage times and the study of the mean first passage time (MFPT) are main objectives in the theory of random walks [192, 195].

In general, there are different approaches to the density $f(x_d, t|x_0)$ of first passage times t to a target at postion x_d when the walker started at position x_0 [192]. In some cases, it is advantageous to solve the master equation 3.10 with appropriate boundary conditions which take the target position into account. This technique is known as the *absorbing boundary approach* [192]. But the first passage time density $f(x_d, t|x_0)$ can also be derived from the displacement density $p(x, t|x_0)$ of the random walk to be at position x at time t when having started at x_0. So in some cases it is sufficient to solve the unrestricted master equation 3.10. The functional relation between first passage time density $f(x_d, t|x_0)$ and displacement density $p(x, t|x_0)$ is given by the *renewal equation* [192, 195]

$$p(x_d, t|x_0) = \int_0^t p(x_d, t - t'|x_d) f(x_d, t'|x_0) \mathrm{d}t' + \delta_{t,0}\delta x_0, x_d \tag{3.21}$$

which is of convolution type and can be solved with the aid of Laplace transformation [192]. If the first passage time density is exponential, the kinetics are fully determined by the *mean first passage time* [72]

$$\mathrm{MFPT} = \int_0^\infty t f(x_d, t|x_0)\, \mathrm{d}t. \tag{3.22}$$

3.1.6. Can intracellular transport be modeled by random walks?

The stochastic motion pattern of cargo suggests a random walk approach to modeling intracellular transport. Active intracellular transport happens on diverse scales - ranging from the stepping of individual motors at the molecular scale to the motion of cargo on the cellular scale [129]. Eventhough theorists also studied the mechanochemical details of molecular motors and their stepping behavior, e.g. [129, 196–199], when investigating intracellular transport on larger length- and timescales coarse grained random walk models are beneficial, e.g. [55, 72, 129, 183, 198]. Such models typically consider the effective motion of cargo inside the cell but ignore the microscopic stepping of and competition among individual motors.

Living cells represent a highly heterogeneous, crowded environment. The cytoskeleton exhibits a specific, generally inhomogeneous and anisotropic spatial organization [2]. Many different motors of diverse species drag a single cargo along the network [17–31]. Accordingly, the trajectories of intracellular cargoes are coined by stochastic transitions between directed transport and reorienting pausing states [29, 33–38]. Consequently, the theoretical investigation of intracellular transport is a challenging task and provides the need for specialized random walk models. In general, three features of intracellular transport are needed to be incorporated into a unified model: the anisotropy and inhomogeneity of the cytoskeleton, the motor activities, and the run-and-pause behavior of the cargo. In the following, a survey on the state of the art of modeling intracellular transport with the aid of random walks is provided. A specific focus is on anomalous diffusion and first passage events.

3.2. Random walk models for anomalous diffusion

Anomalous diffusion is observed in various contexts of physics, chemistry, biology, engineering, economy and so forth [185, 194]. In order to study how anomalous diffusion emerges, more elaborated models than the simple random walk, where stepping directions are uncorrelated and isotropic, are necessary.

3.2.1. Standard models

Normal diffusion, i.e. the linear growth of the MSD in time, is a direct consequence of the central limit theorem, as indicated above exemplarily on the simple random walk model [129]. Hence, asymptotic anomalous diffusion is linked to a breakdown of the central limit theorem and can be generated by two basic mechanisms: broad distributions and long-range correlations [59, 61]. Standard models of sub- and superdiffusion are recapitulated in the following, as reviewed inter alia in [55, 59, 61, 72, 129, 193].

Standard models for subdiffusion

The *continuous time random walk* (CTRW) is a standard model for subdiffusion due to traps and was first introduced by Montroll and Weiss in 1965 [56]. In the model, the walker performs steps in random directions with lengths ℓ characterized by a distribution $\lambda(\ell)$ with finite variance [61, 129]. At each step the particle waits for a time period drawn from a distribution $\psi(\tau)$. If the waiting time distribution $\psi(\tau)$ has a finite mean, normal diffusion is recovered [59–61, 72, 153]. But for heavy-tailed distributions, which asymptotically behave as power laws,

$$\psi(\tau) \propto \frac{1}{\tau^{1+\beta}}, \quad 0 < \beta < 1 \tag{3.23}$$

the mean waiting time is infinite and the motion is subdiffusive with anomalous exponent $\alpha = \beta$ [57, 59–61, 72, 153]. The CTRW models motion of a particle which undergoes transient trapping events. These traps lead to a breakdown of the central limit theorem due to broad waiting time distributions [64, 72, 129].

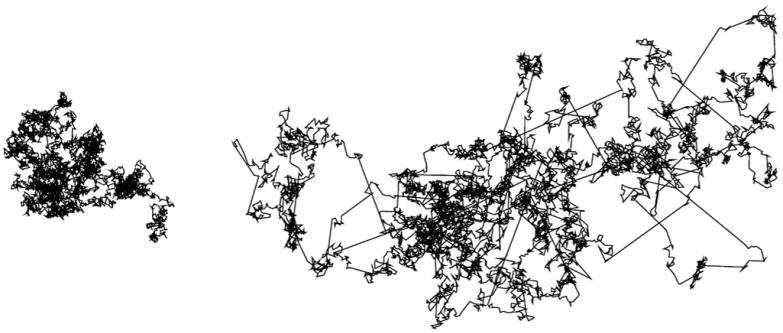

Figure 3.2.: Lévy walk. Sample trajectory of a simple random walk (left) and a Lévy walk (right) with the same number of steps. Reprint of [61]. Reprinted from Physics Reports, 339, Metzler, R. and Klafter, J., The random walk's guide to anomalous diffusion: a fractional dynamics approach, 1-77, Copyright (2000), (`https://dx.doi.org/10.1016/S0370-1573(00)00070-3`), with permission from Elsevier; permission conveyed through Copyright Clearance Center, Inc.

Subdiffusion can also arise due to the crowdedness of the enviroment [129, 200]. The resulting obstructed diffusion can be modeled by *random walks on fractals*. The fractal structure of the surrounding introduces long-range correlations in steps, which result in subdiffusion according to the specific structure and concentration of obstacles in the system [72, 200, 201].

The viscoelastic properties of the cytoplasm can further result in subdiffusion [129]. Elastic elements may lead to strong correlations in a particle's trajectory [129]. Such memory effects can be modeled by *fractional Brownian motion* as introduced by Mandelbort and van Ness in 1968 [202]. It is a Gaussian process where the particle position at time t_2 depends on the one at $t_1 < t_2$ via [72]

$$\langle x(t_1)x(t_2)\rangle \propto t_1^{2H} + t_2^{2H} - |t_1 - t_2|^{2H} . \tag{3.24}$$

For $H = 1/2$ the motion is diffusive, whereas the model yields subdiffusion for $0 < H < 1/2$ and superdiffusion for $1/2 < H < 1$ with anomalous exponent $\alpha = 2H$ due to negatively, respectively positively correlated steps [72, 202–204].

Standard models for superdiffusion

Lévy flights are a specific class of CTRWs coined by Mandelbrot in 1982 [56, 58]. While the mean of the waiting time distribution $\psi(\tau)$ is finite, the variance of the step length distribution $\lambda(\ell)$

$$\lambda(\ell) \propto \frac{1}{\ell^{1+\beta}} \tag{3.25}$$

is diverging [58, 59, 61, 72, 194]. Normal diffusion occurs for $\beta > 2$, whereas $0 < \beta < 2$ leads to superdiffusion with an anomalous exponent $\alpha = 2/\beta$ [72].

Lévy walks were introduced by Shlesinger *et al.* in 1987 as a coupled CTRW [205]. In contrast to Lévy flights, the waiting times and step lengths are not independent anymore, but related via [205]

$$\Psi(\ell, \tau) = \lambda(\ell)\psi(\tau|\ell). \tag{3.26}$$

In particular, the coupling $\psi(\tau|\ell) = \delta(\tau - \ell/v)$ corresponds to a constant speed v of the particle [205]. Lévy walks lead to superdiffusion according to the MSD [205–208,208–212]

$$\langle \Delta x^2 \rangle \propto \begin{cases} t^2, & 0 < \beta < 1, \\ t^2/\ln t, & \beta = 1, \\ t^{3-\beta}, & 1 < \beta < 2, \\ t \ln t, & \beta = 2, \\ t, & \beta > 2. \end{cases} \tag{3.27}$$

The trajectories of Lévy flights and walks exhibit a fractal dimension with large jumps between clustering structures on all lengthscales, as indicated by Fig. 3.2 [58, 194].

3.2.2. Models with pausing states

The standard models for sub- and superdiffusion provide asymptotic anomalous diffusion due to broad distributions or long-range correlations. Otherwise anomalous diffusion appears to be a transient intermediate regime which asymptotically leads to normal diffusion [66, 67, 193]. To differ between transient anomalous regimes and asymptotical anomalous behavior is a challenging task. Especially in biological experiments which generally cover only a few orders of magnitude in time [66, 67, 193].

Transient anomalous diffusion can result from random walks with two states of motility, even without the need for a breakdown of the central limit theorem. Such random walk models are widely used to investigate the run-and-tumble motion of bacteria. Random walks with pausing states are of particular interest for modeling intracellular transport where active motion along the cytoskeleton is frequently interrupted by stationary states [29, 33–38]. See for instance [64, 66, 213–220] and recent reviews on random walk models for intracellular transport [55, 72, 129, 183, 198]. In the following, a selection of random walks with two motility states and their diffusive properties is recapitulated.

"Intermittent random walks: transport regimes" [217]

Portillo *et al.* investigated how waiting periods affect the long time diffusive properties of random flights [217]. In their model, a walker runs with random velocities for a time period chosen according to

$$\phi(\tau) = \frac{\beta}{(1+\tau)^{1+\beta}}, \quad \beta > 0. \tag{3.28}$$

Flights are then interrupted by waiting times distributed according to

$$\varphi(\tau) = \frac{\alpha}{(1+\tau)^{1+\alpha}}, \quad \alpha > 0. \tag{3.29}$$

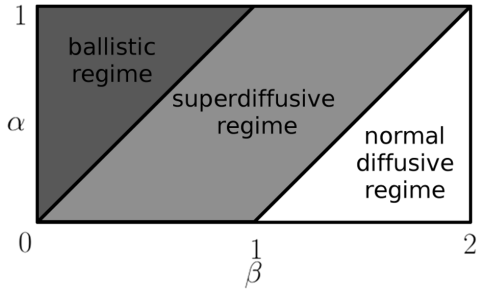

Figure 3.3.: MSD in the model of Thiel *et al.* [218]. The long time behavior of the MSD depends critically on the parameters of the run and tumble time distributions. Reprint of [218]. Reprinted figure with permission from Thiel, F. *et al.*, Physical Review E, 86, 021117, 2012, (`http://dx.doi.org/10.1103/PhysRevE.86.021117`). Copyright (2012) by the American Physical Society. Permission conveyed through SciPris.

Portillo *et al.* analytically showed, that the MSD in the long time limit $t \to \infty$

$$\langle x^2(t)\rangle \sim \begin{cases} t^2, & 0 < \beta < \alpha, \alpha > 0 \\ t^{2-\beta+\alpha}, & \alpha \leqslant \beta < 2, 0 < \alpha < 1 \\ t^{3-\beta}, & \alpha \leqslant \beta < 2, \alpha \geqslant 1 \\ t^{\alpha}, & \beta \geqslant 2, 0 < \alpha < 1 \\ t, & \beta \geqslant 2, \alpha \geqslant 1 \end{cases} \tag{3.30}$$

exhibits all kinds of anomalous diffusive behavior [217].

"Anomalous diffusion in run-and-tumble motion" [218]

Within a similar model, Thiel *et al.* studied the run-and-tumble motion of bacteria in d dimensions. Randomly oriented run phases are interrupted by tumbling phases [218]. Run phases are modeled by Lévy steps with speed c and duration $\psi_r(\tau_r)$. Tumbling phases correspond to Brownian diffusion with diffusion constant D and duration $\psi_t(\tau_t)$ [218]. If the run and the tumbling times are exponentially distributed, both the short time and the long time behavior of the MSD is diffusive [218]

$$\langle x^2(t)\rangle \sim dDt, \quad t \to 0, \langle x^2(t)\rangle \sim 2\frac{dD\tau_t + c^2\tau_r^2}{\tau_t + \tau_r}t, \quad t \to \infty. \tag{3.31}$$

However, if run and tumbling times are heavy-tailed distributed

$$\psi_t(\tau_t) \propto t^{-1-\alpha}, \psi_r(\tau) \propto t^{-1-\beta}, \tag{3.32}$$

the behavior of the MSD in the limit $t \to \infty$ may also be superdiffusive, as shown in Fig. 3.3 [218]. Subdiffusion cannot be obtained [218]. Note that for $\alpha, \beta \geqslant 1$ the second moment of the distribution diverges, while for $0 < \alpha, \beta < 1$ both the first and the second moment are infinite.

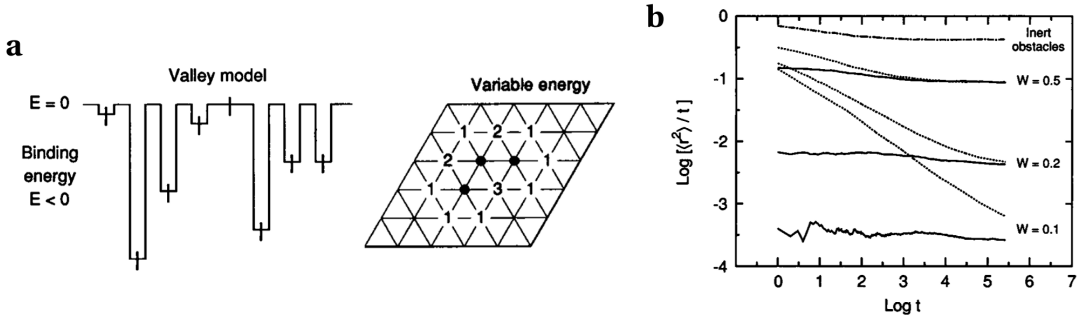

Figure 3.4.: The model of Saxton [64]. (**a**) A triangular lattice is occupied with obstacles (•) at random positions. The walker experiences trapping events at sites adjacent to obstacles with binding energies proportional to the number of occupied nearest neighbour sites. (**b**) The MSD depends on the initial condition of the random walk. Dashed lines correspond to random initial condition, while solid lines are associated to an equilibrated initial condition. For comparison the MSD in the case of pure obstruction by inert obstacles is shown. Reprint of [64]. Reprinted from Biophysical Journal, 70, Saxton, M. J., Anomalous diffusion due to binding: a Monte Carlo study, 1250-1262, Copyright (1996), (`http://dx.doi.org/10.1016/S0006-3495(96)79682-0`), with permission from Elsevier; permission conveyed through Copyright Clearance Center, Inc.

"Anomalous diffusion due to binding" [64]

Saxton studied the diffusion of random walks on a triangular lattice [64]. Each site of the lattice is assigned a well depth. In the model of Saxton, a fraction of C random lattice sites is occupied by immobile obstacles. A site adjacent to n obstacles has a well depth of $-n|\Delta E|$, the occupied site has a level ∞, and all other sites have a level 0, as sketched in Fig. 3.4, a. Since the particle is not allowed to step on lattice sites occupied by obstacles, it is an obstructed random walk. In order to move the particle has to reach E=0. Hence, when being at a lattice site with n neighboring obstacles, the walker waits for a time determined by $\exp(+\beta n|\Delta E|)$ until it moves to a random empty site [64].

With the aid of computer simulations, Saxton showed that the MSD depends critically on the initial condition of the walker [64]. If the walker starts at a random position of the lattice, the motion is subdiffusive at short times and normal diffusive in the long time limit. If the particle is propagated until thermal equilibrium is reached prior to the measurement, the MSD is purely diffusive over all timescales, as shown in Fig. 3.4, b.

3.2.3. Models with anisotropy

The models presented above lead to anomalous diffusion due to broad distributions, long time correlations or random alternations of run and pausing states. But so far only isotropic random walks with uniformly distributed, independent velocity directions have been considered. These models neglect the complex architecture of the cytoskeleton which is neither isotropic nor homogeneous [2].

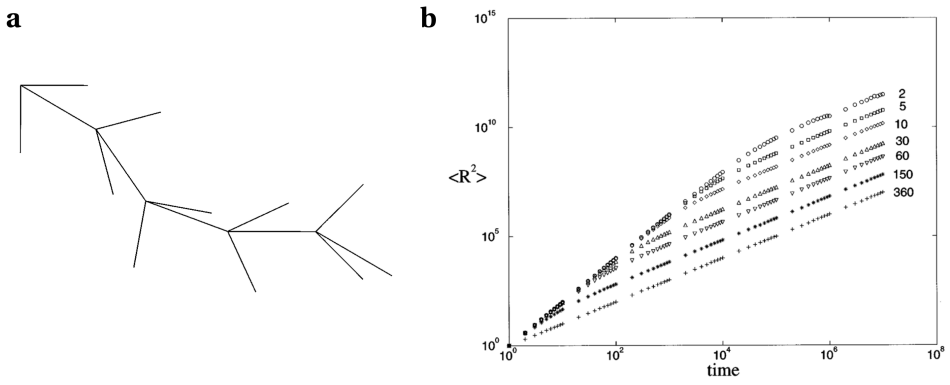

Figure 3.5.: The model of Tojo and Argyrakis [62]. A sample trajectory of the walk (**a**) is shown FOR $\theta = \pi/2$. The MSD (**b**) exhibits initial anomalous diffusion in response to various values of θ. Reprint of [62]. Reprinted figure with permission from Tojo, C. and Argyrakis, P., Physical Review E, 54, 58-63, 1996, (`http://dx.doi.org/10.1103/PhysRevE.54.58`). Copyright (1996) by the American Physical Society. Permission conveyed through SciPris.

Anomalous diffusion can also result from *anisotropic, persistent random walks* without the need for a breakdown of the central limit theorem, only by short-range correlations in successive velocity directions. Early studies of persistent random walks include [221,222]. In the following, a selection of persistent random walk models is given and it is presented how these models lead to anomalous diffusion.

"Correlated random walk in continuous space" [62]

In 1996, Tojo and Argyrakis numerically studied a persistent random walk in continuous, two-dimensional space and discrete time with correlated stepping directions, such that the walker has a memory of the previous direction [62].

Tojo and Argyrakis introduced a correlation in stepping directions as follows [62]: A new direction ϕ' is always restricted to an interval $[\phi - \theta/2; \phi + \theta/2]$ with regard to the previous direction ϕ. Within that interval, the new direction is chosen uniformly. A sample trajectory is sketched in Fig. 3.5, a.

With the aid of Monte Carlo simulations, the MSD was measured as a function of time steps for various values of $\theta \in [0; 2\pi]$ [62]. The case $\theta = 0$ corresponds to a fully correlated random walk on a straight line. The thus introduced long time correlation leads to a breakdown of the central limit theorem and asymptotic ballistic motion. Contrarily, the case $\theta = 2\pi$ is associated with a simple, isotropic random walk and consequently leads to normal diffusion over all timescales [62]. Figure 3.5, b, shows the behavior of the MSD for arbitrary values of θ. Accordingly, intermediate values of θ, and thus finite correlation in stepping directions, result in initial superdiffusive dynamics [62]. However, the asymptotic behavior of the MSD is normal diffusive. The crossover time is a hallmark of the correlation strength defined by θ [62].

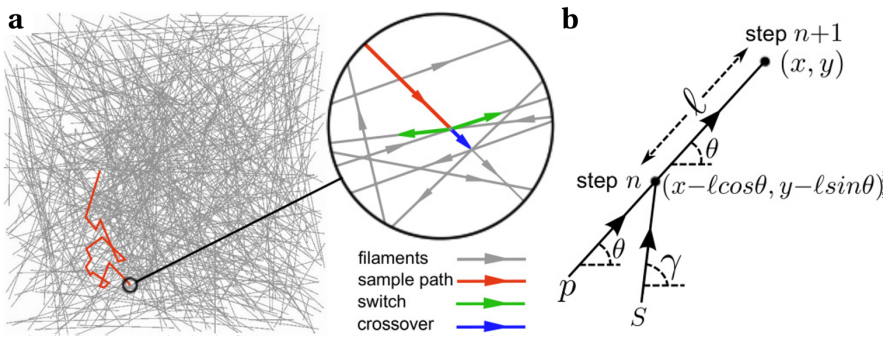

Figure 3.6.: The model of Shaebani *et al.* [63]. (**a**) The sample trajectory of a particle which moves along a random, directed network shows crossovers and switchings at filament crossings. (**b**) The random walker may either continue to walk along the same direction with probability p or it changes its direction according to a specific rotation angle $\phi = \theta - \gamma$ with respect to its previous direction γ. Reprint of [63]. Reprinted figure with permission from Shaebani, M. R. *et al.*, Physical Review E, 90, 030701, 2014, (`http://dx.doi.org/10.1103/PhysRevE.90.030701`). Copyright (2014) by the American Physical Society. Permission conveyed through SciPris.

"Anomalous diffusion of self-propelled particles in directed random environments" [63]

Within a persistent random walk approach, Shaebani *et al.* studied the motion of self-propelled particles, such as intracellular cargo, on random but directed networks, such as the cytoskeleton [63]. With the aid of an analytic framework, they investigated the impact of the interplay between cytoskeletal architecture and cargo processivity on the diffusive transport properties [63, 223].

Shaebani *et al.* implicitly modeled the motion of particles on randomly interlinked, polarized networks as sketched in Fig. 3.6, a. The walker performs steps in discrete time and continuous, two-dimensional space. As visualized in Fig. 3.6, b, at each step the walker either moves in the same direction as in the previous step with probability p, associated with the *processivity* of the particle, or it changes its direction with probability $(1-p)$ [63]. The step length ℓ and the turning angle ϕ are drawn from specific distributions which mimic the underlying cytoskeletal network [63].

The step length ℓ is distributed according to $\mathcal{F}(\ell)$, as shown in Fig. 3.7, a. The *heterogeneity* of the network

$$\lambda = \frac{\langle \ell^2 \rangle}{\langle \ell \rangle^2} \tag{3.33}$$

corresponds to the width of the step length distribution $\mathcal{F}(\ell)$ [63]. A constant step length $\mathcal{F}(\ell) = \delta(\ell - L)$ leads to a heterogeneity $\lambda = 1$, whereas larger values of λ are associated with broader distributions [63].

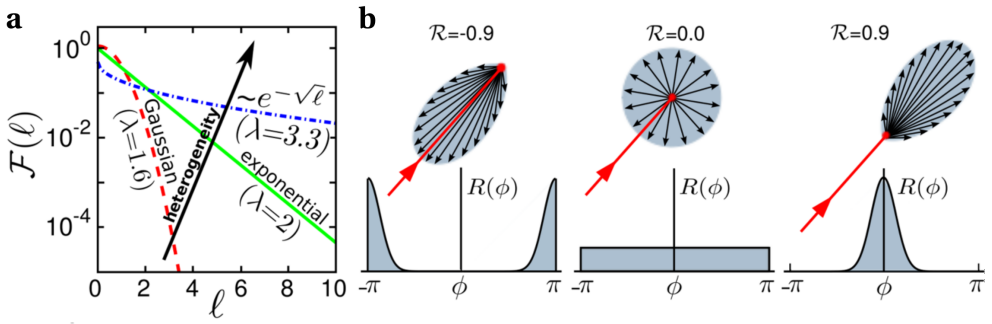

Figure 3.7.: The model of Shaebani *et al.* - network properties [63]. Step length (**a**) and turning angle (**b**) distributions mimic the underlying cytoskeleton. Reprint of [63]. Reprinted figure with permission from Shaebani, M. R. *et al.*, Physical Review E, 90, 030701, 2014, (`http://dx.doi.org/10.1103/PhysRevE.90.030701`). Copyright (2014) by the American Physical Society. Permission conveyed through SciPris.

The turning angle ϕ is chosen according to a distribution $R(\phi)$, which is generally symmetric in biological contexts, as depicted in Fig. 3.7, b [63]. Correlations in subsequent stepping directions are introduced in a Markovian manner, such that the new direction $\theta = \gamma + \phi$ is chosen with regard to the previous direction γ [63]. The *anisotropy* of the network

$$\mathcal{R}_m = \int_{-\pi}^{\pi} \mathrm{d}\phi \; e^{im\phi} \, R(\phi), \qquad \text{with } \mathcal{R}_{-1} = \mathcal{R}_{+1} \equiv \mathcal{R} \in [-1;1] \tag{3.34}$$

is the Fourier transform of the rotation angle distribution $R(\phi)$ [63]. For instance, $\mathcal{R} = 0$ corresponds to an isotropic random walk, which models the movement of cargo on random actin networks. In contrast, positive values $\mathcal{R} > 0$ lead to a higher chance of the particle to step in the forward direction with regard to the previous step. Such persistent motion occurs for instance alongside microtubule bundles. Negative values $\mathcal{R} < 0$ corresponds to highly anti-persistent motion of the particle as found in the crowded cytoplasm [63].

In essence, the random walk model proposed by Shaebani *et al.* is determined by three model parameters, which are the processivity p of the cargo, the heterogeneity λ, and the anisotropy $\mathcal{R}$ of the cytoskeleton network.

In order to study the impact of the cargo processivity and the cytoskeleton structure on the diffusive properties of the walk, Shaebani and Sadjadi *et al.* developed an analytical framework based on the master equation of the process [63, 223–225]

$$\begin{aligned} P_{n+1}(x,y|\theta) = p \int \mathrm{d}\ell \, \mathcal{F}(\ell) \, P_n \left(x - \ell\cos(\theta), y - \ell\sin(\theta)|\theta\right) \\ + s \int \mathrm{d}\ell \, \mathcal{F}(\ell) \int_{-\pi}^{\pi} \mathrm{d}\gamma \, R(\theta-\gamma) \, P_n \left(x - \ell\cos(\theta), y - \ell\sin(\theta)|\gamma\right). \end{aligned} \tag{3.35}$$

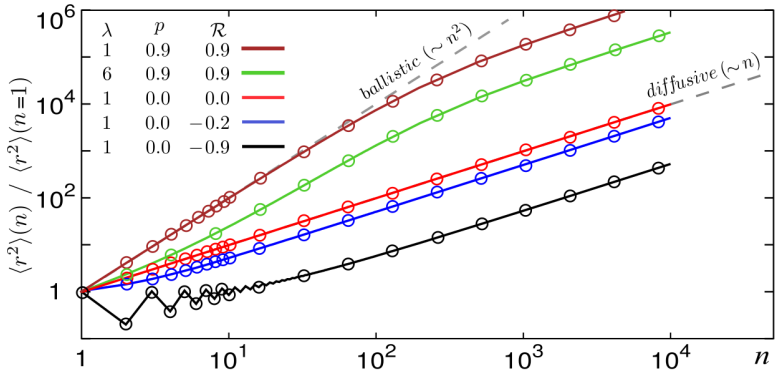

Figure 3.8.: The model of Shaebani *et al.* - MSD [63]. The MSD exhibits diverse anomalous regimes at short and intermediate timescales in response to the model parameters p, λ, and $\mathcal{R}$. The long time limit is purely diffusive. The analytic results (solid lines) and the simulation results (symbols) are in perfect agreement. Reprint of [63]. Reprinted figure with permission from Shaebani, M. R. *et al.*, Physical Review E, 90, 030701, 2014, (`http://dx.doi.org/10.1103/PhysRevE.90.030701`). Copyright (2014) by the American Physical Society. Permission conveyed through SciPris.

It describes the temporal evolution of the probability density function $P_n(x, y|\theta)$ of the particle to arrive in the n-th step at position $\boldsymbol{r} = (x, y)$ along the direction θ [63, 223]. The first term takes processive events into account, whereas the second term corresponds to directional changes.

With the aid of Fourier and z-transformation, it is possible to calculate exact analytic expressions of arbitrary moments of the particle displacement $P_n(x, y|\theta)$ [63, 223]. For the initial condition $P_0(x, y|\theta) = \frac{1}{2\pi}\delta(x)\delta(y)$, the MSD yields [63, 223]

$$\langle r^2\rangle_n = n\langle\ell\rangle^2\left[\lambda + \frac{2(p+\mathcal{R}-p\mathcal{R})}{(1-p)(1-\mathcal{R})}\right] + \langle\ell\rangle^2\frac{2(p+\mathcal{R}-p\mathcal{R})}{(1-p)^2(1-\mathcal{R})^2}\left[(p+\mathcal{R}-p\mathcal{R})^n - 1\right].$$

Figure 3.8 shows the MSD as a function of time for various values of the model parameters p, λ, and $\mathcal{R}$ [63]. The analytic results and the results of Monte Carlo simulations are in perfect agreement. Remarkably, the full range of anomalous diffusive behavior arises on short and intermediate timescales [63]. The type of anomaly is defined by the model parameters p, λ, and $\mathcal{R}$. Both the processivity p and the anisotropy $\mathcal{R}$ determine the correlation in consecutive steps [63]. While p by definition only leads to positive correlations, $\mathcal{R} \in [-1; 1]$ may lead to positively or negatively correlated steps. Consequently, if p and $\mathcal{R}$ are positive, the motion is superdiffusive as both parameters contribute to persistent motion of the particle [63]. However, if p=0 and $\mathcal{R}$=0, the motion is uniformly random which is manifested by normal diffusion over all timescales. In contrast, for negative values of $\mathcal{R}$ and p=0, anti-persistent motion arises which leads to subdiffusion or oscillatory back-and-forth motion of the walker [63].

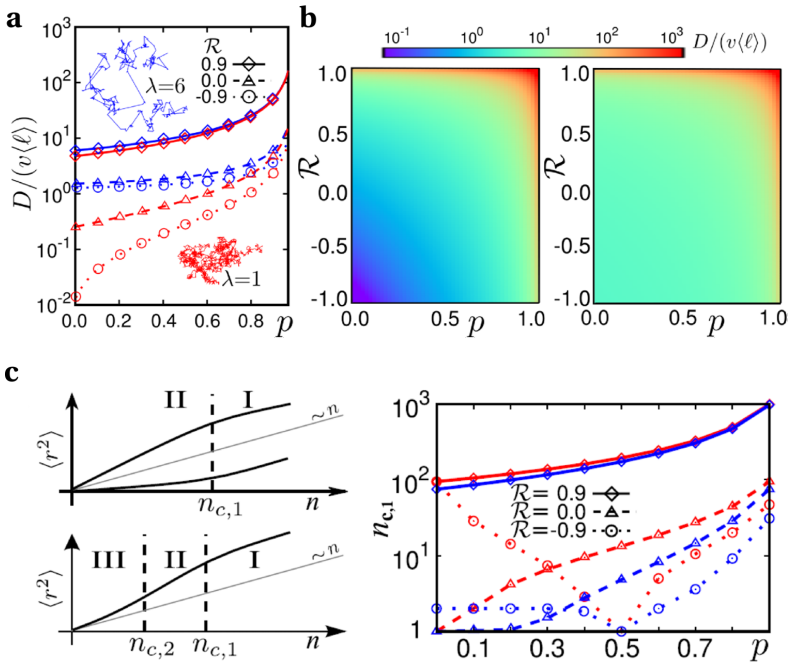

Figure 3.9.: The model of Shaebani *et al.* - asymptotic diffusion constant [63]. (**a**) The asymptotic diffusion constant is shown as a function of p for various values of $\mathcal{R}$ and $\lambda = 1$ (red lines) or $\lambda = 6$ (blue lines). Symbols represent simulation results, lines represent analytical data. (**b**) The asymptotic diffusion constant versus p and $\mathcal{R}$ for $\lambda = 1$ (left) and $\lambda = 6$ (right). (**c**) The crossover time $n_{c,1}$ is plotted as a function of p for various values of $\mathcal{R}$ and $\lambda = 1$ (red lines) or $\lambda = 6$ (blue lines). Reprint of [63]. Reprinted figure with permission from Shaebani, M. R. *et al.*, Physical Review E, 90, 030701, 2014, (`http://dx.doi.org/10.1103/PhysRevE.90.030701`). Copyright (2014) by the American Physical Society. Permission conveyed through SciPris.

The correlations are generally of short-range, except for p=1 or $\mathcal{R}$=1, which leads to ballistic motion over all timescales [223]. In agreement to the central limit theorem, the long time behavior is thus diffusive [63]. The crossover time to asymptotic diffusion and the corresponding diffusion constant

$$D = \frac{1}{4} v\langle\ell\rangle \left[\lambda + \frac{2(p + \mathcal{R} - p\mathcal{R})}{(1-p)(1-\mathcal{R})}\right] \tag{3.36}$$

depend critically on the model parameters and may vary over several orders of magnitude, as shown in Fig. 3.9 [63].

3.3. Random walk models for search problems

Search processes are very common in nature and occur on all lengthscales [72]. When the searcher has low cognitive abilities or no hint on the target position, the search process is random and can be well described with the aid of random walks [72]. On the macroscopic scale animals search for food, mate, or shelter, as for instance studied by [70–72, 226–234]. On the microscopic scale, random search processes are a hallmark of active intracellular transport, where cargo has to find reaction partners or specific regions within the cell or alongside the plasma membrane, as discussed in Chapter 2. Search processes generally depend on a vast array of parameters, as for instance the velocity distribution of the searcher or the properties of the environment. A specific set of these parameters determines a search strategy [72]. The efficiency of a given search strategy is usually quantified by the first passage time to target detection and minimization of the MFPT is essential for establishing efficient search strategies [72]. In the following, a recapitulation of random search strategies in the context of active intracellular transport is given. Reviews on that topic include [72, 129].

3.3.1. Diffusive search strategies

Narrow escape problem on the circular disk [171]

The narrow escape problem specifies the search for a specific region on the boundary of a domain. It is coined by studies in the context of passively diffusing particles of Holcman, Schuss, and Singer, e.g. [169–175], eventhough earlier work on escapes through bottlenecks exist, e.g. [235–237]. When considering search problems during active intracellular transport, studies of the narrow escape problem in spherical domains are most relevant. Singer *et al.* investigated the escape of particles, which are passively diffusing with diffusion constant D, through a narrow opening in a circular disk Ω of radius R [171]. The surface $\partial\Omega$ is reflecting except for a small absorbing region $\partial\Omega_a$ of arc length $|\partial\Omega_a| = 2\epsilon R$, as depicted in Fig. 3.10 [171]. Singer *et al.* derived an asymptotic expansion of the MFPT to the absorbing boundary in the limit of $\epsilon \ll 1$ [171]. If the particle starts at the center of the cell, the MFPT is determined by

$$\mathrm{MFPT}_{x(0)=0} = \frac{R^2}{D}\left[\log\frac{1}{\epsilon} + \log 2 + \frac{1}{4} + \mathcal{O}(\epsilon)\right]. \tag{3.37}$$

When averaging over uniformly distributed initial conditions, it is

$$\mathrm{MFPT}_{\int x(0)} = \frac{R^2}{D}\left[\log\frac{1}{\epsilon} + \log 2 + \frac{1}{8} + \mathcal{O}(\epsilon)\right]. \tag{3.38}$$

And the MFPT has a maximum value of

$$\max \mathrm{MFPT}_{x(0)\in\Omega} = \frac{R^2}{D}\left[\log\frac{1}{\epsilon} + 2\log 2 + \mathcal{O}(\epsilon)\right], \tag{3.39}$$

if the particle initially is located at the pole opposite to the escape region. As expected, the MFPT diverges for $\epsilon \to 0$ [171].

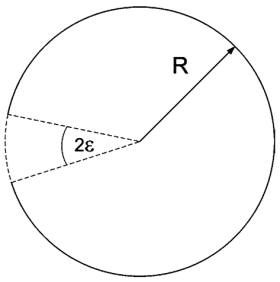

Figure 3.10.: The model of Singer *et al.* - diffusive narrow escape problem [171]. When moving in a circular disk of radius R a Brownian particle experiences reflecting walls (solid line) except for a small absorbing area (dashed line). Reprint of [171]. Reprinted by permission from Springer Customer Service Centre GmbH: Springer Nature, Journal of Statistical Physics, Narrow escape, part II: the circular disk, Singer, A. *et al.*, Copyright (2006), (`http://dx.doi.org/10.1007/s10955-005-8027-5`); permission conveyed through Copyright Clearance Center, Inc.

Reaction problem on the circular disk [238]

Condamin *et al.* considered a Brownian particle which is searching for an immobile target within a confined domain [238]. This is reminiscent of the reaction problem. The particle performs Brownian motion with diffusion constant D on a circular disk of radius R until it reaches the target of radius a. Condamin *et al.* showed that the MFPT depends on the initial distance between searcher and target d [238]

$$\text{MFPT} \sim \frac{R^2}{2D} \ln \frac{d}{a}. \tag{3.40}$$

3.3.2. Intermittent search strategies

However, purely diffusive models are insufficient in the context of active intracellular transport which consists of alternating phases of active, directed motion along the cytoskeleton and reorienting arrest states [29, 33–38]. In order to take such movement pattern into account, the group of Bénichou and Voituriez coined so-called intermittent search strategie [68–75]. Intermittent random walks consist of two states of motility: a fast non-reactive phase and a slow detective phase [72]. In [73–75] these two phases are denoted as *phase 1* and *phase 2*. In phase 1 the particle undergoes Brownian motion with diffusion constant D or it exhibits a static arrest state. Phase 2 is characterized by ballistic runs at constant speed v in uniformly random directions. The particle experiences stochastic transitions between phase 1 and phase 2, which are exponentially distributed with mean τ_1 (τ_2) [73–75].The searcher starts in phase 1 at a random position in a spherical domain of radius b with reflecting boundaries [73–75]. The target is immobile and located at the center of the sphere. Target detection is only possible in phase 1 as it is assumed that the particle is inactive when being in phase 2 [73–75]. Reaction occurs if searcher and target are closer than a distance a. In the case of intermittent diffusion, reaction is instantaneous, whereas it takes place with a finite rate k in the case of intermittent arrest states [73–75].

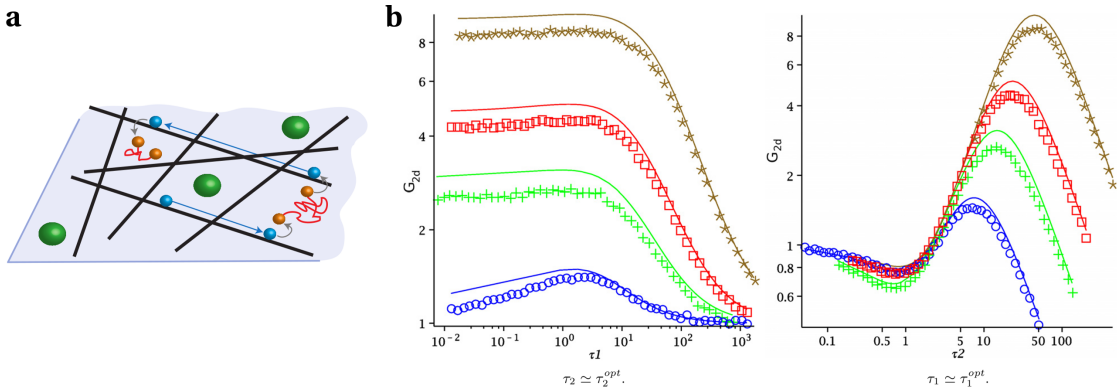

Figure 3.11.: The model of Loverdo *et al.* - intermittent random walk in 2D [73, 75]. (**a**) The sketch of the intermittent random walk model visualizes transitions between ballistic runs along the cytoskeleton and diffusive motion in the cytoplasm. (**b**) The gain of reactivity G_{2d} is shown as a function of τ_1 and τ_2 for v=1, D=1, and a=20, b=2000 (brown), a=10, b=1000 (red), a=10, b=100 (green), a=2.5, b=250 (blue). Analytical results are shown as solid lines and numerical simulations are represented by symbols. Part (a) is a reprint of [73]. Reprinted by permission from Springer Customer Service Centre GmbH: Springer Nature, Nature Physics, Enhanced reaction kinetics in biological cells, Loverdo, C. *et al.*, Copyright (2008), (`http://dx.doi.org/10.1038/nphys830`); permission conveyed through Copyright Clearance Center, Inc. Part (b) is a reprint of [75], Loverdo *et al.*, Reaction kinetics in active media, J. Stat. Mech., 9:P02045, 2009, (`http://dx.doi.org/10.1088/1742-5468/2009/02/P02045`). ©SISSA Medialab Srl. Reproduced by permission of IOP Publishing. All rights reserved.

Within that framework, Loverdo *et al.* analytically investigated the search efficiency in terms of a reaction constant $K = 1/\mathrm{MFPT}$, which is the inverse of the MFPT to the target [73–75]. In order to check whether intermittent strategies are favorable to purely diffusive strategies, they identify maximum values of the reaction constant K as a function of τ_1 and τ_2. Their results are recapitulated in order [73–75].

Intermittent diffusion

For intermittent diffusion, Loverdo *et al.* showed, that in the regime $D/v \ll a \ll b$ intermittent search strategies are favorable in a two-dimensional circular disk. The reaction rate K_{2d} is then maximized for [73–75]

$$\tau_{1,2d}^{\mathrm{opt}} \approx \frac{D}{2v^2} \frac{\ln^2(b/a)}{2\ln(b/a) - 1} \quad \text{and} \quad \tau_{2,2d}^{\mathrm{opt}} \approx \frac{a}{v}\sqrt{\ln(b/a) - 1/2}. \tag{3.41}$$

The gain $G_{2d} = K_{2d}/K_{2d}^{\mathrm{p}}$ in reaction efficiency by intermittent strategies with regard to then one K_{2d}^{p} of purely diffusive search strategies is shown in Fig. 3.11 [73–75]. It has a maximum value of [73–75]

$$G_{2d}^{\max} \approx \frac{av}{4D}\sqrt{\ln(b/a)}. \tag{3.42}$$

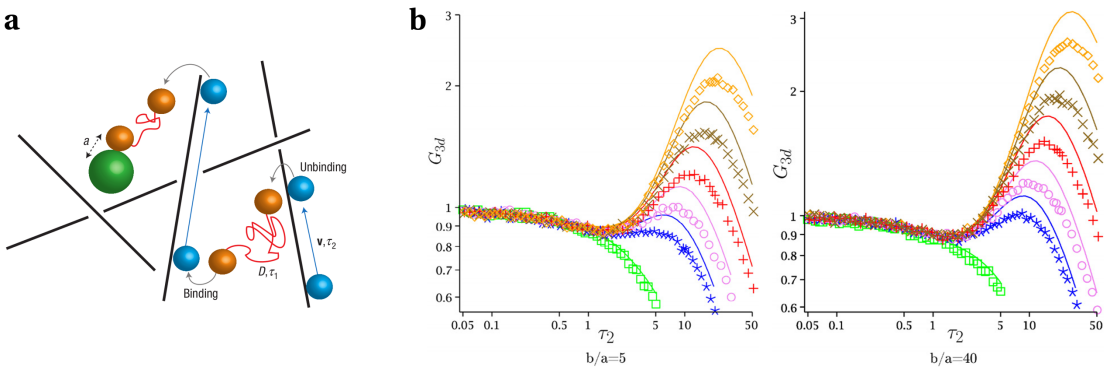

Figure 3.12.: The model of Loverdo *et al.* - intermittent random walk in 3D [73, 75]. (**a**) The sketch of the intermittent random walk model visualizes transitions between ballistic runs along the cytoskeleton and diffusive motion in the cytoplasm. (**b**) The gain of reactivity G_{3d} can be maximized as a function of τ_2 if $a \gtrsim D/v$. Parameters are determined by τ_1=6, v=1, D=1, and a=1 (green), a=5 (blue), a=7 (purple), a=10 (red), a=14 (brown), a=20 (orange). Analytical results are shown as solid lines and numerical simulations are represented by symbols. Part (a) is a reprint of [73]. Reprinted by permission from Springer Customer Service Centre GmbH: Springer Nature, Nature Physics, Enhanced reaction kinetics in biological cells, Loverdo, C. *et al.*, Copyright (2008), (`http://dx.doi.org/10.1038/nphys830`); permission conveyed through Copyright Clearance Center, Inc. Part (b) is a reprint of [75], Loverdo *et al.*, Reaction kinetics in active media, J. Stat. Mech., 9:P02045, 2009, (`http://dx.doi.org/10.1088/1742-5468/2009/02/P02045`). ©SISSA Medialab Srl. Reproduced by permission of IOP Publishing. All rights reserved.

For reaction problems in three-dimensional spheres, Loverdo *et al.* showed, that intermittent strategies are beneficial in the regime $6D/v \lesssim a \ll b$ [73–75]. The reaction rate K_{3d} is maximized for [73–75]

$$\tau_{1,3d}^{\text{opt}} \approx \frac{6D}{v^2} \quad \text{and} \quad \tau_{2,3d}^{\text{opt}} \approx 1.1\frac{a}{v}, \quad \rightarrow \quad G_{3d}^{\max} = \frac{K_{3d}^{\max}}{K_{3d}^{\text{p}}} \approx 0.26\frac{av}{D}, \tag{3.43}$$

as shown in Fig. 3.12. Consequently, in the limit of low target densities $a \ll b$, intermittent search strategies improve the reaction kinetics for large tracer particles with a reaction radius $a \approx D/v$ both in two- and three-dimensional spheres [73–75].

Intermittent arrests

In the case of a static mode in phase 2, intermittent strategies are naturally favourable in three and two dimensions as they are needed to explore space [74]. The reaction rate K can universally be maximized for [74]

$$\tau_{1,2d}^{\text{opt}} \approx \sqrt{\frac{a}{2vk}}\,(\ln(b/a) - 1/2)^{1/4} \quad \text{and} \quad \tau_{2,2d}^{\text{opt}} \approx \frac{a}{v}\sqrt{\ln(b/a) - 1/2} \tag{3.44}$$

in circular disks and in the case of spheres for

$$\tau_{1,3d}^{\text{opt}} \approx \left(\frac{3}{10}\right)^{1/4}\sqrt{\frac{a}{vk}} \quad \text{and} \quad \tau_{2,3d}^{\text{opt}} \approx 1.1\frac{a}{v}. \tag{3.45}$$

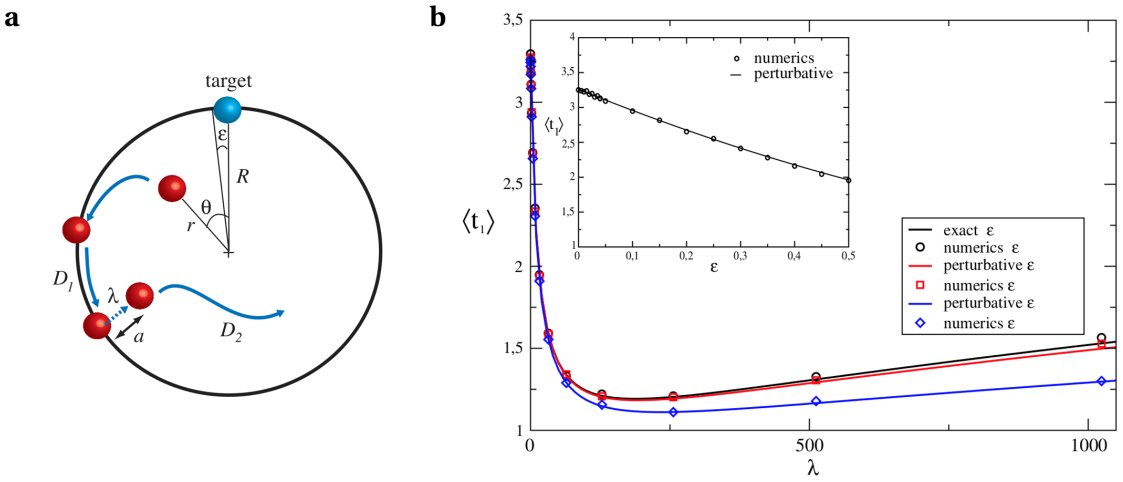

Figure 3.13.: The model of Bénichou *et al.* - surface-mediated diffusion [76]. (**a**) Sketch of a particle which performs surface-mediated diffusion in a sphere S with random alternations of bulk diffusion with diffusion constant D_2 and surface diffusion with diffusion constant D_1. (**b**) The MFPT is minimized as a function of the desorption rate λ for D_1=1, D_2=5, a=0.1, and R=1. Reprint of [76]. Reprinted figure with permission from Bénichou, O. *et al.*, Physical Review Letters, 105, 150606, 2010, (`http://dx.doi.org/10.1103/PhysRevLett.105.150606`). Copyright (2010) by the American Physical Society. Permission conveyed through SciPris.

Remarkably, the optimal residence time spent in the ballistic phase $\tau_{2,2d}^{\text{opt}}$ does not depend on the properties of the slow motion state [72–75]. It does neither depend on the mode of phase 1, diffusive or static, nor on the diffusion constant D or the rate k.

3.3.3. Inhomogeneous search strategies

The findings of Loverdo *et al.* show that intermittent search strategies are very robust strategies to optimize intracellular search problems [73–75]. However, they neglect the specific internal organization of cells by studying random walks in a homogeneous and isotropic environment. In the following, a model for surface-mediated diffusion and models which take a specific cytoskeleton organization into account are listed.

"Optimal reaction time for surface-mediated diffusion" [76]

Models of surface-mediated diffusion include a spatial inhomogeneity of the diffusion constant [76, 239–245]. Bénichou *et al.* investigated the narrow escape problem in two- and three-dimensional spheres S of radius R [76]. A particle performs alternating phases of bulk diffusion with diffusion constant D_2 and surface-mediated diffusion along ∂S with diffusion constant D_1 [76]. When detaching from the surface after an exponentially distributed timescale with rate λ, the particle is radially delocated at a distance $a \ll R$ from the surface into the bulk, where it exhibits bulk diffusion until it reaches the surface again and eventually the target of angular size 2ϵ is detected, as visualized in Fig. 3.13, a [76].

Bénichou *et al.* analytically showed, that the MFPT of a searcher, which is initially uniformly distributed on ∂S, can be minimized as a function of the desorption rate λ in dependence of D_1/D_2, as displayed in Fig. 3.13, b, for the two-dimensional disk [76]. In a very similar approach Calandre *et al.* further showed that also the MFPT to a target in the bulk, reminiscent of the reaction problem, can be minimized as a function of the desorption rate λ [243]. Consequently, the spatial inhomogeneity in the diffusion constant can substantially increase the search efficiency.

"Particle invasion, survival, and non-ergodicity in 2D diffusion processes with space-dependent diffusivity" [77]

Cherstvy *et al.* investigated the transport of particles from the center to the surface of a circular disk [77]. The particle performs Brownian motion with a diffusion constant

$$D(r) = D_0 \frac{A}{A + r^2}, \quad A > 0 \tag{3.46}$$

which is a function of the radial position r. The diffusion constant is thus the highest close to the center and gradually decreases with increasing distance. For $r \gg A$, the diffusion constant scales like a power-law $D(r) \sim 1/r^2$, whereas for $r \ll A$ diffusion is almost Brownian. With the aid of computer simulations, Cherstvy *et al.* found that the timescale $t_{1/2}$, at which the fastest half of the population arrives at the membrane, is defined by two asymptotes [77]. Namely, the one with the slowest diffusivity $D(r = R)$

$$t_{1/2}(R) \simeq \frac{R^2}{2D(R)} \simeq \frac{R^4}{2D_0 A} \tag{3.47}$$

and the one with average diffusivity $\langle D \rangle = \int_a^R D(r)\mathrm{d}r/(2(R^2 - a^2))$

$$t_{1/2}(R) \simeq \frac{R^2}{2\langle D \rangle} \simeq \frac{R^4}{2D_0 A \log[1 + R^2/A^2]}, \tag{3.48}$$

such that $t_{1/2}$ scales like R^4 in the leading order [77].

"Cytoskeleton network morphology regulates intracellular transport dynamics" [78]

Ando *et al.* investigated the influence of the topology of the cytoskeleton on the transport efficiency of particles which travel from the nucleus to an arbitrary position alongside the membrane [78]. Their model system is a two dimensional circular disk of radius R=10 μm, which possesses a nucleus of radius R_n. Tracer particles are initially positioned on the surface of the nucleus. In the cytoplasm they perform Brownian diffusion with diffusion constant D=0.011 $\mu\mathrm{m}^2/s$ [78].

The cytoskeleton is modeled as a shell of width w whose inner radius is positioned at R_a, see Fig. 3.14, a [78]. In order to account for active transport, the diffusion constant is increased within the shell to $D_a = 100D$. They found that the MFPT can be minimized for shells positioned close to the nucleus if $R_n \gtrsim R/4$, as shown in Fig. 3.14, b [78].

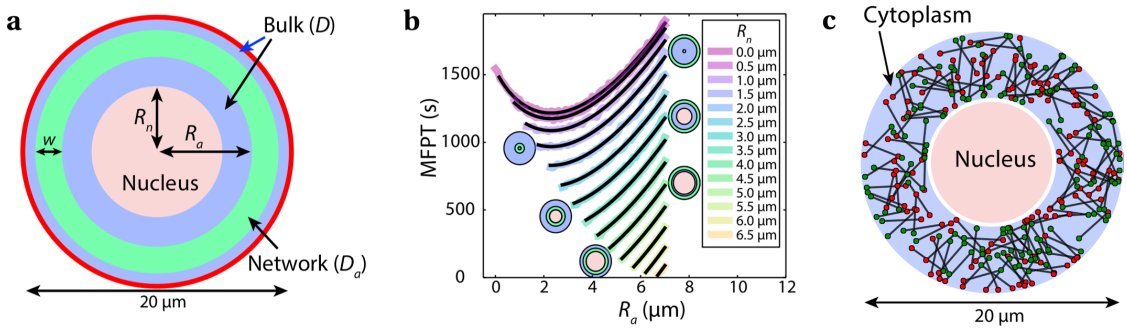

Figure 3.14.: The model of Ando *et al.* - accelerated diffusion in a shell [78]. (**a**) The particle experiences a higher diffusion constant in the network shell (green) than in the bulk (blue). (**b**) The MFPT can be minimized as a function of the shell position R_a. The MFPT is plotted for diverse nucleus radii and a shell width w=3 μm. (**c**) Sample realization of randomly oriented filaments in the cytoplasm. The green (red) circles indicate minus (plus) end of the filaments. Reprint of [78]. Reprinted from Biophysical Journal, 109, Ando, D. *et al.*, Cytoskeletal network morphology regulates intracellular transport dynamics, 1574-1582, Copyright (2015), (`http://dx.doi.org/10.1016/j.bpj.2015.08.034`), with permission from Elsevier; permission conveyed through Copyright Clearance Center, Inc.

Ando *et al.* further explicitly simulated filaments with fixed length which are randomly distributed in the cytoplasm, as sketched in Fig. 3.14, c [78]. Tracer particles experience alternations of ballistic motion alongside the filaments and diffusion in the bulk. They found that the transport efficiency from the nucleus to the membrane is increased if the filament polarities collectively point towards the membrane [78].

"Optimality of spatially inhomogeneous search strategies" [79]

However, the cytoskeleton exhibits a very specifc architecture, where microtubules emanate radially from the center, while actin filaments are found in a cortex underneath the membrane. In 2016, Schwarz *et al.* studied the impact of an inhomogeneous, anisotropic organization of the cytoskeleton on the efficiency of various intermittent search processes [79, 80]. The tracer particle undergoes phases of Brownian diffusion in the cytoplasm (with diffusion constant D and k-exponentially distributed duration) and ballistic motion alongside cytoskeleton (with k'-exponentially distributed duration) which prohibits target detection [79]. The distribution of filament orientations Ω is space-dependent

$$\rho_\Omega(\boldsymbol{r}) = \begin{cases} p\delta_{\Omega,\Omega'(\boldsymbol{r})} + (1-p)\delta_{\Omega,\Omega'(-\boldsymbol{r})}, & 0 < |\boldsymbol{r}| < R - \Delta, \\ 1/4\pi, & R - \Delta < |\boldsymbol{r}| < R, \end{cases} \tag{3.49}$$

where $\Omega'(\boldsymbol{r})$ specifies the direction of position $\boldsymbol{r}$ [79]. Hence, a cell is modeled as a three-dimensional sphere of radius R with radial microtubules in the interior and randomly oriented actin filaments in a shell beneath the membrane of thickness Δ, as indicated by the sample trajectory in Fig. 3.15, a [79]. The search efficiency is measured in terms of the MFPT to the target, but target detection is only allowed when the searcher is in

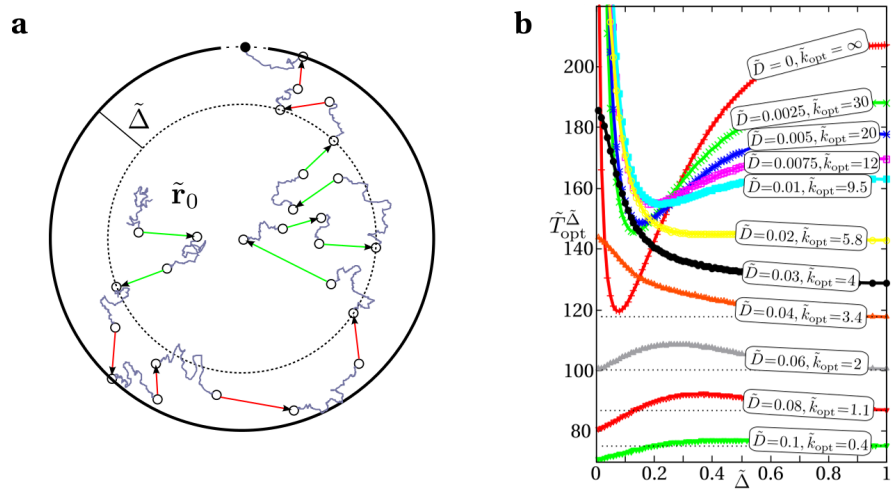

Figure 3.15.: The model of Schwarz *et al.* - spatially inhomogeneous, intermittent search strategies [79]. (**a**) The sample trajectory exhibits the intermittent diffusive phase and the space-dependent directions of the ballistic phases. (**b**) The MFPT of the narrow-escape problem can be minimized as a function of Δ in dependence of the diffusivity D. Rates k'_{opt}=0 and k_{opt}, which are optimal for a homogeneous, uniformly random filament distribution $\Delta = R$, are applied. Reprint of [79]. Reprinted figure with permission from Schwarz, K. *et al.*, Physical Review Letters, 117, 068101, 2016, (`http://dx.doi.org/10.1103/PhysRevLett.117.068101`). Copyright (2016) by the American Physical Society. Permission conveyed through SciPris.

the slow, diffusive phase. With the aid of a Monte Carlo method, specific to reaction-diffusion problems presented in [246], Schwarz *et al.* found that the MFPT can generally be minimized as a function of Δ for diverse transport tasks, as exemplary shown for the narrow escape problem in Fig. 3.15, b [79, 80].

3.4. Summary

Intracellular transport can be modeled with the aid of specific random walks.

Random walk models which display asymptotic anomalous diffusion rely on a breakdown of the central limit theorem and take advantage of broad distributions and long-range correlations in the walker's trajectory [56–61]. However, anomalous diffusion can also occur on short and intermediate timescales without the need for broad distributions and long-range correlations. Random walks in anisotropic environments and random walks with pausing states show non-trivial transient anomalous diffusion [62–64].

Intermittent random walks have been widely studied in the context of diverse search problems. In general, intermittent search strategies have been shown to be favorable, because the MFPT can be minimized as a function of the transition rates between

the two motility states [68–75]. Typically, such search strategies are studied in homogeneous, isotropic environments. But this assumption is not valid for intracellular transport processes which cover the whole cell range on which the cytoskeleton is neither homogeneous nor isotropic. The crucial impact of the exact topology of the cellular environment on the search efficiency of various transport tasks has very recently gained scientific interest [76–80].

The impact of the key properties of intracellular transport, i.e. the cytoskeletal architecture, the motor activity, and the pausing frequency of the cargo, on anomalous diffusion and first passage events have been studied individually in the past. In Chapter 4 and 5, we present unified random walk models which enable us to elucidate how the interplay between the key properties of intracellular transport effects anomalous diffusion and first passage events. A specific focus is on the role of the inhomogeneity and anisotropy of the cytoskeleton.

Chapter 4.

Anomalous diffusion: the role of anisotropy

Contents

4.1. Motivation

Anomalous diffusion of tracer particles is frequently observed in living cells [39–55]. However, the origin is often elusive and it is further not known whether the anomaly is a transient effect or not [65–67]. Modeling intracellular transport is challenging: The movement of cargoes is determined by the cellular environment. Transitions between ballistic motion along the cytoskeleton and reorienting pauses [29, 33–38] are regulated by the concentration of accessory proteins or crossings of the filamentous network [2, 37, 130]. Moreover, the cytoskeleton exhibits a space-dependent anisotropy. Microtubules often form aligned bundles, while actin filaments are typically random [2].

While standard models of asymptotic anomalous diffusion necessitate broad distributions and long-range correlations [56–61], waiting states and the anisotropy of the environment are candidates to provide transient anomalous diffusion [62–64], as recapitulated in Chapter 3. How the interplay between the local anisotropy of the cytoskeleton, the motor behavior, and the pausing states effects anomalous diffusion of intracellular tracer particles is not fully understood. Here, we investigate how cells are able to regulate anomalous diffusion by transient arrest states on anisotropic filaments and networks. We present a coarse grained random walk perspective of intracellular transport by monitoring the effective motion of cargo while disregarding the mechanochemical details of the motor stepping. This approach enables us to identify the influence of the local

anisotropy of the cytoskeleton, the cargo processivity, and the transition frequency between the two states of motility on the diffusive properties of intracellular transport. In the following, we investigate the motion of cargo which experience pauses on a single filament and on cytoskeletal networks.

At first, a model for motion on a single anisotropic filament is introduced. An exact analytic expression of the probability density function of the tracer's displacement is derived and the resulting MSD is studied. Within an analytic approach, we monitor the anomalous exponent over all timescales and estimate the crossover time to the asymptotic behavior as a function of the transition rates between the two motility states [Hafner2016B].

In [Hafner2014], a model of intermittent motion on two-dimensional anisotropic networks, based on the model of Shaebani *et al.* [63], was introduced. In Section 4.4, the model and main results of [Hafner2014] are briefly recapitulated. Then, we study the temporal evolution of the anomalous exponent and the crossover time to asymptotic diffusion, which provides further insight into the transient nature of the discovered anomalous diffusion. Moreover, we focus on the diffusion constant in the long time limit [Hafner2016B].

The investigations which are presented in this chapter are published in [Hafner2016B].

4.2. Model

4.2.1. Description

Here, we investigate how transient arrest states influence the transport of cargoes which move unidirectionally along a single cytoskeletal filament [Hafner2016B]. We introduce a random walk model in discrete time and continuous, one-dimensional space which incorporates stochastic transitions between two states of motility: (i) ballistic transport along the filament is frequently interrupted by (ii) stationary pauses. Such arrest states arise when cargoes are stopped by roadblocks, such as accessory proteins which are attached to the filament, so that they have to maneouvre around the obstruction [37, 130, 144, 247], or, although unlikely [31], when cargoes fully detach of the filament and subdiffusve dynamics in the crowded cytoplasm are approximately stationary [31, 39–41, 50, 51, 55]. The model is also relevant for the motion of highly proccessive cargoes on cytoskeletal networks, where filament crossings cause cargoes to pause until they overcome the barrier [29, 33–38].

In the model, state transitions are assumed to occur in a Markovian manner with constant probabilities κ_w and κ_m per time step to switch from the motion to the waiting state and vice versa [Hafner2016B]. This leads to an exponentially distributed duration of each motility state; the smaller the probability κ_w (κ_m), the longer the mean duration in the motion (waiting) state. Since active lifetimes during intracellular transport are reported to be exponentially distributed as well [248], this is in good agreement to biological observations.

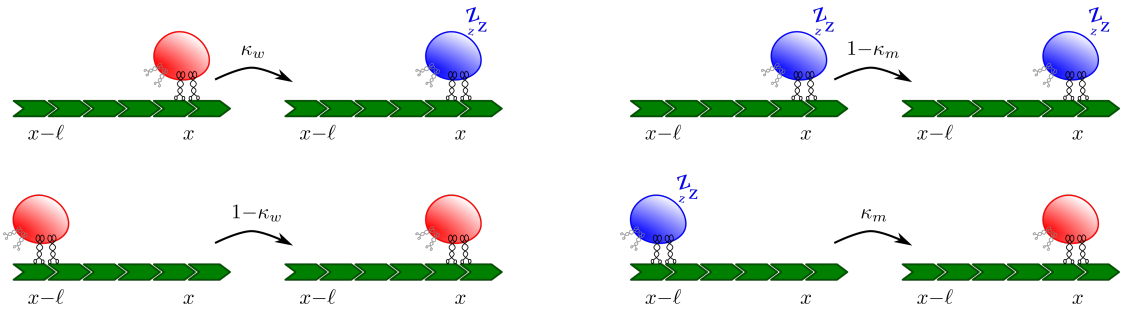

Figure 4.1.: Run-and-pause random walk on a single filament - the model. The four possible state transitions between two consecutive steps are sketched. Blue color indicates a cargo in the arrest state, while red color corresponds to a cargo in the motion state. In the style of a figure published in [Hafner2016B], Scientific Reports, 6, 37162, 2016, (`http://dx.doi.org/10.1038/srep37162`).

We assume that the cargo is transported by a single motor species. Consequently, it performs unidirectional motion along the filament. At each time step of the walk, the tracer particles either waits or moves a distance ℓ drawn from a distribution $\mathcal{F}(\ell)$, as sketched in Fig. 4.1 [Hafner2016B]. Following [63], the step length distribution $\mathcal{F}(\ell)$ is characterized by $\lambda = \langle \ell^2 \rangle / \langle \ell \rangle^2$, but in what follows, the step length is often assumed to be constant, i.e. $\mathcal{F}(\ell) = \delta(\ell - L) \Rightarrow \lambda = 1$ [Hafner2016B].

4.2.2. Analytic approach

The temporal evolution of the probability density function $P_n^M(x)$, $P_n^W(x)$ to find the particle at time step n at position x in the motion, waiting state, respectively, is given by a set of coupled master equations

$$\begin{cases} P_{n+1}^M(x) = \int \mathrm{d}\ell\, \mathcal{F}(\ell) \left[\kappa_m P_n^W(x-\ell) + (1-\kappa_w) P_n^M(x-\ell) \right], \\ P_{n+1}^W(x) = \kappa_w P_n^M(x) + (1-\kappa_m) P_n^W(x). \end{cases} \tag{4.1}$$

The master equation takes the four possible transitions of the cargo, presented in Fig. 4.1, into account [Hafner2016B]. The first equation corresponds to position updates from $x-\ell$ to x between steps n and $n+1$ if the particle either switches from the waiting to the motion state with probability κ_m or if it remains in the motion state with probability $1-\kappa_w$. The second equation represents a stationary particle position which occurs if the particle switches from the motion to the waiting state with probability κ_w or if it stays in the waiting state with probability $1-\kappa_m$.

Within an analytic approach, which involves Fourier and z-transformation [63, 223–225], it is possible to solve the coupled set of Eq. 4.1 in terms of the probability density functions $P_n^M(x)$ and $P_n^W(x)$ [Hafner2016B]. Note that this is specific to the here presented one-dimensional model.

The Fourier transform of Eq. 4.1 reads

$$\begin{cases} P^M_{n+1}(\omega) &= \int \mathrm{d}x\, e^{i\omega x} P^M_{n+1}(x) = \int \mathrm{d}\ell\, \mathcal{F}(\ell)\, e^{i\omega\ell} \left[\kappa_m P^W_n(\omega) + (1-\kappa_w) P^M_n(\omega)\right], \\ P^W_{n+1}(\omega) &= \int \mathrm{d}x\, e^{i\omega x} P^M_{n+1}(x) = \kappa_w P^M_n(\omega) + (1-\kappa_m) P^W_n(\omega), \end{cases} \tag{4.2}$$

and generates the moments of displacement according to

$$\langle x^k \rangle^j_n = \int \mathrm{d}x\, x^k P^j_n(x) = (-i)^k \frac{\partial^k P^j_n(\omega)}{\partial \omega^k}\bigg|_{\omega=0}. \tag{4.3}$$

The coupled set of Eq. 4.2 can be solved with the aid of z-transformation

$$T^j(z) = \sum_{n=0}^{\infty} T^j_n z^{-n}, \tag{4.4}$$

which leads to

$$\begin{cases} P^M(z,\omega) &= \frac{1}{\kappa_w}\left[(z-(1-\kappa_m))\; P^W(z,\omega) - z\, P^W_{n=0}(\omega)\right], \\ P^W(z,\omega) &= \frac{1}{\kappa_m}\left[\left(\frac{z}{\langle e^{i\omega\ell}\rangle} - (1-\kappa_w)\right)\; P^M(z,\omega) - \frac{z}{\langle e^{i\omega\ell}\rangle}\, P^M_{n=0}(\omega)\right], \end{cases} \tag{4.5}$$

with $\langle e^{i\omega\ell}\rangle = \int \mathrm{d}\ell\, \mathcal{F}(\ell)\, e^{i\omega\ell}$. By applying the initial condition

$$P^M_{n=0}(x) = P^M_0\, \delta(x), \tag{4.6}$$
$$P^W_{n=0}(x) = (1-P^M_0)\, \delta(x), \tag{4.7}$$
$$P_{n=0}(x) = P^M_{n=0}(x) + P^W_{n=0}(x) = \delta(x), \tag{4.8}$$

where P^M_0 is the probability to start the walk in the motion state, and solving the coupled set of Eq. 4.5, we obtain the full solution of the master equation 4.1 in Fourier- and z-space [Hafner2016B]

$$P(z,\omega) = P^M(z,\omega) + P^W(z,\omega) \tag{4.9}$$
$$= \frac{z\left[\langle e^{i\omega\ell}\rangle \left(P^M_0 - 1\right)(\kappa_m + \kappa_w - 1) - P^M_0\,(\kappa_m + \kappa_w - 1) - z\right]}{\langle e^{i\omega\ell}\rangle\,(z - z\kappa_w + \kappa_m + \kappa_w - 1) - z\,(z + \kappa_m - 1)}. \tag{4.10}$$

Arbitrary moments of the particle displacement can thus be derived by z-transformation of Eq. 4.3. For instance the temporal evolution of the MSD is determined by

$$\langle x^2 \rangle^j(z) = \sum_{n=0}^{\infty} z^{-n} \langle x^2 \rangle^j_n = (-i)^2\; \frac{\partial^2 P^j(z,\omega)}{\partial \omega^2}\bigg|_{\omega=0}. \tag{4.11}$$

Consequently, the MSD of a particle which experiences transient arrest states while moving unidirectionally along a single filament is given by [Hafner2016B]

$$
\begin{aligned}
\langle x^2\rangle_n = {} & 1/(\kappa_m+\kappa_w)^4\times \\
& \Bigg\{ \langle \ell^2\rangle(\kappa_m+\kappa_w)^2\Big[-\kappa_m+P_0^M\kappa_m+\kappa_m^2-P_0^M\kappa_m^2+\kappa_m^2 n+P_0^M\kappa_w+\kappa_m\kappa_w-2P_0^M\kappa_m\kappa_w \\
& \qquad +\kappa_m\kappa_w n-P_0^M\kappa_w^2+(1-\kappa_m-\kappa_w)^{(1+n)}(\kappa_m-P_0^M\kappa_m-P_0^M\kappa_w)\Big] \\
& +\langle\ell\rangle^2\Big[\kappa_m^4 n(1-2P_0^M+n) \\
& \quad +2\kappa_m^3\Big(P_0^M-1-n+P_0^M n-\kappa_w+P_0^M\kappa_w-3P_0^M n\kappa_w+n^2\kappa_w \\
& \qquad +(P_0^M-1)(1-\kappa_m-\kappa_w)^n\big(-1+(-1+n)\kappa_w\big)\Big) \\
& \quad +2P_0^M(-1+\kappa_w)\kappa_w^2\Big(\kappa_w-1+(1-\kappa_m-\kappa_w)^n\big(1+(-1+n)\kappa_w\big)\Big) \\
& \quad +\kappa_m^2\Big(2-2P_0^M+4\kappa_w+4P_0^M n\kappa_w-4\kappa_w^2+6P_0^M\kappa_w^2-3n\kappa_w^2-6P_0^M n\kappa_w^2+n^2\kappa_w^2 \\
& \qquad +2(1-\kappa_m-\kappa_w)^n\big(P_0^M-1+(n-P_0^M n-2)\kappa_w+(3P_0^M-2)(n-1)\kappa_w^2\big)\Big) \\
& \quad +2\kappa_m\kappa_w\Big(-(\kappa_w-1)\big(-2+(1+P_0^M(-3+n)+n)\kappa_w\big)(1-\kappa_m-\kappa_w)^n\times \\
& \qquad +\big(2+\kappa_w(3P_0^M-3+n-2P_0^M n+(3P_0^M-1)(n-1)\kappa_w)\big)\Big)\Big]\Bigg\}.
\end{aligned}
\tag{4.12}
$$

The MSD is a complex function of the transition probabilities κ_m and κ_w, the first and second moment of the step length distribution $\langle\ell^2\rangle$, and the initial condition P_0^M.

4.2.3. Monte Carlo simulation

Due to the complexity of the calculations, we perform Monte Carlo simulations in order to validate the analytic predictions 4.12, as described in the Appendix A.1. The MSD is calculated as an ensemble average over of the order of 10^6 independent realizations of the walk [Hafner2016B].

4.3. Results

4.3.1. Transient anomalous diffusion

In Fig. 4.2, a, the analytic predictions for the MSD, given in Eq. 4.12, are compared to the results of Monte Carlo simulations. Analytic results and simulations are in perfect agreement. Remarkably, the MSD exhibits several crossovers in anomalous diffusion as a function of time [Hafner2016B]. In response to the transition probabilities κ_w and κ_m, crossovers from super- to subdiffusion and vice versa arise at short and intermediate timescales. The initial superdiffusive regime is a direct consequence of the unidirectional motion of cargoes along anisotropic filaments of the cytoskeleton.

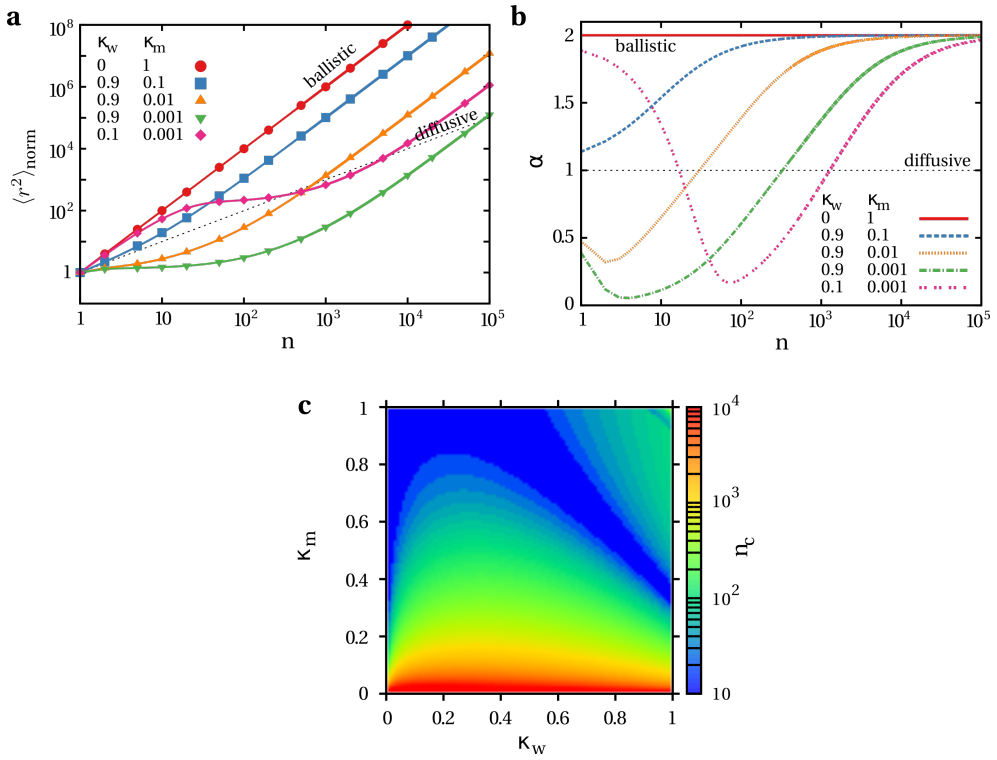

Figure 4.2.: Run-and-pause random walk on a single filament - transient anomalous diffusion. (**a**) The normalized MSD $\langle x^2\rangle(n)/\langle x^2\rangle(n{=}1)$ displays transient anomalous diffusion as a function of time n in response to various combinations of the transition probabilities κ_w and κ_m for the initial condition $P_0^M{=}1$ and $\lambda{=}1$. Analytic predictions are displayed by lines, whereas the results of Monte Carlo simulations are represented by symbols. (**b**) The transient behavior of the MSD is highlighted by the temporal evolution of the anomalous exponent for the same parameters as in a. (**c**) The crossover time to asymptotic ballistic motion varies over several orders of magnitude depending on the transition probabilities κ_w and κ_m for $P_0^M{=}1$ and $\lambda{=}1$. Reprint of [Hafner2016B], Scientific Reports, 6, 37162, 2016, (`http://dx.doi.org/10.1038/srep37162`).

The transient behavior of anomalous diffusion can be quantified in terms of the temporal evolution of the anomalous exponent $\alpha(n)$ [Hafner2016B]. It can be estimated via a power-law fit $\langle x^2\rangle{\sim}t^\alpha$ [67] of the analytic expression of the MSD, given in Eq. 4.12, as follows

$$\alpha(n) = \ln\left[\frac{\langle r^2\rangle_{n+1}}{\langle r^2\rangle_n}\right] \Big/ \ln\left[\frac{n+1}{n}\right]. \tag{4.13}$$

For instance the initial anomalous exponent $\alpha^\star{=}\alpha(1)$ reads [Hafner2016B]

$$\alpha^\star = \ln\left[2 - \frac{2(\kappa_w{-}1)}{\lambda} - \kappa_w + \kappa_m\Big(-1{+}\frac{1}{\kappa_m{-}P_0^M(-1{+}\kappa_m{+}\kappa_w)}\Big)\right] \Big/ \ln[2], \tag{4.14}$$

which reduces to

$$\alpha^\star = \ln\left[4 - 3\kappa_w - \kappa_m + \frac{\kappa_m}{1-\kappa_w}\right] \Big/ \ln[2]. \tag{4.15}$$

for the initial condition P_0^M=1 and λ=1. Hence, without any pauses, i.e. κ_w=0 and κ_m=1, the initial exponent $\alpha^\star$=2 is ballistic, as expected for unidirectional motion along a single filament [Hafner2016B].

In Fig. 4.2, b, the temporal evolution of the anomalous exponent is shown for P_0^M=1. Crossovers in anomaly are highlighted by intersections with the constant line α=1. In response to the interplay between the key parameters of the walk, i.e. κ_w, κ_m, and P_0^M=1, the anomalous exponent is a complex function of time [Hafner2016B], which is reminiscent of transient anomalous diffusion [67]. Consequently, the presented analytic approach to monitor the temporal evolution of the anomalous exponent $\alpha(n)$ provides a powerful tool to discriminate between transient anomalous diffusion with a time-dependent exponent and stationary anomalous diffusion with a constant exponent [67]. Different regimes in anomalous diffusion can be easily visualized and crossovers in anomaly correspond to intersections of $\alpha(n)$ with α=1. Furthermore, knowing $\alpha(n)$ is advantageous for identifying the crossover time to the diffusive limit [Hafner2016B]. In the long time limit $n \to \infty$, the MSD, given in Eq. 4.12, is determined by [Hafner2016B]

$$\langle x^2 \rangle_{n\to\infty} \approx \frac{\kappa_m^2(\kappa_m+1)^2}{(\kappa_m+\kappa_w)^4} \langle \ell \rangle^2 \, n^2. \tag{4.16}$$

The asymptotic behavior is ballistic due to the unidirectional motion along the filament. The crossover time to asymptotic ballistic motion can be estimated by [Hafner2016B]

$$|\alpha(n_c)-2| < \epsilon = 10^{-2} \tag{4.17}$$

where α=2 corresponds to ballistic motion. Note that Eq. 4.17 needs to be valid for a sufficient timescale to guarantee that the asymptotic limit is reached. We further checked that the arbitrary choice of ϵ does not influence our conclusions. Figure 4.2, c, shows that the crossover time is a complex function of the transition probabilities κ_w and κ_m and varies by several orders of magnitude [Hafner2016B]. As expected, the crossover time n_c increases with decreasing κ_m, since the particle remains longer in the waiting state. Remarkably, the crossover can also be delayed by frequent state transitions due to large values of κ_m and κ_w.

4.3.2. Impact of the initial condition

The transient nature of the observed anomalous diffusion is a direct consequence of aging processes, see for instance [193]. A sequence of state transitions of the walk is described by a Markov chain with two states, i.e. motion and waiting [Hafner2016B, Hafner2014]. The transition probabilities κ_m and κ_w define an equilibrium state with probabilities

$$\begin{aligned} P_\infty^M &= \frac{\kappa_m}{(\kappa_m+\kappa_w)}, \\ P_\infty^W &= \frac{\kappa_w}{(\kappa_m+\kappa_w)}, \end{aligned} \tag{4.18}$$

to be in the motion or the waiting state, respectively [249,250] [Hafner2016B,Hafner2014].

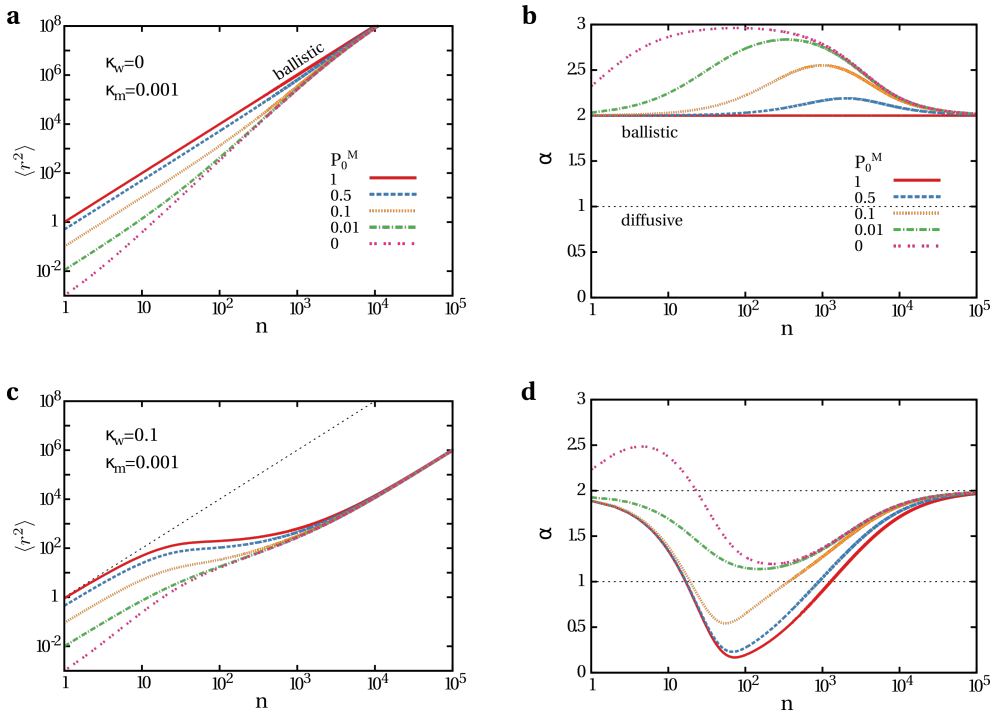

Figure 4.3.: Run-and-pause random walk on a single filament - impact of the initial condition. (**a,c**) The MSD is shown as a function of time for diverse initial conditions P_0^M and transition probabilities κ_w and κ_m; λ=1 is applied. (**b,d**) The temporal evolution of the anomalous exponent highlights the impact of the initial condition. Accordingly, a superballistic regime may arise. Reprint of [Hafner2016B], Scientific Reports, 6, 37162, 2016, (`http://dx.doi.org/10.1038/srep37162`).

The MSD presented in Fig. 4.2 is an ensemble average over trajectories with fixed initial condition P_0^M=1, i.e. all particles start in the motion state. In the course of time, the Markov chain relaxes from the initial condition (P_0^M, P_0^W=1−P_0^M) to the equilibrium state (P_∞^M, P_∞^W) [249, 250] [Hafner2016B, Hafner2014]. Hence, aging processes occur due to the relaxation of the chain during the measurement of the MSD, which lead to transient anomalous diffusion, as shown in Fig. 4.2.

Figure 4.3 shows the MSD and the anomalous exponent as a function of time for various initial conditions P_0^M and transition probabilities κ_w and κ_m. Accordingly, anomalous diffusion critically depends on the choice of the initial condition [Hafner2016B]. Remarkably, the anomalous exponent can also exceed values of α=2, such that the MSD grows faster than for ballistic motion due to an acceleration in the system, which can be understood as follows [Hafner2016B]. Consider the case, that all particles start in the waiting state with P_0^M=0 and switch to the motion state with probability κ_m per time step. Once in the motion state, no transitions back to the waiting state are allowed via κ_w=0. Consequently, all particles are gradually injected into the motion state, as shown by the squared displacement of single particle trajectories in Fig. 4.4, a. This

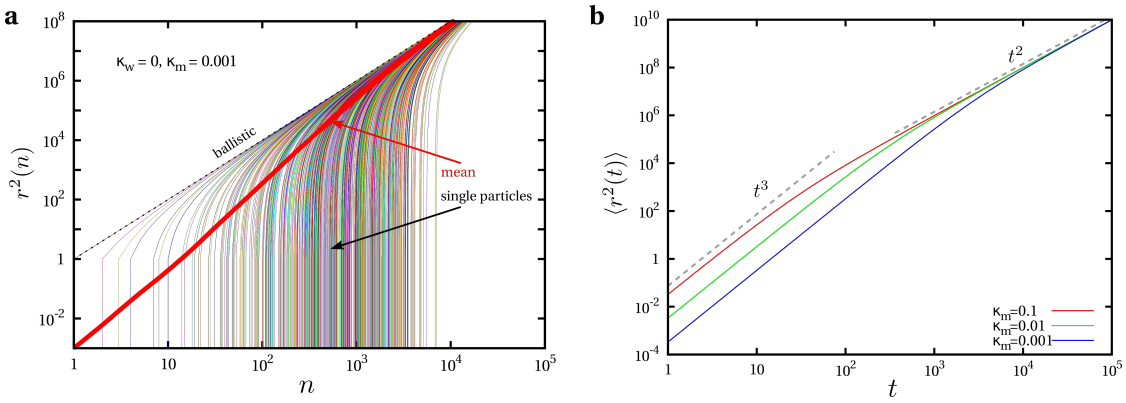

Figure 4.4.: Run-and-pause random walk on a single filament - impact of the initial condition II. (**a**) Simulation results of single trajectories and the corresponding ensemble averaged mean are shown for P_0^M=0, κ_w=0, κ_m=0.001, and λ=1. (**b**) The MSD, predicted by Eq. 4.21, explains the observed initial exponent $\alpha^\star \approx 3$ for P_0^M=0, κ_w=0, λ=1, and various values of κ_m. Reprint of [Hafner2016B], Scientific Reports, 6, 37162, 2016, (`http://dx.doi.org/10.1038/srep37162`).

particle injection accelerates the MSD as manifested by an anomalous exponent greater than α=2 [Hafner2016B]. In a continuous time approach, the initial residence time in the waiting state t_0 is exponentially distributed

$$p(t_0) = \kappa_m' e^{-\kappa_m' t_0} \tag{4.19}$$

Hence, the particles switch at times t_0 to the motion state. When being in the motion state, they undergo ballistic motion with speed v, such that the displacement of a particle at time t is given by [Hafner2016B]

$$r(t) = \begin{cases} 0, & t < t_0 \\ v\,|t - t_0|\,, & t \geqslant t_0 \end{cases} \tag{4.20}$$

The MSD is determined by integration over the transition times

$$\langle r^2(t) \rangle = \int_0^t \mathrm{d}t_0 \; p(t_0) v^2 \,|t - t_0|^2 = \frac{v^2}{\kappa_m^2} \left[2 - 2\kappa_m t + \kappa_m^2 t^2 - 2e^{-\kappa_m t} \right] \tag{4.21}$$

and Taylor expansion of Eq. 4.21

$$\langle r^2(t) \rangle \approx \frac{v^2}{\kappa_m^2} \left[\frac{1}{3} \kappa_m^3 t^3 + \dots \right] \tag{4.22}$$

highlights the initial behavior $\langle r^2(t) \rangle \sim t^3$, as displayed in Fig. 4.4, b [Hafner2016B].

Note that our analytic findings are in qualitative agreement to the conclusions of Saxton drawn from simulations in a similar context [64, 66]. Saxton showed in his model, as recapitulated in Section 3.2.2 of Chapter 3, that transient anomalous diffusion critically depends on the initial position of the particle, which defines its initial state [64, 66].

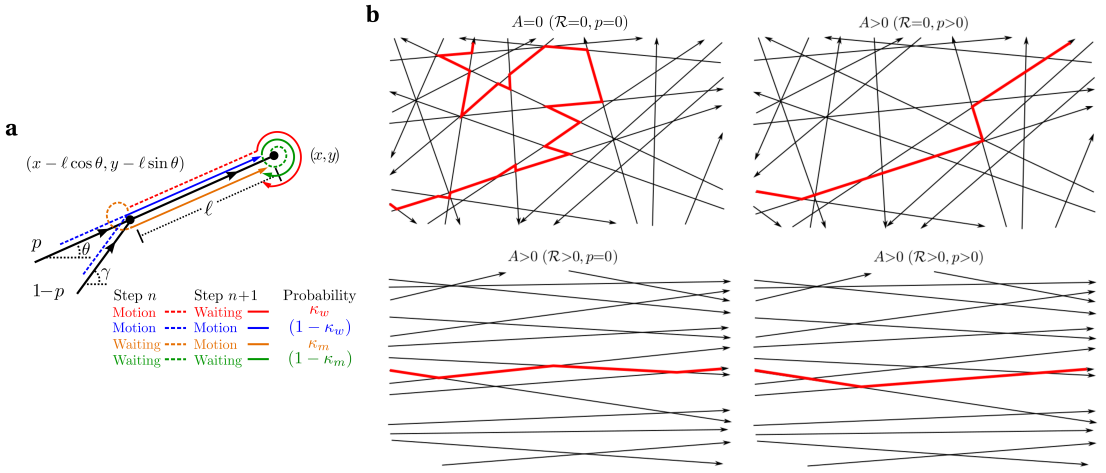

Figure 4.5.: Run-and-pause random walk on anisotropic networks - the model. (**a**) A sketch of the walk during two successive steps is shown. (**b**) Networks with anisotropy $\mathcal{R}$ and sample trajectories (red lines) with processivity p lead to diverse generalized anisotropies $\mathcal{A}$ of the walk. Reprint of [Hafner2016B], Scientific Reports, 6, 37162, 2016, (`http://dx.doi.org/10.1038/srep37162`).

4.4. Generalization to two-dimensional networks

In [Hafner2014], a run-and-pause random walk on two-dimensional anisotropic networks, based on the model of Shaebani *et al.* [63], was introduced. The model and main results of [Hafner2014] are briefly recapitulated here. We then provide further insight into the transient nature of the discovered anomalous diffusion by studying the temporal evolution of the anomalous exponent over all timescales, the crossover time to asymptotic diffusion, and the asymptotic diffusion constant [Hafner2016B].

Since intracellular cargoes frequently pause at filament crossings of cytoskeleton [29, 33–38], we consider a persistent random walk with transient arrest states [Hafner2014, Hafner2016B]. Transitions between the motion and the waiting states occur in a Markovian manner with probabilities κ_w (from motion to waiting) and κ_m (from waiting to motion). At each time step, the tracer particle either waits or it performs a step of length ℓ. The step length ℓ is distributed according to $\mathcal{F}(\ell)$ with $\lambda = \langle\ell^2\rangle/\langle\ell\rangle^2$, but the focus is on constant step lengths with $\mathcal{F}(\ell) = \delta(\ell - L)$ and λ=1. In the motion state, the particle either continues to move in the same direction as in the previous step with processivity p or a new direction $\theta = \gamma + \phi$ is chosen with respect to the old direction γ according to a specific rotation angle drawn from a distribution $\mathcal{R}(\phi)$, which is in analogy to [63]. A sketch of the walk is presented in Fig. 4.5, a.

Within an analytic approach, based on [63,223–225], it is possible to derive exact analytic expressions of arbitrary moments of the particle displacement, as shown in [Hafner2014, Hafner2016B]. But in contrast to the one-dimensional model, the coupled set of master equations [Hafner2014, Hafner2016B]

$$\begin{cases} P_{n+1}^{M}(x,y|\theta) & = p\int \mathrm{d}\ell\, \mathcal{F}(\ell)\, \left[\kappa_m P_n^W\left(x',y'|\theta\right) + (1-\kappa_w) P_n^M\left(x',y'|\theta\right)\right] \\ & \quad + (1-p)\int \mathrm{d}\ell\, \mathcal{F}(\ell) \int_{-\pi}^{\pi} \mathrm{d}\gamma\, R(\phi)\left[\kappa_m P_n^W\left(x',y'|\gamma\right) + (1-\kappa_w) P_n^M\left(x',y'|\gamma\right)\right], \\ P_{n+1}^{W}(x,y|\theta) & = \kappa_w P_n^M(x,y|\theta) + (1-\kappa_m) P_n^W(x,y|\theta), \end{cases} \tag{4.23}$$

cannot be solved in terms of the probability density function $P_n(x,y|\theta)$ to find the particle at position (x,y) along direction θ at time step n [Hafner2014, Hafner2016B]. In [Hafner2014] we showed that the exact analytic expression for the ensemble averaged MSD

$$\begin{aligned} \langle r^2\rangle_n = & -\frac{\langle \ell^2\rangle}{(A-1)^2\lambda} \times \\ & \Bigg\{ 2A + 2AP_0^M - 2A^2P_0^M + P_0^M\lambda - 2AP_0^M\lambda + A^2P_0^M\lambda \\ & + \frac{(A-1)(A(\lambda-2)-\lambda)\kappa_m}{(\kappa_m+\kappa_w)^2} - \frac{(A-1)P_0^M(A(\lambda-2)-\lambda)}{\kappa_m+\kappa_w} - \frac{(A-1)(A(\lambda-2)-\lambda)\kappa_m(1+n)}{\kappa_m+\kappa_w} \\ & + \frac{(A-1)(A(\lambda-2)-\lambda)(1-\kappa_m-\kappa_w)^{1+n}((P_0^M-1)\kappa_m+P_0^M\kappa_w)}{(\kappa_m+\kappa_w)^2} \\ & - \frac{2^{-n}A}{\sqrt{(\kappa_m-1+A(\kappa_w-1))^2+4A(\kappa_m+\kappa_w-1)}} \times \\ & \Bigg[\left(1+A-\kappa_m-A\kappa_w+\sqrt{(\kappa_m-1+A(\kappa_w-1))^2+4A(\kappa_m+\kappa_w-1)}\right)^n \times \\ & \quad \Big(1-2P_0^M-\kappa_m+2P_0^M\kappa_m+2P_0^M\kappa_w+\sqrt{(\kappa_m-1+A(\kappa_w-1))^2+4A(\kappa_m+\kappa_w-1)} \\ & \quad +A(2\kappa_m+\kappa_w-1-2P_0^M(\kappa_m+\kappa_w-1))\Big) \\ & + \left(1+A-\kappa_m-A\kappa_w-\sqrt{(\kappa_m-1+A(\kappa_w-1))^2+4A(\kappa_m+\kappa_w-1)}\right)^n \times \\ & \quad \Big(2P_0^M-1+\kappa_m-2P_0^M\kappa_m-2P_0^M\kappa_w+\sqrt{(\kappa_m-1+A(\kappa_w-1))^2+4A(\kappa_m+\kappa_w-1)} \\ & \quad +A(1-2\kappa_m-\kappa_w+2P_0^M(\kappa_m+\kappa_w-1))\Big)\Bigg]\Bigg\}. \end{aligned} \tag{4.24}$$

depends on the generalized anisotropy $\mathcal{A}=p+\mathcal{R}-p\mathcal{R}$, where $\mathcal{R}$ which is the Fourier transform of $\mathcal{R}(\phi)$ characterizes the anisotropy of the network and p corresponds to the processivity of the cargo. As depicted in Fig. 4.5, b, $\mathcal{A}=0$ corresponds to non-processive motion on isotropic networks, whereas $\mathcal{A}>0$ takes into account persistent motion and anisotropic environments [Hafner2014, Hafner2016B].

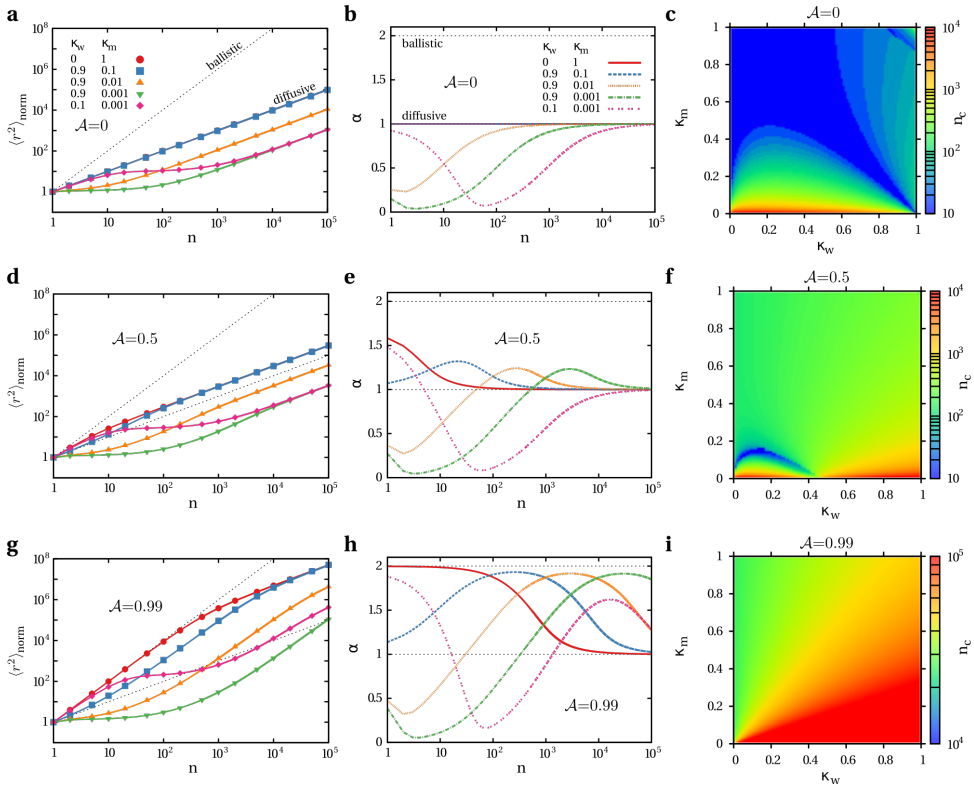

Figure 4.6.: Run-and-pause random walk on anisotropic networks - transient anomalous diffusion. (**a, d, g**) The MSD exhibits diverse crossovers in anomaly as a consequence of the interplay between generalized anisotropy $\mathcal{A}$ and transient arrest states determined by κ_m and κ_w for P_0^M=1 and λ=1. Lines correspond to analytic expressions, whereas symbols represent simulation results. (**b, e, h**) The temporal evolution of the anomalous exponent highlights the transient nature for the same parameters as in a, d, g, respectively. (**c, f, i**) The crossover time to asymptotic diffusion varies over several orders of magnitude in response to κ_m and κ_w for P_0^M=1 and λ=1. Reprint of [Hafner2016B], Scientific Reports, 6, 37162, 2016, (`http://dx.doi.org/10.1038/srep37162`).

In [Hafner2014], the analytic results of the MSD were also verified with the aid of Monte Carlo simulations. We showed that the MSD exhibits non-trivial crossovers between different types of anomalous diffusion at short and intermediate timescales [Hafner2014, Hafner2016B], see Fig. 4.6, a, d, and g, in response to the interplay between generalized anisotropy $\mathcal{A}$ and waiting frequency. Note that in the limit $\mathcal{A}$=1, the 2D-simulation yields the same results as the 1D-simulation described in the Appendix A.1. But, the analytic expression of the MSD, given in Eq. 4.24, exhibits a singularity for $\mathcal{A}$=1. Consequently, an analytic investigation of the walk is not possible for $\mathcal{A}$=1, which highlights the need for the above presented 1D-model of run-and-pause motion along a single filament.

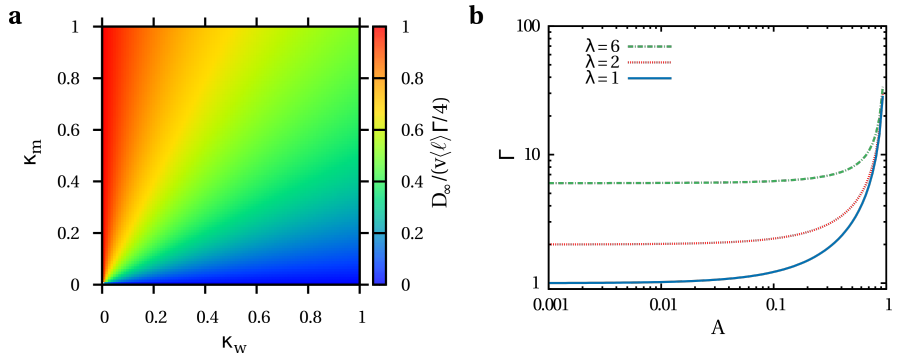

Figure 4.7.: Run-and-pause random walk on anisotropic networks - asymptotic diffusion constant. (**a**) The long time diffusion constant D_∞ scaled by $(v\langle\ell\rangle\Gamma/4)$ is mapped in the κ_w-κ_m-plane. (**b**) The parameter Γ is plotted as a function of the generalized anisotropy $\mathcal{A}$ for several values of λ. Reprint of [Hafner2016B], Scientific Reports, 6, 37162, 2016, (`http://dx.doi.org/10.1038/srep37162`).

According to Eq. 4.13, we can now track the anomalous exponent over all timescales and thus easily identify crossover in anomaly. Figures 4.6, b, e, and h, show that the anomalous exponent is a complex function of time in response to the interplay between generalized anisotropy $\mathcal{A}$ and transient arrest states defined by the transition probabilities κ_m and κ_w [Hafner2016B]. Consequently, the observed anomaly is a highly transient effect.

In the long time limit the MSD exhibits normal diffusion, since the correlations in consecutive velocity directions vanish in the course of time [Hafner2016B]

$$\langle r^2\rangle_{n\to\infty} \approx \frac{\kappa_m}{\kappa_m+\kappa_w}\,\frac{A(\lambda-2)-\lambda}{A-1}\,\langle\ell\rangle^2\,n. \tag{4.25}$$

Analogous to the 1D-model, the crossover time to asymptotic diffusion can be estimated by

$$|\alpha(n_c)-1| < \epsilon = 10^{-2}. \tag{4.26}$$

Figures 4.6, c, f, and i, show that the crossover time n_c varies over several orders of magnitude as a function of the transition probabilities κ_m and κ_w [Hafner2016B]. According to Eq. 4.25 and $\langle r^2\rangle_{n\to\infty} = 4D_\infty n\langle\ell\rangle/v$, the long time diffusion constant can be deduced

$$D_\infty = \frac{v\langle\ell\rangle}{4}\,\frac{\kappa_m}{\kappa_m+\kappa_w}\,\frac{A(\lambda-2)-\lambda}{A-1} = \frac{v\langle\ell\rangle}{4}\,\Gamma\,\frac{\kappa_m}{\kappa_m+\kappa_w}, \tag{4.27}$$

with $\Gamma=\frac{A(\lambda-2)-\lambda}{A-1}$ and the average cargo velocity v [Hafner2016B]. Figure 4.7, a, shows that the scaled diffusion constant $D_\infty/(v\langle\ell\rangle\Gamma/4)$ is increased by decreasing κ_w or increasing κ_m. The diffusion constant D_∞ varies over several orders of magnitude in response to the network topology, as shown by plotting Γ as a function of the generalized anisotropy A in Fig. 4.7, b. The asymptotic diffusion constant does not depend on the initial condition P_0^M since aging effects vanish for $n\to\infty$ [Hafner2016B].

4.5. Summary

Within an analytic framework, we identified the impact of the interplay between cytoskeleton architecture, motor behavior, and arrest states of the cargoes on anomalous diffusion of intracellular cargoes. We investigated the MSD and its dependence on the initial condition of the measurements, we monitored the anomalous exponent over all timescales, and we studied diffusion in the long time limit [Hafner2016B].

We found that the interplay between anisotropy of the motion and arrest states lead to complex anomalous diffusion phenomena. Crossovers between different anomalous regimes occur on short and intermediate timescales. By monitoring the temporal evolution of the anomalous exponent we revealed that the observed anomaly is a highly transient effect based on aging processes out of a predefined initial state. The crossover time to the asymptotic limit and the long time diffusion constant varies by several orders of magnitude in response to the pausing frequency.

In essence, a cell is able to control the diffusive properties of intracellular cargoes by regulating the network morphology, the motor behavior, and the cargo's arrest frequency. However, the initial condition and the averaging procedure of measurements is of crucial importance for the interpretation of the results.

Chapter 5.

Search efficiency: the role of anisotropy and inhomogeneity

Contents

5.1. Motivation

The efficient delivery of intracellular cargo is vital for cells and organisms. Cargo particles, such as organelles or macromolecules, have to be transported from their source to specific target locations. Thereby, cargoes often cover long distances within the cell, which is facilitated by active intracellular transport along the cytoskeleton [2].

Intracellular transport is a stochastic process which is shaped by the interplay between the cytoskeleton and its spatial architecture, the molecular motors and their activity, and the cargo which undergoes random alternations between active, directed motion along the cytoskeleton and reorienting arrest states. The cytoskeleton of metazoan cells exhibits a space-dependent structure which is highly inhomogeneous and anisotropic. Microtubules radiate from the cell center, whereas actin filaments randomly populate the cortex [2]. Typically diverse molecular motors are attached to a single cargo and drag it along the cytoskeleton [17–31]. Large cargo-motor complexes frequently experience arrest states at filament crossings of the network. These barriers cause the cargoes to pause until they either overcome the constriction or until they switch the filament [29, 33–38].

Due to its complexity, modeling intracellular transport is a challenging theoretical task. The stochastic movement pattern of intracellular cargo suggests a random walk approach. Intermittent search strategies with stochastic transitions between a slow detective phase and a fast non-reactive phase are shown to be favorable in the context of various search problems, e.g. [68–75]. Such random walks are typically studied in homogeneous and isotropic environments. But, this assumption is not valid for intracellular transport processes which cover the whole cell range. Very recently, the effect of the exact topology of the cytoskeleton on intracellular transport has gained scientific interest [76–80].

Nonetheless, up to now the influence of the specific cytoskeleton architecture, the motor activity, and the arrest states a cargo experiences during its travel have been considered separately in the literature, as recapitulated in Chapter 3. It is still obscure how the efficiency of targeted intracellular transport is influenced by this interaction. Here, we introduce a unified random walk model for intracellular transport with stationary pauses [Hafner2016, Hafner2018]. The cytoskeleton and the action of diverse motor proteins is implicitly modeled by a specific, space-dependent distribution of random velocities of the cargo. We thus present a coarse grained perspective of intracellular transport by considering the effective motion of cargo along the cytoskeleton - from intersection node to intersection node - while neglecting the mechanochemical details of the underlying motor stepping. With the aid of extensive Monte Carlo simulations, we systematically analyze how the interplay between cytoskeleton architecture, motor activity, and a cargo's pausing frequency effects the transport efficiency [Hafner2016, Hafner2018]. Efficiency is measured in terms of the MFPT to target detection. We consider three paradigmatic intracellular transport tasks, as biologically motivated in Chapter 2:

- the narrow escape problem, which models transport to a specific area on the plasma membrane
- the reaction problem, which evaluates the reaction time of two particles within the cell, and
- the reaction-escape problem, which emerges when two particles first react inside the cell before the product particle is stochastically transported to a narrow exit on the plasma membrane.

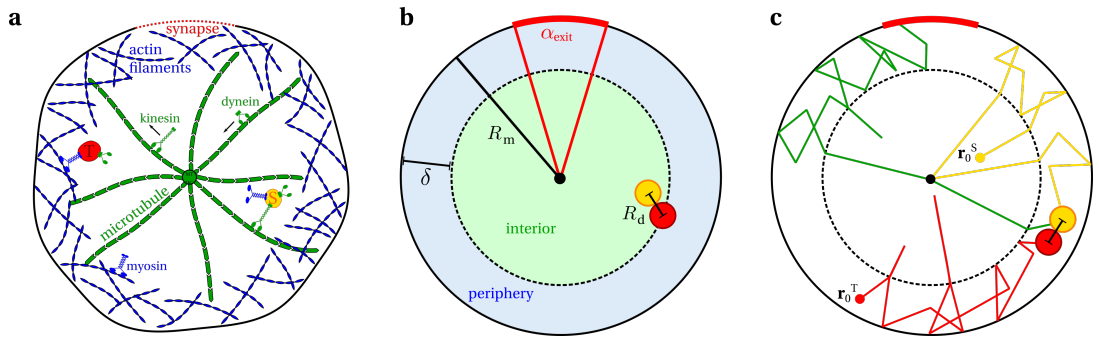

Figure 5.1.: Run-and-pause random walk on a spatially inhomogeneous and anisotropic cytoskeleton - the model. (**a**) Targeted intracellular transport is a stochastic process based on the spatial organization of the cytoskeleton. (**b**) We idealize a cell as a sphere of radius R_{m}. The inhomogeneity of the cytoskeleton is taken into account by a cortex of width δ which splits the sphere into interior and periphery. An exit of angle α_{exit} is located on the membrane and R_{d} denotes the detection radius for reaction of two particles. (**c**) The reaction-escape problem combines the reaction of searcher (yellow) and target (red) particle, which start at $\boldsymbol{r}_0^S$, $\boldsymbol{r}_0^T$, and the escape of the product (green). Reprint of [Hafner2018], Biophysical Journal, 114, 1420-1432, 2018, (`http://dx.doi.org/10.1016/j.bpj.2018.01.042`).

Results which are presented in this chapter are published in [Hafner2016] and [Hafner2018].

Note that Schwarz *et al.* focussed on intermittent diffusion [79, 80], as recapitulated in chapter 3. In contrast, we systematically analyze the impact of transient arrest states on spatially inhomogeneous and anisotropic search strategies in two and three dimensions [Hafner2016, Hafner2018]. Our findings are in qualitative agreement for small diffusion constants. The limit of a vanishing diffusion constant is biologically relevant for intracellular cargo, such as vesicles, mitochondria, or macromolecules, which experience size-dependent subdiffusion in the crowded cytoplasm and thus undergo effectively stationary states [39–41, 50, 51, 55]. But more importantly, since a single cargo is typically attached to several motor proteins concurrently [17–31], a full dissociation of the filament is rather unlikely [31]. Instead, arrest states at filament crossings are observed in *in vitro* experiments as well as in live-cell microscopy [29, 33–38]. In contrast to Schwarz *et al.* [79, 80], we further investigate non-intermittent search strategies and take several steps towards more physiological conditions.

5.2. Model

5.2.1. Description

In order to study the impact of the cytoskeleton architecture, the motor activity, and the arrest states on active intracellular transport, we formulate a unified random walk model in continuous time and two-dimensional space [Hafner2016, Hafner2018].

We idealize a cell by a sphere of radius R_m, as sketched in Fig. 5.1. In order to take the inhomogeneity of the cytoskeleton into account, we include a cortex of width δ underneath the cell boundary, which divides the sphere into interior and periphery [Hafner2016, Hafner2018]. The interior is characterized by a radial microtubule aster, whereas the periphery is dominated by the cortical actin filaments.

The random walk is characterized by stochastic transitions between two states of motility [Hafner2016, Hafner2018]:

- a ballistic motion state at velocity $\boldsymbol{v}(v, \phi_v)$ which corresponds to active transport by molecular motors between successive intersections nodes of the cytoskeleton at constant speed v, and
- a waiting state, which is associated to arrests of the cargo when stuck at filament crossings.

State transitions are arranged in a Markovian manner by constant transition rates $k_{m\to w}$ ($k_{w\to m}$) to switch from motion to waiting (from waiting to motion). Therefore, the residence times t_m and t_w in each state are exponentially distributed

$$p(t_m) = k_{m\to w} e^{-k_{m\to w} t_m}, \tag{5.1}$$

$$p(t_w) = k_{w\to m} e^{-k_{w\to m} t_w}, \tag{5.2}$$

with means $1/k_{m\to w}$ and $1/k_{w\to m}$, which is in agreement to experiments [248]. In the context of active intracellular transport, the rate $k_{w\to m}$ determines the mean waiting time per arrest state, whereas the rate $k_{m\to w}$ is associated to the mesh size ℓ of the cytoskeleton, i.e. the mean distance between successive filament crossings, via $k_{m\to w}{=}v/\ell$ [Hafner2016, Hafner2018]. In general, both rates depend on the cytoskeleton architecture and the size of the cargo [29, 38]. Due to the inhomogeneity of the cytoskeleton, the transition rate

$$k_{m\to w}(r) = \begin{cases} k^i_{m\to w}, & \text{for } 0 \le r < R_\mathrm{m}{-}\delta, \\ k^p_{m\to w}, & \text{for } R_\mathrm{m}{-}\delta \le r \le R_\mathrm{m}, \end{cases} \tag{5.3}$$

generally depends on the current particle position $\boldsymbol{r}(r, \phi_r)$ which takes into account different mesh sizes in cell interior and periphery. For simplicity, the mean waiting time per arrest state $k_{w\to m}$ is assumed to be space-independent.

Intracellular cargo is reported to move either processively along the same track or switch to a crossing filament at intersection nodes [29, 33–38]. Therefore, after each waiting period, the model particle either continues to move along the previous direction with probability ω, reminiscent of the processivity of intracellular cargoes, or it changes its direction with probability $(1{-}\omega)$ according to a specific rotation angle α_rot [Hafner2016]. Note that this leads to a timescale $((1-\omega)k_{w\to m})^{-1}$ to change direction subsequent to a waiting state. With regard to the rotational symmetry of a cell, the new direction of the velocity $\boldsymbol{v}(v, \phi_v)$ is determined by a rotation angle α_rot which is chosen with respect to the radial direction of the current particle position $\boldsymbol{r}(r, \phi_r)$, i.e. $\phi_v = \phi_r + \alpha_\mathrm{rot}$ [Hafner2016, Hafner2018]. The new position is then determined by $\boldsymbol{r'}{=}\boldsymbol{r} + \boldsymbol{v}t_m$ according

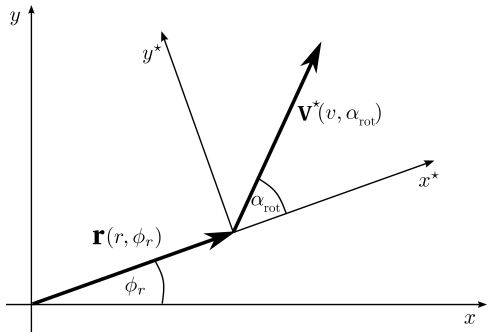

Figure 5.2.: Run-and-pause random walk on a spatially inhomogeneous and anisotropic cytoskeleton - the rotation angle. The velocity vector $\boldsymbol{v}^\star(v, \phi_v^\star)$ is defined via the rotation angle α_{rot} in a rotated coordinate system. Transformation between coordinate systems is conveyed by the rotation matrix M.

to the residence time of the particle in the motion state. Note that, as sketched in Fig. 5.2, the simple relation $\phi_v = \phi_r + \alpha_{\mathrm{rot}}$ only holds in the two-dimensional case

$$\boldsymbol{v} = M\boldsymbol{v}^\star = \begin{pmatrix} \cos\phi_r & -\sin\phi_r \\ \sin\phi_r & \cos\phi_r \end{pmatrix} \cdot v \begin{pmatrix} \cos\alpha_{\mathrm{rot}} \\ \sin\alpha_{\mathrm{rot}} \end{pmatrix} = v \begin{pmatrix} \cos(\phi_r{+}\alpha_{\mathrm{rot}}) \\ \sin(\phi_r{+}\alpha_{\mathrm{rot}}) \end{pmatrix} = v \begin{pmatrix} \cos\phi_v \\ \sin\phi_v \end{pmatrix} \quad (5.4)$$

but is more complex for motion in three-dimensional spheres. The rotation angle α_{rot} is drawn from a specific distribution which is shaped by the cytoskeleton architecture and takes into account the activity levels of the three motor species kinesin, dynein, and myosin [Hafner2016, Hafner2018]

$$f(\alpha_{\mathrm{rot}}) = \begin{cases} p_{\mathrm{antero}}\, f_{\mathrm{K}}(\alpha_{\mathrm{rot}}) + (1{-}p_{\mathrm{antero}})\, f_{\mathrm{D}}(\alpha_{\mathrm{rot}}), & \text{for } 0 < r < R_{\mathrm{m}}{-}\delta, \\ q_{\mathrm{K}}\, f_{\mathrm{K}}(\alpha_{\mathrm{rot}}) + q_{\mathrm{D}}\, f_{\mathrm{D}}(\alpha_{\mathrm{rot}}) + q_{\mathrm{M}}\, f_{\mathrm{M}}(\alpha_{\mathrm{rot}}), & \text{for } R_{\mathrm{m}}{-}\delta < r < R_{\mathrm{m}}, \end{cases} \quad (5.5)$$

with $q_{\mathrm{K}}{+}q_{\mathrm{D}}{+}q_{\mathrm{M}}{=}1$ and the current particle position $\boldsymbol{r}(r, \phi_r)$. The cytoskeleton polarity and the walking direction of the motors are considered by

$$f_{\mathrm{K}}(\alpha_{\mathrm{rot}}) = \delta(\alpha_{\mathrm{rot}}), \quad f_{\mathrm{D}}(\alpha_{\mathrm{rot}}) = \delta(\alpha_{\mathrm{rot}} - \pi), \quad f_{\mathrm{M}}(\alpha_{\mathrm{rot}}) = \frac{1}{2\pi}, \quad (5.6)$$

with $\alpha_{\mathrm{rot}} \in (-\pi; \pi]$. While microtubules are radial, actin filaments are assumed to be isotropically oriented. Which filament type is currently used is determined by the activity p_{antero} and q_i with $i \in \{\mathrm{K}, \mathrm{D}, \mathrm{M}\}$ in interior and periphery [Hafner2016, Hafner2018]. It describes in how much a given motor species contributes to the apparent motion of the cargo. The motor activity depends on the activity potential of the motor itself and the density of the corresponding filament type in its vicinity. Hence, activity levels are generally space-dependent. In the interior of the cell, the activity levels of kinesins and dyneins are represented by the probabilities p_{antero} and $(1{-}p_{\mathrm{antero}})$, respectively. In the periphery, the activity levels of kinesins, dyneins, and myosins are characterized by q_i with $i \in \{\mathrm{K}, \mathrm{D}, \mathrm{M}\}$. For instance if $q_{\mathrm{M}}{=}1$, motion in the cortex is solely managed by myosins on actin filaments.

Initially, the tracer particle is assumed to be in the motion state at position $\boldsymbol{r}(t{=}0) = \boldsymbol{r}_0$, which is either at the center ($r{=}0$) or uniformly distributed throughout the whole cell ($f(r_0){=}1/R_\mathrm{m}$, $f(\phi_{r_0}){=}1/(2\pi)$). The particle experiences confinement events [Hafner2016, Hafner2018]

- at the MTOC ($r{=}0$):
  After a waiting period defined by $((1{-}\omega)\, k_{w\to m})$, the particle chooses a uniformly random direction $\alpha_\mathrm{rot} \in (-\pi;\pi]$ if $p_\mathrm{antero} \neq 0$, otherwise the particle is stuck at the MTOC.

- at the inner border of the cortex ($r{=}R_\mathrm{m}{-}\delta$):
  If the particle is currently transported by kinesins or dyneins and $q_\mathrm{M} \neq 1$, it traverses the inner border on microtubules which extend into the periphery. Otherwise, it waits for a time period defined by $((1{-}\omega)\, k_{w\to m})$. After the pause, the particle is radially-inward transported by dyneins with probability $(1{-}p_\mathrm{antero})$, and with probability p_antero the particle selects a random direction into the periphery according to $f_{R_\mathrm{m}-\delta<r<R_\mathrm{m}}(\alpha_\mathrm{rot})$ but restricted to $\alpha_\mathrm{rot} \in (-\pi/2;\pi/2)$.

- at the membrane ($r{=}R_\mathrm{m}$):
  After a waiting period defined by $((1{-}\omega)\, k_{w\to m})$, the particle takes a random direction back into the periphery drawn from $f_{R_\mathrm{m}-\delta<r<R_\mathrm{m}}(\alpha_\mathrm{rot})$ but restricted to $\alpha_\mathrm{rot} \in (-\pi;-\pi/2) \cup (\pi/2;\pi]$.

Pauses at confinement events consider that filaments typically end there.

The random walk is terminated upon target detection [Hafner2016, Hafner2018]. In case of the narrow escape problem, the target is a small opening of angle α_exit on the plasma membrane, as illustrated in Fig. 5.1, b. For the reaction problem, two different detection modes are considered: reaction either occurs by encounter of searcher and target particle $|\boldsymbol{r}^\mathrm{S}{-}\boldsymbol{r}^\mathrm{T}|{=}R_\mathrm{d}$ regardless of their current motility states, or it is only possible if both particles are in the waiting state. Note that only the latter detection mode constitutes an intermittent search strategy. In either way, reaction takes place instantaneously at detection radius R_d. In case of the reaction-escape problem, searcher and target first have to pair, before the product particle is stochastically transported to the escape zone on the membrane. Note that the exit on the membrane is only absorbing for the product particle, whereas searcher and target particles experience scattering boundaries. A schematic trajectory is sketched in Fig. 5.1, c.

A certain combination of transition rates $k_{m\to w}$ and $k_{w\to m}$, processivity ω, and turning angle distribution $f(\alpha_\mathrm{rot})$, given in Eq. 5.5, defines a specific search strategy which is generally inhomogeneous and anisotropic [Hafner2016, Hafner2018]. A homogeneous search strategy is recovered for $\delta{=}R_\mathrm{m}$. Table 5.1 summarizes the model parameters and their biological interpretation. If not stated otherwise, in order to reduce parameter space we use rescaled, dimensionless coordinates and parameters

$$\boldsymbol{r} \mapsto \boldsymbol{r}/R_\mathrm{m}, \quad t \mapsto vt/R_\mathrm{m}, \quad k_{m\to w} \mapsto R_\mathrm{m}k_{m\to w}/v, \quad k_{w\to m} \mapsto R_\mathrm{m}k_{w\to m}/v. \tag{5.7}$$

Table 5.1.: Run-and-pause random walk on a spatially inhomogeneous and anisotropic cytoskeleton - model parameters and biological interpretation.

Model parameter	biological interpretation
R_{m}	radius of the cell
δ	thickness of the actin cortex
α_{exit}	opening angle of the exit zone on the membrane
R_{d}	detection distance, i.e. sum of radii of searcher and target
$k_{w\to m}$	associated with the mesh size of the cytoskeleton
$k_{w\to m}$	mean waiting time per filament crossing
v	effective speed of the cargo on the cytoskeleton
ω	processivity of the cargo at filament crossings
$f(\alpha_{\mathrm{rot}})$	cytoskeleton structure
p_{antero}, q_i	motor activity levels

5.2.2. Monte Carlo simulation

With the aid of Monte Carlo simulations, we measure the efficiency of a specific search strategy in terms of the MFPT to target detection. We use an event-driven algorithm, as sketched in the Appendix A.2, to generate the stochastic process and derive the MFPT by ensemble averaging over at least 10^6 independent realizations of the walk [Hafner2016, Hafner2018].

In the following, we analyze the dependence of the MFPT on the key parameters of the model: the spatial cytoskeleton architecture, the motor activities, and the frequencies of arrest states. We monitor the MFPT as a function of the model parameters to identify optimal search strategies.

5.3. Narrow escape problem

In this section, we study the narrow escape problem. A tracer particle which is initially either uniformly distributed throughout the cell, or located at the cell center is stochastically propagated until it detects a small window on the boundary of the domain. A prominent example is directed secretion by T cells where toxic granules are actively transported and exclusively released at the synapse [2, 8–14]. With the aid of Monte Carlo simulations we analyze how the interplay between cytoskeleton organization, motor activity, and frequent pausing of the cargo effects the efficiency of the narrow escape problem [Hafner2016, Hafner2018]. We first focus on homogeneous search strategies and then point out the crucial impact of the cytoskeleton inhomogeneity.

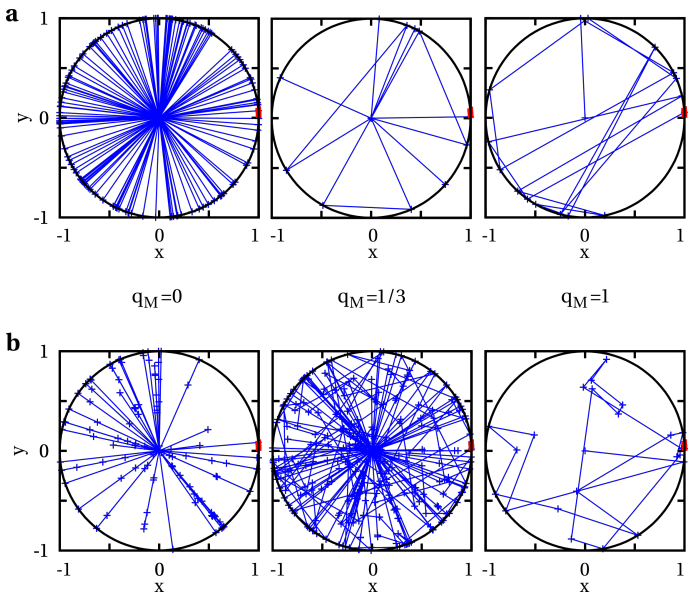

Figure 5.3.: The narrow escape problem on a homogeneous cytoskeleton - trajectories. Sample trajectories (blue lines) of a tracer particle which is initially located at the cell center and searches for a window of arclength α_{exit}=0.1 on the membrane are shown for a homogeneous cytoskeleton architecture with δ=1. The trajectories reflect the motor activity q_{M}, q_{K}=q_{D}=(1−q_{M})/2. Network intersections at which the particle changes its direction (ω=0) are represented by blue crosses and occur on scales defined by (**a**) $k_{m\to w}$=0, and (**b**) $k_{m\to w}$=1. The waiting rate $k_{w\to m}$=∞ is not visualized. Reprint of [Hafner2016], Physical Biology, 13, 066003, 2016, (`http://dx.doi.org/10.1088/1478-3975/13/6/066003`).

5.3.1. Homogeneous search strategies

Here, we fix δ=1 and assume that the cytoskeleton is homogeneously distributed within the cell according to

$$f_{1-\delta<r<1}(\alpha_{\text{rot}}) = q_{\text{K}}\,\delta(\alpha_{\text{rot}}) + q_{\text{D}}\,\delta(\alpha_{\text{rot}}-\pi) + q_{\text{M}}\,\frac{1}{2\pi}. \tag{5.8}$$

A tracer particle reaches filament crossings at rate $k_{m\to w}$. At each crossing it waits for a time period defined by $k_{w\to m}$ and unexceptionally changes its direction, since ω=0.

Trajectories

Figure 5.3 displays sample trajectories for different motor activities q_{M}, q_{K}, and q_{D}, and network mesh sizes $k_{m\to w}$ [Hafner2016]. For simplicity, we assume equal activities of kinesins and dyneins, i.e. q_{K}=q_{D}=(1−q_{M})/2. Particles start at the cell center r_0=0 and search for a narrow escape of arclength α_{exit}=0.1. The trajectories reflect the interplay between cytoskeleton architecture and motor activity [Hafner2016]. While a high activity of myosins by q_{M}=1 leads to isotropic transport, the motion is determined by a radial aster of microtubules for q_{M}=0. Intermediate values correspond to motion on a mixture of random actin filaments and radial microtubules.

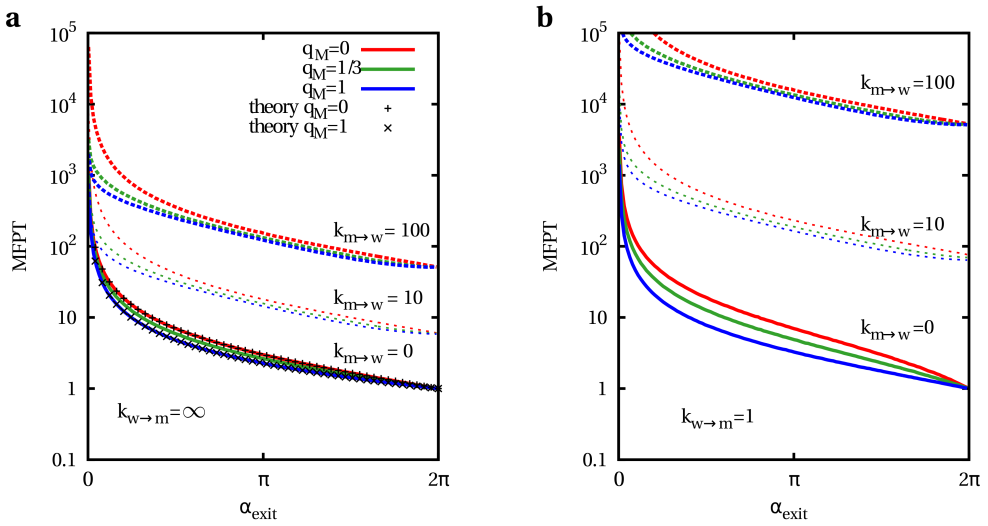

Figure 5.4.: The narrow escape problem on a homogeneous cytoskeleton - impact of the motor activity. The MFPT is measured as a function of the target size α_{exit} for particles which are initially located at the center of the cell and move along a homogeneous cytoskeleton with different motor activities q_{M}, q_{K}=q_{D}=$(1-q_{\text{M}})/2$. Various values of the transition rates $k_{m\to w}$ are applied for (**a**) $k_{w\to m}$=∞ and (**b**) $k_{w\to m}$=1. For $k_{m\to w}$=0 and $k_{w\to m}$=∞, the simulation results (lines) are compared to analytic results (symbols), given in Eq. 5.9 and 5.11, respectively. Figure a is a modification of [Hafner2016], Physical Biology, 13, 066003, 2016, (`http://dx.doi.org/10.1088/1478-3975/13/6/066003`).

Impact of the motor activity

Keeping the sample trajectories in mind, we study the influence of the motor activity q_{M} and the target size α_{exit} on the MFPT of searchers which are initially located at the center of the cell r_0=0 [Hafner2016]. In Fig. 5.4, the MFPT is plotted as a function of α_{exit} for various values of the transition rates $k_{m\to w}$ and $k_{w\to m}$, and diverse probabilities q_{M}, q_{K}=q_{D}=$(1-q_{\text{M}})/2$ [Hafner2016]. As expected, the MFPT monotonically decreased with increasing target size α_{exit} and diverges in the limit $\alpha_{\text{exit}} \to 0$. Directional changes in the bulk with $k_{m\to w} \neq 0$, as well as the introduction of arrest states by $k_{w\to m} \neq \infty$ do not improve the search efficiency. The MFPT increases for increasing $k_{m\to w}$ and decreasing $k_{w\to m}$. Remarkably, we find that transport on an isotropic cytoskeleton with q_{M}=1 is favorable to $q_{\text{M}} \neq 1$. Consequently, we will focus on a high activity of myosin motors with q_{M}=1 in the following.

The results can be analytically verified for $k_{m\to w}$=0 and $k_{w\to m}$=∞. In that case, the particle only changes its direction at confinements events. By assumption that consecutive collision positions at the membrane are independent random numbers (Bernoulli process), the escape window is detected with probability $P = \alpha_{\text{exit}}/(2\pi)$ per collision and on average $1/P$ collisions are necessary for target detection. In the case of a radial microtubule network, i.e. $q_{\text{M}} = 0$, the time lapse between successive collisions with the

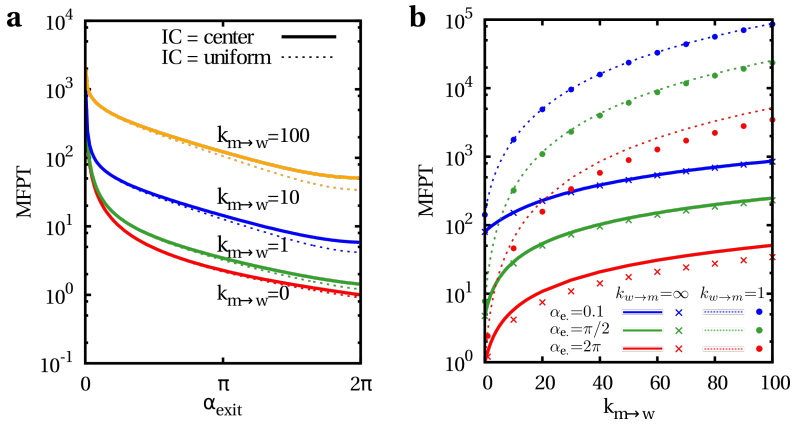

Figure 5.5.: The narrow escape problem on a homogeneous cytoskeleton - impact of the initial condition. (**a**) The MFPT is shown as a function of the target size α_{exit} for various transition rates $k_{m\to w}$ and $k_{w\to m}=\infty$ on an isotropic network with $q_{\text{M}}=1$. Two different initial conditions are applied: the particle is either initially located at the cell center (solid lines) or it is uniformly distributed throughout the cell (dashed lines). (**b**) The MFPT is measured in dependence of the transition rate $k_{m\to w}$ for diverse target sizes α_{exit}, rates $k_{w\to m}$, and centered initial condition (lines) or uniform initial condition (symbols). Reprint of [Hafner2018], Biophysical Journal, 114, 1420-1432, 2018, (`http://dx.doi.org/10.1016/j.bpj.2018.01.042`).

membrane is $\langle \Delta t \rangle = 2R_{\text{m}}/v$, such that the MFPT yields

$$\text{MFPT}_{[q_{\text{M}}=0]} = \left(\frac{2\pi}{\alpha_{\text{exit}}} - 1\right)\frac{2R_{\text{m}}}{v} + \frac{R_{\text{m}}}{v}, \tag{5.9}$$

where it is taken into account that the last interval to target detection only takes $\langle \Delta t \rangle/2$. In the case of isotropic motion on a uniformly random actin network with $q_{\text{M}} = 1$, the time lapse between successive collisions can be calculated by the law of cosines $R_{\text{m}}^2 = R_{\text{m}}^2 + l^2 - 2R_{\text{m}} l \cos\gamma$, such that

$$\langle \Delta t \rangle = \frac{\langle l \rangle}{v} = \frac{1}{v}\int_{-\pi/2}^{\pi/2} \mathrm{d}\gamma \frac{1}{\pi} 2R_{\text{m}} \cos(\gamma) = \frac{4R_{\text{m}}}{\pi v} \tag{5.10}$$

where l denotes the distance between consecutive collision positions. Thus, the MFPT is given by

$$\text{MFPT}_{[q_{\text{M}}=1]} = \left(\frac{2\pi}{\alpha_{\text{exit}}} - 1\right)\frac{4R_{\text{m}}}{\pi v} + \frac{R_{\text{m}}}{v}, \tag{5.11}$$

because the first time to collision only takes R_{m}/v due to the centered initial position of the particle. The analytic results are in perfect agreement to simulation results, as shown in Fig. 5.4, a.

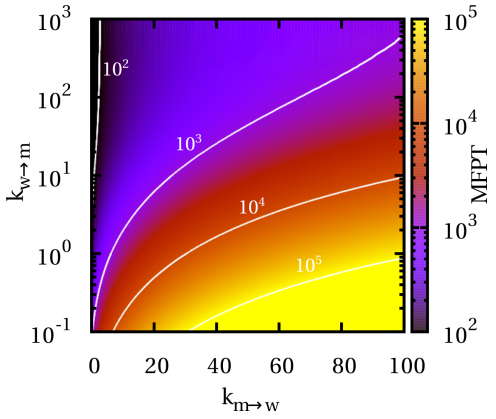

Figure 5.6.: The narrow escape problem on a homogeneous cytoskeleton - optimal transition rates. The MFPT is mapped as a function of the transition rates $k_{m\to w}$ and $k_{w\to m}$ for α_{exit}=0.1, centered initial condition, and isotropic cytoskeleton with q_{M}=1. Reprint of [Hafner2018], Biophysical Journal, 114, 1420-1432, 2018, (`http://dx.doi.org/10.1016/j.bpj.2018.01.042`).

Impact of the initial condition

So far, we focused on particles which are initially located at the center of the cell r_0=0. In Fig. 5.5, we study the impact of the initial condition on the homogeneous, isotropic (q_{M}=1) narrow escape problem [Hafner2018]. We distinguish between two initial positions: (i) the particle starts at the center of the cell, i.e. r_0=0, and (ii) the particle is initially uniformly distributed within the cell, i.e. $f(r_0)$=$1/R_{\text{m}}$, $f(\phi_{r_0})$=$1/(2\pi)$. According to Fig. 5.5, a, the uniform initial condition is slightly advantageous for large target sizes $\alpha_{\text{exit}} \approx 2\pi$ [Hafner2018]. The larger the target, the more likely is a detection at the first collision with the membrane and accordingly the initial condition has a strong impact on the MFPT. Uniformly distributed initial positions are beneficial as the particle is on average closer to the membrane than for the centered initial condition. In contrast, for small escapes zones α_{exit} the initial condition becomes gradually irrelevant. The smaller the target, the more collisions with the membrane are necessary for target detection and consequently the impact of the initial condition vanishes [Hafner2018]. This is also valid when pauses are involved, as shown by Fig. 5.5, b.

Optimal transition rates

In order to identify the optimal search strategy to a narrow escape in the case of a homogeneous cytoskeleton, we measure the MFPT as a function of the transition rates $k_{m\to w}$ and $k_{w\to m}$ for q_{M}=1, as shown in Fig. 5.6 [Hafner2018]. The particle is initially located at the center of the cell, but as discussed the impact of the initial condition is negligible for target sizes as small as α_{exit}=0.1. Apparently, an uninterrupted motion pattern with $k^{\text{opt}}_{m\to w}$=0 and $k^{\text{opt}}_{w\to m}$=∞ is optimal for the detection of narrow escapes when the tracer particle is transported along a homogeneous cytoskeleton [Hafner2018], as already indicated by Fig. 5.4 and 5.5.

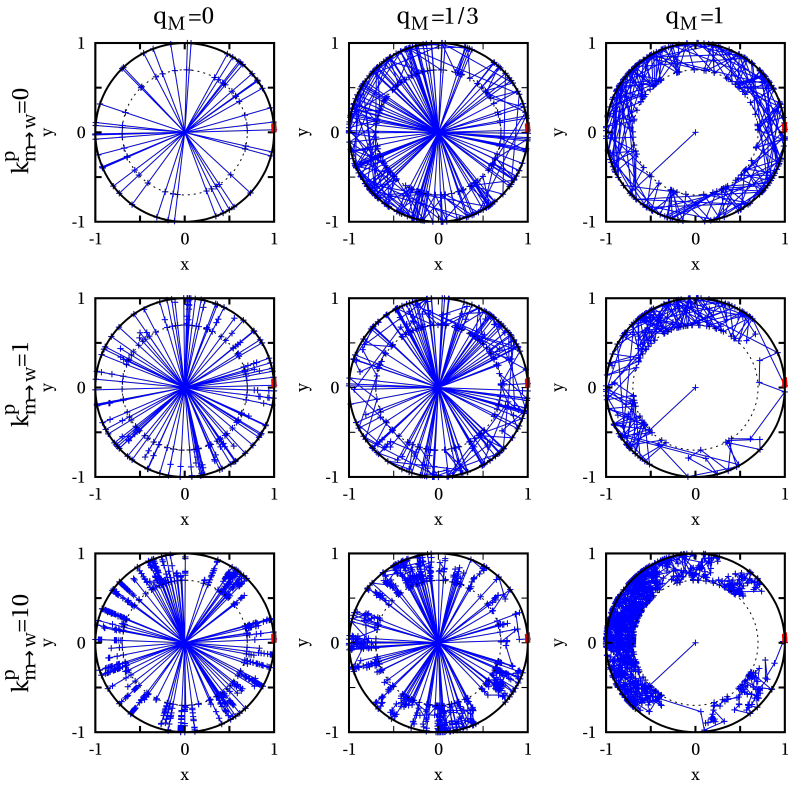

Figure 5.7.: The narrow escape problem on an inhomogeneous cytoskeleton - trajectories. Sample trajectories (blue lines) are shown for a tracer particle which is initially located at the center of the cell and searches for an opening of arclength α_{exit}=0.1 (red zone). The cytoskeleton is inhomogeneous, as defined by δ=0.3. The motion on the cortical network is characterized by various transition rates $k^p_{m\to w}$, and motor activities q_{M}, q_{K}=q_{D}=(1−q_{M})/2. The particle moves uninterruptedly in the interior by $k^i_{m\to w}$=0 and changes its direction at the MTOC. Otherwise $k_{w\to m}$=∞, ω=0, and p_{antero}=1 are applied. Partial reprint of [Hafner2016], Physical Biology, 13, 066003, 2016, (`http://dx.doi.org/10.1088/1478-3975/13/6/066003`).

5.3.2. Inhomogeneous search strategies

In the previous section, we optimized the narrow escape problem for a homogeneous cytoskeleton architecture with δ=1 and found that q_{M}=1, $k^{\text{opt}}_{m\to w}$=0, and $k^{\text{opt}}_{w\to m}$=∞ are beneficial. But in general the cytoskeleton is spatially inhomogeneous, as defined in Eq. 5.5. Here, we address the impact of the spatial inhomogeneity of the cytoskeleton, i.e. $\delta \in (0;1)$, on the search efficiency of the narrow escape problem.

Trajectories

Inhomogeneous search strategies are characterized by a well-defined width $\delta \in (0;1)$ of the actin cortex, as given in Eq. 5.5. The interplay between inhomogeneous cytoskeleton, motor activity, and motility transitions is manifested by the trajectories of intracellular cargoes plotted in Fig. 5.7 [Hafner2016]. The actin cortex is fixed to δ=0.3 and the

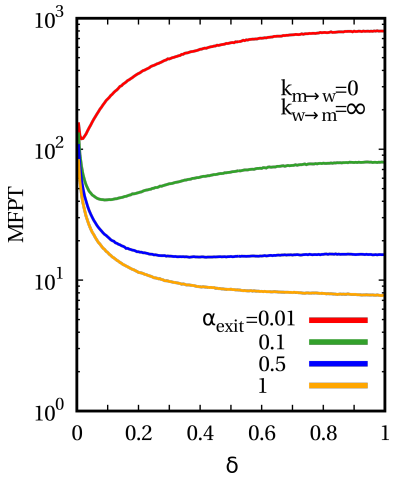

Figure 5.8.: The narrow escape problem on an inhomogeneous cytoskeleton - impact of the cortex width. The MFPT is plotted as a function of the cortex width δ for various target sizes α_{exit}. As a reference case, the following parameters are applied: $k_{m\to w}$=0, $k_{w\to m}$=∞, q_{M}=1, p_{antero}=1, and ω=0.

particle is initially located at the center of the cell. The motion along the cortical network is characterized by various transition rates $k^p_{m\to w}$ and motor activities q_{M}, q_{K}=q_{D}=(1−q_{M})/2. Directional changes occur instantaneously at each filament crossing, i.e. ω=0, $k_{w\to m}$=∞. For instance, in the case of $k^p_{m\to w}$=0 the particle is reoriented only at confinement events, whereas it frequently changes its direction in the bulk of the cortex for $k^p_{m\to w} \neq 0$. In the interior, the tracer moves uninterruptedly by $k^i_{m\to w}$=0 and changes its direction only at the MTOC. Since p_{antero}=1, transitions from periphery to interior are only possible via dyneins moving on microtubules which extend into the periphery for $q_{\text{M}} \neq 1$. According to Fig. 5.7, diverse motor activities q_{M} in the cortex drastically change the exploration of space [Hafner2016]. For q_{M}=1, motion is isotropic and restricted to the cortex as soon as it is reached. In contrast, transport in the periphery is also radially oriented for q_{M}=0 and intermediate values of $q_{\text{M}} \in (0;1)$ lead to a mixture of microtubules and actin filaments.

Impact of the cortex width

At first, we investigate the MFPT as a function of the cortex width δ for the reference case q_{M}=1, p_{antero}=1, ω=0, $k_{m\to w}$=0 and $k_{w\to m}$=∞. In Fig. 5.8 the MFPT is plotted in dependence of δ for various target sizes α_{exit}. Remarkably, for small targets α_{exit} the MFPT exhibits a non-trivial minimum at $\delta \in (0;1)$ which becomes more pronounced as the target size decreases. Hence, an inhomogeneous cytoskeleton is beneficial in the case of narrow escapes on the cell membrane and can improve the search by several orders of magnitude. In contrast, a homogeneous strategy with δ=1 is most efficient for large targets. In the following, we focus on small exit zones α_{exit}=0.1 which constitute only 1.59% of the total cell circumference [Hafner2016, Hafner2018].

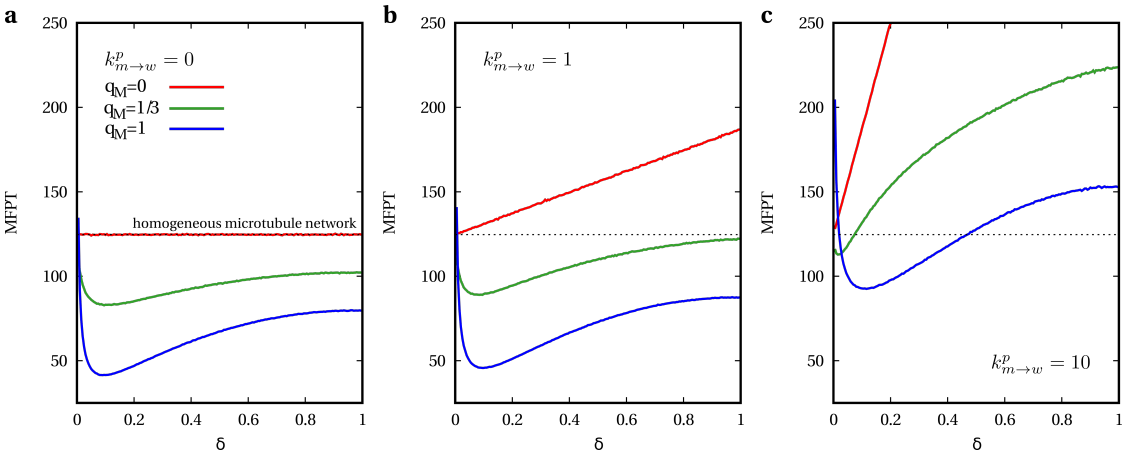

Figure 5.9.: The narrow escape problem on an inhomogeneous cytoskeleton - impact of the motor activity I. The MFPT is measured as a function of the cortex width δ for various motor activities $q_M \in \{0; 1/3; 1\}$, $q_K{=}q_D{=}(1{-}q_M)/2$, and $p_{antero}{=}1$. (**a-c**) Inhomogeneous transition rates $k^p_{m\to w} \in \{0; 1; 10\}$ and $k^i_{m\to w}{=}0$ are considered for detection of a target $\alpha_{exit}{=}0.1$. Waiting times and processivity are neglected, i.e. $k_{w\to m}{=}\infty$, $\omega{=}0$. The dashed black line corresponds to a homogeneous search strategy on radial microtubule network, i.e. $\delta{=}0$. Reprint of [Hafner2016], Physical Biology, 13, 066003, 2016, (`http://dx.doi.org/10.1088/1478-3975/13/6/066003`).

In order to analyze the influence of the cytoskeleton architecture, the motor activity, and the cargo's arrests states on the search efficiency to narrow escapes, we measure the MFPT as a function of the cortex width δ for various motor activities q_M and p_{antero}, processivities ω, and transition rates $k_{m\to w}(r)$ and $k_{w\to m}$, in what follows. In either way, the particle starts at the center of the cell. But as discussed, our conclusions are largely independent of the particle's initial condition.

Impact of the motor activity

Here, we address the impact of various motor activities q_M, $q_K{=}q_D{=}(1{-}q_M)/2$ in the periphery and p_{antero} in the interior of the cell on the efficiency of the narrow escape problem [Hafner2016, Hafner2018].

First, we consider the most general case of spatially inhomogeneous motor activities, i.e. p_{antero} in interior and q_M, $q_K{=}q_D{=}(1{-}q_M)/2$ in periphery, and spatially inhomogeneous mesh sizes, i.e. $k^i_{m\to w}$ in interior and $k^p_{m\to w}$ in periphery [Hafner2016]. Since radial microtubules manage rapid long-range transport [2, 16], we focus on $k^i_{m\to w}{=}0$. This is the fastest relocation in the cell interior which leads to a change in radial direction at the MTOC. We further neglect the processivity, i.e. $\omega{=}0$, as well as arrest states, i.e. $k_{w\to m}{=}\infty$. Hence, the cargo changes its direction instantaneously at each filament crossing. In order to separately study the effect of the peripheral motor activity q_M, we choose $p_{antero}{=}1$ in Fig. 5.9. Hence, as soon as the particle reaches the cortex, excursions back to the interior are only possible via dyneins for $q_M \neq 1$, compare to the sample

trajectories in Fig. 5.7. Figure 5.9 displays the MFPT as a function of the cortex width δ for various transition rates $k^p_{m\to w}$ and motor activities q_{M} [Hafner2016]. Remarkably, the optimization of the MFPT as a function of the cortex width $\delta \in (0;1)$ is largely robust against alterations in transitions rates and motor activity q_{M} [Hafner2016, Hafner2018]. An inhomogeneous search strategy improves the search efficiency by several orders of magnitude in comparison to the two homogeneous limits δ=1 and δ=0. The minimum of the MFPT at a thin cortex $\delta \in (0;1)$ vanishes for q_{M}=0, but is most pronounced for q_{M}=1, i.e. when motion is restricted to a cortex which is dominated by the action of myosins on random actin filaments [Hafner2016]. For q_{M}=0 the MFPT is generally minimal for δ=0, because the motion is handled solely by kinesins and dyneins on radial microtubules [Hafner2016]. In that case, the inhomogeneity defined by δ is entirely manifested by a change in the mesh size between cortex and interior. However, the inhomogeneity in mesh size vanishes for $k^p_{m\to w}$=$k^i_{m\to w}$=0, such that the MFPT is constant in Fig. 5.9, a. In contrast, for $k^p_{m\to w} \neq k^i_{m\to w}$=0 the cargo performs a local back-and-forth motion in the cortex on a lengthscale $v/k^p_{m\to w}$. Consequently, target detection is hindered with increasing cortex width δ, as shown in Fig. 5.9, b and c. With increasing δ, it becomes more and more unlikely that the particle either reaches the membrane or the MTOC to change its radial direction which is necessary for target detection [Hafner2016]. Figure 5.9 further indicates that a high activity of myosins q_{M}=1 is favorable for the narrow escape problem [Hafner2016]. Apparently, the search efficiency does not benefit from any relocation along the internal microtubule network for $q_{\mathrm{M}} \neq 1$; even not for the here studied fastest possible relocation determined by $k^i_{m\to w}$=0. Instead, an optimal search strategy is characterized by the restriction of transport to a thin actin cortex without frequent interference by microtubules. Hence from now on, we neglect the inhomogeneity of the mesh size as defined by Eq. 5.3 and focus on transition rates

$$k_{m\to w}(r) = k_{m\to w}$$

which are constant throughout the cell. We further assume that the cortex is dominated by actin filaments, such that Eq. 5.5 is simplified to

$$f(\alpha_{\mathrm{rot}}) = \begin{cases} p_{\mathrm{antero}}\,\delta(\alpha_{\mathrm{rot}}) + (1-p_{\mathrm{antero}})\,\delta(\alpha_{\mathrm{rot}}-\pi), & \text{for } 0 < r < R_{\mathrm{m}}-\delta, \\ 1/(2\pi), & \text{for } R_{\mathrm{m}}-\delta < r < R_{\mathrm{m}}. \end{cases} \tag{5.12}$$

Within that model, we study the impact of the kinesin motor activity p_{antero} [Hafner2018]. For instance p_{antero}=1 denotes a high activity of kinesins, such that particles are transported from the cell interior to the periphery and stay in the cortex as soon as it is reached. In contrast, p_{antero}=0 takes into account a high activity of dyneins, such that cargoes are likely to get stuck at the MTOC sooner or later. A frequent exchange between interior and periphery is only possible for intermediate values of p_{antero}, as manifested by the sample trajectories in Fig. 5.10. Figure 5.10 shows that small values of p_{antero}, for which the particle is mainly moving in the interior of the cell, are highly deficient [Hafner2018]. They hinder the detection of a target which is located on the membrane. In contrast, the MFPT exhibits a pronounced minimum at $\delta \in (0;1)$ for p_{antero}=1. Furthermore, Fig. 5.10 displays that the MFPT increases with increasing transition rate $k_{m\to w}$. Hence, directional changes in the bulk are disadvantageous and the optimal transition rates are given by $k^{\mathrm{opt}}_{m\to w}$=0 and $k^{\mathrm{opt}}_{w\to w}$=$\infty$ [Hafner2018]. Waiting times increase the MFPT, as discussed below.

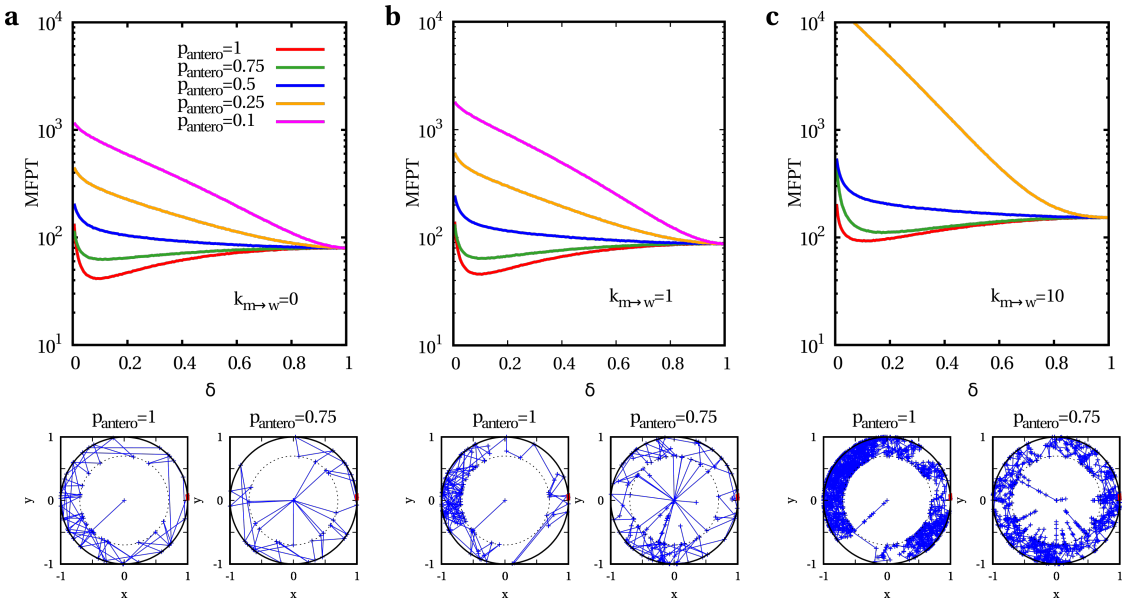

Figure 5.10.: The narrow escape problem on an inhomogeneous cytoskeleton - impact of the motor activity II. The MFPT is shown versus the cortex width δ for diverse motor activities p_{antero}, and transition rates (**a**) $k_{m\to w}$=0, (**b**) $k_{m\to w}$=1, and (**c**) $k_{m\to w}$=10. Apart from that $k_{w\to m}$=∞, ω=0, and α_{exit}=0.1 are applied. Sample trajectories (blue lines) are given for δ=0.3. The target is shown as the red zone on the membrane. Blue crosses indicate directional changes at filament crossings. The motor activity p_{antero} determines the frequency of excursions in the interior of the cell, which hinder the detection of narrow escapes on the membrane. Figures a and b are reprints of [Hafner2018], Biophysical Journal, 114, 1420-1432, 2018, (`http://dx.doi.org/10.1016/j.bpj.2018.01.042`).

Optimal cortex width and motor activity

In order to determine the best search strategy for narrow escapes, we apply the optimal transition rates $k^{\text{opt}}_{m\to w}$=0 and $k^{\text{opt}}_{w\to m}$=∞ and map the MFPT in dependence of the cortex width δ and the motor activity p_{antero}, as shown in Fig. 5.11. The MFPT displays a global minimum at roughly δ=0.1 and p_{antero}=1 [Hafner2018]. In essence, the search efficiency to narrow escapes on spherical domains is optimized by an uninterrupted motion pattern ($k_{m\to w}$=0, $k_{w\to m}$=∞) which is restricted to a thin cortex ($\delta \in (0;1)$, p_{antero}=1). Inhomogeneous search strategies are generally more efficient than the homogeneous counterparts. Confining the motion to a thin cortex is beneficial, because it downsizes the search domain and prohibits excursions to the cell interior where the target is not located [Hafner2016, Hafner2018]. Consequently, reducing the cortex width provisionally decreases the MFPT. However, the cortex must not bee too thin either. As evident from Fig. 5.8, 5.9, and 5.10, the MFPT diverges in the limit of $\delta \to 0$ [Hafner2016,Hafner2018]. Target detection is drastically slowed down for particles of the ensemble which initially reach the cortex at a polar angle far from the exit window. Especially those which reach the cortex at the pole opposite to the target will need very long to reach the escape zone. A very narrow cortex increases the lateral distance to the target, while at the

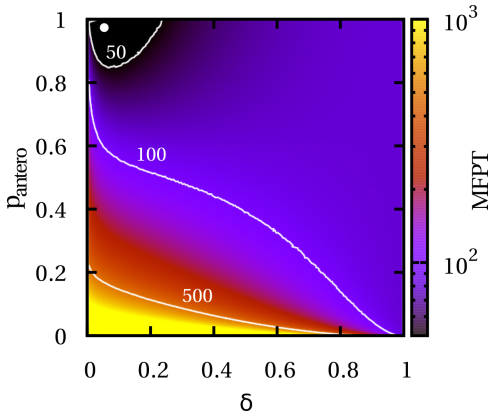

Figure 5.11.: The narrow escape problem on an inhomogeneous cytoskeleton - optimal cortex width and motor activity. The MFPT is mapped in the δ-p_{antero}-plane for $k^{\text{opt}}_{m\to w}$=0, $k^{\text{opt}}_{w\to m}$=∞, ω=0, centered initial condition, and α_{exit}=0.1. Reprint of [Hafner2018], Biophysical Journal, 114, 1420-1432, 2018, (`http://dx.doi.org/10.1016/j.bpj.2018.01.042`).

same time decreases the lateral diffusion of the walker by frequent confinement events with the two borders of the cortex. Such rare events are manifested by the probability density function of first passage times (FPT) [Hafner2018]. Figure 5.12 shows that the density is far from being exponential and the statistics are thus not fully covered by the MFPT. Instead a power-law is observed at intermediate timescales, as expected for Brownian search processes on bounded domains [251, 252]. Decreasing the cortex width δ significantly broadens the intermediate power-law regime [Hafner2018].

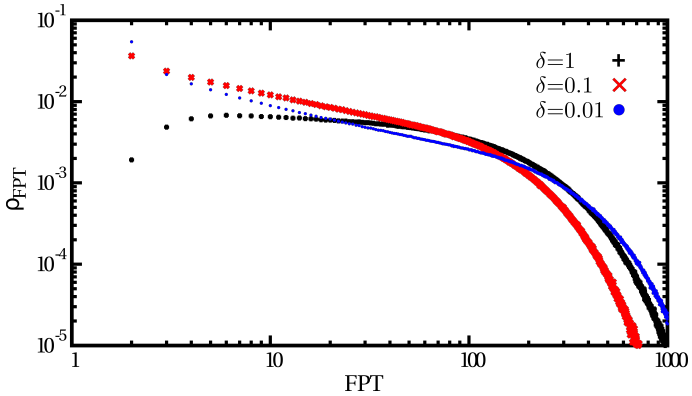

Figure 5.12.: The narrow escape problem on an inhomogeneous cytoskeleton - FPT distribution. The probability density function ρ_{FPT} of FPT to a narrow escape of size α_{exit}=0.1 is plotted for various cortex widths δ, $k_{m\to w}$=10, $k_{w\to m}$=∞, p_{antero}=1, and centered initial condition. Modification of [Hafner2018], Biophysical Journal, 114, 1420-1432, 2018, (`http://dx.doi.org/10.1016/j.bpj.2018.01.042`).

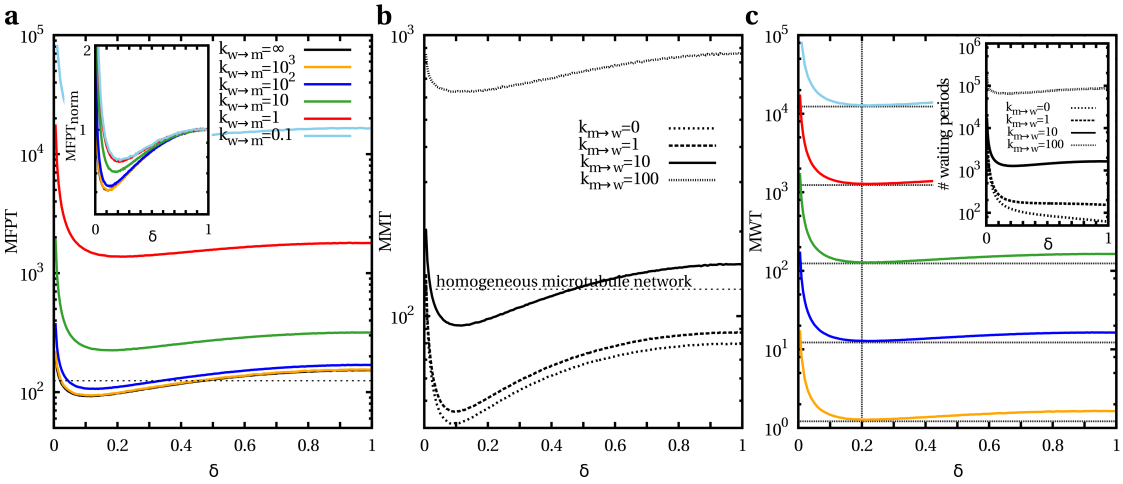

Figure 5.13.: The narrow escape problem on an inhomogeneous cytoskeleton - impact of arrest states. (**a**) The MFPT is plotted as a function of the cortex width δ for $k_{m\to w}$=10 and various $k_{w\to m}$. Otherwise p_{antero}=1, ω=0, and α_{exit}=0.1 are applied. The inset shows the MFPT normalized to $\text{MFPT}_{\text{norm}}$=MFPT/MFPT($\delta$=1). (**b**) The MMT versus δ is shown for diverse transition rates $k_{m\to w}$, p_{antero}=1, ω=0, and α_{exit}=0.1. It is independent of $k_{w\to m}$. (**c**) The MWT is given in dependence of δ for the same parameters as in (a). The inset displays the mean number of waiting periods which only depends on the mesh size of the cytoskeleton $k_{m\to w}$. Reprint of [Hafner2016], Physical Biology, 13, 066003, 2016, (`http://dx.doi.org/10.1088/1478-3975/13/6/066003`).

Impact of arrest states

Recapitulating, the search efficiency to narrow escapes can be significantly improved by spatially inhomogeneous cytoskeletal structures, $\delta \in (0;1)$. The optimal choice of parameters, $k_{m\to w}$=0, $k_{w\to m}$=∞, p_{antero}=1, $\delta \in (0;1)$, indicates that a restriction of cargo motion to a thin cortex is beneficial. But so far, we mainly neglected arrest states and assumed that waiting states at filament crossings are instantaneously left with rate $k_{w\to m}$=∞. Here, we systematically investigate how the duration of arrest states effects the search efficiency to narrow escapes on the plasma membrane. We ask to what extent inhomogeneous search strategies are still favorable for non-optimal transition rates $k_{m\to w} \neq 0$, $k_{w\to m} \neq \infty$ [Hafner2016]. In order to separate the effect of the transition rates on the search efficiency, we fix the other model parameters to p_{antero}=1, ω=0, and α_{exit}=0.1.

In Fig. 5.13, a, the MFPT is plotted as a function of the cortex width δ for $k_{m\to w}$=10 and various values of $k_{w\to m}$ [Hafner2016]. As expected, a decrease of the transition rate $k_{w\to m}$, i.e. a longer mean waiting time per arrest state, leads to an increase of the MFPT. Remarkably, the optimal value of the cortex width δ^{opt} is shifted, as displayed in the inset of Fig. 5.13, a, by normalization to $\text{MFPT}_{\text{norm}}$=MFPT/MFPT($\delta$=1) [Hafner2016].

The origin of that shift can obviously be traced back to an enhanced impact of arrests in the particle's trajectory. The MFPT can be divided into the total mean motion time (MMT) and the total mean waiting time (MWT) a particle experiences on average until target detection [Hafner2016]. Since each arrest state exhibits the same mean waiting time $1/k_{w\to m}$, it is

$$\mathrm{MFPT} = \mathrm{MMT} + \mathrm{MWT} = \mathrm{MMT} + \#\,\text{waiting periods}/k_{w\to m}, \tag{5.13}$$

where (# waiting periods) denotes the mean number of arrest states which occur until target detection [Hafner2016]. Accordingly, the contribution of the MMT and the MWT to the MFPT can be studied separately.

In the limit $k_{w\to m}{=}\infty$ the MFPT is fully determined by the MMT [Hafner2016]. Figure 5.13, b, shows that the MMT exhibits a minimum as a function of the inhomogeneity δ which is highly robust against changes of the transition rate $k_{m\to w}$ and is of course independent of $k_{w\to m}$ [Hafner2016].

Contrarily, in the limit of $k_{w\to m} \to 0$ the MFPT is dominated by the MWT [Hafner2016]. The MWT depends on both transition rates $k_{m\to w}$, which defines the mean number of filament crossings and thus the mean number of arrest states (# waiting periods), and $k_{w\to m}$, which defines the mean waiting time per arrest state. Figure 5.13, c, displays that the rate $k_{w\to m}$ does only contribute multiplicatively to the MWT, in agreement to Eq. 5.13. Furthermore, the (# waiting periods) does only depend on the transition rate $k_{m\to w}$. Remarkably, the inset of Fig. 5.13, c, shows that the (# waiting periods) can also be minimized as a function of the cortex width δ. The occurrence of the minimum is largely robust against alterations of $k_{m\to w}$; the only exception is $k_{m\to w}{=}0$. In all other cases, the MFPT is optimized by an inhomogeneous cytoskeleton even in the limit of very long pauses during the search process [Hafner2016].

With that we can understand the shift of the optimal width δ^{opt} in Fig. 5.13, a, as follows [Hafner2016]. Focus on the behavior of the MMT and the MWT for $k_{m\to w}{=}10$. While the MMT displays a minimum at about $\delta{=}0.1$, see Fig. 5.13, b, the MWT exhibits a minimum at approximately $\delta{=}0.2$, see Fig. 5.13, c. Accordingly, the MFPT experiences a shift of the optimal cortex width from $\delta^{\mathrm{opt}}{=}0.1$ to $\delta^{\mathrm{opt}}{=}0.2$ with decreasing rate $k_{w\to m}$, i.e. increasing the mean waiting time per arrest state.

To conclude, the occurrence of a minimal MFPT as a function of the cortex width is very robust against stochastic transitions between the two studied motility states. An inhomogeneous cytoskeleton constitutes the most efficient search strategy also in the limit of very long pauses during the search process. This is biologically relevant since the mean waiting time per arrest state is reported to be of the order of seconds [29,146,152].

Impact of the processivity

So far, we assumed that the particle changes its direction at each filament crossing. But cargo is reported to also be able to overcome intersections [29, 33–38]. Here, we investigate the impact of the processivity ω on the search efficiency to narrow escapes [Hafner2016]. For that purpose we fix the motor activity to the preferable value p_{antero}=1.

Sample trajectories of a processive ($\omega > 0$) and a non-processive tracer particle are compared in Fig. 5.14, a. While a non-processive searcher changes its direction at each filament crossing, a processive searcher overcomes the constriction with probability ω [Hafner2016].

Figure 5.14, b, displays the MFPT as a function of the cortex width δ for various processivities ω. When considering instantaneous quitting of the waiting state $k_{w\to m}$=∞, the MFPT is systematically decreased by an increase of the processivity ω and optimal for ω=1 [Hafner2016]. This reflects the optimal choice of $k^{\text{opt}}_{m\to w}$=0. Figure 5.14, c, highlights the benefit by showing that the MFPT as a function of the processivity is minimal for ω=1 [Hafner2016].

But, when introducing prolonged arrest states by $k_{m\to w} < \infty$, an optimal processivity $\omega < 1$ is found which minimizes the MFPT [Hafner2016], as shown in Fig. 5.14, d-f. While the MMT, as given in Fig. 5.14, b, as well as the mean number of arrest states (# waiting periods), as shown in Fig. 5.14, e, are optimal for ω=1, the MWT exhibits a minimum at $\omega < 1$, as demonstrated by Fig. 5.14, e [Hafner2016]. Here, Eq. 5.13 does not hold since the mean waiting time per arrest state is not universal for all arrest states. While pauses at filament crossings in the bulk are left with rate $k_{w\to m}$, waiting periods at confinement events (r=0, r=1 − δ, r=1) are extended according to $((1-\omega)k_{w\to m})$ [Hafner2016]. The timescales are assumed to be different since confinement events disallow subsequent processive runs whereas waiting processes in the bulk do not. Since the mean waiting time per confinement event consequently diverges for ω=1, an optimal processivity $\omega < 1$ is observed for the MFPT shown in Fig. 5.14, f [Hafner2016]. Consequently, an intermediate processivity is favorable due to inevitable pauses at confinement events. Intermediate probabilities for processive runs subsequent to a filament crossing are reported during active intracellular transport too [29, 33–35]. Note that from now on the cargo processivity is neglected for simplicity.

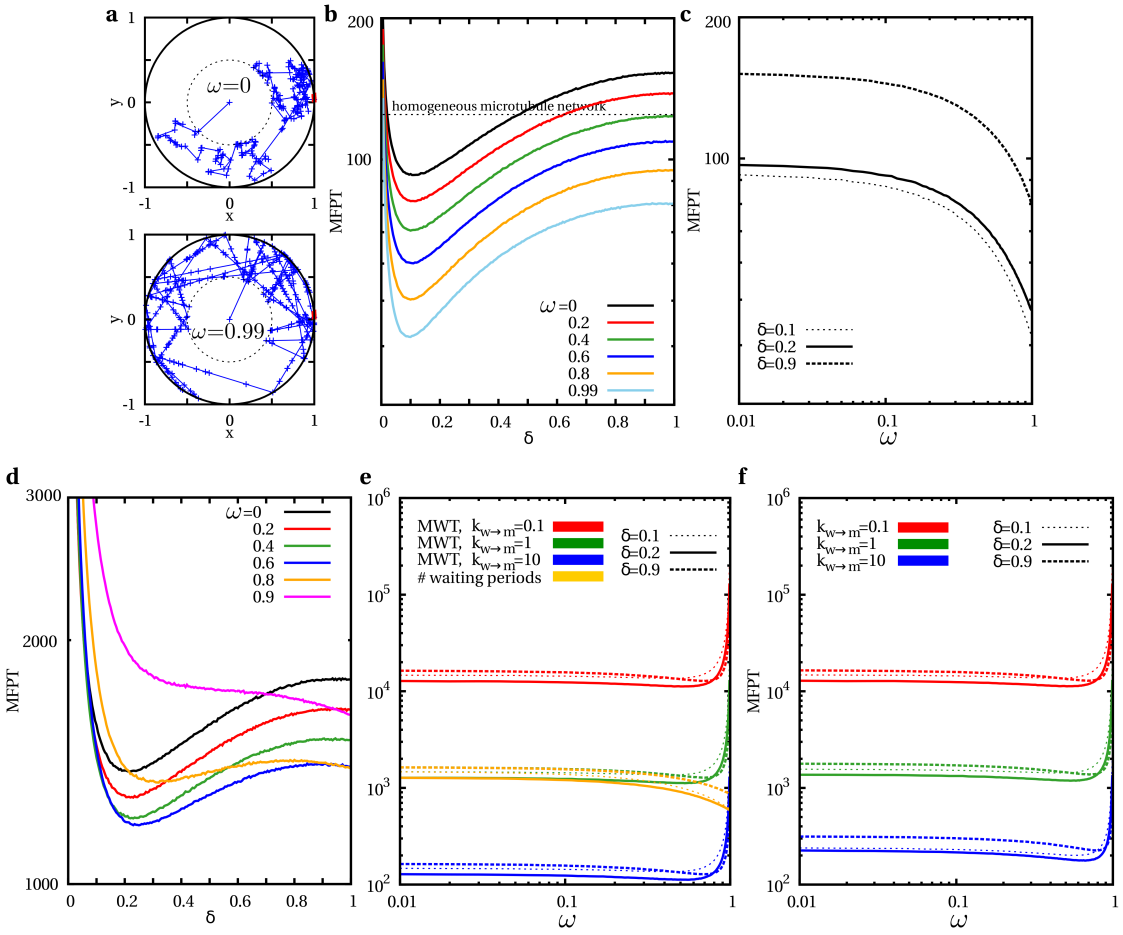

Figure 5.14.: The narrow escape problem on an inhomogeneous cytoskeleton - impact of the processivity. (**a**) Sample trajectories (blue lines) are shown for a cortex width δ=0.5. A non-processive particle with ω=0 changes its direction at each filament crossing (blue cross), while a highly processive searcher with ω=0.99 often overcomes the nodes. (**b**) The MFPT is plotted as a function of the cortex width δ for diverse processivities ω and $k_{w\to m}$=∞. (**c**) The MFPT versus the processivity ω is shown for various fixed cortical widths δ and $k_{w\to m}$=∞. (**d**) The MFPT is plotted as a function of the cortex width δ for diverse processivities ω and $k_{w\to m}$=1. (**e**) The MMT and the mean number of waiting periods are plotted versus the processivity ω for various fixed cortical widths δ and diverse transition rates $k_{w\to m}$. (**f**) The MFPT is shown in dependence of the processivity ω for various fixed cortical widths δ and diverse transition rates $k_{w\to m}$. Otherwise $k_{m\to w}$=10, p_{antero}=1, and α_{exit}=0.1 are applied for all graphs. Reprint of [Hafner2016], Physical Biology, 13, 066003, 2016, (`http://dx.doi.org/10.1088/1478-3975/13/6/066003`).

5.4. Reaction problem - motile target

In this section, we study the enhancement of reaction kinetics between two independently motile reaction partners by active transport within the cell [Hafner2018]. First, the focus is on particles which have the same motility properties, i.e. motor activity p_{antero} and transition rates $k_{m\to w}$ and $k_{w\to m}$. Then, we take into account particles with different motility parameters, before we study the limit of immotile targets in the next section.

Searcher and target particle are initially uniformly distributed within the cell, i.e. $\boldsymbol{r}(t{=}0) = \boldsymbol{r}_0,\ f(r_0){=}1/R_{\text{m}},\ f(\phi_{r_0}){=}1/(2\pi)$. They are propagated until reaction which is assumed to occur instantaneously if searcher and target particle are closer than the reaction radius $|\boldsymbol{r}^{\text{S}}{-}\boldsymbol{r}^{\text{T}}| \leq R_{\text{d}}$, see Fig. 5.1 for a sketch. In the theory of intermittent search strategies, it is usually assumed that the fast motility state prohibits target detection, such that reaction only occurs in the slow state, e.g. [72, 79, 80]. Nontheless, the literature on a relation between the mobility state of cargoes and the likelihood for intracellular reactions is limited, see for instance [253, 254]. It remains unclear whether all intracellular cargoes are non-reactive when being actively transported along the cytoskeleton with the aid of molecular motors. Hence, we consider two different detection modes which depend on the motility state of the tracer particles [Hafner2018]. Reaction either occurs by encounter regardless of the motility states both reaction partners are in, or it is only possible if both particles are in the waiting state [Hafner2018]. The latter alternative constitutes an intermittent search strategy. Remarkably, we show that the detection mode has no significant impact on the reaction kinetics under biologically reasonable conditions.

5.4.1. Homogeneous search strategies

At first, we consider the reaction problem in a homogeneous, isotropic environment with $\delta{=}1$ and ask whether the MFPT to reaction can be optimized as a function of the transition rates $k_{m\to w}$ and $k_{w\to m}$, which are assumed to be equal for searcher and target particle [Hafner2018].

If detection occurs by simple encounter regardless of the motility state of searcher and target particle, Fig. 5.15, a and b, show that the MFPT is universally optimal for $k^{\text{opt}}_{m\to w}{=}0$ and $k^{\text{opt}}_{w\to m}{=}\infty$, no matter how small the target is [Hafner2018]. In contrast, when detection is exclusively possible if both particles are in the arrest state, the MFPT is minimized for non-trivial transition rates $k^{\text{opt}}_{m\to w} > 0$ and $k^{\text{opt}}_{w\to m} < \infty$ which strongly depend on the detection radius R_{d}, see Fig. 5.15, c and d [Hafner2018]. Interestingly, the minimum is quite broad, as demonstrated by the contour lines.

Remarkably, Fig. 5.15, e, shows that the MFPT becomes more and more independent of the detection mode with increasing transition rate $k_{m\to w}$. In the limit of large transition rates $k_{m\to w}$, searcher and target particle change direction on very short timescales such that they explore the domain very slowly. Due to the uniform distributed initial position of both particles, the reaction problem is then determined by getting the particles close to each other in the first place, regardless of the detection mode [Hafner2018].

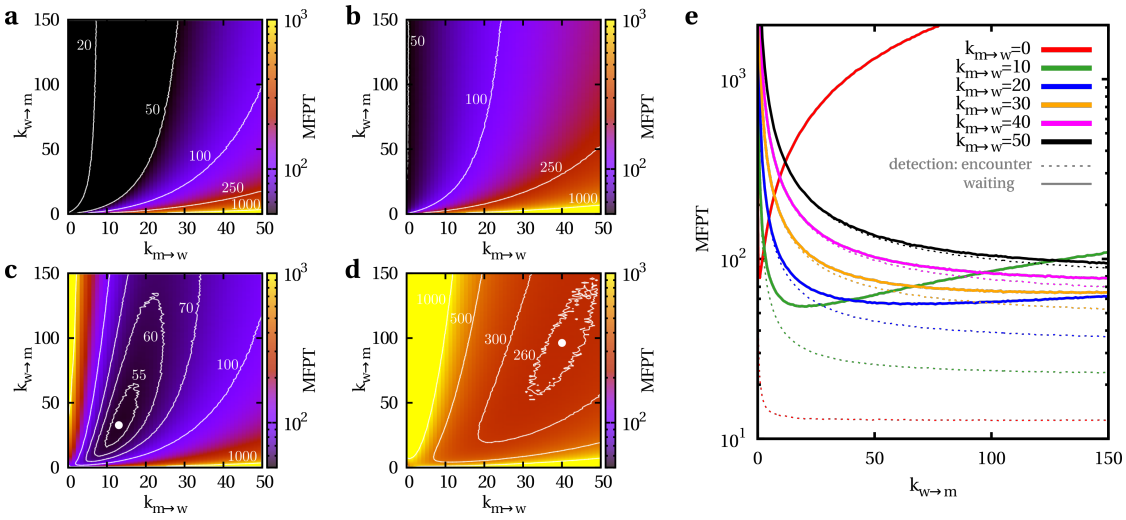

Figure 5.15.: The reaction problem on a homogeneous cytoskeleton to a motile target - optimal transition rates. (**a**) The MFPT is mapped as a function of the transition rates $k_{m\to w}$ and $k_{w\to m}$ for R_d=0.1. Reaction occurs upon encounter regardless of the motility state. (**b**) The same as in (a) but for R_d=0.025. (**c**) The MFPT is shown in dependence of $k_{m\to w}$ and $k_{w\to m}$ for R_d=0.1. But reaction is limited to the waiting state. (**d**) The same as in (c) but for R_d=0.025. (**e**) The MFPT is plotted as a function of the transition rate $k_{w\to m}$ for diverse values of $k_{m\to w}$ and both detection modes with R_d=0.1. Reprint of [Hafner2018], Biophysical Journal, 114, 1420-1432, 2018, (`http://dx.doi.org/10.1016/j.bpj.2018.01.042`).

5.4.2. Inhomogeneous search strategies

By applying the transition rates $k^{\mathrm{opt}}_{m\to w}$ and $k^{\mathrm{opt}}_{w\to m}$ which are optimal in the homogeneous case δ=1, we study the impact of the motor activity p_{antero} and the cytoskeleton inhomogeneity δ on the efficiency of intracellular reactions [Hafner2018].

Figures 5.16, a and b, show that a universally optimal reaction strategy is determined by a motor activity p_{antero}=0, independently of the detection mode [Hafner2018]. For p_{antero}=0 the motion of the tracer particles in the cell interior is determined by radial transport to the center with the aid of dynein motors. In that case, reaction predominantly takes place close to the MTOC. The distribution of reaction locations r_{react} is measured for both detection modes in Fig. 5.16, c and d. The distribution changes drastically in response to the motor activity p_{antero}. Figure 5.16, e, emphasizes that reaction takes place in the cell interior close to the MTOC for p_{antero}=0, whereas it occurs in the cortex for p_{antero}=1. Consequently, a cell is not only able to adjust the efficiency of intracellular reactions, but also to regulate the spatial distributions of reaction products by control of the motor activity levels [Hafner2018].

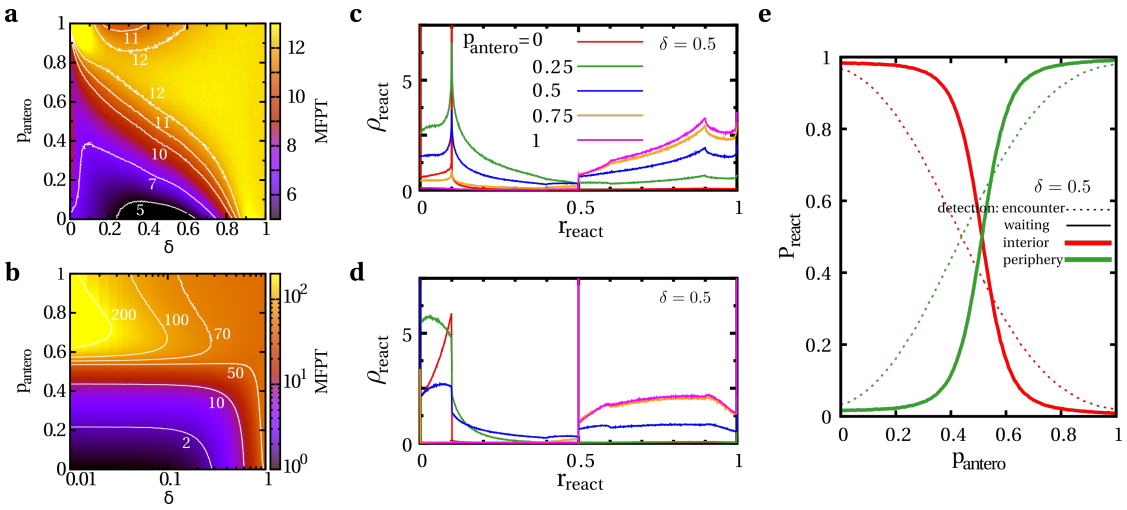

Figure 5.16.: The reaction problem on an inhomogeneous cytoskeleton to a motile target - impact of the motor activity. (**a**) The MFPT is plotted as a function of δ and p_{antero} for R_{d}=0.1. Detection occurs by encounter regardless of the motility state. The transition rates $k^{\text{opt}}_{m\to w}$=0 and $k^{\text{opt}}_{w\to m}$=∞ which are optimal in the homogeneous case δ=1 are applied. (**b**) The MFPT is shown versus δ and p_{antero} for R_{d}=0.1. Reaction is only possible in the waiting state. The rates $k^{\text{opt}}_{m\to w}$=13 and $k^{\text{opt}}_{m\to w}$=34 which are optimal in the homogeneous case δ=1 are applied. (**c**) The distribution of reaction locations r_{react} is shown for diverse motor activities p_{antero} and a cortex width δ=0.5. The transition rates $k^{\text{opt}}_{m\to w}$, $k^{\text{opt}}_{w\to m}$ are applied. Reaction occurs by encounter at R_{d}=0.1 regardless of the motility state of both particles. (**d**) The same as in (c) but detection is restricted to the waiting state. (**e**) The probability P_{react} that the reaction takes place in the interior or the periphery of the cell is measured as a function of the motor activity p_{antero} for δ=0.5, R_{d}=0.1, and both detection modes. The rates $k^{\text{opt}}_{m\to w}$, $k^{\text{opt}}_{w\to m}$ are applied. Reprint of [Hafner2018], Biophysical Journal, 114, 1420-1432, 2018, (`http://dx.doi.org/10.1016/j.bpj.2018.01.042`).

Note that the peaks of the distributions in Fig. 5.16, c and d, arise either due to the detection radius R_{d} at r_{react}=R_{d} and r_{react}=1−R_{d}, or due to automatic transitions to the waiting state at confinement events $r \in \{0; 1-\delta; 1\}$ which is especially beneficial when both particles have to be in the waiting state in order to react [Hafner2018].

The superiority of a low probability for radially outward transport p_{antero}=0 is very robust against changes in the transition rates $k_{m\to w}$ and $k_{w\to m}$, as shown in Fig. 5.17, a and b [Hafner2018]. In general, the optimal reaction strategy is determined by p_{antero}=0, δ=0, $k_{m\to w}$=0, and $k_{w\to m}$=∞. Initially uniformly distributed searcher and target particles are transported on the shortest route to the MTOC in order to react. The optimality of this strategy is independent of the detection mode, as particles switch to the arrest state at the MTOC automatically.

However, as already indicated by Fig. 5.16, a, there may also arise a local minimum of the MFPT for high probabilities of radially outward directed transport p_{antero}.

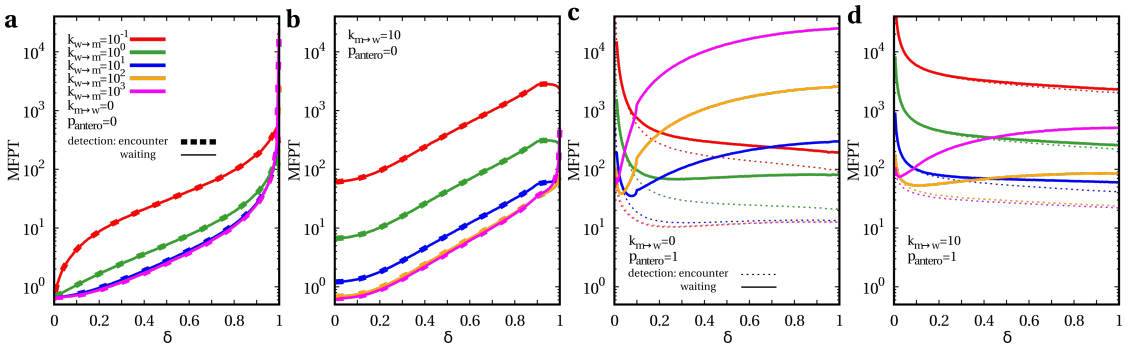

Figure 5.17.: The reaction problem on an inhomogeneous cytoskeleton to a motile target - impact of the cortex width. (**a**) The MFPT is plotted as a function of the cortex width δ for p_{antero}=0, $k_{m\to w}$=0, diverse rates $k_{w\to m}$, and R_{d}=0.1. The results of both detection modes are compared. (**b**) The same as in (a) but for $k_{m\to w}$=10. (**c**) The same as in (a) but for p_{antero}=1. (**d**) The same as in (b) but for p_{antero}=1. Figures b-d are reprints of [Hafner2018], Biophysical Journal, 114, 1420-1432, 2018, (`http://dx.doi.org/10.1016/j.bpj.2018.01.042`).

Accordingly and as indicated by Fig. 5.17, c and d, the reaction time can also be minimized as a function of the cortex width δ for p_{antero}=1 [Hafner2018]. Hence, another efficient search strategy is given by the restriction of motion to a thin cortex by p_{antero}=1 and $\delta^{\text{opt}} \in (0;1)$. However, the occurrence of the minimum is not very robust [Hafner2018]. Whether such inhomogeneous search strategies with $\delta^{\text{opt}} \in (0;1)$ and p_{antero}=1 are favorable to a homogeneous search strategy δ=1 depends critically on the transition rates $k_{m\to w}$ and $k_{w\to m}$, as displayed in Fig. 5.18. Note that Fig. 5.18 again emphasizes that the detection mode significantly loses impact on the reaction efficiency with increasing transition rate $k_{m\to w}$.

As evident from for instance Fig. 5.17 and 5.18, the MFPT displays kinks as a function of the cortex width δ when detection is only possible in the waiting state [Hafner2018]. These kinks are especially prominent for $k_{m\to w}$=0 and occur at δ=R_{d} and δ=1−R_{d}. For $k_{m\to w}$=0 the tracer particle never switches to the waiting state in the bulk and thus reaction critically depends on automatic arrests at confinement events at the MTOC r=0, the inner cortex border r=1−δ, and the membrane r=1. If $\delta \leq R_{\text{d}}$, reaction may occur for four different searcher-target configurations: both are at the MTOC, both are on the inner cortex border, both are on the membrane, or one is on the inner cortex border and one is on the membrane. There are also four configurations in the case of $\delta \geq 1-R_{\text{d}}$: both are at the MTOC, both at the inner cortex border, both are at the membrane, or one is at the MTOC and the other one is on the inner cortex border. But, for $R_{\text{d}} < \delta < 1-R_{\text{d}}$ there are only three searcher-target configurations which allow reaction since the mixed configurations are far off [Hafner2018].

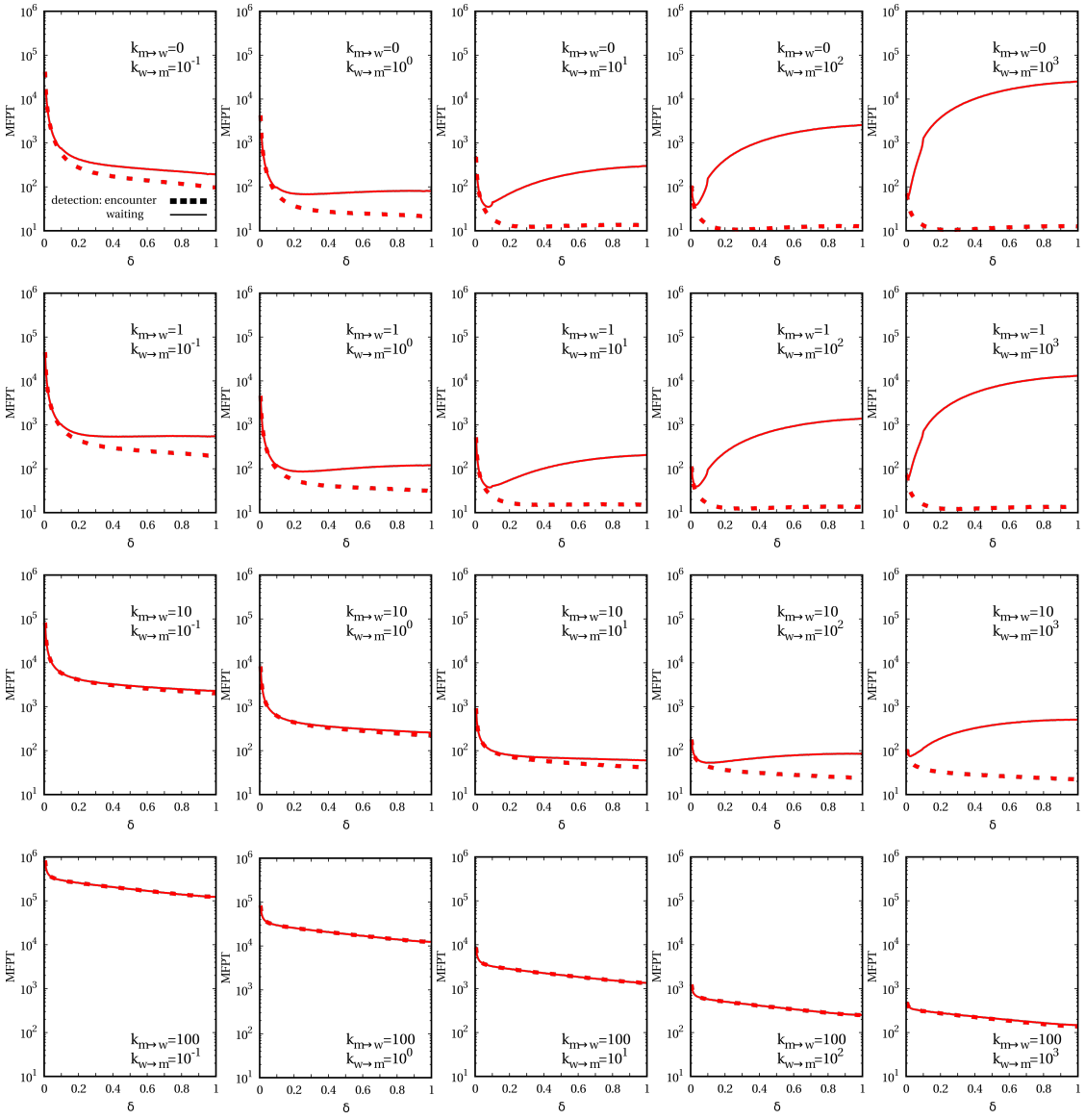

Figure 5.18.: The reaction problem on an inhomogeneous cytoskeleton to a motile target - impact of the transition rates. The MFPT is measured as a function of the cortex width δ for p_{antero}=1 and various transition rates $k_{m\to w}$ and $k_{w\to m}$. Results of the two considered detection modes are compared.

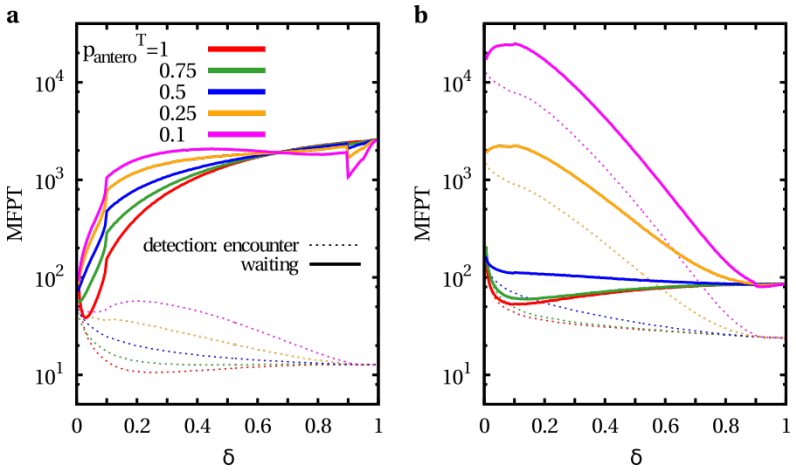

Figure 5.19.: The reaction problem on an inhomogeneous cytoskeleton to a motile target - impact of nonidentical motor activities. (**a**) The MFPT is shown as a function of the cortex width δ for nonidentical motor activities $p_{\text{antero}}^{\text{S}}$=1 and diverse $p_{\text{antero}}^{\text{T}}$. The two detection modes are compared for R_{d}=0.1 and $k_{m\to w}^{\text{S}}$=$k_{m\to w}^{\text{T}}$=0, $k_{w\to m}^{\text{S}}$=$k_{w\to m}^{\text{T}}$=100. (**b**) The same as in (a) but for $k_{m\to w}^{\text{S}}$=$k_{m\to w}^{\text{T}}$=10. Figure b is a reprint of [Hafner2018], Biophysical Journal, 114, 1420-1432, 2018, (`http://dx.doi.org/10.1016/j.bpj.2018.01.042`).

Impact of nonidentical particle properties

So far, we only considered the reaction problem for identical searcher and target particles with equal motility parameters p_{antero}, $k_{m\to w}$, and $k_{w\to m}$. However, target and searcher particle are rarely identical in intracellular reaction problems. They may differ according to their size, which effects the transition rates $k_{m\to w}$, $k_{w\to m}$ [29,38], or according to their attached motor proteins, which alters p_{antero} [Hafner2018]. In the following we analyze the impact of nonidentical properties of searcher, i.e. $p_{\text{antero}}^{\text{S}}$, $k_{m\to w}^{\text{S}}$, and $k_{w\to m}^{\text{S}}$, and target particle, i.e. $p_{\text{antero}}^{\text{T}}$, $k_{m\to w}^{\text{T}}$, and $k_{w\to m}^{\text{T}}$, on their reaction efficiency [Hafner2018].

As expected and demonstrated by Fig. 5.19, nonidentical motor activities $p_{\text{antero}}^{\text{S}} \neq p_{\text{antero}}^{\text{T}}$ are highly deficient for reaction as they drive searcher and target particle apart [Hafner2018]. Particles with p_{antero}=0 stick to the MTOC, whereas particles with p_{antero}=1 are only moving in the cortex. As a result, a homogeneous search strategy δ=1 is favorable, since the impact of p_{antero} vanishes in this limit and the particles are isotropically moving within the cell. Figure 5.19 shows that the MFPT increases by several orders of magnitude with increasing difference in the motor activity. This finding is robust against alterations of the transition rates $k_{m\to w}^{\text{S}}$, and $k_{w\to m}^{\text{S}}$ [Hafner2018]. Note that $k_{m\to w}$=0 is a specific exception if reaction is only possible in the waiting state, because target detection then critically depends on automatic transitions to arrest states at confinement events, as indicated by Fig. 5.19, a.

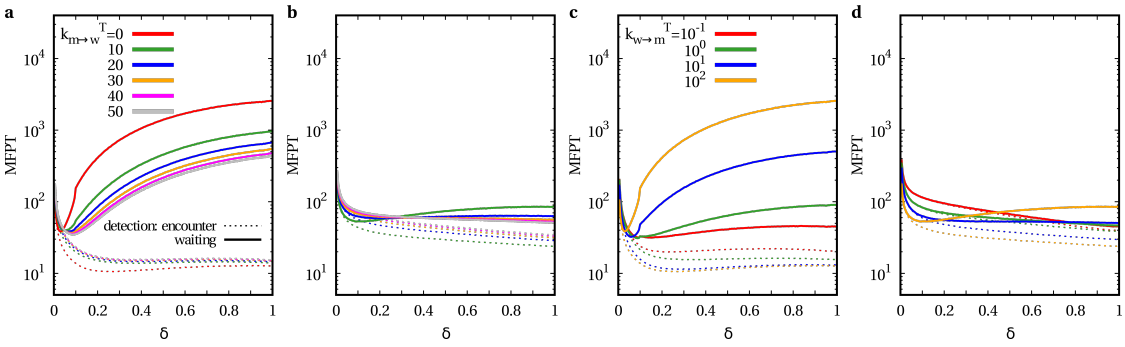

Figure 5.20.: The reaction problem on an inhomogeneous cytoskeleton to a motile target - impact of nonidentical transition rates. (**a**) The MFPT is shown versus the cortex width δ for nonidentical transition rates $k^{\mathrm{S}}_{m\to w}$=0 and various $k^{\mathrm{T}}_{m\to w} > k^{\mathrm{S}}_{m\to w}$, such that the target is more localized than the searcher due to shorter step lengths. Apart from that, particles are identical, i.e. $k^{\mathrm{S}}_{w\to m}$=$k^{\mathrm{T}}_{w\to m}$=100 and p_{antero}=1. The two detection modes are considered for R_{d}=0.1. (**b**) The same as in (a) but for $k^{\mathrm{S}}_{m\to w}$=10. (**c**) The MFPT is plotted as a function of the cortex width δ for nonidentical transition rates $k^{\mathrm{S}}_{w\to m}$=100 and diverse values of $k^{\mathrm{T}}_{w\to m} < k^{\mathrm{S}}_{w\to m}$, such that the target is more localized than the searcher due to longer waiting periods. Otherwise, particles are identical, i.e. $k^{\mathrm{S}}_{m\to w}$=$k^{\mathrm{T}}_{m\to w}$=0 and p_{antero}=1. The two detection modes are considered for R_{d}=0.1. (**d**) The same as in (c) but for $k_{m\to w}$=10. Figures a and c are reprints of [Hafner2018], Biophysical Journal, 114, 1420-1432, 2018, (`http://dx.doi.org/10.1016/j.bpj.2018.01.042`).

Contrarily, Fig. 5.20 shows that the impact of nonidentical transition rates on the reaction efficiency depends on the detection mode [Hafner2018]. A less motile target, either by $k^{\mathrm{S}}_{m\to w} < k^{\mathrm{T}}_{m\to w}$, as studied in Fig. 5.20, a and b, or by $k^{\mathrm{S}}_{w\to m} > k^{\mathrm{T}}_{w\to m}$, as shown in Fig. 5.20, c and d, is universally deficient if detection occurs by pure encounter regardless of the motility state. However, the case is more peculiar when reaction is exclusively allowed in the waiting state. The overall trend shows that a less motile target is largely beneficial for the reaction efficiency, but the effect vanishes for increasing rate $k^{\mathrm{T}}_{m\to w}$, as indicated by Fig. 5.20, c and d.

5.5. Reaction problem - immotile target

Hooked by the study of nonidentical particle properties, we investigate the reaction efficiency to immotile targets which are uniformly distributed within the cell in the following section [Hafner2018].

5.5.1. Homogeneous search strategies

First, we consider the detection of an immotile target by a searcher which is moving on a homogeneous cytoskeleton with δ=1 and transition rates $k_{m\to w}$ and $k_{w\to m}$ [Hafner2018].

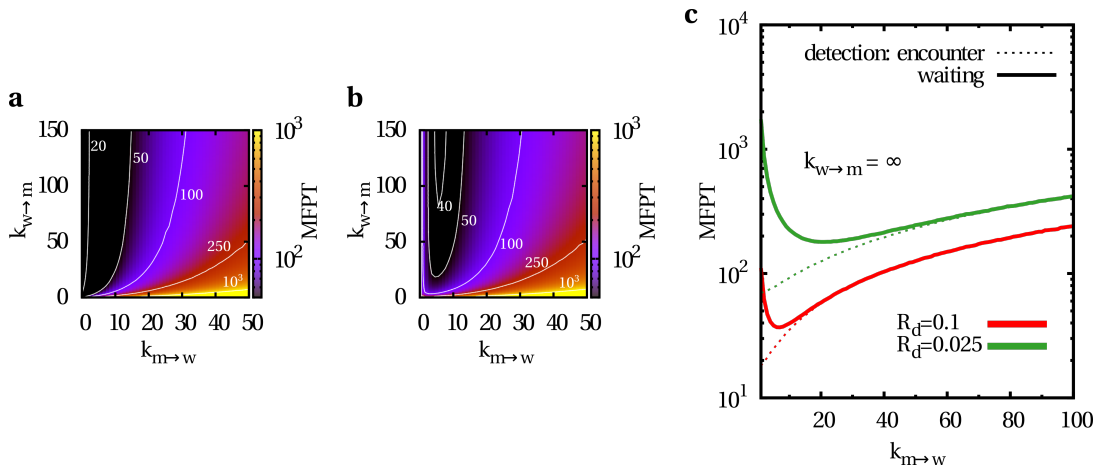

Figure 5.21.: The reaction problem on a homogeneous cytoskeleton to an immotile target - optimal transition rates. (**a**) The MFPT to a uniformly distributed, immotile target is shown versus the transition rates $k_{m\to w}$ and $k_{w\to m}$ of the searching tracer particle for a reaction radius R_d=0.1. Detection occurs by encounter, regardless of the motility state of the searcher. (**b**) The same as in (a) but the searcher may detect the target only in the waiting state. (**c**) The MFPT is measured as a function of the transition rate $k_{m\to w}$ for the universally optimal rate $k_{w\to m}$=∞ and reaction radii $R_\mathrm{d} \in \{0.025; 0.1\}$. The two detection modes are compared. Reprint of [Hafner2018], Biophysical Journal, 114, 1420-1432, 2018, (`http://dx.doi.org/10.1016/j.bpj.2018.01.042`).

Figure 5.21, a and b, show that the MFPT to an immotile target, which is initially uniformly distributed within the cell is globally minimal for $k_{w\to m}$=∞, as a tribute to the considered instantaneous reactions [Hafner2018]. In the case of detection by encounter regardless of the searcher's motility state, the reaction efficiency is optimized by an uninterrupted motion pattern without directional changes in the bulk, i.e. $k_{m\to w}$=0 and $k_{w\to m}$=∞ [Hafner2018]. This is independent of the reaction radius R_d as shown in Fig. 5.21, c. In contrast, Fig. 5.21, c, underlines that the MFPT is minimized by a non-zero transition rate $k_{m\to w} > 0$ which strongly depends on the reaction radius R_d if reaction is only possible in the waiting state [Hafner2018]. Hence, it is necessary for the particle to stop more frequently in the bulk and scan for the target the smaller the reaction radius R_d is.

Supplementary to the previous paragraph on nonidentical reaction partners, note by comparison of Fig. 5.21, a and b, and Fig. 5.15, a and c, respectively, that an immotile target is disadvantageous with regard to the reaction efficiency when detection occurs by encounter, whereas the situation is more complex and depends sensitively on the transition rates when reaction is only possible in the waiting state.

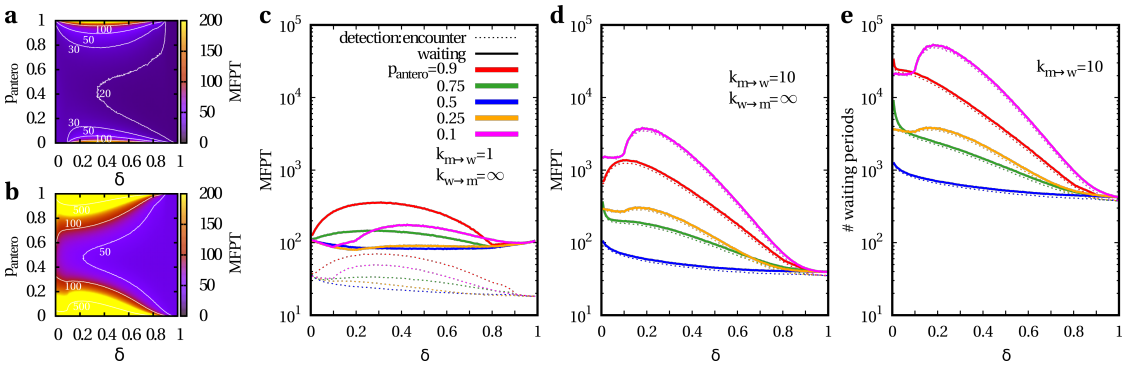

Figure 5.22.: The reaction problem on an inhomogeneous cytoskeleton to an immotile target - optimal cortex width and motor activity. (**a**) The MFPT is measured as a function of the cortex width δ and the motor activity p_{antero} for an immotile target with reaction radius R_{d}=0.1. The rates $k^{\text{opt}}_{m\to w}$=0 and $k^{\text{opt}}_{w\to m}$=∞ which are optimal in the homogeneous case δ=1 are applied. Detection occurs by encounter, regardless of searcher's the motility state. (**b**) The same as in (a), but detection is only possible in the waiting state. The rates $k^{\text{opt}}_{m\to w}$=7, $k^{\text{opt}}_{w\to m}$=∞ are applied. (**c**) The MFPT is plotted in dependence of the inhomogeneity δ for diverse motor activities p_{antero}, $k_{m\to w}$=1, $k_{w\to m}$=∞, and R_{d}=0.1. Both detection modes are considered. (**d**) The same as in (c) but for $k_{m\to w}$=10. (**e**) The mean number of waiting periods, which defines the MFPT in the limit of $k_{w\to m} \gg 1$ is shown as a function of the cortex width δ for diverse motor activities p_{antero}, $k_{m\to w}$=10 and R_{d}=0.1. Both detection modes are applied. Figures a and b are reprints of [Hafner2018], Biophysical Journal, 114, 1420-1432, 2018, (`http://dx.doi.org/10.1016/j.bpj.2018.01.042`).

5.5.2. Inhomogeneous search strategies

In order to analyze how the interplay between spatial inhomogeneity of the cytoskeleton and motor activity effects the reaction efficiency with immotile targets, we plot the MFPT as a function of δ and p_{antero} and fix the transition rates $k^{\text{opt}}_{m\to w}$, $k^{\text{opt}}_{w\to m}$=∞ to the values which are optimal for the homogeneous counterpart [Hafner2018]. Figures 5.22, a and b, elucidate that for both detection modes a homogeneous cytoskeleton with δ=1 is optimal as it explores the space isotropically and thus enhances the detection of a uniformly distributed target. Nonetheless, for all inhomogeneities δ, a motor activity p_{antero}=0.5 is advantageous [Hafner2018]. In that case radially outward and inward directed transport are balanced in the interior, such that the searcher explores the whole cell homogeneously. The MFPT diverges for $p_{\text{antero}} \to 0$ and $p_{\text{antero}} \to 1$, because the searcher is then stuck to the MTOC or the cortex and targets which are distributed somewhere else in the cell are never found. The superiority of a search strategy which involves a homogeneous cytoskeleton δ=1 or at least a motor activity p_{antero}=0.5 is very robust against changes of the transition rates $k_{m\to w}$ and $k_{w\to m}$, as emphasized by Fig. 5.22, c-e [Hafner2018]. Figure 5.22, e, shows that prolonged arrest states systematically increase the MFPT to immotile targets analogously to Eq. 5.13 of the narrow escape problem where the target is immobile as well.

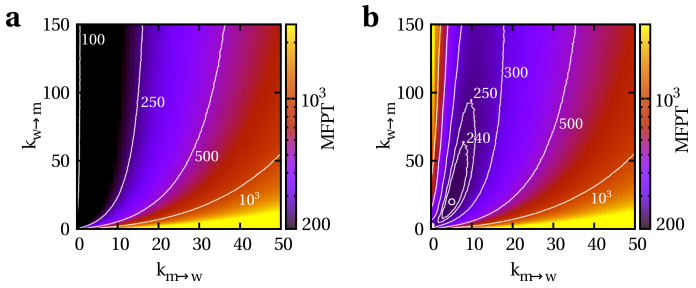

Figure 5.23.: The reaction-escape problem on a homogeneous cytoskeleton - optimal transition rates. (**a**) The MFPT is plotted versus the transition rates $k_{m\to w}$ and $k_{w\to m}$ for a reaction radius R_d=0.1 and an exit size α_exit=0.1. Reaction occurs regardless of the motility state. (**b**) The same as in (a) but reaction is only possible in the waiting state. Reprint of [Hafner2018], Biophysical Journal, 114, 1420-1432, 2018, (`http://dx.doi.org/10.1016/j.bpj.2018.01.042`).

5.6. Reaction-escape problem

In this section, we investigate how the interplay between cytoskeleton organization, motor activity, and arrest frequency of the cargo effects the efficiency of the combined reaction-escape problem [Hafner2018]. A searching particle first has to pair with another motile target particle before the product is stochastically transported to the exit zone on the cell membrane. We assume that searcher and target particle are initially uniformly distributed within the cell and possess the same motor activity p_antero and transition rates $k_{m\to w}$ and $k_{w\to m}$. Reaction of searcher and target particle occurs for $|\boldsymbol{r}^\mathrm{S}-\boldsymbol{r}^\mathrm{T}| \leq R_\mathrm{d}$ and is either possible regardless of the motility state, or only possible if both particles are in the waiting state. Subsequent to reaction, the characteristics of the searcher, i.e. $\boldsymbol{r}^\mathrm{S}$, p_antero, $k_{m\to w}$, and $k_{w\to m}$, are transmitted to the product particle for escaping the cell via a narrow window in the plasma membrane of arc length α_exit. Consequently, the MFPT of the reaction-escape problem is the sum MFPT=$\mathrm{MFPT}_\mathrm{react}$+$\mathrm{MFPT}_\mathrm{escape}$ of the reaction-MFPT and the escape-MFPT [Hafner2018]. Note that the initial position of the product particle for the narrow escape problem is typically not uniformly distributed within the cell but defined by the reaction location, as studied in Fig. 5.16, c-e.

5.6.1. Homogeneous search strategies

First, we analyze the efficiency of the reaction-escape problem on a homogeneous cytoskeleton defined by δ=1. Figure 5.23, displays the MFPT of the reaction-escape problem as a function of the transition rates $k_{m\to w}$ and $k_{w\to m}$ for R_d=0.1 and α_exit=0.1. The optimal transition rates which minimize the MFPT depend critically on the reaction mode [Hafner2018]. If reaction occurs by encounter regardless of the motility state, the MFPT is universally minimal for $k^\mathrm{opt}_{m\to w}$=0 and $k^\mathrm{opt}_{w\to m}$=∞, as shown in Fig. 5.23, a. This comes as no surprise as both the homogeneous escape and the homogeneous reaction problem are optimized by these rates, see Fig. 5.6 and 5.15, a [Hafner2018]. However, if reaction is only possible in the waiting state, Fig. 5.23, b, shows that the MFPT displays two minima as a function of the transition rates $k_{m\to w}$ and $k_{w\to m}$. The reason is that the

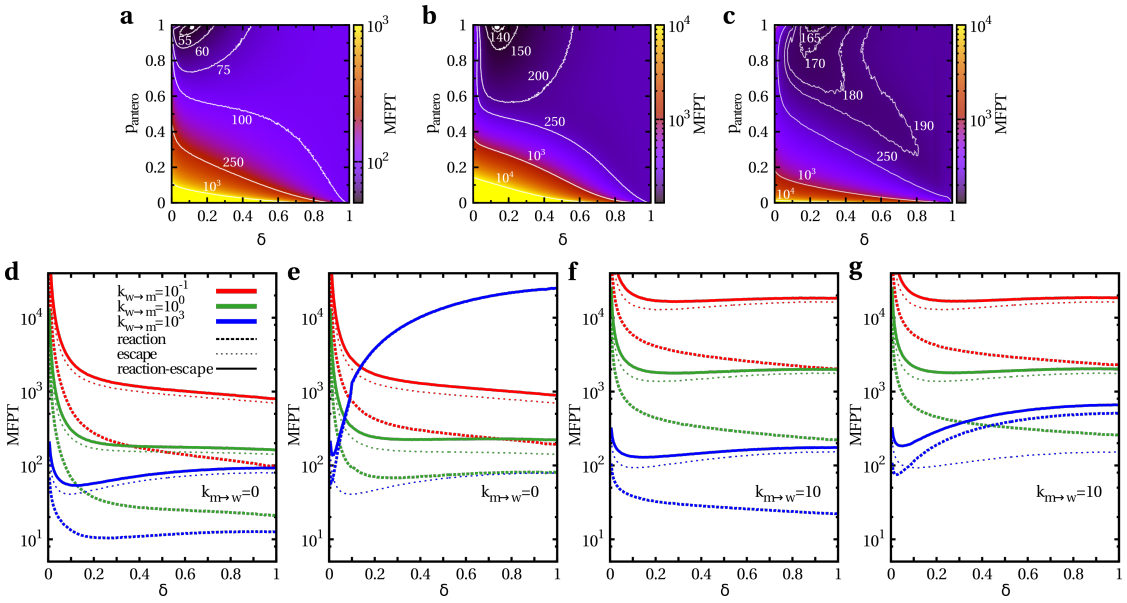

Figure 5.24.: The reaction-escape problem on an inhomogeneous cytoskeleton - optimal cortex width and motor activity. (**a**) The MFPT is shown as a function of the cortex width δ and the motor activity p_{antero} for $k^{\mathrm{opt}}_{m\to w}$=0, $k^{\mathrm{opt}}_{m\to w}$=$\infty$, R_{d}=0.1 and α_{exit}=0.1. Reaction occurs by encounter regardless of the motility state. (**b**) The same as in (a) but for $k^{\mathrm{opt}}_{m\to w}$=5 and $k^{\mathrm{opt}}_{w\to m}$=22. Reaction is restricted to the waiting state. (**c**) The same as in (b) but for $k_{m\to w}$=0 and $k_{w\to m}$=1. Note that the minimum of the MFPT is larger than the one in (b) even though the transition rates are more optimal for the homogeneous counterpart. (**d**) The MFPT of the reaction, the subsequent escape, and the reaction-escape problem is shown in dependence of the inhomogeneity δ for $k_{m\to w}$=0, various $k_{w\to m}$, and p_{antero}=1, R_{d}=0.1, α_{exit}=0.1. Reaction occurs by encounter regardless of the motility state. (**e**) The same as in (d) but reaction is restricted to the waiting state. (**f**) The same as in (d) but for $k_{m\to w}$=10. (**g**) The same as in (e) but for $k_{m\to w}$=10. Figures a, b, d-g are reprints of [Hafner2018], Biophysical Journal, 114, 1420-1432, 2018, (`http://dx.doi.org/10.1016/j.bpj.2018.01.042`).

homogeneous escape problem is optimized by $k_{m\to w}$=0, $k_{w\to m}$=∞, whereas the homogeneous reaction problem is minimal for $k_{m\to w}$=13, $k_{w\to m}$=34, if reaction is restricted to the waiting state, see Fig. 5.6 and 5.15, c. Whereas the global minimum at $k_{m\to w}$=0, $k_{w\to m}$=1 is highly deficient, the local minimum at $k^{\mathrm{opt}}_{m\to w}$=5, $k^{\mathrm{opt}}_{w\to m}$=22 is robust and leads to only 5% loss in efficiency in comparison to the global minimum [Hafner2018].

5.6.2. Inhomogeneous search strategies

In order to analyze the impact of the interplay between spatial organization of the cytoskeleton and motor activity on the efficiency of the reaction-escape problem, we apply for both reaction modes the transition rates $k^{\mathrm{opt}}_{m\to w}$ and $k^{\mathrm{opt}}_{w\to m}$ which are optimal in the homogeneous case and evaluate the MFPT as a function of δ and p_{antero} in Fig. 5.24, a-c. Remarkably, for both reaction modes the MFPT is minimized for about p_{antero}=1

and $\delta^{\mathrm{opt}} \in (0;1)$ [Hafner2018]. Although the reaction problem is universally minimized for p_{antero}=0, such a high probability of radially inward directed transport is disadvantageous for the narrow escape problem, which actually diverges for p_{antero}=0 as particles are stuck at the MTOC. In consequence, an efficient search strategy for the reaction-escape problem relies on the restriction of cargo motion to a thin actin cortex. Figures 5.24, d-g, show that inhomogeneous search strategies which are more efficient than the homogeneous counterpart exist also for transition rates which are not optimal in the homogeneous case [Hafner2018]. But the occurrence of a minimal MFPT for inhomogeneous cytoskeleton organizations $\delta \in (0;1)$ is not as robust as for the narrow escape problem alone, see Fig. 5.13, because the reaction problem is sensitive to alterations in transition rates, see Fig. 5.18. However, a cell is able to regulate the search efficiency by controlling the cytoskeleton organization and the motor activity, which potentially reduces the MFPT by several orders of magnitude.

5.7. Steps towards more realistic cells

So far, we investigated two-dimensional, spherical cell which exhibit a constant density of microtubules and uniformly random oriented actin filaments. Here we take several steps towards more physiological conditions [Hafner2016, Hafner2018]. First, we generalize our approach to three-dimensional, spherical cells. We take into account biologically reasonable parameters and compare the predictions of our model to experimental measurements. For that reason, we mainly use non-scaled parameters, in contrast to Eq. 5.7, in this section. Furthermore, we investigate how the cell shape, the space-dependent microtubule density, and non-uniformly distributed actin orientations effect the search efficiency of targeted intracellular transport.

5.7.1. Generalization to three-dimensional spherical cells

A generalization of our approach to three dimensions is straightforward. The main difference constitutes the update procedure of the particle velocity [Hafner2018]. The new velocity $\boldsymbol{v}^{\star}(v, \theta_v^{\star}, \phi_v^{\star})$ is defined in a rotated coordinate system with $z^{\star}$-axis pointing in the direction of the current particle position $\boldsymbol{r}(r, \theta_r, \phi_r)$, similar to Fig. 5.2 in two dimensions [Hafner2018]. In order to take the distribution of cytoskeletal filaments into account the azimuthal angle $\phi_v^{\star}$ is uniformly distributed in $(-\pi;\pi]$ and the polar angle $\theta_v^{\star}$=$\alpha_{\mathrm{rot}} \in [0;\pi]$ is chosen according to a specific rotation angle distribution

$$f_{\mathrm{3D}}(\alpha_{\mathrm{rot}}) = \begin{cases} p_{\mathrm{antero}}\,\delta(\alpha_{\mathrm{rot}}) + (1-p_{\mathrm{antero}})\,\delta(\alpha_{\mathrm{rot}}-\pi), & \text{for } 0 < r < R_{\mathrm{m}}-\delta, \\ 1/\pi, & \text{for } R_{\mathrm{m}}-\delta < r < R_{\mathrm{m}}, \end{cases} \tag{5.14}$$

which is the three-dimensional generalization of Eq. 5.12 [Hafner2018]. The velocity vector $\boldsymbol{v}(v, \theta_v, \phi_v)$ in the primal coordinate system is given by rotation according to

$$\boldsymbol{v} = \begin{pmatrix} \cos\theta_r \cos\phi_r & -\sin\phi_r & \sin\theta_r \cos\phi_r \\ \cos\theta_r \sin\phi_r & \cos\phi_r & \sin\theta_r \sin\phi_r \\ -\sin\theta_r & 0 & \cos\theta_r \end{pmatrix} \cdot v \begin{pmatrix} \sin\theta_v^{\star}\cos\phi_v^{\star} \\ \sin\theta_v^{\star}\sin\phi_v^{\star} \\ \cos\theta_v^{\star} \end{pmatrix} = v \begin{pmatrix} \sin\theta_v\cos\phi_r \\ \sin\theta_v\sin\phi_r \\ \cos\theta_v \end{pmatrix}. \tag{5.15}$$

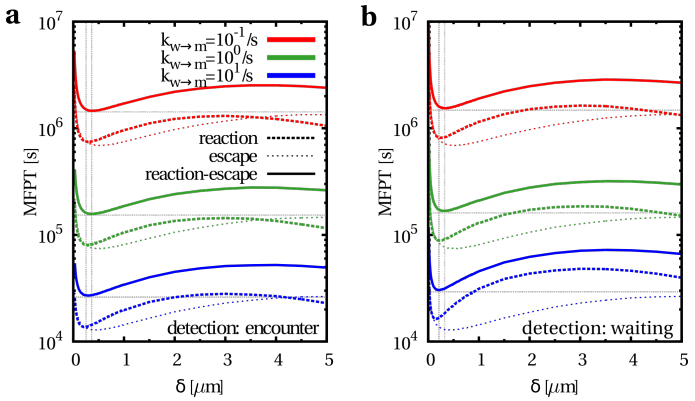

Figure 5.25.: Transport efficiency in 3D cells - comparison to biological measurements. The MFPT of the reaction, the subsequent escape, and the combined reaction-escape problem are shown as a function of the cortex width δ for spherical cells of radius R_m=5μm. Biologically reasonable transition rates $k_{m\to w}$=10/s, $k_{w\to m} \in \{10^{-1}/\mathrm{s}; 10^{0}/\mathrm{s}; 10^{1}/\mathrm{s}\}$ and target sizes R_d=0.1 μm, α_exit=0.2 are applied for p_antero=1 and v=1 μm/s. (**a**) Reaction occurs by encounter regardless of the motility state. (**b**) Reaction is limited to the waiting state. Reprint of [Hafner2018], Biophysical Journal, 114, 1420-1432, 2018, (`http://dx.doi.org/10.1016/j.bpj.2018.01.042`).

In order to compare our model predictions to experimental measurements of the actin cortex, we take into account biologically reasonable parameters [Hafner2016,Hafner2018]. T cells typically posses a radius R_m=5 μm. By fixing α_exit=0.2, we consider exits of arc length 0.2×5 μm =1 μm, which is consistent with the size of an immunological synapse [10, 12–14]. Lytic vesicles posses a radius R_d=0.1 μm [12] and are roughly transported by an effective motor speed v=1 μm/s [2]. Biologically reasonable mesh sizes ℓ=100 nm [93,96,98,99] are taken into account by a transition rate $k_{m\to w}$=v/ℓ=10/s. The mean waiting time per arrest state is reported to be of the order of seconds [29,146,152], which is captured in our model by $k_{w\to m} \in \{10^{-1}/\mathrm{s}; 10^{0}/\mathrm{s}; 10^{1}/\mathrm{s}\}$. We further assume a high motor activity of kinesins p_antero=1, which is optimal for the reaction-escape problem, as shown in Fig. 5.24.

Under these conditions, Fig. 5.25 shows that the efficiency of the three studied transport tasks can substantially be increased by the establishment of a thin cortex [Hafner2016, Hafner2018]. The model predicts an optimal width of the actin cortex of approximately δ^opt=0.3 μm, which is in good agreement to experimental results [93, 95]. We emphasize that the reaction mode has no significant effect on the search efficiency under biological conditions, as demonstrated by comparison of Fig. 5.25, a and b. By considering the rescaled parameter $k_{m\to w} \mapsto R_\mathrm{m} k_{m\to w}/v$=50, this was already indicated earlier by Fig. 5.15 and 5.18 [Hafner2018].

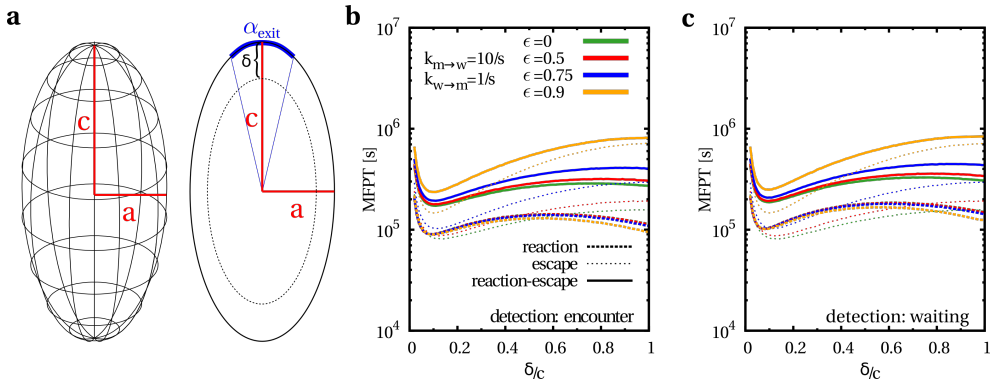

Figure 5.26.: Transport efficiency in 3D cells - impact of the cell shape. (**a**) A sketch of an ellipsoidal cell with symmetry axis z and semi-axes $c > a$ is shown. (**b**) The MFPT of the reaction, the subsequent escape, and the combined reaction-escape problem are shown as a function of δ/c for spheroidal cells of volume $V{=}4\pi(5\,\mu\text{m})^3/3$ and diverse eccentricities ϵ. Biologically reasonable transition rates $k_{m\to w}{=}10/\text{s}$ and $k_{w\to m}{=}1/\text{s}$ are applied. The exit zone is fixed to an arc length of 1 μm and the reaction radius $R_\text{d}{=}0.1$ μm takes typical vesicles sizes into account. Otherwise, $p_\text{antero}{=}1$ and $v{=}1$ μm/s are applied. Reaction occurs by encounter regardless of the motility state. (**c**) The same as in (b) but reaction is limited to the waiting state. Figures b and c are reprints of [Hafner2018], Biophysical Journal, 114, 1420-1432, 2018, (`http://dx.doi.org/10.1016/j.bpj.2018.01.042`).

5.7.2. Impact of the cell shape

Up to now, we investigated spherical cells. However, many cells are polarized [2]. Here we evaluate the impact of cell polarization on the efficiency of intracellular transport by considering ellipsoidal cells. The cell membrane is modeled as a prolate spheriod with symmetry axis z and semi-axes $c > a$ [Hafner2018]. Consequently, the cortex is not spherical as well, as sketched in Fig. 5.26, a. For the narrow escape problem, we assume that the exit zone is located at the north pole of the spheroid. Since we would like to isolate the impact of the cell shape on the search efficiency, we exclude any volume or target size effects [Hafner2018]. Therefore, we fix the volume $V{=}4\pi ca^2/3{=}4\pi(5\,\mu\text{m})^3/3$ and vary the eccentricity $\epsilon{=}\sqrt{1-a^2/c^2} \in [0;1)$ of the spheroid. The greater the eccentricity ϵ, the more does the cell shape differ from the spherical case $\epsilon{=}0$. Furthermore, we adjust α_exit to assure a target size of arc length 1 μm, as given in Table 5.2.

Table 5.2.: Transport efficiency in 3D cells - impact of the cell shape.

eccentricity ϵ	semi-axis c	semi-axis a	α_exit
0	5 μm	5 μm	0.2
0.5	5.503 μm	4.766 μm	0.182
0.75	6.586 μm	4.356 μm	0.152
0.9	8.697 μm	3.791 μm	0.115

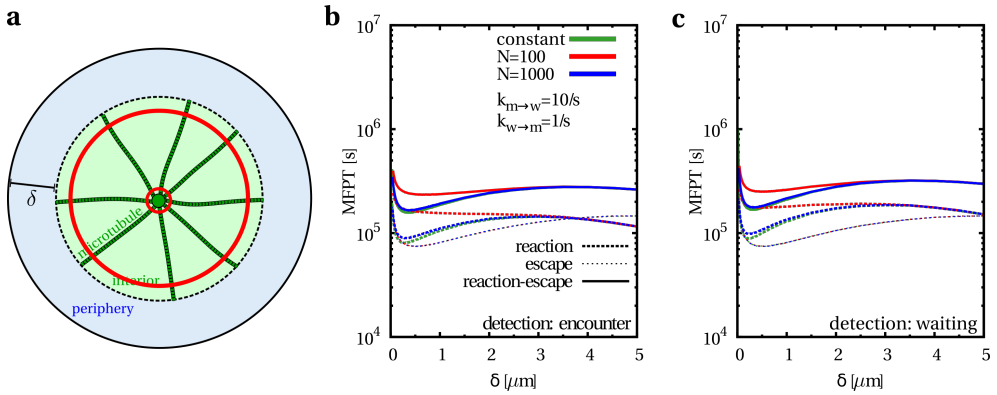

Figure 5.27.: Transport efficiency in 3D cells - impact of the microtubule density. (**a**) A sketch of the microtubule distribution within the cell visualizes the space-dependent filament concentration. Whereas the inner red circle is densely occupied by microtubules, the outer red circle is only sparsely intersected by microtubules. (**b**) The MFPT of the reaction, the subsequent escape, and the combined reaction-escape problem are shown as a function of the cortex width δ for spherical cells of radius R_m=5μm. The varying microtubule density is considered by space-dependent transition rates $\tilde{k}_{w\to m}(r)$ and a total mean number $N_\mathrm{MT} \in \{10^2; 10^3\}$ of microtubules in the cell. The results are compared to constant waiting times. Biologically reasonable transition rates $k_{m\to w}$=v/ℓ=10/s, $k_{w\to m}$=1/s and target sizes R_d=0.1 μm, α_exit=0.2 are applied for p_antero=1 and v=1 μm/s. Reaction occurs by encounter regardless of the motility state. (**c**) The same as in (b) but reaction is limited to the waiting state. Figures b and c are reprints of [Hafner2018], Biophysical Journal, 114, 1420-1432, 2018, (`http://dx.doi.org/10.1016/j.bpj.2018.01.042`).

Remarkably, Fig. 5.26, b and c, show that for biologically reasonable parameters the MFPT is again minimized by a thin actin cortex [Hafner2018]. While the eccentricity of the spheroid has little effect on the reaction problem, increasing the eccentricity leads to a more pronounced minimum of the MFPT in the case of the escape and the combined reaction-escape problem. In the following, we focus on spherical cells again.

5.7.3. Impact of the microtubule density

Here, we investigate how the space-dependent density of microtubules in the interior of the cell effects the efficiency of targeted intracellular transport [Hafner2018]. In general, the concentration of microtubules is not constant throughout the cell. It is greatest close to the MTOC and gradually dilutes, as depicted in Fig. 5.27, a. Hence, the concentration of microtubules $\rho(r)$ decreases with increasing distance r from the cell center and can be approximated by [Hafner2018]

$$\rho_\mathrm{2D}(r) = \frac{N_\mathrm{MT}\, d_\mathrm{MT}}{2\pi r}, \tag{5.16}$$

$$\rho_\mathrm{3D}(r) = \frac{N_\mathrm{MT}\, \pi\, (d_\mathrm{MT}/2)^2}{4\pi r^2} = \frac{N_\mathrm{MT}\, d_\mathrm{MT}^2}{16 r^2}, \tag{5.17}$$

in two and three dimensions, respectively. The mean number of microtubules within the cell is roughly N_{MT}=10^2−10^3 [86, 87] and d_{MT}=25nm corresponds to the diameter of a single microtubule [2]. Such a decreasing concentration of microtubules can be incorporated into our probabilistic model by introduction of a space-dependent transition rate $\tilde{k}_{w\to m}(r)$ in the cell interior, according to [Hafner2018]

$$\tilde{k}_{w\to m}(r)=\rho(r)\cdot k_{w\to m}. \tag{5.18}$$

Hence, the mean waiting time per arrest state increases gradually with the distance r from the cell center as the concentration of microtubules decreases likewise [Hafner2018].

Figure 5.27, b and c, displays the MFPT of the reaction, the subsequent escape, and the combined reaction-escape problem for biologically reasonable parameters and space-dependent transition rates $\tilde{k}_{w\to m}(r)$ in comparison to the results for a constant transition rate $k_{w\to m}$ [Hafner2018]. Remarkably, a space-dependent internal transition rate $\tilde{k}_{w\to m}(r)$ has a strong impact on the reaction problem for small cortex widths $\delta < 1$ even though p_{antero}=1 restricts the motion of the tracer particles to the cortex once it is reached. For N_{MT}=100 a homogeneous cytoskeleton with δ=1 is most efficient for the reaction problem. As expected, the narrow escape problem which subsequently follows the reaction problem is not affected by the the space-dependent microtubule density at all. The reason is the high probability for radially outward transport p_{antero}=1, such that reactions mainly occur in the cell periphery, see Fig. 5.16, c-e, and the motion of the product particle is restricted to the cortex as well. Inhomogeneous search strategies are still favorable for the reaction escape problem. Overall, a space-dependent transition rate has only a strong impact for small cortex widths δ, which lead to long waiting periods in the interior. For $\delta \to 1$ the impact of the space-dependent microtubule concentration vanishes as there is no interior with microtubules at all.

5.7.4. Impact of the actin orientation

So far, we studied isotropic actin orientations in the cortex, as indicated by Eq. 5.5, 5.12, and 5.14. Although actin filaments typically are thought to be isotropically oriented [2, 93], elucidating the exact distribution of cortical filaments in living cells is objective of ongoing research. Actually, it is reported that actin filaments align to microtubules [105] and actin filaments in cellular blebs are tangentially oriented to the membrane [97].

Here, we analyze the influence of non-isotropic actin filaments on the search efficiency of various intracellular transport tasks [Hafner2016, Hafner2018]. First, we focus on three-dimensional, spherical cells with biologically relevant parameters, i.e. R_{m}=5μm, R_{d}=0.1 μm, α_{exit}=0.2, v=1 μm/s, $k_{m\to w}$=10/s, $k_{w\to m}$=1/s, and p_{antero}=1 and investigate non-uniform, cut-off-gaussian rotation angle distributions in the cell cortex according to [Hafner2018]

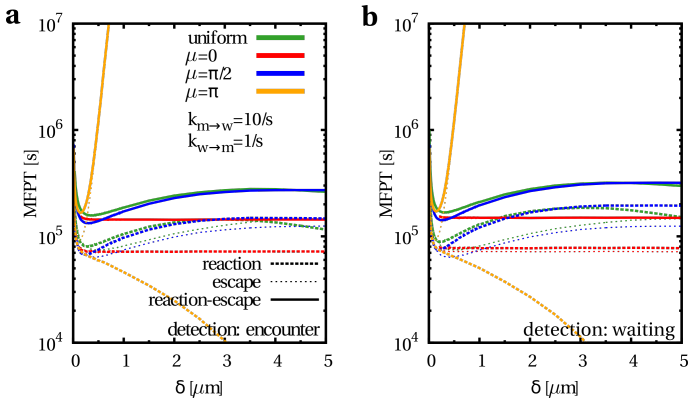

Figure 5.28.: Transport efficiency in 3D cells - impact of the actin orientation. The MFPT of the reaction, the subsequent escape, and the combined reaction-escape problem are shown as a function of the cortex width δ for spherical cells of radius R_m=5μm. Actin filaments in the cortex are either uniformly distributed, according to Eq. 5.14, or gaussian distributed with diverse mean values $\mu \in \{0;\pi/2;\pi\}$ and standard deviation σ=1, according to Eq. 5.19. Biologically reasonable transition rates $k_{m\to w}$=10/s, $k_{w\to m}$=1/s and target sizes R_d=0.1 μm, α_exit=0.2 are applied for p_antero=1 and v=1 μm/s. (**a**) Reaction occurs by encounter regardless of the motility state. (**b**) Reaction is limited to the waiting state. Reprint of [Hafner2018], Biophysical Journal, 114, 1420-1432, 2018, (`http://dx.doi.org/10.1016/j.bpj.2018.01.042`).

$$\tilde{f}_\mathrm{3D}(\alpha_\mathrm{rot}) = \begin{cases} p_\mathrm{antero}\,\delta(\alpha_\mathrm{rot}) + (1-p_\mathrm{antero})\,\delta(\alpha_\mathrm{rot}-\pi), & \text{for } 0 < r < R_\mathrm{m}-\delta, \\ \frac{\mathcal{N}}{\sqrt{2\pi\sigma^2}} \exp\left(-\frac{(\alpha_\mathrm{rot}-\mu)^2}{2\sigma^2}\right), & \text{for } R_\mathrm{m}-\delta < r < R_\mathrm{m}, \end{cases} \tag{5.19}$$

with mean $\pi \geq \mu \geq 0$, variance σ^2, and normalization $\mathcal{N}$ such that $\alpha_\mathrm{rot} \in [0;\pi]$. In consequence, a mean $\mu \in [0;\pi/2)$ ($\mu \in (\pi/2;\pi]$) corresponds to actin filaments which predominantly point outwards (inwards), whereas μ=$\pi/2$ takes into account tangentially oriented filaments in the cortex. In Fig. 5.28, we study the impact of gaussian distributed actin filaments in comparison to isotropic filaments in the cortex. In order to isolate the effect of the mean value $\mu \in \{0;\pi/2;\pi\}$, we first fix the variance to σ=1. Remarkably, we find that the MFPT as a function of the cortex width δ drastically changes in response to the mean μ [Hafner2018]. For laterally oriented actin filaments characterized by μ=$\pi/2$, there is no significant deviation from the uniform case, because of the equal likelihood of radially outward- and inward-directed transport [Hafner2018]. Generally, an inhomogeneous search strategy is most efficient for the three studied transport tasks. However, for μ=0, the minimum of the MFPT at a thin cortex $\delta \in (0;1)$ vanishes and a homogeneous search strategy with δ=1 is advantageous for the reaction, the subsequent escape, as well as the combined reaction-escape problem [Hafner2018]. In contrast, for μ=π, the establishment of a thin actin cortex is crucially important for an efficient escape, and reaction-escape problem, whereas the reaction problem is improved by several orders of magnitude for a homogeneous search strategy with δ=1 [Hafner2018]. This emphasizes the strong impact of the actin polarity on the search efficiency of various transport tasks.

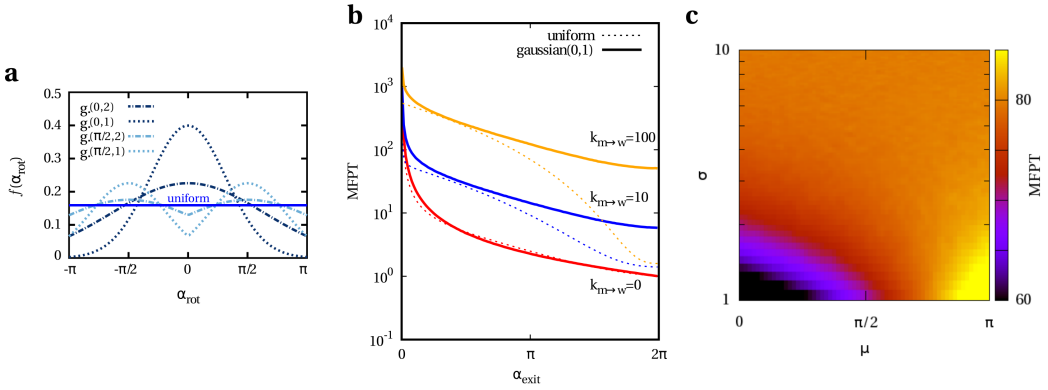

Figure 5.29.: The narrow escape problem on a homogeneous cytoskeleton - impact of the actin orientation. (**a**) The distribution of actin filaments in the cortex is plotted according to Eq. 5.20 for diverse values of (μ, σ). (**b**) The MFPT is shown in dependence of the exit size α_{exit} for $k_{m\to w} \in \{0; 10; 100\}$ and $k_{w\to m}{=}\infty$. The results for a homogeneous isotropic cytoskeletal network are compared to the ones of a gaussian network with mean $\mu{=}0$ and standard deviation $\sigma{=}1$. (**c**) The MFPT to a narrow escape $\alpha_{\text{exit}}{=}0.1$ is measured as a function of the mean μ and the standard deviation σ of the actin filament distribution 5.20 for $k_{m\to w}{=}0$ and $k_{w\to m}{=}\infty$. Figures a and b are modifications of [Hafner2016], Physical Biology, 13, 066003, 2016, (`http://dx.doi.org/10.1088/1478-3975/13/6/066003`).

In order to shed a light on the impact of the actin polarity, we consider the narrow escape problem for two-dimensional cells, because particle trajectories are easier to visualize. We use the two-dimensional complement of the rotation angle distribution, given in Eq. 5.19 [Hafner2016]

$$\tilde{f}_{2\text{D}}(\alpha_{\text{rot}}) = \begin{cases} p_{\text{antero}}\,\delta(\alpha_{\text{rot}}) + (1{-}p_{\text{antero}})\,\delta(\alpha_{\text{rot}}{-}\pi), & \text{for } 0 < r < R_{\text{m}}{-}\delta, \\ \frac{1}{2}f^{+} + \frac{1}{2}f^{-}, & \text{for } R_{\text{m}}{-}\delta < r < R_{\text{m}}, \end{cases} \tag{5.20}$$

with

$$f^{\pm} = \frac{\mathcal{N}}{\sqrt{2\pi\sigma^2}} \exp\left(-\frac{(\alpha_{\text{rot}} \mp \mu)^2}{2\sigma^2}\right), \text{ for } \alpha_{\text{rot}} \in [0;\pi],\ \alpha_{\text{rot}} \in [-\pi;0], \text{ respectively} \tag{5.21}$$

and mean $0 \le \mu \le \pi$, variance σ^2, and normalization $\mathcal{N}$ such that $\alpha_{\text{rot}} \in (-\pi;\pi]$. The distribution is plotted in Fig. 5.29, a, for diverse mean values μ and variances σ^2.

We first focus on a homogeneous cytoskeleton with $\delta{=}1$, such that the whole cell body is filled with actin filaments [Hafner2016]. Figure 5.29, b, displays the MFPT as a function of the exit size α_{exit} for $k_{m\to w} \in \{0; 10; 100\}$ and $k_{w\to m}{=}\infty$. The MFPT on a radially outward-pointing cytoskeleton, defined by Eq. 5.20 with $\mu{=}0$ and $\sigma{=}1$, is compared to the one of an isotropic network, according to Eq. 5.12. As already expected by the study of Ando *et al.* [78], a radially outward-oriented network is highly advantageous to the isotropic one in the limit of large exit zones $\alpha_{\text{exit}} \to 2\pi$. But, remarkably, it also significantly improves the search efficiency

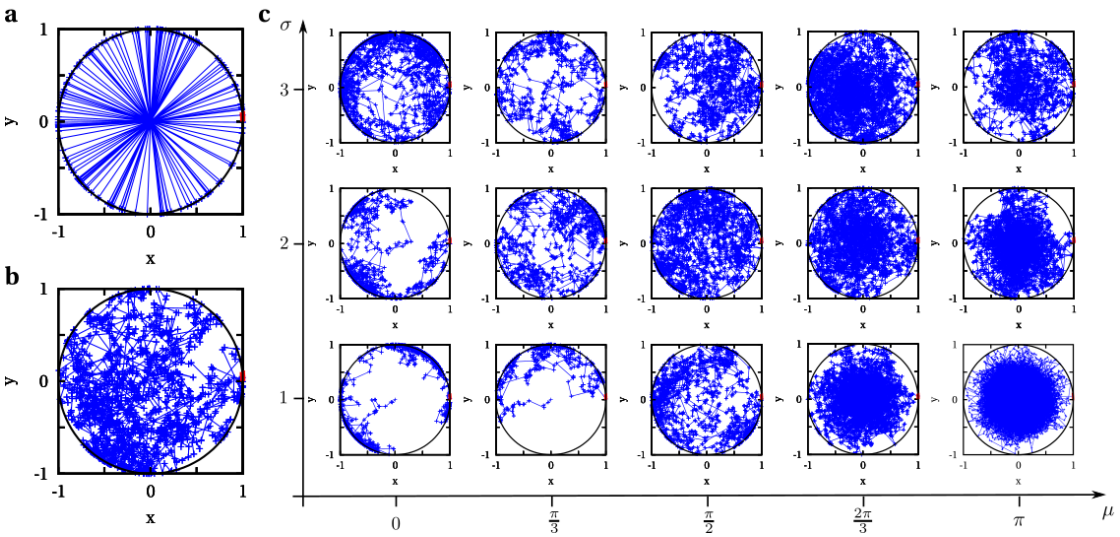

Figure 5.30.: The narrow escape problem on a homogeneous cytoskeleton - impact of the actin orientation on sample trajectories. Sample trajectories are shown for the narrow escape problem with α_{exit}=0.1 (red zone) on a homogeneous cytoskeleton organization. State transitions occur at $k_{m\to w}$=10 and $k_{w\to m}$=∞. Different orientations of filaments are applied as follows. (**a**) Trajectory on a radial microtubule network, i.e. δ=0. (**b**) Trajectory on an isotropic actin network, i.e. according to Eq. 5.12 with δ=1. (**c**) Trajectories on a gaussian distributed actin network with various mean values μ and standard deviations σ, i.e. according to Eq. 5.20 with δ=1. Reprint of [Hafner2016], Physical Biology, 13, 066003, 2016, (`http://dx.doi.org/10.1088/1478-3975/13/6/066003`).

for small exits $\alpha_{\text{exit}} \to 0$ [Hafner2016]. Figure 5.29, c, emphasizes that the search for narrow escapes on a homogeneous cytoskeleton benefits from outward-directed networks ($\mu < \pi/2$), whereas inward-directed networks ($\mu > \pi/2$) impede target detection on the membrane. As expected, the larger σ, the less the impact of the mean μ, since the distribution gradually broadens and aligns to the isotropic case [Hafner2016].

The sample trajectories shown in Fig. 5.30 for σ=1 clearly demonstrate that the tracer particle exhibits different residence areas within the cell in response to the mean μ [Hafner2016]. For outward-directed filaments with $\mu < \pi/2$, the cargoes are mainly moving alongside the plasma membrane of the cell, whereas for inward-directed filaments with $\mu > \pi/2$, particles are driven towards the cell center. Increasing the standard deviation σ randomizes the trajectories as the distribution 5.20 broadens. Outward-directed filaments with $\mu < \pi/2$ provide a topologically induced technique to efficiently examine the membrane for the target [Hafner2016]. Targets are detected faster than for isotropic filaments, since the particle is predominantly moving alongside the plasma membrane - even without a confining cortex. In contrast, the search efficiency is significantly decreased by inward-directed networks, which drive the particle to the cell center and thus hinder the detection of targets on the cell membrane [Hafner2016].

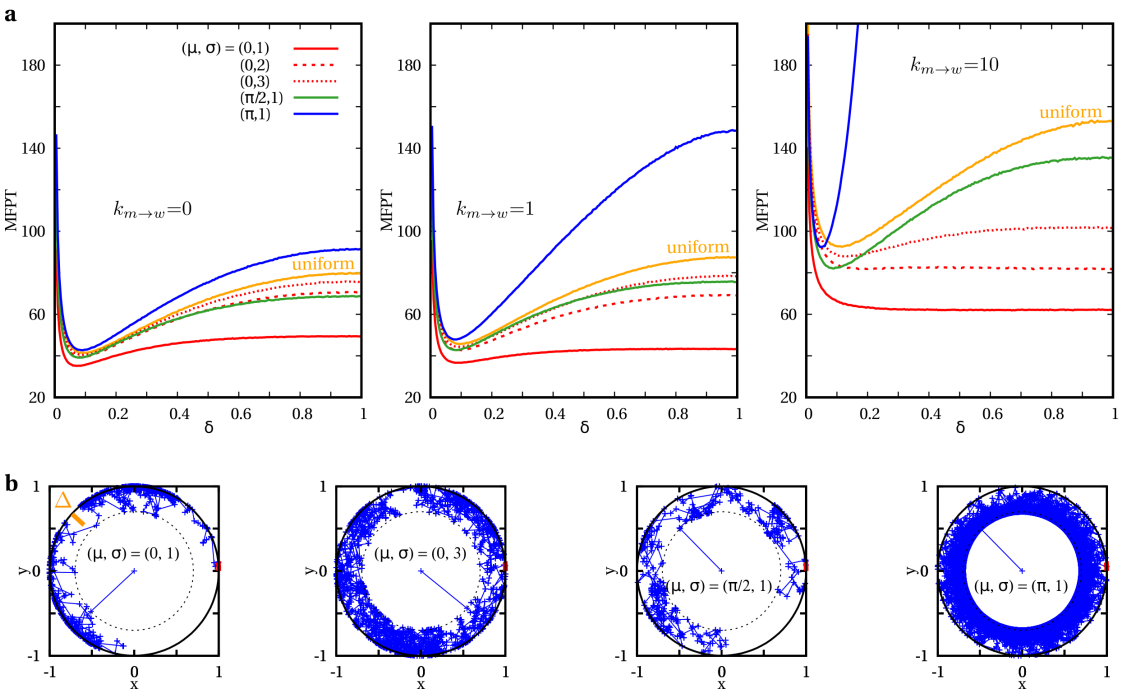

Figure 5.31.: The narrow escape problem on an inhomogeneous cytoskeleton - impact of the actin orientation. (**a**) The MFPT is measured as a function of the cortex width δ for gaussian distributions of the cortical filaments with mean μ and standard deviation σ. The results are compared to the case of uniformly distributed cortical filaments. Otherwise $k_{m\to w} \in \{0; 1; 10\}$, $k_{w\to m}=\infty$, $p_{\text{antero}}=1$, and $\alpha_{\text{exit}}=0.1$ are applied. (**b**) Sample trajectories of the narrow escape problem with $k_{m\to w}=10$, $k_{w\to m}=\infty$, $p_{\text{antero}}=1$, and $\alpha_{\text{exit}}=0.1$ are plotted for $\delta=0.3$ and diverse values of the mean μ and the standard deviation σ. Figure b is a modification of [Hafner2016], Physical Biology, 13, 066003, 2016, (`http://dx.doi.org/10.1088/1478-3975/13/6/066003`).

Figure 5.31 shows the MFPT of the narrow escape problem as a function of the cortex width δ for various gaussian distributions of cortical filaments in comparison to the uniformly distributed case [Hafner2016]. The results are in complete analogy to the three-dimensional case shown in Fig. 5.28. First, we focus on peaked distributions with σ=1. Outward-directed cortical networks with $\mu < \pi/2$ drive the particle towards the membrane such that it is mainly moving alongside the boundary on a ring of width Δ which is sketched in Fig. 5.31, b, and depends on the mean μ, the standard deviation σ, and the transition rate $k_{m\to w}$. Consequently changing the cortex width δ does not effect the MFPT of either intracellular search problem as long as δ is not within the range of Δ [Hafner2016], as shown in Fig. 5.28 and 5.31. Under biological conditions, a homogeneous search strategy with δ=1 is most efficient, whereas a minimum of the MFPT still occurs for small transition rates $k_{m\to w}$, as shown in Fig. 5.31, a. Tangentially-oriented cortical networks with μ=$\pi/2$ do not introduce a higher chance for outward- or inward-directed transport. Thus, search problems on lateral networks are very similar to the ones on isotropic cortical networks [Hafner2016], as manifested by the results

shown in Fig. 5.28 and 5.31. An inhomogeneous cytoskeleton is generally advantageous. Inward-directed cortical networks with $\mu > \pi/2$ move the particles in radially inward direction. Since the reaction problem is generally optimal for a high probability of motion directed to the cell center, see Fig. 5.16 and 5.17, inward-directed homogeneous networks significantly improve the reaction efficiency [Hafner2018], as shown in Fig. 5.28. In contrast, the escape problem is substantially hindered as the particle rarely touches the membrane. Thus, the establishment of a thin cortex is crucial, as illustrated by the sample trajectories in Fig. 5.31, b. A thin actin cortex forces the particles closer to the membrane and thus decreases the MFPT by several orders of magnitude [Hafner2016], as shown in Fig. 5.28 and 5.31, a. Increasing the standard deviation σ randomizes the cortical network as the distribution gradually broadens. Consequently, the MFPT converges to the uniform case, as shown in Fig. 5.31, a, exemplary for μ=0 [Hafner2016]. Again, an inhomogeneous cytoskeleton constitutes the most efficient search strategy.

5.8. Summary

The efficiency of intracellular transport is strongly influenced by the interplay between cytoskeleton organization, motor activity, and pausing states of the cargo. Despite the many insightful biological and theoretical investigations, as recapitulated in Chapters 2 and 3, it is still obscure how this interplay effects the efficiency of targeted intracellular transport. Due to its complexity, modeling intracellular transport is a challenging theoretical task. We presented a coarse grained run-and-pause random walk model in inhomogeneous and anisotropic environments to study three paradigmatic transport tasks: the narrow escape, the reaction, and the combined reaction-escape problem [Hafner2016, Hafner2018]. The particle exhibits two states of motility: ballistic motion at random velocities and waiting periods at filament crossings. State transitions are arranged in a Markovian manner by constant transition rates from one state to another. The spatial inhomogeneity of the cytoskeleton is taken into account by a distinct cortex underneath the plasma membrane which divides the cell into interior and periphery. While in the interior only radial transport is possible, the periphery is dominated by isotropic motion on actin filaments. The different motor activity levels are incorporated into the model by certain probabilities for anterograde, or retrograde transport along microtubules, or isotropic transport along actin filaments. In essence, we introduced a probabilistic approach by considering a complex distribution of the random walker's velocity instead of explicitly modeling the underlying cytoskeletal structure. With the aid of Monte Carlo simulations we systematically analyze how the search efficiency in terms of the MFPT to specific targets is influenced by the spatial organization of the cytoskeleton, the motor activity levels, and the frequency of arrest states of the cargo [Hafner2016, Hafner2018].

We showed that the narrow escape problem, which models transport to a small exit zone on the plasma membrane of a cell, is universally optimized by restricting cargo motion to a thin cortex [Hafner2016, Hafner2018]. Within that cortex an uninterrupted motion pattern is beneficial, but the superiority of inhomogeneous search strategies is very robust against changes in the transition rates. Remarkably, we showed that even

in the limit of very long pauses in a cargo's trajectory, an inhomogeneous cytoskeleton is generally advantageous to its homogeneous counterpart.

In the case of the reaction problem, where a searcher has to fuse with another motile particle within the cell, we investigated the reaction efficiency for two different detection modes [Hafner2018]: reaction may occur regardless of the motility state of both particles solely by encounter, or reaction may only be possible if both particles are in the waiting state. The reaction problem is universally optimized by a high activity of dynein motors, such that intracellular cargoes are quickly transported to the center where they react. Nonetheless, inhomogeneous search strategies which are more efficient than the homogeneous counterpart exist also for high probabilities of anterograde transport. But the efficiency of these inhomogeneous search strategies is fragile and depends critically on the pausing behavior of the cargo. Remarkably, we found that the reaction mode has no significant impact on the efficiency under physiological conditions.
We further showed that nonidentical motor activities of searcher and target particle are highly disadvantageous for the reaction efficiency [Hafner2018]. And we saw that less motile target particle are disadvantageous if detection occurs regardless of the motility state, whereas they are beneficial when reaction is restricted to the arrest state [Hafner2018].
In the limit of uniformly distributed immotile targets, homogeneous search strategies or at least an equal motor activity of kinesins and dyneins are most efficient, because they allow the particle to explore the search domain homogeneously [Hafner2018].
In essence, the optimal search strategy for the reaction problem strongly depends on the properties of searcher and target particle. In the case of identically motile particles, the restriction of motility space either to the MTOC or to the cortex is essential. In contrast, for uniformly distributed immotile targets a search strategy which guarantees a homogeneous exploration of space is necessary [Hafner2018].

The reaction-escape problem combines the prior findings on reaction of two identically motile particles and the subsequent escape of the reaction product. A high probability of retrograde transport is optimal for the reaction problem, but is highly disadvantageous for the escape problem, since it prevents particles from reaching the membrane and detecting the escape window. Remarkably, in the case that motility properties are transmitted from searcher to product, the reaction-escape problem is also optimized by a high probability of anterograde transport and the establishment of a thin actin cortex [Hafner2018].

The best search strategies for the various studied transport tasks are summarized in Table 5.3.

Remarkably, by considering biologically reasonable model parameters we found that the optimal width of the actin cortex predicted by our model is in good agreement to experimental measurements. We further took several steps towards a more realistic cell [Hafner2016, Hafner2018]: We showed that inhomogeneous search strategies are also beneficial in the case of polarized, spheroidal cells, we concluded that the space-dependent density of microtubules within the cell may change the efficiency of

the reaction, but not of the subsequent narrow escape problem, and we investigated the impact of non-isotropic distributions of cortical filaments on the efficiency of various intracellular transport tasks. Remarkably, laterally oriented filaments do not significantly alter the search efficiency, but inward- and outward-directed networks do have very opposite effects. Cortical networks which display mainly inward-directed polarities enhance the gain in search efficiency by a thin cortex for the escape and the reaction-escape problem, such that an inhomogeneous search strategy is crucial for efficient search strategies. But, inward-directed homogeneous networks are favorable for the reaction problem as they drive the particles towards the cell center. In contrast, cortical networks which exhibit mainly outward-directed polarities significantly improve the search efficiency in comparison to isotropic cortical networks. The network topology provides a mechanisms to propagate the particles alongside the plasma membrane for efficient target detection even without a confining cortex.

To conclude, we showed that a cell is able to regulate the efficiency of diverse intracellular transport tasks, as well as the spatial distribution of intracellular reaction products by controlling the cytoskeleton architecture, the motor activities, and the pausing frequency of cargo particles. A spatially inhomogeneous cytoskeleton architecture with a thin actin cortex can substantially increase the efficiency of various transport tasks in comparison to its homogeneous complement [Hafner2016, Hafner2018].

Table 5.3.: Run-and-pause random walk on a spatially inhomogeneous and anisotropic cytoskeleton - recap of optimal search strategies. Optimal search strategies for narrow escapes α_{exit}=0.1 and reaction radii R_{d}=0.1 are recapitulated. The transition rates $k^{\text{opt}}_{m\to w}$ and $k^{\text{opt}}_{w\to m}$ of a homogeneous cytoskeleton structure are applied for the inhomogeneous case [Hafner2018].

	homogeneous		inhomogeneous	
	$k^{\text{opt}}_{m\to w} \approx$	$k^{\text{opt}}_{w\to m} \approx$	$p^{\text{opt}}_{\text{antero}} \approx$	$\delta^{\text{opt}} \approx$
narrow escape	0	∞	1	$\in]0;1[$
reaction: motile target				
· detection: encounter	0	∞	0	0
· detection: waiting	13	34	0	0
reaction: immotile target				
· detection: encounter	0	∞	0.5	1
· detection: waiting	7	∞	0.5	1
reaction-escape				
· detection: encounter	0	∞	1	$\in]0;1[$
· detection: waiting	5	22	1	$\in]0;1[$

Chapter 6.

Conclusion and discussion

Intracellular transport is shaped by the interplay between the cytoskeleton architecture, the motor activity, and the waiting frequency of cargo particles. Typically, the cytoskeleton is highly inhomogeneous and anisotropic. Actin filaments randomly populate the cell cortex, whereas microtubules radiate from the central MTOC [2]. A single cargo is dragged along the cytoskeleton with the aid of several motor species [17–31], whose activity is controlled by the cell to ensure correct delivery [19–28, 31, 32]. Thereby, the large cargo-motor complexes frequently pause at filament crossings until they either overcome the barrier or switch to another track [29, 33–38]. Hence, intracellular cargoes undergo a stochastic motion pattern with random alternations between directed transport along the cytoskeleton and reorienting arrest states.

How the interplay between the cytoskeleton architecture, the motor activity, and the cargo pausing, affects anomalous diffusion and the efficiency of targeted intracellular transport is elusive.

Due to its complexity, the theoretical modeling intracellular transport is a challenging task. But, the stochastic motion pattern suggests a random walk approach. It is known, that anomalous diffusion can arise either due to the anisotropy of the cytoskeleton [62,63] or due to transient trapping events [64]. Moreover, intermittent search strategies with two states of motility, i.e. a slow reactive state and a fast relocation state, are shown to have a positive impact on the temporal efficiency of intracellular transport [68–75]. But, such search strategies are usually studied in homogeneous environments. The inhomogeneity of the cytoskeleton is typically neglected. Very recently, the impact of the exact topology of the cytoskeleton on intracellular transport tasks has gained scientific interest, see for instance [76–80], which highlights the topicality of our research.

However, up to now the impact of the cytoskeleton architecture, the motor activity, and the arrest states of the cargo have been investigated only separately in the literature, as discussed in chapter 3. In this thesis, we presented a unified random walk perspective on intracellular transport. We addressed how such physiological conditions effect anomalous diffusion and efficiency of cargo delivers.

In chapter 4, we focused on anomalous diffusion of intracellular tracer particles. A random walk model was introduced to investigate the unidirectional motion of cargo on a single, polarized filament which is frequently interrupted by pauses [Hafner2016B]. Within an analytic framework, we derived an exact expression for the probability density

function of the tracer's displacement, which is only possible in the one-dimensional case [Hafner2016B]. Due to non-trivial correlations in the particle's velocity, the two-dimensional model requires a more elaborate analytic technique which allows the calculation of arbitrary moments of the particle's displacement probability density function [Hafner2014, Hafner2016B].
The resulting MSD revealed complex anomalous diffusion. Crossovers between different anomalous regimes appear on short and intermediate timescales. Fitting the analytic expression of the MSD to a power law enables us to monitor the temporal evolution of the anomalous exponent over all timescales [Hafner2016B]. Remarkably, the anomalous exponent is a complex function of time, which emphasizes that the observed anomaly is a highly transient effect based on aging processes out of a predefined initial state.
The impact of the initial state is of crucial importance for the interpretation of experimental results. Even though it is experimentally difficult to identify diverse internal motility states of intracellular cargoes and correlations therein (which is objective of ongoing research, see for instance [255]), it is important to acknowledge that the initial state of the measurements as well as the chosen averaging procedure have a strong impact on the results. We explored the MSD as an ensemble averaged quantity, which fully captures the equilibration of the underlying Markov chain of states and consequently leads to transient subdiffusive regimes [Hafner2016B]. These subdiffusive regimes would not appear in a time averaged MSD for the very same process, since the impact of the initial condition would vanish due to the averaging technique [64, 66] [Hafner2014]. Consequently, the same biological process can lead to apparently different results depending on the measurement procedure.
We further showed that the crossover time to the asymptotic limit as well as the long time diffusion constant cover several orders of magnitude in response to the pausing frequency of the cargo and the anisotropy of the cytoskeleton [Hafner2016B]. It is questionable whether these regimes can ever be reached in practice. By assuming the smallest possible cargo step length of 8 nm and a typical motor velocity of 1 μm/s [2], the crossover occurs on a lengthscale 0.1 μm - 1000 μm and a timescale 0.01 s - 1000 s, depending on the frequency of state transitions [Hafner2016B]. Even in that case, the confinement of cargo within the cell and the time range which is accessible in experiments should play a crucial role.

In chapter 5, we studied the temporal efficiency of targeted intracellular transport. We introduced a random walk model [Hafner2016, Hafner2018] with stochastic transitions between two states of motility: ballistic motion at random velocities along the cytoskeleton and reorienting stationary states at filament crossings. State transitions are arranged in a Markovian manner by generally asymmetric rates. In general, the transition rates may depend on each other. For instance the effective mesh size of the cytoskeleton, which defines the transition rate to the waiting state, and the mean waiting time at filament crossings depend on the size of the transported cargo [29, 38]. In order to cover the full parameter space, we investigated the most general case of independent transition rates. The cytoskeleton architecture is implicitly taken into account by a space-dependent distribution of the particle velocity. The particle experiences radial transport in the cell interior, whereas multi-directional transport is restricted to a cortex underneath the plasma membrane. The different motor activity levels are incorporated

into the model by certain probabilities for anterograde/retrograde transport along microtubules, respectively, or transport along actin filaments. In essence, we presented a powerful probabilistic approach to intracellular transport by considering a complex distribution of the random walker's velocity instead of explicitly modeling the underlying cytoskeletal structure together with the dynamic instability of the filaments. With the aid of extensive Monte Carlo simulations, we systematically analyzed how the interplay between the structural characteristics of the cytoskeleton, the motor activity, and the waiting states of the cargo effects the efficiency of targeted intracellular transport [Hafner2016, Hafner2018]. The transport efficiency was measured in terms of the MFPT to a specific target. We considered three paradigmatic tasks: the narrow escape problem, which models transport to a specific area on the plasma membrane, the reaction problem, which evaluates the time until fusion of two reactants within the cell, and the reaction-escape problem, which emerges when two particles first have to react inside the cell before the product particle is transported to a narrow exit on the plasma membrane [Hafner2016, Hafner2018].

Note that in the limit of small diffusion constants our findings are in qualitative agreement to search strategies with intermittent diffusion which were recently studied by Schwarz *et al.* [79, 80]. The limit of a vanishing diffusion constant is biologically relevant for large intracellular cargo, such as vesicles, mitochondria, or macromolecules, which experience size-dependent subdiffusion in the crowded cytoplasm and thus exhibit effectively stationary states [39–41, 50, 51, 55]. But more importantly, since a single cargo is typically attached to several motor proteins concurrently [17–31], a full detachment off the filament is rather unlikely [31]. Instead, arrest states at filament crossings are observed in *in vitro* experiments as well as in live-cell microscopy [29, 33–38]. In contrast to Schwarz *et al.* [79, 80], we systematically analyzed the impact of transient pauses on intracellular transport and performed several steps towards more physiological conditions [Hafner2016, Hafner2018].

We showed that the narrow escape problem is universally optimized by the confinement of cargo motion to a thin cortex with the aid of a high activity level of anterograde motors [Hafner2016, Hafner2018]. However, in the limit of an infinitesimal thin cortex, excursions in the cell interior, which are mediated by dyneins, are advantageous, compare to "surface-mediated diffusion" [76, 239–245]. Within the cortex an uninterrupted motion pattern is beneficial, but the advantage of spatially inhomogeneous search strategies is very robust against changes in the transition rates. Remarkably, we showed that even in the limit of very long pauses in a cargo's trajectory, an inhomogeneous cytoskeleton is generally favorable to its homogeneous counterpart [Hafner2016, Hafner2018].

The efficiency of intracellular reactions was studied for two different detection modes [Hafner2018]: On the one hand, reaction occurs solely by encounter regardless of the motility state of both particles. On the other hand, reaction partners are assumed to be inactive when walking along the cytoskeleton, such that reaction is only possible if both particles are in the waiting state, which is reminiscent of intermittent search strategies, e.g. [68–75]. Basically, other detection modes are possible as well: Reaction could exclusively depend on the searcher's or the target's motility state, or reaction could only be possible in the motion state. For symmetric particles, the first two alternatives would yield the same results. But, as long as biological evidence for the actual reaction mode is lacking, the two modes under investigation appear to be the most reasonable

ones. Remarkably, we find that for physiological conditions the reaction mode has no significant impact on the reaction efficiency [Hafner2018].In the case of two identically motile particles within the cell, efficient reaction depends on the restriction of motility space either to the MTOC or to a thin cortex. The reaction problem is universally optimized by a high activity of dynein motors. Cargoes are transported on the shortest route to the center where they react [Hafner2018]. In the case of a high probability of anterograde transport, inhomogeneous search strategies exist which are more efficient than the homogeneous counterpart. But the efficiency of these inhomogeneous search strategies is fragile and depends critically on the pausing frequency of the cargo particles [Hafner2018].We further showed that nonidentical motor activities of searcher and target particle are highly disadvantageous for the reaction efficiency [Hafner2018]. And we saw that less motile target particles are disadvantageous if detection occurs regardless of the motility state, whereas they are beneficial when reaction is restricted to the arrest state [Hafner2018]. In the limit of uniformly distributed immotile targets, homogeneous search strategies or at least an equal motor activity of kinesins and dyneins are essential, since they allow a homogeneous exploration of space [Hafner2018]. Note that the optimal motor activity depends critically on the exact spatial distribution of immotile targets within the cell. If targets were located at the center a high probability of retrograde transport would be favorable, whereas a high probability of anterograde transport is advantageous for targets which are distributed close to the membrane [79, 80].
The reaction-escape problem combines the prior findings on reactions of two identically motile particles and the subsequent escape of the reaction product [Hafner2018]. We showed that a high probability of radially inward directed transport is optimal for the reaction problem, but is highly disadvantageous for the escape problem, since it prevents the particles from reaching the membrane and detecting the escape window. Consequently, in the case that motility properties are inherited from searcher to product, the reaction-escape problem is also optimized by a high probability of anterograde transport and the establishment of a thin actin cortex [Hafner2018]. However, the reaction-escape problem would be solved most efficiently if the reaction and the subsequent escape problem would decouple: First the reaction problem is solved by a high activity of dynein motors. Then, motor activities are changed and a high activity of anterograde transport solves the narrow escape problem.
In order to investigate the transport efficiency under physiological conditions, we took several steps towards a more realistic picture of a cell [Hafner2016, Hafner2018]: We showed that inhomogeneous search strategies are also beneficial in the case of polarized, spheroidal cells. We concluded that the space-dependent density of microtubules within the cell may change the efficiency of the reaction, but not of the subsequent narrow escape problem. And we investigated the impact of non-isotropic distributions of cortical filaments on the efficiency of various intracellular transport tasks. Remarkably, laterally oriented filaments do not significantly alter the search efficiency, but inward- or outward-directed networks do have very opposite effects. For cortical networks which display mainly inward-directed actin polarities, an inhomogeneous search strategy with a thin cortex is crucial for the escape and the reaction-escape problem, but a homogeneous strategy is sufficient for the reaction problem as the actin polarities automatically drive the particles towards the cell center. In contrast, cortical networks which exhibit mainly outward-directed polarities generally improve the efficiency of all transport tasks in

comparison to isotropic cortical networks for a high probability of anterograde transport. The network topology provides a mechanisms to propagate the particles alongside the plasma membrane for efficient target detection even without a confining cortex.

In principle, our probabilistic approach to intracellular transport enables us to implicitly take into account several other aspects of transport in living cells. For instance, the cytoplasm is highly crowded with cell organelles or macromolecules [2, 50]. Hard-sphere-interactions with such obstacles can be studied implicitly within our model by a higher frequency of arrest states. For the narrow escape problem we showed that the superiority of inhomogeneous search strategies is highly robust against changes in the transition rates [Hafner2016, Hafner2018]. However, our results suggest that efficient search strategies for the reaction problem will be critically affected by obstacles [Hafner2018]. Based on our results, it would be informative to address in future studies how the speed of diverse motor proteins affects the transport efficiency instead of assuming a constant effective motor speed. Furthermore, we assumed instantaneous reactions, but how a certain reaction rate influences the reaction kinetics is elusive for motile targets. When considering cells which are not rotationally symmetric, such as polarized spheroidal cells, it is obscure how the position of the exit zone on the plasma membrane affects the narrow escape problem. And concerning T cell killing, although collecting lytic granules at an MTOC which is located close to the synapse improves specific killing, the impact of the massive reorganization of the cytoskeleton on the transport efficiency is not clear per se [8–10, 13, 14, 256–260]. Furthermore, we started to investigate the full distribution of first passage times and found a broadening with decreasing cortex width [Hafner2018]. It is worth studying how far the MFPT is significant for the efficiency of intracellular transport [251, 252]. And, in particular, studying multiple searcher and target particles within a cell is promising and opens a new range of questions. Instead of focusing on the MFPT, the study of extreme statistics (i.e. when does the first x particles arrive at a given target) has recently gained scientific interest in the context of biological systems [261] and is certainly relevant for e.g. T cell killing as well.

To conclude, within a random walk approach we showed that a cell is able to regulate anomalous diffusion and the efficiency of targeted intracellular transport by control of the interplay between cytoskeleton architecture, motor activity, and pausing frequency of the cargoes [Hafner2016B, Hafner2016, Hafner2018]. Transient anomalous diffusion defines the spatiotemporal spreading of intracellular cargo on short and intermediate timescales [Hafner2016B] and the efficiency of targeted intracellular transport is substantially increased by a spatially inhomogeneous cytoskeleton which involves a thin actin cortex [Hafner2016, Hafner2018]. In this way, we have contributed to a deeper understanding of intracellular transport phenomena.

Appendix A.

Pseudo codes

Contents

Here, we present pseudo codes of the Monte Carlo simulations to evaluate the MSD and the MFPT of run-and-pause random walks in inhomogeneous and anisotropic environments, as studied in Chapters 4 and 5. For a general introduction to Monte Carlo simulations, see for instance textbooks such as [262, 263].

A.1. MSD of random walks studied in Chapter 4

Here, we sketch the Monte Carlo simulation to study the MSD of the random walks studied in Chapter 4. The MSD $\langle x_n^2 \rangle$ of a particle at time step n is evaluated by averaging over an ensemble of N independent realizations of the walk $\{x_n^j\}_{j=1,\dots,N}$ according to

$$\langle x_n^2 \rangle = \int x^2 \, P_n(x) \, \mathrm{d}x = \lim_{N\to\infty} \frac{1}{N} \sum_{j=1}^{N} {x_n^j}^2, \tag{A.1}$$

where the random variable x_n^j is distributed according to $P_n(x)$.

The basic procedure to generate the random variable x_n^j is sketched in the following pseudo code. At each step of the walk, the particle's position is updated according to its current motility state: motion (M) or waiting (W). Furthermore, the MSD is updated and averaged over an ensemble of at least $N{=}10^6$ independent random walks.

input : The motion of a tracer particle is defined by:
time step $i \in 1, \ldots, n$,
position x_i,
state $s_i \in \{M; W\}$,
step length distribution $\mathcal{F}(\ell)$,
transition probabilities κ_m, κ_w, and
initial condition P_0^M.
output: MSD_i, $i \in 1, \ldots, n$

```
// ensemble loop:
for (i=0; i < (n+1); i++) do MSD_i=0;
for (j=0; j < N; j++) do
    // initialization:
    x_0=0;
    s_0 ∈ {M, W} according to P_0^M;
    // step loop:
    for (i=0; i < n; i++) do
        random number r ∈ [0; 1];
        if (s_i=M) then
            if (r < κ_w) then
                s_{i+1}=W;
                x_{i+1}=x_i;
            end
            else
                s_{i+1}=M;
                ℓ according to F(ℓ);
                x_{i+1}=x_i+ℓ;
            end
        end
        else
            if (r < κ_m) then
                s_{i+1}=M;
                ℓ according to F(ℓ);
                x_{i+1}=x_i+ℓ;
            end
            else
                s_{i+1}=W;
                x_{i+1}=x_i+;
            end
        end
        MSD_{i+1}+=x_{i+1}^2/N;
    end
end
```

In the case of motion on a two-dimensional network, correlations in the random walker's velocity have to be taken into account [Hafner2014, Hafner2016B].

A.2. MFPT of random walks studied in Chapter 5

Here, we sketch the basic Monte Carlo simulation to study the MFPT of the random walks studied in Chapter 5. We present the general pseudo code exemplarily for the narrow escape problem of a single particle. A generalization to the reaction problem of two particles and the combined reaction-escape problem is straightforward but extensive. For all search problems, we measure the MFPT to target detection by use of an event-driven algorithm which is based on Gillespie's method [264–266] and calculates the MFPT as an ensemble average over at least $N{=}10^6$ independent realizations of the walk.

In the following, $\Delta t_{\text{gillespie}}$ denotes the time to the next transition between the two motility states, i.e. motion and waiting. Whereas $\Delta t_{\text{confinement}}$ characterizes the time to the next confinement event, i.e. when the particle hits the MTOC ($r{=}0$), the inner border ($r{=}R_{\text{m}}{-}\delta$), or the membrane ($r{=}R_{\text{m}}$).

input : The motion of a tracer particle is defined by:
time t,
position $\boldsymbol{r}(r, \phi_r)$,
state $\in$ {motion; waiting},
location $\in$ {MTOC, interior, inner border, periphery, membrane},
velocity $\boldsymbol{v}(v, \phi_v)$,
radius of the sphere R_{m},
width of the actin cortex δ,
escape opening angle α_{exit},
transition rates $k^i_{m\to w}$, $k^p_{m\to w}$, $k_{w\to m}$,
speed v,
processivity ω, and
rotation angle distribution $f(\alpha_{\text{rot}})$
with motor activities p_{antero} and q_i with $i \in \{\text{K}, \text{D}, \text{M}\}$.
For simplicity, assume $\omega{=}0$ and $q_{\text{M}}{=}1$.
output: MFPT

```
// ensemble loop:
MFPT=0;
for (j=0; j < N; j++) do
    // initialization:
    t=0;
    r=r_0;
    state = motion;
    location = according to r;
    φ_v = according to f(α_rot) and r;
```

```
// step loop:
repeat
    if (state=motion & location=interior) then
        Δt_gillespie = according to k^i_{m→w};
        Δt_confinement = time to r=0 or r=R_m−δ;
        if (Δt_gillespie < Δt_confinement) then
            t+ = Δt_gillespie;
            r= update according to Δt_gillespie;
            state = waiting;
            location = interior;
        end
        else
            t+ = Δt_confinement;
            r= update according to Δt_confinement;
            state = waiting;
            location = MTOC or inner border;
        end
    end
    else if (state=motion & location=periphery) then
        Δt_gillespie = according to k^p_{m→w};
        Δt_confinement = time to r=R_m−δ or r=R_m;
        if (Δt_gillespie < Δt_confinement) then
            t+ = Δt_gillespie;
            r= update according to Δt_gillespie;
            state = waiting;
            location = periphery;
        end
        else
            t+ = Δt_confinement;
            r= update according to Δt_confinement;
            state = waiting;
            location = inner border or membrane;
        end
    end
    else if (state=waiting & location=MTOC) then
        Δt_gillespie = according to k_{w→m};
        t+ = Δt_gillespie;
        state = motion;
        location = interior;
        φ_v = uniformly distributed in α_rot ∈ (−π; π];
    end
```

```
    else if (state=waiting & location=interior) then
        Δt_gillespie = according to k_{w→m};
        t+ = Δt_gillespie;
        state = motion;
        location = interior;
        φ_v = according to f_{0<r<R_m−δ}(α_rot);
    end
    else if (state=waiting & location=inner border) then
        Δt_gillespie = according to k_{w→m};
        t+ = Δt_gillespie;
        state = motion;
        location = interior;
        φ_v = with probability p_antero according to f_{R_m−δ<r<R_m}(α_rot)
              but restricted to α_rot ∈ (−π/2; π/2)
              and with probability (1−p_antero) according to f_D(α_rot);
    end
    else if (state=waiting & location=periphery) then
        Δt_gillespie = according to k_{w→m};
        t+ = Δt_gillespie;
        state = motion;
        location = periphery;
        φ_v = according to f_{R_m−δ<r<R_m}(α_rot);
    end
    else if (state=waiting & location=membrane) then
        Δt_gillespie = according to k_{w→m};
        t+ = Δt_gillespie;
        state = motion;
        location = periphery;
        φ_v = according to f_{R_m−δ<r<R_m}(α_rot)
              but restricted to α_rot ∈ (−π; −π/2) ∪ (π/2; π);
    end
  until (exit is detected);
  MFPT+=t/N;
end
```

Bibliography: own works

[Hafner2014] Anne E. Hafner. A random walk approach to intracellular transport. Master's thesis, Saarland University, 2014. For access to the thesis, please send a query to: anne_hafner@web.de.

[Hafner2016] A. E. Hafner and H. Rieger. Spatial organization of the cytoskeleton enhances cargo delivery to specific target areas on the plasma membrane of spherical cells. *Phys. Biol.*, 13:066003, 2016. (`http://dx.doi.org/10.1088/1478-3975/13/6/066003`).

[Hafner2016B] A. E. Hafner, L. Santen, H. Rieger, and M. R. Shaebani. Run-and-pause dynamics of cytoskeletal motor proteins. *Sci. Rep.*, 6:37162, 2016. (`http://dx.doi.org/10.1038/srep37162`). This work includes results of my master thesis [Hafner2014].

[Hafner2018] A. E. Hafner and H. Rieger. Spatial cytoskeleton organization supports targeted intracellular transport. *Biophys. J.*, 114:1420–1432, 2018. (`http://dx.doi.org/10.1016/j.bpj.2018.01.042`).

Bibliography: references

[1] E. Schrödinger. *What is life? and Mind and Matter*. Cambridge University Press, 1967.

[2] B. Alberts, A. Johnson, J. Lewis, M. Raff, K. Roberts, and P. Walter. *Molecular biology of the cell*. Garland Science, Taylor & Francis Group, 2008.

[3] `https://en.wikipedia.org/wiki/Cell_(biology)`. 13.04.2018.

[4] G. Karp. *Cell and molecular biology concepts and experiments*. John Wiley and Sons, Inc., 1996, 1999.

[5] S. R. Bolsover, J. S. Hyams, E. A. Shephard, H. A. White, and C. G. Wiedemann. *Cell biology: a short course*. John Wiley & Sons, Inc., 2004.

[6] J. Monod. *Chance and necessity*. William Collins Sons & Co Ltd, Fontana Books, 1972.

[7] P. Hunter. Biology is the new physics. *EMBO Reports*, 11:350–352, 2010. (`http://dx.doi.org/10.1038/embor.2010.55`).

[8] G. M. Griffiths. The cell biology of ctl killing. *Curr. Opin. Immunol.*, 7:343–348, 1995. (`http://dx.doi.org/10.1016/0952-7915(95)80108-1`).

[9] G. M. Griffiths. Protein sorting and secretion during ctl killing. *Immunology*, 9: 109–115, 1997. (`http://dx.doi.org/10.1006/smim.1997.0059`).

[10] A. Grakoui, S. K. Bromley, C. Sumen, M. M. Davis, A. S. Shaw, P. M. Allen, and M. L. Dustin. The immunological synapse: a molecular machine controlling t cell activation. *Science*, 285:221–227, 1999. (`http://dx.doi.org/10.1126/science.285.5425.221`).

[11] S. K. Bromley, W. R. Burack, K. G. Johnson, K. Somersalo, T. N. Sims, C. Sumen, M. M. Davis, A. S. Shaw, P. M. Allen, and M. L. Dustin. The immunological synapse. *Annu. Rev. Immunol.*, 19:375–396, 2001. (`http://dx.doi.org/10.1146/annurev.immunol.19.1.375`).

[12] B. Qu, V. Pattu, C. Junker, E. C. Schwarz, S. S. Bhat, C. Kummerow, M. Marshall, U. Matti, M. Pfreundschuh, U. Becherer, H. Rieger, J. Rettig, and M. Hoth. Docking of lytic granules at the immunological synapse in human ctl required vti1b-dependent pairing with cd3 endosomes. *J. Immunol.*, 186:6894–6904, 2011. (`http://dx.doi.org/10.4049/jimmunol.1003471`).

[13] K. L. Angus and G. M. Griffiths. Cell polarisation and the immunological synapse. *Curr. Opin. Cell Biol.*, 25:85–91, 2013. (http://dx.doi.org/10.1016/j.ceb.2012.08.013).

[14] A. T. Ritter, K. L. Angus, and G. M. Griffiths. The role of the cytoskeleton at the immunological synapse. *Immunol. Rev.*, 256:107–117, 2013. (http://dx.doi.org/10.1111/imr.12117).

[15] P. H. St. George-Hyslop, W. C. Mobley, and Y. Christen, editors. *Intracellular traffic and neurodegenerative disorders*. Springer-Verlag Berlin Heidelberg, 2009.

[16] S. J. Atkinson, S. K. Doberstein, and T. D. Pollard. Moving off the beaten track. *Curr. Biol.*, 2:326–328, 1992. (http://dx.doi.org/10.1016/0960-9822(92)90896-I).

[17] A. Ashkin, K. Schütze, J. M. Dziedzic, U. Euteneuer, and M. Schliwa. Force generation of organelle transport measured in vivo by an infrared laser trap. *Nature*, 348:346–348, 1990. (http://dx.doi.org/10.1038/348346a0).

[18] M. A. Welte, S. P. Gross, M. Postner, S. M. Block, and E. F. Wieschaus. Developmental regulation of vesicle transport in drosophila embryos: forces and kinetics. *Cell*, 92:547–557, 1998. (http://dx.doi.org/10.1016/S0092-8674(00)80947-2).

[19] S. P. Gross, M. C. Tuma, S. W. Deacon, A. S. Serpinskaya, A. R. Reilin, and V. I. Gelfand. Interactions and regulation of molecular motors in xenopus melanophores. *J. Cell Biol.*, 156:855–865, 2002. (http://dx.doi.org/10.1083/jcb.200105055).

[20] S. P. Gross, M. A. Welte, S. M. Block, and E. F. Wieschaus. Coordination of opposite-polarity microtubule motors. *J. Cell Biol.*, 156:715–724, 2002. (http://dx.doi.org/10.1083/jcb.200109047).

[21] M. A. Welte. Bidirectional transport along microtubules. *Curr. Biol.*, 14:R525–R537, 2004. (http://dx.doi.org/10.1016/j.cub.2004.06.045).

[22] S. P. Gross. Hither and yon: a review of bi-directional microtubule-based transport. *Phys. Biol.*, 1:R1–R11, 2004. (http://dx.doi.org/10.1088/1478-3967/1/2/R01).

[23] C. Kural, H. Kim, S. Syed, G. Goshima, V. I. Gelfand, and P. R. Selvin. Kinesin and dynein move a peroxisome in vivo: A tug-of-war or coordinated movement? *Science*, 308:1469–1472, 2005. (http://dx.doi.org/10.1126/science.1108408).

[24] C. Kural, A. S. Serpinskaya, Y.-H. Chou, R. D. Goldman, V. I. Gelfand, and P. R. Selvin. Tracking melanosomes inside a cell to study molecular motors and their interaction. *P. Natl. Acad. Sci. USA*, 104:5378–5382, 2007. (http://dx.doi.org/10.1073/pnas.0700145104).

[25] M. Vershinin, B. C. Carter, D. S. Razafsky, S. J. King, and S. P. Gross. Multiple-motor based transport and its regulation by tau. *P. Natl. Acad. Sci. USA*, 104:87–92, 2007. (http://dx.doi.org/10.1073/pnas.0607919104).

[26] S. P. Gross, M. Vershinin, and G. T. Shubeita. Cargo transport: two motors are sometimes better than one. *Curr. Biol.*, 17:R478–R486, 2007. (http://dx.doi.org/10.1016/j.cub.2007.04.025).

[27] A. Kunwar, S. K. Tripathy, J. Xu, M. K. Mattson, P. Anand, R. Sigua, M. Vershinin, R. J. McKenney, C. C. Yu, A. Mogilner, and S. P. Gross. Mechanical stochastic tug-of-war models cannot explain bidirectional lipid-droplet transport. *P. Natl. Acad. Sci. USA*, 108:18960–18965, 2011. (http://dx.doi.org/10.1073/pnas.1107841108).

[28] R. P. Erickson, Z. Jia, S. P. Gross, and C. C. Yu. How molecular motors are arranged on a cargo is important for vesicular transport. *PLoS Comput. Biol.*, 7: e1002032, 2011. (http://dx.doi.org/10.1371/journal.pcbi.1002032).

[29] Š. Bálint, I. Verdeny Vilanova, Á. Sandoval Álvarez, and M. Lakadamyali. Correlative live-cell and superresolution microscopy reveals cargo transport dynamics at microtubule intersections. *P. Natl. Acad. Sci. USA*, 110:3375–3380, 2013. (http://dx.doi.org/10.1073/pnas.1219206110).

[30] W. O. Hancock. Bidirectional cargo transport: moving beyond tug of war. *Nat. Rev. Mol. Cell Biol.*, 15:615–628, 2014. (http://dx.doi.org/10.1038/nrm3853).

[31] C. Appert-Rolland, M. Ebbinghaus, and L. Santen. Intracellular transport driven by cytoskeletal motors: General mechanisms and defects. *Phys. Rep.*, 593:1–59, 2015. (http://dx.doi.org/10.1016/j.physrep.2015.07.001).

[32] R. Mallik and S. P. Gross. Molecular motors: strategies to get along. *Curr. Biol.*, 14:R971–R982, 2004. (http://dx.doi.org/10.1016/j.cub.2004.10.046).

[33] M. Y. Ali, E. B. Krementsova, G. G. Kennedy, R. Mahaffy, T. D. Pollard, K. M. Trybus, and D. M. Warshaw. Myosin va maneuvers through actin intersections and diffuses along microtubules. *P. Natl. Acad. Sci. USA*, 104:4332–4336, 2007. (http://dx.doi.org/10.1073/pnas.0611471104).

[34] J. L. Ross, M. Y. Ali, and D. M. Warshaw. Cargo transport: molecular motors navigate a complex cytoskeleton. *Curr. Opin. Cell Biol.*, 20:41–47, 2008. (http://dx.doi.org/10.1016/j.ceb.2007.11.006).

[35] J. L. Ross, H. Shuman, E. L. F. Holzbaur, and Y. E. Goldman. Kinesin and dynein-dynactin at intersecting microtubules: motor density affects dynein function. *Biophys. J.*, 94:3115–3125, 2008. (http://dx.doi.org/10.1529/biophysj.107.120014).

[36] H. W. Schröder, C. Mitchell, H. Shuman, E. L. F. Holzbaur, and Y. E. Goldman. Motor number controls cargo switching at actin-microtubule intersections in vitro. *Curr. Biol.*, 20:687–696, 2010. (http://dx.doi.org/10.1016/j.cub.2010.03.024).

[37] M. Lakadamyali. Navigating the cell: how motors overcome roadblocks and traffic jams to efficiently transport cargo. *Phys. Chem. Chem. Phys.*, 16:5907, 2014. (http://dx.doi.org/10.1039/C3CP55271C).

[38] I. Verdeny-Vilanova, F. Wehnekamp, N. Mohan, A. S. Alvares, J. S. Borbely, J. J. Otterstrom, D. C. Lamb, and M. Lakadamyali. 3d motion of vesicles along microtubules helps them to circumvent obstacles in cells. *J. Cell Sci.*, 130:1904–1916, 2017. (http://dx.doi.org/10.1242/jcs.201178).

[39] K. Luby-Phelps, P. E. Castle, D. L. Taylor, and F. Lanni. Hindered diffusion of inert tracer particles in the cytoplasm of mouse 3t3 cells. *P. Natl. Acad. Sci. USA*, 84:4910–4913, 1987. (http://dx.doi.org/10.1073/pnas.84.14.4910).

[40] O. Seksek, J. Biwersi, and A. S. Verkman. Translational diffusion of macromolecule-sized solutes in cytoplasm and nucleus. *J. Cell Biol.*, 138:131–142, 1997. (http://dx.doi.org/10.1083/jcb.138.1.131).

[41] M. Arrio-Dupont, G. Foucault, M. Vacher, P. F. Devaux, and S. Cribier. Translational diffusion of globular proteins in the cytoplasm of cultured muscle cells. *Biophys. J.*, 78:901–907, 2000. (http://dx.doi.org/10.1016/S0006-3495(00)76647-1).

[42] A. Caspi, R. Granek, and M. Elbaum. Enhanced diffusion in active intracellular transport. *Phys. Rev. Lett.*, 85:5655–5658, 2000. (http://dx.doi.org/10.1103/PhysRevLett.85.5655).

[43] A. Caspi, R. Granek, and M. Elbaum. Diffusion and directed motion in cellular transport. *Phys. Rev. E*, 66:011916, 2002. (http://dx.doi.org/10.1103/PhysRevE.66.011916).

[44] H. Salman, Y. Gil, R. Granek, and M. Elbaum. Microtubules, motor proteins, and anomalous mean squared displacements. *Chem. Phys.*, 284:389–397, 2002. (http://dx.doi.org/10.1016/S0301-0104(02)00669-9).

[45] R. P. Kulkarni, K. Castelino, A. Majumdar, and S. E. Fraser. Intracellular transport dynamics of endosomes containing dna polyplexes along the microtubule network. *Biophys. J.*, 90:L42–L44, 2006. (http://dx.doi.org/10.1529/biophysj.105.077941).

[46] I. M. Kulić, A. E. X. Brown, H. Kim, C. Kural, B. Blehm, P. R. Selvin, P. C. Nelson, and V. I. Gelfand. The role of microtubule movement in bidirectional cargo transport. *P. Natl. Acad. Sci. USA*, 105:10011–10016, 2008. (http://dx.doi.org/10.1073/pnas.0800031105).

[47] L. Bruno, V. Levi, M. Brunstein, and M. A. Despósito. Transition to superdiffusive behavior in intracellular actin-based transport mediated by molecular motors. *Phys. Rev. E*, 80:011912, 2009. (http://dx.doi.org/10.1103/PhysRevE.80.011912).

[48] F. Santamaria, S. Wils, E. De Schutter, and G. J. Augustine. Anomalous diffusion in purkinje cell dendrites caused by spines. *Neuron*, 52:635–648, 2006. (http://dx.doi.org/10.1016/j.neuron.2006.10.025).

[49] F. Santamaria, S. Wils, E. De Schutter, and G. J. Augustine. The diffusional properties of dendrites depend on the density of dendritic spines. *Eur. J. Neurosci.*, 34:561–568, 2011. (http://dx.doi.org/10.1111/j.1460-9568.2011.07785.x).

[50] R. J. Ellis and A. P. Minton. Cell biology: join the crowd. *Nature*, 425:27–28, 2003. (http://dx.doi.org/10.1038/425027a).

[51] M. Weiss, M. Elsner, F. Kartberg, and T. Nilsson. Anomalous subdiffusion is a measure for cytoplasmic crowding in living cells. *Biophys. J.*, 87:3518–3524, 2004. (http://dx.doi.org/10.1529/biophysj.104.044263).

[52] I. M. Tolić-Nørrelykke, E.-L. Munteanu, G. Thon, L. Oddershede, and K. Berg-Sørensen. Anomalous diffusion in living yeast cells. *Phys. Rev. Lett.*, 93:078102, 2004. (http://dx.doi.org/10.1103/PhysRevLett.93.078102).

[53] I. Golding and E. C. Cox. Physical nature of bacterial cytoplasm. *Phys. Rev. Lett.*, 96:098102, 2006. (http://dx.doi.org/10.1103/PhysRevLett.96.098102).

[54] S. C. Weber, A. J. Spakowitz, and J. A. Theriot. Bacterial chromosomal loci move subdiffusively through a viscoelastic cytoplasm. *Phys. Rev. Lett.*, 104:238102, 2010. (http://dx.doi.org/10.1103/PhysRevLett.104.238102).

[55] F. Höfling and T. Franosch. Anomalous transport in the crowded world of biological cells. *Rep. Prog. Phys.*, 76:046602, 2013. (http://dx.doi.org/10.1088/0034-4885/76/4/046602).

[56] E. W. Montroll and G. H. Weiss. Random walks on lattices. ii. *J. Math. Phys.*, 6: 167–181, 1965. (http://dx.doi.org/10.1063/1.1704269).

[57] E. W. Montroll and G. H. Weiss. Random walks on lattices. iv. continuous-time walks and influence of absorbing boundaries. *J. Stat. Phys.*, 9:101–135, 1973.

[58] B. Mandelbrot. *The fractal geometry of nature*. W. H. Freeman and Co., 1982.

[59] J.-P. Bouchaud and A. Georges. Anomalous diffusion in disordered media: statistical mechanisms, models and physical applications. *Phys. Rep.*, 195:127–293, 1990. (http://dx.doi.org/10.1016/0370-1573(90)90099-N).

[60] B. D. Hughes. *Random walks and random environments; volume 1: random walks*. Oxford University Press: Clarendon Press, 1995.

[61] R. Metzler and J. Klafter. The random walk's guide to anomalous diffusion: a fractional dynamics approach. *Phys. Rep.*, 339:1–77, 2000. (http://dx.doi.org/10.1016/S0370-1573(00)00070-3).

[62] C. Tojo and P. Argyrakis. Correlated random walk in continuous space. *Phys. Rev. E*, 54:58–63, 1996. (http://dx.doi.org/10.1103/PhysRevE.54.58).

[63] M. R. Shaebani, Z. Sadjadi, I. M. Sokolov, H. Rieger, and L. Santen. Anomalous diffusion of self-propelled particles in directed random environments. *Phys. Rev. E*, 90:030701, 2014. (http://dx.doi.org/10.1103/PhysRevE.90.030701).

[64] M. J. Saxton. Anomalous diffusion due to binding: a monte carlo study. *Biophys. J.*, 70:1250–1262, 1996. (http://dx.doi.org/10.1016/S0006-3495(96)79682-0).

[65] P. C. Bressloff. *Stochastic processes in cell biology*. Springer International Publishing Switzerland, 2014.

[66] M. J. Saxton. A biological interpretation of transient anomalous subdiffusion. i. qualitative model. *Biophys. J.*, 92:1178–1191, 2007. (http://dx.doi.org/10.1529/biophysj.106.092619).

[67] A. M. Berezhkovskii, L. Dagdug, and S. M. Bezrukov. Discriminating between anomalous diffusion and transient behavior in microheteogeneous environments. *Biophys. J.*, 106:L09–L011, 2014. (http://dx.doi.org/10.1016/j.bpj.2013.12.013).

[68] M. Coppey, O. Bénichou, R. Voituriez, and M. Moreau. Kinetics of target site localization of a protein on dna: a stochastic approach. *Biophys. J.*, 87:1640–1649, 2004. (http://dx.doi.org/10.1529/biophysj.104.045773).

[69] O. Bénichou, M. Coppey, M. Moreau, P-H. Suet, and R. Voituriez. Optimal search strategies for hidden targets. *Phys. Rev. Lett.*, 94:198101, 2005. (http://dx.doi.org/10.1103/PhysRevLett.94.198101).

[70] O. Bénichou, M. Coppey, M. Moreau, and R. Voituriez. Intermittent search strategies: when losing time becomes efficient. *Europhys. Lett.*, 75:349–354, 2006. (http://dx.doi.org/10.1209/epl/i2006-10100-3).

[71] O. Bénichou, C. Loverdo, M. Moreau, and R. Voituriez. Two-dimensional intermittent search processes: an alternative to lévy flight strategies. *Phys. Rev. E*, 74: 020102, 2006. (http://dx.doi.org/10.1103/PhysRevE.74.020102).

[72] O. Bénichou, C. Loverdo, M. Moreau, and R. Voituriez. Intermittent search strategies. *Rev. Mod. Phys.*, 83:81–129, 2011. (http://dx.doi.org/10.1103/RevModPhys.83.81).

[73] C. Loverdo, O. Bénichou, M. Moreau, and R. Voituriez. Enhanced reaction kinetics in biological cells. *Nat. Phys.*, 4:137, 2008. (http://dx.doi.org/10.1038/nphys830).

[74] C. Loverdo, O. Bénichou, M. Moreau, and R. Voituriez. Robustness of optimal intermittent search strategies in one, two, and three dimensions. *Phys. Rev. E*, 80: 031146, 2009. (http://dx.doi.org/10.1103/PhysRevE.80.031146).

[75] C. Loverdo, O. Bénichou, M. Moreau, and R. Voituriez. Reaction kinetics in active media. *J. Stat. Mech.*, 9:P02045, 2009. (http://dx.doi.org/10.1088/1742-5468/2009/02/P02045).

[76] O. Bénichou, D. Grebenkov, P. Levitz, C. Loverdo, and R. Voituriez. Optimal reaction time for surface-mediated diffusion. *Phys. Rev. Lett.*, 105:150606, 2010. (http://dx.doi.org/10.1103/PhysRevLett.105.150606).

[77] A. G. Cherstvy, A. V. Chechkin, and R. Metzler. Particle invasion, survival, and non-ergodicity in 2d diffusion processes with space-dependent diffusivity. *Soft Matter*, 10:1591–1601, 2014. (http://dx.doi.org/10.1039/c3sm52846d).

[78] D. Ando, N. Korabel, K. C. Huang, and A. Gopinathan. Cytoskeletal network morphology regulates intracellular transport dynamics. *Biophys. J.*, 109:1574–1582, 2015. (http://dx.doi.org/10.1016/j.bpj.2015.08.034).

[79] K. Schwarz, Y. Schröder, B. Qu, M. Hoth, and H. Rieger. Optimality of spatially inhomogeneous search strategies. *Phys. Rev. Lett.*, 117:068101, 2016. (http://dx.doi.org/10.1103/PhysRevLett.117.068101).

[80] K. Schwarz, Y. Schröder, and H. Rieger. Numerical analysis of homogeneous and inhomogeneous intermittent search strategies. *Phys. Rev. E*, 94:042133, 2016. (http://dx.doi.org/10.1103/PhysRevE.94.042133).

[81] D. A. Fletcher and R. D. Mullins. Cell mechanics and the cytoskeleton. *Nature*, 463:485–492, 2010. (http://dx.doi.org/10.1038/nature08908).

[82] F. Huber, J. Schnauß, S. Rönicke, P. Rauch, K. Müller, C. Fütterer, and J. Käs. Emergent complexity of the cytoskeleton: from single filaments to tissue. *Adv. Phys.*, 62:1–112, 2013. (http://dx.doi.org/10.1080/00018732.2013.771509).

[83] A. Akhmanova and M. O. Steinmetz. Tracking the ends: a dynamic protein network controls the fate of microtubule tips. *Nat. Rev. Mol. Cell Biol.*, 9:309–322, 2008. (http://dx.doi.org/10.1038/nrm2369).

[84] A. Desai and T. J. Mitchison. Microtubule polymerization dynamics. *Annu. Rev. Cell Dev. Biol.*, 13:83–117, 1997. (http://dx.doi.org/10.1146/annurev.cellbio.13.1.83).

[85] C. Allen and G. G. Borisy. Structural polarity and directional growth of microtubules of chlamydomonas flagella. *J. Mol. Biol.*, 90:381–386, 1974. (http://dx.doi.org/10.1016/0022-2836(74)90381-7).

[86] W. D. Cohen and L. I. Rebhun. An estimate of the amount of microtubule protein in the isolated mitotic apparatus. *J. Cell Sci.*, 6:159–176, 1970.

[87] E. Schulze and M. Kirschner. Dynamic and stable populations of microtubules in cells. *J. Cell Biol.*, 104:277–288, 1987. (http://dx.doi.org/10.1083/jcb.104.2.277).

[88] F. J. Nédelec, T. Surrey, A.C. Maggs, and S. Leibler. Self-organization of microtubules and motors. *Nature*, 389:305–308, 1997. (http://dx.doi.org/10.1038/38532).

[89] M. L. Gardel, J. H. Shin, F. C. MacKintosh, L. Mahadevan, P. Matsudaira, and D. A. Weitz. Elastic behavior of cross-linked and bundled actin networks. *Science*, 304:1301–1305, 2004. (http://dx.doi.org/10.1126/science.1095087).

[90] R. D. Mullins, J. A. Heuser, and T. D. Pollard. The interaction of arp2/3 complex with actin: nucleation, high affinity pointed end capping, and formation of branching networks of filaments. *P. Natl. Acad. Sci. USA*, 95:6181–6186, 1998. (http://dx.doi.org/10.1073/pnas.95.11.6181).

[91] V. I. Risca, E. B. Wang, O. Chaudhuri, J. J. Chia, P. L. Geissler, and D. A. Fletcher. Actin filament curvature biases branching direction. *P. Natl. Acad. Sci. USA*, 109:2913–2918, 2012. (http://dx.doi.org/10.1073/pnas.1114292109).

[92] D. Bray, J. Heath, and D. Moss. The membrane-associated 'cortex' of animal cells: its structure and mechanical properties. *J. Cell Sci. Suppl.*, 4:71–88, 1986. (http://dx.doi.org/10.1242/jcs.1986.Supplement_4.5).

[93] G. Salbreux, G. Charras, and E. Paluch. Actin cortex mechanics and cellular morphogenesis. *Trends Cell Biol.*, 22:536–545, 2012. (http://dx.doi.org/10.1016/j.tcb.2012.07.001).

[94] F. Hanakam, R. Albrecht, C. Eckerskorn, M. Matzner, and G. Gerisch. Myristoylated and non-myristoylated forms of the ph sensor protein hisactophilin ii: intracellular shuttling to plasma membrane and nucleus monitored in real time by a fusion with green fluorescent protein. *EMBO J.*, 15:2935–2943, 1996.

[95] A. G. Clark, K. Dierkes, and E. Paluch. Monitoring actin cortex thickness in live cells. *Biophys. J.*, 105:570–580, 2013. (http://dx.doi.org/10.1016/j.bpj.2013.05.057).

[96] F. Eghiaian, A. Rigato, and S. Scheuring. Structural, mechanical, and dynamical variability of the actin cortex in living cells. *Biophys. J.*, 108:1330–1340, 2015. (http://dx.doi.org/10.1016/j.bpj.2015.01.016).

[97] M. Bovellan, Y. Romeo, M. Biro, A. Boden, C. Priyamvada, A. Yonis, M. Vaghela, M. Fritzsche, D. Moulding, R. Thorogate, A. Jégou, A. J. Thrasher, G. Romet-Lemonne, P. P. Roux, E. K. Paluch, and G. Charras. Cellular control of cortical actin nucleation. *Curr. Biol.*, 24:1628–1635, 2014. (http://dx.doi.org/10.1016/j.cub.2014.05.069).

[98] G. T. Charras, C.-K. Hu, M. Coughlin, and T. J. Mitchison. Reassembly of contractile actin cortex in cell blebs. *J. Cell Biol.*, 175:477–490, 2006. (http://dx.doi.org/10.1083/jcb.200602085).

[99] N. Morone, T. Fujiwara, K. Murase, R. S. Kasai, H. Ike, S. Yuasa, J. Usukura, and A. Kusumi. Three-dimensional reconstruction of the membrane skeleton at the plasma membrane interface by electron tomography. *J. Cell Biol.*, 174:851–862, 2006. (http://dx.doi.org/10.1083/jcb.200606007).

[100] E. Fuchs and I. Karakesisoglou. Bridging cytoskeletal intersections. *Gene. Dev.*, 15:1–14, 2001. (http://dx.doi.org/10.1101/gad.861501).

[101] G. G. Gundersen and J. C. Bulinski. Selective stabilization of microtubules oriented toward the direction of cell migration. *P. Natl. Acad. Sci. USA*, 85:5946–5950, 1988. (http://dx.doi.org/10.1073/pnas.85.16.5946).

[102] G. G. Gundersen, E. R. Gomes, and Y. Wen. Cortical control of microtubule stability and polarization. *Curr. Opin. Cell Biol.*, 16:106–112, 2004. (http://dx.doi.org/10.1016/j.ceb.2003.11.010).

[103] G. Lansbergen and A. Akhmanova. Microtubule plus end: a hub of cellular activities. *Traffic*, 7:499–507, 2006. (http://dx.doi.org/10.1111/j.1600-0854.2006.00400.x).

[104] E. Sackmann, F. Keber, and D. Heinrich. Physics of cellular movements. *Annu. Rev. Condens. Matter Phys.*, 1:257–276, 2010. (http://dx.doi.org/10.1146/annurev-conmatphys-070909-104105).

[105] M. P. López, F. Huber, I. Grigoriev, M. O. Steinmetz, A. Akhmanova, G. H. Koenderink, and M. Dogterom. Actin-microtubule coordination at growing microtubule ends. *Nat. Commun.*, 5:4778, 2014. (http://dx.doi.org/10.1038/ncomms5778).

[106] A. J. Tooley, J. Gilden, J. Jacobelli, P. Beemiller, W. S. Trimble, M. Kinoshita, and M. F. Krummel. Ameboid t lymphocytes require the septin cytoskeleton for cortical integrity and persistent motility. *Nat. Cell Biol.*, 11:17–26, 2009. (http://dx.doi.org/10.1038/ncb1808).

[107] P. Kunda and B. Baum. The actin cytoskeleton in spindle assembly and positioning. *Trends Cell Biol.*, 19:174–179, 2009. (http://dx.doi.org/10.1016/j.tcb.2009.01.006).

[108] K. Wolf, I. Mazo, H. Leung, K. Engelke, U. H. von Andrian, E. I. Deryugina, A. Y. Strongin, E.-B. Bröcker, and P. Friedl. Compensation mechanism in tumor cell migration: mesenchymal-amoeboid transition after blocking of pericellular proteolysis. *J. Cell Biol.*, 160:267–277, 2003. (http://dx.doi.org/10.1083/jcb.200209006).

[109] G. Woehlke and M. Schliwa. Walking on two heads: the many talents of kinesin. *Nat. Rev. Mol. Cell Biol.*, 1:50–58, 2000. (http://dx.doi.org/10.1038/35036069).

[110] R. D. Vale and R. A. Milligan. The way things move: looking under the hood of molecular motor proteins. *Science*, 288:88–95, 2000. (http://dx.doi.org/10.1126/science.288.5463.88).

[111] R. D. Vale. The molecular motor toolbox for intracellular transport. *Cell*, 112:467–480, 2003. (http://dx.doi.org/10.1016/S0092-8674(03)00111-9).

[112] M. Schliwa and G. Woehlke. Molecular motors. *Nature*, 422:759–765, 2003. (http://dx.doi.org/10.1038/nature01601).

[113] J. Howard. Molecular motors: structural adaptations to cellular functions. *Nature*, 389:561–567, 1997. (http://dx.doi.org/10.1038/39247).

[114] D. D. Hackney. Evidence for alternating head catalysis by kinesin during microtubule-stimulated atp hydrolysis. *P. Natl. Acad. Sci. USA*, 91:6865–6869, 1994. (http://dx.doi.org/10.1073/pnas.91.15.6865).

[115] J. Howard, A. J. Hudspeth, and R. D. Vale. Movement of microtubules by single kinesin molecules. *Nature*, 342:154–158, 1989. (http://dx.doi.org/10.1038/342154a0).

[116] S. M. Block, L. S. B. Goldstein, and B. J. Schnapp. Bead movement by single kinesin molecules studied with optical tweezers. *Nature*, 348:348–352, 1990. (http://dx.doi.org/10.1038/348348a0).

[117] A. D. Mehta, R. S. Rock, M. Rief, J. A. Spudich, M. S. Mooseker, and R. E. Cheney. Myosin-v is a processive actin-based motor. *Nature*, 400:590–593, 1999. (http://dx.doi.org/10.1038/23072).

[118] Z. Wang, S. Khan, and M. P. Sheetz. Single cytoplasmic dynein molecule movements: characterization and comparison with kinesin. *Biophys. J.*, 69:2011–2023, 1995. (http://dx.doi.org/10.1016/S0006-3495(95)80071-8).

[119] S. J. King and T. A. Schroer. Dynactin increases the processivity of the cytoplasmic dynein motor. *Nat. Cell Biol.*, 2:20–24, 2000. (http://dx.doi.org/10.1038/71338).

[120] C. L. Asbury, A. N. Fehr, and S. M. Block. Kinesin moves by an asymmetric hand-over-hand mechanism. *Science*, 302:2130–2134, 2003. (http://dx.doi.org/10.1126/science.1092985).

[121] A. Yildiz, M. Tomishige, R. D. Vale, and P. R. Selvin. Kinesin walks hand-over-hand. *Science*, 303:676–678, 2004. (http://dx.doi.org/10.1126/science.1093753).

[122] A. Yildiz, J. N. Forkey, S. A. McKinney, T. Ha, Y. E. Goldman, and P. R. Selvin. Myosin v walks hand-over-hand: singel fluorophore imaging with 1.5-nm localization. *Science*, 300:2061–2065, 2003. (http://dx.doi.org/10.1126/science.1084398).

[123] S. Toba, T. M. Watanabe, L. Yamaguchi-Okimoto, Y. Y. Toyoshima, and H. Higuchi. Overlapping hand-over-hand mechanism of single molecular motility of cytoplasmic dynein. *P. Natl. Acad. Sci. USA*, 103:5741–5745, 2006. (http://dx.doi.org/10.1073pnas.0508511103).

[124] S. L. Reck-Peterson, A. Yildiz, A. P. Carter, A. Gennerich, N. Zhang, and R. D. Vale. Single-molecule analysis of dynein processivity and stepping behavior. *Cell*, 126:335–348, 2006. (http://dx.doi.org/10.1016/j.cell.2006.05.046).

[125] D. Tsygankov, A. W. R. Serohijos, N. V. Dokholyan, and T. C. Elston. Kinetic models for the coordinated stepping of cytoplasmic dynein. *J. Chem. Phys.*, 130:025101, 2009. (http://dx.doi.org/10.1063/1.3050098).

[126] M. A. DeWitt, A. Y. Chang, P. A. Combs, and A. Yildiz. Cytoplasmic dynein moves through uncoordinated stepping of the aaa+ ring domains. *Science*, 335:221–225, 2012. (http://dx.doi.org/10.1126/science.1215804).

[127] W. Qiu, N. D. Derr, B. S. Goodman, E. Villa, D. Wu, W. Shih, and S. L. Reck-Peterson. Dynein achieves processive motion using both stochastic and coordinated stepping. *Nat. Struct. Mol. Biol.*, 9:193–200, 2012. (http://dx.doi.org/10.1038/nsmb.2205).

[128] A. J. Roberts, K. Takahide, P. J. Knight, K. Sutoh, and S. A. Burgess. Functions and mechanics of dynein motor proteins. *Nat. Rev. Mol. Cell Biol.*, 14:713–726, 2013. (http://dx.doi.org/10.1038/nrm3667).

[129] P. C. Bressloff and J. M. Newby. Stochastic models of intracellular transport. *Rev. Mod. Phys.*, 85:135–196, 2013. (http://dx.doi.org/10.1103/RevModPhys.85.135).

[130] B. Trinczek, A. Ebneth, E.M. Mandelkow, and E. Mandelkow. Tau regulates the attachment/detachment but not the speed of motors in microtubule-dependent transport of single vesicles and organelles. *J. Cell Sci.*, 112:2355–2367, 1999.

[131] C. J. Lawrence, R. K. Dawe, K. R. Christie, D. W. Cleveland, S. C. Dawson, S. A. Endow, L. S.B. Goldstein, H. V. Goodson, N. Hirokawa, J. Howard, R. L. Malmberg, J. R. McIntosh, H. Miki, T. J. Mitchison, Y. Okada, A. S.N. Reddy, W. M. Saxton, M. Schliwa, J. M. Scholey, R. D. Vale, C. E. Walczak, and L. Wordeman. A standardized kinesin nomenclature. *J. Cell Biol.*, 167:19–22, 2004. (http://dx.doi.org/10.1083/jcb.200408113).

[132] K. Svoboda, C. F. Schmidt, B. J. Schnapp, and S. M. Block. Direct observation of kinesin stepping by optical trapping interferometry. *Nature*, 365:721–727, 1993. (http://dx.doi.org/10.1038/365721a0).

[133] A. N. Fehr, C. L. Asbury, and S. M. Block. Kinesin steps do not alternate in size. *Biophys. J.*, 94:L20–L22, 2008. (http://dx.doi.org/10.1529/biophysj.107.126839).

[134] K. Ray. How kinesins walk, assemble and transport: A birds-eye-view of some unresolved questions. *Physica A*, 372:52–64, 2006. (http://dx.doi.org/10.1016/j.physa.2006.05.007).

[135] M. Sakato and S. M. King. Design and regulation of the aaa+ microtubule motor dynein. *J. Struct. Biol.*, 146:58–71, 2004. (http://dx.doi.org/10.1016/j.jsb.2003.09.026).

[136] R. A. Cross. Molecular motors: dynein's gearbox. *Curr. Biol.*, 14:R355–R356, 2004. (http://dx.doi.org/10.1016/j.cub.2004.04.026).

[137] R. Mallik, B. C. Carter, S. A. Lex, S. J. King, and S. P. Gross. Cytoplasmic dynein functions as a gear in response to load. *Nature*, 427:649–652, 2004. (http://dx.doi.org/10.1038/nature02293).

[138] G. M. Langford. Myosin-v, a versatile motor for short-range vesicle transport. *Traffic*, 3:859–865, 2002. (http://dx.doi.org/10.1034/j.1600-0854.2002.31202.x).

[139] V. Muresan and Z. Muresan. Unconventional functions of microtubule motors. *Arch. Biochem. Biophys.*, 520:17–29, 2012. (http://dx.doi.org/10.1016/j.abb.2011.12.029).

[140] G. M. Langford. Actin- and microtubule-dependent organelle motors: interrelationships between the two motility systems. *Curr. Opin. Cell Biol.*, 7:82–88, 1995. (http://dx.doi.org/10.1016/0955-0674(95)80048-4).

[141] S. S. Brown. Cooperation between microtubule- and actin-based motor proteins. *Annu. Rev. Cell Dev. Biol.*, 15:63–80, 1999. (http://dx.doi.org/10.1146/annurev.cellbio.15.1.63).

[142] S. A. Kuznetsov, G. M. Langford, and D. G. Weiss. Actin-dependent organelle movement in squid axoplasm. *Nature*, 356:722–725, 1992. (http://dx.doi.org/10.1038/356722a0).

[143] J. I. Rebhun. Structural aspects of saltatory particle movement. *J. Gen. Physiol.*, 50:223–239, 1967. (http://dx.doi.org/PMC2225743).

[144] A. L. Jolly and V. I. Gelfand. Bidirectional intracellular transport: utility and mechanism. *Biochem. Soc. Trans.*, 39:1126–1130, 2011. (http://dx.doi.org/10.1042/BST0391126).

[145] B. L. Goode, D. G. Drubin, and G. Barnes. Functional cooperation between the microtubule and the actin cytoskeletons. *Curr. Opin. Cell Biol.*, 12:63–71, 2000. (http://dx.doi.org/10.1016/S0955-0674(99)00058-7).

[146] B. M. Slepchenko, I. Semenova, I. Zaliapin, and V. Rodionov. Switching of membrane organelles between cytoskeletal transport systems is determined by regulation of the microtubule-based transport. *J. Cell Biol.*, 179:635–641, 2007. (http://dx.doi.org/10.1083/jcb.200705146).

[147] V. Rodionov, J. Yi, A. Kashina, A. Oladipo, and S. P. Gross. Switching between microtubule- and actin-based transport systems in melanophores is controlled by camp levels. *Curr. Biol.*, 13:1837–1847, 2003. (http://dx.doi.org/10.1016/j.cub.2003.10.027).

[148] M. Suomalainen, M.Y. Nakano, K. Boucke, S. Keller, and U.F. Greber. Adenovirus-activated pka and p38/mapk pathways boost microtubule-mediated nuclear targeting of virus. *EMBO J.*, 20:1310–1319, 2001. (http://dx.doi.org/10.1093/emboj/20.6.1310).

[149] S. P. Gross, Y. Guo, J. E. Martinez, and M. A. Welte. A determinant for directionality of organelle transport in drosophila embryos. *Curr. Biol.*, 13:1660–1668, 2003. (http://dx.doi.org/10.1016/j.cub.2003.08.032).

[150] S. P. Gross. Dynactin: coordinating motors with opposite inclinations. *Curr. Biol.*, 13:R320–R322, 2003. (http://dx.doi.org/10.1016/S0960-9822(03)00237-9).

[151] J. Snider, F. Lin, N. Zahedi, V. Rodionov, C. C. Yu, and S. P. Gross. Intracellular actin-based transport: how far you go depends on how often you switch. *P. Natl. Acad. Sci. USA*, 101:13204–13209, 2004. (http://dx.doi.org/10.1073/pnas.0403092101).

[152] I. Zaliapin, I. Semenova, A. Kashina, and V. Rodionov. Multiscale trend analysis of microtubule transport in melanophores. *Biophys. J.*, 88:4008–4016, 2005. (http://dx.doi.org/10.1529/biophysj.104.057083).

[153] J. Klafter and I. M. Sokolov. *First steps in random walks: from tools to applications.* Oxford University Press, 2011.

[154] A. B. Fulton. How crowded is the cytoplasm? *Cell*, 30:345–347, 1982. (http://dx.doi.org/10.1016/0092-8674(82)90231-8).

[155] M. R. Shaebani, A. E. Hafner, and L. Santen. Geometrical considerations for anomalous transport in complex neuronal dendrites. *(in preparation)*, ?:?, ?

[156] G. Guigas and M. Weiss. Sampling the cell with anomalous diffusion - the discovery of slowness. *Biophys. J.*, 94:90–94, 2008. (http://dx.doi.org/10.1529/biophysj.107.117044).

[157] L. E. Sereshki, M. A. Lomholt, and R. Metzler. A solution to the subdiffusion-efficiency paradox: Inactive states enhance reaction efficiency at subdiffusion conditions in living cells. *Europhys. Lett.*, 97:20008, 2012. (http://dx.doi.org/10.1209/0295-5075/97/20008).

[158] I. Wacker, C. Kaether, A. Kromer, A. Migala, W. Almers, and H. H. Gerdes. Microtubule-dependent transport of secretory vesicles visualized in real time with a gfp-tagged secretory protein. *J. Cell Sci.*, 110:1453–1463, 1997.

[159] J. E. Rothman. Mechanisms of intracellular protein transport. *Nature*, 372:55–63, 1994. (http://dx.doi.org/10.1038/372055a0).

[160] H. Cai, K. Reinisch, and S. Ferro-Novick. Coats, tethers, rabs, and snares work together to mediate the intracellular destination of a transport vesicle. *Dev. Cell*, 12:671–682, 2007. (http://dx.doi.org/10.1016/j.devcel.2007.04.005).

[161] R. D. Vale, F. Malik, and D. Brown. Directional instability of microtubule transport in the presence of kinesin and dynein, two opposite polarity motor proteins. *J. Cell Biol.*, 119:1589–1596, 1992. (http://dx.doi.org/10.1083/jcb.119.6.1589).

[162] P. L. McNeil, S. S. Vogel, K. Miyake, and M. Terasaki. Patching plasma membrane disruptions with cytoplasmic membrane. *J.Cell Sci.*, 113:1891–1902, 2000.

[163] P. L. McNeil and T. Kirchhausen. An emergency response team for membrane repair. *Nat. Rev. Mol. Cell Biol.*, 6:499–505, 2005. (http://dx.doi.org/10.1038/nrm1665).

[164] N. W. Andrews, P. E. Almeida, and M. Corrotte. Damage control: cellular mechanisms of plasma membrane repair. *Trends Cell Biol.*, 24:734–742, 2014. (http://dx.doi.org/10.1016/j.tcb.2014.07.008).

[165] N. W. Andrews. Lysosome recruitment during host cell invasion by trypanosoma cruzi. *Trends Cell Biol.*, 5:133–137, 1995. (http://dx.doi.org/10.1016/S0962-8924(00)88965-5).

[166] P. Alberts and T. Galli. The cell outgrowth secretory endosome (cose): a specialized compartment involved in neuronal morphogenesis. *Biol. Cell*, 95:419–424, 2003. (http://dx.doi.org/10.1016/S0248-4900(03)00074-1).

[167] E. Marco, R. Wedlich-Soldner, R. Li, S. J. Altschuler, and L. F. Wu. Endocytosis optimizes the dynamic localization of membrane proteins that regulate cortical polarity. *Cell*, 129:411–422, 2007. (http://dx.doi.org/10.1016/j.cell.2007.02.043).

[168] S. J. Altschuler, S. B. Angenent, Y. Wang, and L. F. Wu. On the spontaneous emergence of cell polarity. *Nature*, 454:886–889, 2008. (http://dx.doi.org/10.1038/nature07119).

[169] D. Holcman and Z. Schuss. Escape through a small opening: receptor trafficking in a synaptic membrane. *J. Stat. Phys.*, 117:975–1014, 2004. (http://dx.doi.org/0022-4715/04/1200-0975/0).

[170] A. Singer, Z. Schuss, D. Holcman, and R. S. Eisenberg. Narrow escape, part i. *J. Stat. Phys.*, 122:437–463, 2006. (http://dx.doi.org/10.1007/s10955-005-8026-6).

[171] A. Singer, Z. Schuss, and D. Holcman. Narrow escape, part ii: the circular disk. *J. Stat. Phys.*, 122:465–489, 2006. (http://dx.doi.org/10.1007/s10955-005-8027-5).

[172] A. Singer, Z. Schuss, and D. Holcman. Narrow escape, part iii: non-smooth domains and riemann surfaces. *J. Stat. Phys.*, 122:491–509, 2006. (http://dx.doi.org/10.1007/s10955-005-8028-4).

[173] A. Biess, E. Korkotian, and D. Holcman. Diffusion in a dendritic spine: the role of geometry. *Phys. Rev. E*, 76:021922, 2007. (http://dx.doi.org/10.1103/PhysRevE.76.021922).

[174] Z. Schuss, A. Singer, and D. Holcman. The narrow escape problem for diffusion in cellular microdomains. *P. Natl. Acad. Sci. USA*, 104:16098–16103, 2007. (http://dx.doi.org/10.1073/pnas.0706599104).

[175] Z. Schuss. The narrow escape problem - a short review of recent results. *J. Sci. Comput.*, 53:194–210, 2012. (http://dx.doi.org/10.1007/s10915-012-9590-y).

[176] S. A. Gorski, M. Dundr, and T. Misteli. The road much traveled: trafficking in the cell nucleus. *Curr. Opin. Cell Biol.*, 18:284–290, 2006. (http://dx.doi.org/10.1016/j.ceb.2006.03.002).

[177] T. Misteli. Physiological importance of rna and protein mobility in the cell nucleus. *Histochem. Cell Biol.*, 129:5–11, 2008. (http://dx.doi.org/10.1007/s00418-007-0355-x).

[178] A. Biess, E. Korkotian, and D. Holcman. Barriers to diffusion in dendrites and estimation of calcium spread following synaptic inputs. *PLoS Comput. Biol.*, 7: e1002182, 2011. (http://dx.doi.org/10.1371/journal.pcbi.1002182).

[179] E. Granger, G. McNee, V. Allan, and P. Woodman. The role of the cytoskeleton and molecular motors in endosomal dynamics. *Sem. Cell Dev. Biol.*, 31:20–29, 2014. (http://dx.doi.org/10.1016/j.semcdb.2014.04.011).

[180] B. Brandenburg and X. Zhuang. Virus trafficking - learning from single-virus tracking. *Nat. Rev. Mircobiol.*, 5:197–208, 2007. (http://dx.doi.org/10.1038/nrmicro1615).

[181] S.-L. Liu, L.-J. Zhang, Z.-G. Wang, Z.-L. Zhang, Q.-M. Wu, E.-Z. Sun, Y.-B. Shi, and D.-W. Pang. Globally visualizing the microtubule-dependent transport behaviors of influenza virus in live cells. *Anal. Chem.*, 86:3902–3908, 2014. (http://dx.doi.org/10.1021/ac500640u).

[182] R. Brown. Xxvii. a brief account of microscopical observations made in the months of june, july and august 1827, on the particles contained in the pollen of plants; and on the general existence of active molecules in organic and inorganic bodies. *Phil. Mag.*, 4:161–173, 1828. (http://dx.doi.org/10.1080/14786442808674769).

[183] E. A. Codling, M. J. Plank, and S. Benhamou. Random walk models in biology. *J. R. Soc. Interface*, 5:813–834, 2008. (http://dx.doi.org/10.1098/rsif.2008.0014).

[184] L. Bachelier. Théorie de la spéculation. *Ann. sci. ecole norm. s.*, 17:21–86, 1900.

[185] J. Klafter and I. M. Sokolov. Anomalous diffusion spreads its wings. *Phys. World*, 18:29–32, 2005.

[186] K. Pearson. The problem of the random walk. *Nature*, 72:294, 1905. (http://dx.doi.org/10.1038/072294b0).

[187] Rayleigh. The problem of the random walk. *Nature*, 72:318, 1905.

[188] K. Pearson. The problem of the random walk. *Nature*, 72:342, 1905.

[189] A. Einstein. Über die von der molekularkinetischen theorie der wärme geforderte bewegung von in ruhenden flüssigkeiten suspendierten teilchen. *Ann. Phys.*, 322: 549–560, 1905. (http://dx.doi.org/10.1002/andp.19053220806).

[190] A. Einstein. Zur theorie der brownschen bewegung. *Ann. Phys.*, 324:371–381, 1906. (http://dx.doi.org/10.1002/andp.19063240208).

[191] M. Smoluchowski. Zur kinetischen theorie der brownschen molekularbewegung und der suspensionen. *Ann. Phys.*, 326:756–780, 1906. (http://dx.doi.org/10.1002/andp.19063261405).

[192] N. G. Van Kampen. *Stochastic processes in physics and chemistry (third edition)*. Elsevier, 2007.

[193] I. M. Sokolov. Models of anomalous diffusion in crowded environments. *Soft Matter*, 8:9043–9052, 2012. (http://dx.doi.org/10.1039/C2SM25701G).

[194] R. Metzler and J. Klafter. The restaurant at the end of the random walk: recent developments in the description of anomalous transport by fractional dynamics. *J. Phys. A: Math. Gen.*, 37:R161–R208, 2004. (http://dx.doi.org/10.1088/0305-4470/37/31/R01).

[195] S. Redner. *A guide to first-passage processes*. Cambridge University Press, 2001.

[196] M. E. Fisher and A. B. Kolomeisky. The force exerted by a molecular motor. *P. Natl. Acad. Sci. USA*, 96:6597–6602, 1999. (http://dx.doi.org/10.1073/pnas.96.12.6597).

[197] P. Reimann. Brownian motors: noisy transport far from equilibrium. *Phys. Rep.*, 361:57–265, 2002. (http://dx.doi.org/10.1016/S0370-1573(01)00081-3).

[198] R. Lipowsky and S. Klumpp. 'Life is motion': multiscale motility of molecular motors. *Physica A*, 352:53–112, 2005. (http://dx.doi.org/10.1016/j.physa.2004.12.034).

[199] A. B. Kolomeisky and M. E. Fisher. Molecular motors: a theorist's perspective. *Annu. Rev. Phys. Chem.*, 58:675–695, 2007. (http://dx.doi.org/10.1146/annurev.physchem.58.032806.104532).

[200] M. J. Saxton. Anomalous diffusion due to obstacles: a monte carlo study. *Biophys. J.*, 66:394–401, 1994. (http://dx.doi.org/10.1016/S0006-3495(94)80789-1).

[201] J. C. Angles d'Auriac, A. Benoit, and A. Rammal. Random walk on fractals: numerical studies in two dimensions. *J. Phys. A: Math. Gen.*, 16:4039–4051, 1983. (http://dx.doi.org/10.1088/0305-4470/16/17/020).

[202] B.B. Mandelbrot and J. W. van Ness. Fractional brownian motions, fractional noises and applications. *SIAM Rev.*, 10:422–437, 1968.

[203] K. G. Wang and C. W. Lung. Long-time correlation effects and fractal brownian motion. *Phys. Lett. A*, 151:119–121, 1990. (http://dx.doi.org/10.1016/0375-9601(90)90175-N).

[204] A. Fuliński. Fractional brownian motions: memory, diffusion velocity, and correlation functions. *J. Phys. A: Math. Theor.*, 50:054002, 2017. (http://dx.doi.org/10.1088/1751-8121/50/5/054002).

[205] M. F. Shlesinger, B. J. West, and J. Klafter. Lévy dynamics of enhanced diffusion: application to turbulence. *Phys. Rev. Lett.*, 58:1100–1103, 1987. (http://dx.doi.org/10.1103/PhysRevLett.58.1100).

[206] M. F. Shlesinger and J. Klafter. Comment on 'accelerated diffusion in josephson junctions and related chaotic systems'. *Phys. Rev. Lett.*, 54:2551, 1985. (http://dx.doi.org/10.1103/PhysRevLett.54.2551).

[207] J. Klafter, A. Blumen, and M. F. Shlesinger. Stochastic pathway to anomalous diffusion. *Phys. Rev. A*, 35:3081–3085, 1987. (http://dx.doi.org/10.1103/PhysRevA.35.3081).

[208] G. Zumofen, A. Blumen, J. Klafter, and M. F. Shlesinger. Lévy walks for turbulence: a numerical study. *J. Stat. Phys.*, 54:1519–1527, 1989. (http://dx.doi.org/10.1007/BF01044732).

[209] A. Blumen, G. Zumofen, and J. Klafter. Transport aspects in anomalous diffusion: Lévy walks. *Phys. Rev. A*, 40:3964–3973, 1989. (http://dx.doi.org/10.1103/PhysRevA.40.3964).

[210] J. Klafter, A. Blumen, G. Zumofen, and M. F. Shlesinger. Lévy walk approach to anomalous diffusion. *Physica A*, 168:637–645, 1990. (http://dx.doi.org/10.1016/0378-4371(90)90416-P).

[211] G. Zumofen and J. Klafter. Scale-invariant motion in intermittent chaotic sytsems. *Phys. Rev. E*, 47:851–863, 1993. (http://dx.doi.org/10.1103/PhysRevE.47.851).

[212] J. Klafter, A. Blumen, and M. F. Shlesinger. Beyond brownian motion. *Phys. Today*, 49:33–39, 1996. (http://dx.doi.org/10.1063/1.881487).

[213] R. Lipowsky, S. Klumpp, and T. M. Nieuwenhuizen. Random walks of cytoskeletal motors in open and closed compartments. *Phys. Rev. Lett.*, 87:108101, 2001. (http://dx.doi.org/10.1103/PhysRevLett.87.108101).

[214] T. M. Nieuwenhuizen, S. Klumpp, and R. Lipowsky. Walks of molecular motors in two and three dimensions. *Europhys. Lett.*, 58:468–474, 2002. (http://dx.doi.org/10.1209/epl/i2002-00662-4).

[215] T. M. Nieuwenhuizen, S. Klumpp, and R. Lipowsky. Random walks of molecular motors arising from diffusional encounters with immobilized filaments. *Phys. Rev. E*, 69:061911, 2004. (http://dx.doi.org/10.1103/PhysRevE.69.061911).

[216] S. Klumpp and R. Lipowsky. Active diffusion of motor particles. *Phys. Rev. Lett.*, 95:268102, 2005. (http://dx.doi.org/10.1103/PhysRevLett.95.268102).

[217] I. G. Portillo, D. Campos, and V. Méndez. Intermittent random walks: transport regimes and implications on search strategies. *J. Stat. Mech.*, 11:P02033, 2011. (http://dx.doi.org/10.1088/1742-5468/2011/02/P02033).

[218] F. Thiel, L. Schimansky-Geier, and I. M. Sokolov. Anomalous diffusion in run-and-tumble motion. *Phys. Rev. E*, 86:021117, 2012. (http://dx.doi.org/10.1103/PhysRevE.86.021117).

[219] M. Theves, J. Taktikos, V. Zaburdaev, H. Stark, and C. Beta. A bacterial swimmer with two alternating speeds of propagation. *Biophys. J.*, 105:1915–1924, 2013. (http://dx.doi.org/10.1016/j.bpj.2013.08.047).

[220] I. Pinkoviezky and N. S. Gov. Transport dynamics of molecular motors that switch between an active and inactive state. *Phys. Rev. E*, 88:022714, 2013. (http://dx.doi.org/10.1103/PhysRevE.88.022714).

[221] J. H. Jeans. *An introduction to the kinetic theory of gases*. Cambridge University Press, 1940.

[222] C. S. Patlak. Random walk with persistence and external bias. *Bull. Math. Biophys.*, 15:311–338, 1953. (http://dx.doi.org/10.1007/BF02476407).

[223] Z. Sadjadi, M. R. Shaebani, H. Rieger, and L. Santen. Persistent random walk approach to anomalous transport of self-propelled particles. *Phys. Rev. E*, 91: 062715, 2015. (http://dx.doi.org/10.1103/PhysRevE.91.062715).

[224] Z. Sadjadi, M. Miri, M. R. Shaebani, and S. Nakhaee. Diffusive transport of light in a two-dimensional disordered packing of disks: Analytical approach to transport mean free path. *Phys. Rev. E*, 78:031121, 2008. (http://dx.doi.org/10.1103/PhysRevE.78.031121).

[225] Z. Sadjadi and M. Miri. Diffusive transport of light in two-dimensional granular materials. *Phys. Rev. E*, 84:051305, 2011. (http://dx.doi.org/10.1103/PhysRevE.84.051305).

[226] E. L. Charnov. Optimal foraging, the marginal value theorem. *Theor. Popul. Biol.*, 9:129–136, 1976. (http://dx.doi.org/10.1016/0040-5809(76)90040-X).

[227] W. J. O'Brien, H. I. Browman, and B. I. Evans. Search strategies of foraging animals. *Am. Sci.*, 78:152–160, 1990.

[228] G. M. Viswanathan, S. V. Buldyrev, S. Havlin, M. G. E. da Luz, E. P. Raposo, and H. E. Stanley. Optimizing the sucess of random searches. *Nature*, 401:911–914, 1999. (http://dx.doi.org/10.1038/44831).

[229] D. L. Kramer and R. L. McLaughlin. The behavioral ecology of intermittent locomotion. *Am. Zool.*, 41:137–153, 2001. (http://dx.doi.org/10.1093/icb/41.2.137).

[230] M. F. Shlesinger. Search research. *Nature*, 443:281–282, 2006. (http://dx.doi.org/10.1038/443281a).

[231] A. M. Edwards, R. A. Phililips, N. W. Watkins, M. P. Freeman, E. J. Murphys, V. Afanasyev, S. V. Buldyrev, M. G. da Luz, E. P. Raposo, H. E. Stanley, and G.M. Viswanathan. Revisiting Lévy flight search patterns of wandering albatrosses, bumblebees and deer. *Nature*, 449:1044–1048, 2007. (http://dx.doi.org/10.1038/nature06199).

[232] A. M. Reynolds. Lévy flight patterns are predicted to be an emergent property of a bumblebees foraging strategy. *Behav. Ecol. Sociobiol.*, 64:19–23, 2009. (http://dx.doi.org/10.1007/s00265-009-0813-7).

[233] N. E. Humphries, N. Queiroz, J. R. M. Dyer, N. G. Payde, M. K. Musyl, K. M. Schaefer, D. W. Fuller, J. M. Brunnschweiler, T. K. Doyle, J. D. R. Houghton, G. C. Hays, C. S. Jones, L. R. Noble, V. J. Wearmouth, E. J. Southall, and Sims D. W. Environmental context explains Levy and Brownian movement patterns of marine predators. *Nature*, 465:1066–1069, 2010. (http://dx.doi.org/10.1038/nature09116).

[234] F. Lenz, T. C. Ings, L. Chittka, A. V. Chechkin, and R. Klages. Spatiotemporal dynamics of bumblebees foraging under predation risk. *Phys. Rev. Lett.*, 108: 098103, 2012. (http://dx.doi.org/10.1103/PhysRevLett.108.098103).

[235] J. W. S. B. Rayleigh. *The theory of sound, Volume II.* Dover Publications, 1896.

[236] H.-X. Zhou and R. Zwanzig. A rate process with an entropy barrier. *J. Chem. Phys.*, 94:6147–6152, 1991. (http://dx.doi.org/10.1063/1.460427).

[237] I. V. Grigoriev, Y. A. Makhnovskii, A. M. Berezhkovskii, and V. Y. Zitserman. Kinetics of escape through a small hole. *J. Chem. Phys.*, 116:9574–9577, 2002. (http://dx.doi.org/10.1063/1.1475756).

[238] S. Condamin, O. Bénichou, and M. Moreau. Random walks and brownian motion: a method of computation for first-passage times and related quantities in confined geometries. *Phys. Rev. E*, 75:021111, 2007. (http://dx.doi.org/10.1103/PhysRevE.75.021111).

[239] O. Bénichou, D. S. Grebenkov, P. E. Levitz, C. Loverdo, and R. Voituriez. Mean first-passage time of surface-mediated diffusion in spherical domains. *J. Stat. Phys.*, 142:657–685, 2011. (http://dx.doi.org/10.1007/s10955-011-0138-6).

[240] T. Calandre, O. Bénichou, D. S. Grebenkov, and R. Voituriez. Interfacial territory covered by surface-mediated diffusion. *Phys. Rev. E*, 85:051111, 2012. (http://dx.doi.org/10.1103/PhysRevE.85.051111).

[241] J.-F. Rupprecht, O. Bénichou, D. S. Grebenkov, and R. Voituriez. Kinetics of active surface-mediated diffusion in spherically symmetric domains. *J. Stat. Phys.*, 147:891–918, 2012. (http://dx.doi.org/10.1007/s10955-012-0496-8).

[242] J.-F. Rupprecht, O. Bénichou, D. S. Grebenkov, and R. Voituriez. Exact mean exit time for surface-mediated diffusion. *Phys. Rev. E*, 86:041135, 2012. (http://dx.doi.org/10.1103/PhysRevE.86.041135).

[243] T. Calandre, O. Bénichou, and R. Voituriez. Accelerating search kinetics by following boundaries. *Phys. Rev. Lett.*, 112:230601, 2014. (http://dx.doi.org/10.1103/PhysRevLett.112.230601).

[244] T. Calandre, O. Bénichou, D. S. Grebenkov, and R. Voituriez. Splitting probabilities and interfacial territory covered by two-dimensional and three-dimensional surface-mediated diffusion. *Phys. Rev. E*, 89:012149, 2014. (http://dx.doi.org/10.1103/PhysRevE.89.012149).

[245] O. Bénichou, D. Grebenkov, L. Hillairet, L. Phun, R. Voituriez, and M. Zinsmeister. Mean exit time for surface-mediated diffusion: spectral analysis and asymptotic behavior. *Anal. Math. Phys.*, 5:321–362, 2015. (http://dx.doi.org/10.1007/s13324-015-0098-0).

[246] K. Schwarz and H. Rieger. Efficient kinetic monte carlo method for reaction-diffusion problems with spatially varying annihilation rates. *J. Comput. Phys.*, 237:396–410, 2013. (http://dx.doi.org/10.1016/j.jcp.2012.11.036).

[247] L. A. Lopez and M. P. Sheetz. Steric inhibition of cytoplasmic dynein and kinesin motility by map2. *Cell Motil. Cytoskel.*, 24:1–16, 1993. (http://dx.doi.org/10.1002/cm.970240102).

[248] D. Arcizet, B. Meier, E. Sackmann, J. O. Rädler, and D. Heinrich. Temporal analysis of active and passive transport in living cells. *Phys. Rev. Lett.*, 101:248103, 2008. (http://dx.doi.org/10.1103/PhysRevLett.101.248103).

[249] L. Kleinrock. *Queueing systems; volume I: theory.* Wiley - Interscience, John Wiley & Sons, Inc., 1975.

[250] D. R. Cox and H. D. Miller. *The theory of stochastic processes.* Chapman and Hall Ltd, 1972.

[251] C. Mejía-Monasterio, G. Oshanin, and G. Schehr. First passages for a search by a swarm of independent random searchers. *J. Stat. Mech.*, P06022, 2011. (http://dx.doi.org/10.1088/1742-5468/2011/06/P06022).

[252] T. G. Mattos, C. Mejía-Monasterio, R. Metzler, and G. Oshanin. First passages in bounded domains: When is the mean first passage time meaningful? *Phys. Rev. E*, 86:031143, 2012. (http://dx.doi.org/10.1103/PhysRevE.86.031143).

[253] S. Huet, E. Karatekin, V. S. Tran, I. Fanget, S. Cribier, and J.-P. Henry. Analysis of transient behavior in complex trajectories: application to secretory vesicle dynamics. *Biophys. J.*, 91:3542–3559, 2006. (http://dx.doi.org/10.1529/biophysj.105.080622).

[254] M. Cebecauer, M. Spitaler, A. Sergé, and A. I. Magee. Signalling complexes and clusters: functional advantages and methodological hurdles. *J. Cell Sci.*, 123:309–320, 2010. (http://dx.doi.org/10.1242/jcs.061739).

[255] Y. Lanoiselée and D. S. Grebenkov. Unraveling intermittent features in single-particle trajectories by a local convex hull method. *Phys. Rev. E*, 96:022144, 2017. (http://dx.doi.org/10.1103/PhysRevE.96.022144).

[256] B. Geiger, D. Rosen, and G. Berke. Spatial relationships of microtubuile-organizing centers and the contact area of cytotoxic t lymphocytes and target cells. *J. Cell Biol.*, 95:137–143, 1982. (http://dx.doi.org/10.1083/jcb.95.1.137).

[257] J.-E. Ryser, E. Rungger-Brändle, C. Chaponnier, G. Gabbiani, and P. Vassalli. The area of attachment of cytotoxic t lymphocytes to their target cells shows high motility and polarization of actin, but not myosin. *J. Immunol.*, 128:1159–1162, 1982.

[258] A. Kupfer and G. Dennert. Reorientation of the microtubule-organizing center and the golgi apparatus in cloned cytotoxic lymphocytes triggered by binding to lysable target cells. *J. Immunol.*, 133:2762–2766, 1984.

[259] J. R. Kuhn and M. Poenie. Dynamic polarization of the microtubule cytoskeleton during ctl-mediated killing. *Immunity*, 16:111–121, 2002. (http://dx.doi.org/10.1016/S1074-7613(02)00262-5).

[260] J. C. Stinchcombe, E. Majorovits, G. Bossi, S. Fuller, and G. M. Griffiths. Centrosome polarization delivers secretory granules to the immunological synapse. *Nature*, 443:462–465, 2006. (http://dx.doi.org/10.1038/nature05071).

[261] K. Basnayake, C. Guerrier, Z. Schuss, and D. Holcman. Asymptotics of extreme statistics of escape time in 1, 2, and 3-dimensional diffusions. *arXiv:1711.01330v1*, 2017. https://arxiv.org/abs/1711.01330, (16.04.2018).

[262] M. E. J. Newman and G. T. Barkema. *Monte Carlo methods in statistical physics*. Oxford University Press Inc., New York, 1999.

[263] W. Krauth. *Statistical mechanics: algorithms and computations*. Oxford University Press Inc., New York, 2006.

[264] D. T. Gillespie. A general method for numerically simulating the stochastic time evolution of coupled chemical reactions. *J. Comput. Phys.*, 22:403–434, 1976. (http://dx.doi.org/10.1016/0021-9991(76)90041-3).

[265] D. T. Gillespie. Exact stochastic simulation of coupled chemical reactions. *J. Phys. Chem.*, 81:2340–2361, 1977. (http://dx.doi.org/10.1063/1.2710253).

[266] D. T. Gillespie. Monte carlo simulation of random walks with residence time dependent transition probability rates. *J. Comput. Phys.*, 28:395–407, 1978. (http://dx.doi.org/10.1016/0021-9991(78)90060-8).

Acknowledgments

I would like to thank the people who have supported me.

Foremost, I would like to thank my supervisor Prof. Heiko Rieger for his continuous support and invaluable advice. I have benefited a lot from his expertise and appreciate the freedom he gave and the guidance he provided when needed. In particular, I am very grateful that he has given me the opportunity to present our work at many exciting conferences.

Furthermore, I would like to thank Prof. Ludger Santen and Dr. Reza Shaebani for guiding and supporting my first steps into the world of random walks.

It has been a pleasure to work in such an inspiring research environment.

In this context, I thank the German Research Foundation (DFG) for financial support within the Collaborative Research Center SFB 1027. I have learned so much from the seminars, the lab courses, the trainings, and summer camps.

Many thanks go to my friends and colleagues, especially to Benjamin Blaß, Benjamin Bogner, Thierry Fredrich, Ivan Hornak, Alexander Lück, Zeinab Sadjadi, Barbara Schmidt, Karsten Schwarz, and Christian Thome for fruitful discussions and advice on no matter what topic.

In particular, I would like to express my deep gratitude to my family. I thank my mother for her unreserved support and encouragement. I thank my brother for scientific discussions and for sharing my passion for physics and my sense of humor. This thesis is dedicated to the memory of Ben, who steadily reminded me on the very essence of "What is Life?" [1].